Polysiloxane and Polysilsesquioxane based Materials for Optoelectronic Applications and Organic Dye Integration

Dissertation

Zur Erlangung des Grades des
Doktors der Naturwissenschaften
der Naturwissenschaftlich-Technischen Fakultät
der Universität des Saarlandes

Nils Steinbrück, M.Sc.

Saarbrücken
2020

Tag des Kolloquiums: 14.02.2020

Dekan: Prof. Dr. Guido Kickelbick
Vorsitzender: Prof. Dr. Christopher Kay
Berichterstatter: Prof. Dr. Guido Kickelbick
Prof. Dr. Gregor Jung
Prof. Dr. Holger Frey
Akad. Beisitzer: Dr. Bernd Morgenstern

“The greatest gift we can receive is to have the chance,
just once in our lives, to make a difference.”

Dr. Stephen Strange

The present dissertation was prepared in the time between March 2016 and July 2019 in the Institute of Inorganic Solid State Chemistry of the Faculty of Natural Science and Engineering at the Saarland University under the supervision of *Prof. Dr. Guido Kickelbick*.

The research has been funded by the *Federal Ministry of Education and Research of Germany* in the framework of MatRessource (project number: 03XP0050) in cooperation with *BASF SE, OSRAM GmbH* and *OSRAM Opto Semiconductors GmbH* under the supervision of the *Projektträger Jülich (PTJ).*

Erklärung

Ich erkläre hiermit an Eides statt, dass ich die vorliegende Arbeit ohne unzulässige Hilfe Dritter und ohne Benutzung anderer, nicht angegebener Hilfsmittel angefertigt habe. Die aus anderen Quellen direkt oder indirekt übernommenen Daten und Konzepte sind unter Angabe der Quelle gekennzeichnet. Die Arbeit wurde bisher weder im In- noch im Ausland in gleicher oder ähnlicher Form einer anderen Prüfungsbehörde vorgelegt. Es wurden keine Dienste eines Promotionsvermittlungsinstituts oder ähnlichen Organisationen in Anspruch genommen. Ich habe weder früher noch gleichzeitig bei einer anderen Hochschule oder in einer anderen Fakultät ein Promotionsverfahren beantragt. Weiterhin erkläre ich, dass mir die Promotionsordnung der Naturwissenschaftlich-Technischen Fakultät der Universität des Saarlandes vom 13. November 2013 bekannt ist und von mir anerkannt wird.

Declaration of Authorship

I hereby declare that I have produced the present word without the unauthorized help of third parties and without the use of other resources, which have not been attributed. Any data and concepts taken directly or indirectly from other sources have been assigned by quoting the reference. Before this date, the work has not been submitted to any other examination authority either in Germany or in another country in the same or a similar form. I have not used the service of any doctoral procurement institute or any organization of similar nature. Moreover, I have not applied for a doctoral process either earlier nor currently at any other university of faculty. Furthermore, I declare that I am aware of the doctoral regulation of the Faculty of Natural Science and Engineering of the Saarland University dated 13th of November 2013 and that I fully acknowledged them.

Saarbrücken, 18.02.2020

Nils Steinbrück

List of Publications

Within this Thesis

Effect of polysiloxane encapsulation material compositions on emission behavior and stabilities of perylene dyes
Nils Steinbrück, Martin Könemann, and Guido Kickelbick*, *RSC Adv.*, **2018**, *8*, 18128-18138
https://doi.org/10.1039/c8ra01700j

Perylene Polyphenylmethylsiloxanes for Optoelectronic Applications
Nils Steinbrück and Guido Kickelbick*, *J.Pol.Sci.B.,* **2019**, *57*, 1062-1073
https://doi.org/10.1002/polb.24861

Platinum free thermally curable siloxanes for optoelectronic application – synthesis and properties
Nils Steinbrück, Svenja Pohl and Guido Kickelbick*, *RSC Adv.*, **2019**, *9*, 2205–2216.
https://doi.org/10.1039/C8RA09801H

Others

HBr or not HBr? That is the question: crystal structure of 6-hydroxy-1,4-diazepane-1,4-diium dibromide redetermined
Mateusz Piontek, Bernd Morgenstern, Nils Steinbrück, Bastian Oberhausen, Guido Kickelbick and Kasper Hegetschweiler*, *Acta Cryst.*, **2019**, C75, 6, 678-685.
https://doi.org/10.1107/S2053229619005321

Synthesis, Structure, and Bonding Analysis of Tin(II) Dihalide and Cyclopentadienyltin(II) Halide (Alkyl)(amino)Carbene Complexes
Carsten Müller, Diego M. Andrada, Inga-Alexandra Bischoff, Michael Zimmer, Volker Huch, Nils Steinbrück and André Schäfer*, *Organometallics*, **2019**, 38, *5*, 1052-1061
https://doi.org/10.1021/acs.organomet.8b00861

List of Submitted Patents

Zusammensetzungsprecursor, Zusammensetzung, Verfahren zur Herstellung eines Zusammensetzungsprecursors, Verfahren zur Herstellung einer Zusammensetzung, Verwendung einer Zusammensetzung und Bauelement
G. Kickelbick, N. Steinbrück, S. Pohl, 2018, EP18190475.6

Polymeres Matrixmaterial, Konversionselement, optoelektronisches Bauelement und Verfahren zur Herstellung eines optoelektronischen Bauelements
G. Kickelbick, N. Steinbrück, D. Meier, 2018, EP18190468.1

C2-C3-alkenyl-substituted rylene imide dyes and curing product of curable silicone resin composition and C2-C3-alkenyl-substituted rylene imide dyes
G. Kickelbick, N. Steinbrück, M. Könemann, S. Ivanovici, H. S. Mangold, 2019, WO/2019/137975

Abstract

Commonly applied phosphors in LEDs are made of oxides doped with rare-earth ions that are incorporated into polysiloxane encapsulation materials. Due to the uncertain supply of rare-earth compounds and the high prices of those materials, alternative rare-earth free organic hybrid-LEDs are an object of recent research projects. Within this thesis, the influence of different substituted platinum-containing and thermally curable polysiloxane to the properties of covalent and non-covalent incorporated perylene dyes has been investigated. New liquid perylene polysiloxanes by hydrosilylation, leading to a significant increase of the dye concentration incorporable into a polysiloxane without precipitation and enhance stabilities. Platinum-free curable, gel-like and partially cross-linked phenylmethylsiloxane encapsulation materials with tunable properties could be synthesized able to be thermally cured to elastomeric materials without the use of any catalyst. Using these materials as host for organic fluorescence dyes leads to a significantly increased photostability of the dye and therefore to a sustainable and reliable combination. Spherical, completely condensed and thermally stable fluorescent microparticles has also been synthesized in a newly developed surfactant mediated emulsion technique. The subsequent integration of these particles to a thermally curable polysiloxane has been performed to prove the possibility of an implementation to a Hybrid-LED encapsulation.

Zusammenfassung

Konversionsleuchtstoffe werden in den meisten kommerziell nutzbaren LEDs aus selten-erddotierten, anorganischen Verbindungen hergestellt und mit Polysiloxanen verkapselt. Aus ökonomischen und ökologischen Gründen sind seltenerd-freien organischen Hybrid-LEDs ein äußerst attraktiver Gegenstand aktueller Forschung. Im Rahmen dieser Dissertation wurde zuerst der Einfluss von verschieden substituierten platinhaltigen Polysiloxanmatrices auf die Eigenschaften kovalent und nicht-kovalent eingebrachten Perylenfarbstoffe untersucht. Phenylhaltige polysiloxane erhöhen die Löslichkeit der Farbstoffe, deren Quantenausbeute und thermische sowie fotophysikalische Stabilität stark. Neuartige Perylenpolysiloxane wurden hergestellt, die eine signifikante Erhöhung der einbringbaren Farbstoffkonzentration in Polysiloxanen ermöglichen. Der Einbau dieser flüssigen Polymere in ein thermisch aushärtbares zwei-komponenten Polysiloxan führte zur Darstellung von stark fluoreszierenden festen Probenkörpern, mit hohen Quantenausbeuten, hohen Stabilitäten und einstellbaren Härten. Neue gelartige, teilvernetzte und katalysator-frei thermisch aushärtbare polysilsesquioxane wurden hergestellt. Integrierte Perylenfarbstoffe zeigen eine signifikant erhöhte Lebensdauer bei Bestrahlung im Vergleich zu den platin-haltigen kommerziellen Systemen. Durch ein neu entwickeltes tensidunterstütztes Verfahren wurden vollständig kondensierte und thermisch stabile, fluoreszierendem Hybrid-Glas Mikropartikel hergestellt.

List of Abbreviations

a	Self-Absorption Coefficient
A	Absorbance
ATR	Attenuated Total Reflection
CM	Consolidated Material
CRI	Color Rendering Index
DABCO	1,4-Diazabicyclo[2.2.2]octane
DAS	Dialkoxysilane
DC	Degree of Cross-linking
DSC	Differential scanning calorimetry
Dow(1)	Dow Corning OE6630
ESR	Electron Spin Resonance Spectroscopy
FTIR	Fourier-Transform Infrared Spectroscopy
GC	Gas Chromatography
HMBC	Heteronuclear Multiple Bond Correlation
HOMO	Highest Occupied Molecular Orbital
HRI	High Refractive Index
ISC	Intersystem Crossing
KAIST	Korean Advanced Institute of Science and Technology
LCD	Liquid Crystal Display
LED	Light Emitting Diode
LG305	Lumogen®F Red 305
LRI	Low Refractive Index

LSC	Luminescent Solar Collector
LUMO	Lowest Unoccupied Molecular Orbital
MAS	Magic Angle Spinning
MS	Mass Spectrometry
M_W	Molecular weight
NMR	Nuclear Magnetic Resonance Spectroscopy
OLED	Organic Light Emitting Diode
PC	Polycarbonate
PDMS	Polydimethylsiloxane
PENIS/CP	Proton-Enhanced Nuclear Induction Spectroscopy/Cross Polarization
PMMA	Polymethylmethacrylate
PMPS	Polymethylphenylsiloxane
POSS	Polyhedral Oligomeric Silsesquioxane
ppm	Parts Per Million
PS	Polystyrene
PTCDA	Perylene-3,4,9,10-tetracarboxylic Acid
PTFE	Polytetrafluoroethylene (Teflon)
QLED	Quantum Dot Light Emitting Diode
QY	Quantum yield
RI	Refractive Index
SEM	Scanning Electron Microscopy
SD	Swelling Degree
SEC	Size Exclusion Chromatography

Shin(1)	Shin Estu KJR9022E
TAS	Trialkoxysilane
TEM	Transmission Electron Microscopy
TEOS	Tetraethyl Orthosilicate
TG	Thermogravimetric Analysis
T_g	Glass Transition Temperature
Triton X-405	Polyoxyethylene(40)isooctylphenylether
UV/Vis	Ultraviolet-Visible Spectroscopy
wt%	Weight Percent
XRD	X-ray Diffraction
YAG	Yttrium Aluminum Garnet

Content

1. Introduction and Research Objective

1.1. Motivation

White light-emitting diodes have been investigated and offered for sale for the first time in the 1990s.[1] A high luminance, low production prices, low energy consumption and the possibility of a massive reduction of the dimension of the device makes the LED irreplaceable for today's in and outdoor illumination and the electronic and automotive industries.[2–4] It became the most promising technology for every possible application in which lightning is essential. Despite the circumstance that LED technology gets along without the use of toxic components, like the formerly used mercury lamps, and without a considerable energy loss by heat generation, it is still not sustainable with regards to its raw materials. The device segmented in different parts made from completely diverse materials. The main component responsible for an appropriate white light impression is an inorganic phosphor that is applied on top of a semiconductor chip.[5] This phosphor is consists of rare-earth-containing host lattice, which converts blue light emitted from the semiconductor chips' surface into light with wavelengths from the less energetic visible spectrum. The sum spectrum of the emitted light from the chip and the phosphor material covers the visible spectrum entirely and results in a white light LED. An encapsulation primarily made of polysiloxanes, in general, called silicones, is used to protect this simple setup from external expositions like dirt, water, oxygen, and other gases. This encapsulation is commonly composed of two liquid silicon components that can be hardened by platinum-catalyzed hydrosilylation.[6] After the hardening process, the platinum remains in the LED encapsulation. Due to the massive geopolitical dependence of the supply of rare-earth compounds, the high correlated prices of those materials, sustainable alternatives must be found.

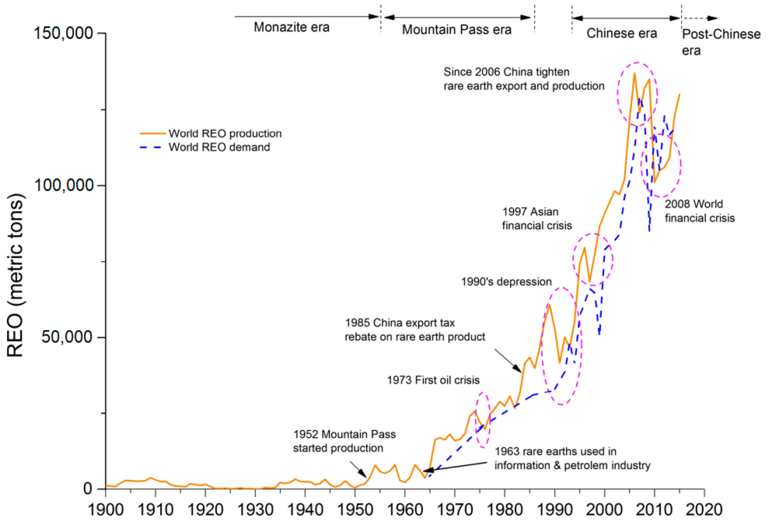

Figure 1. Globale rare-earh production and demand. Reprinted from Zhou, B., Li, Z. & Chen, C., Minerals 7, 203 (2017), licensed under CC-BY 4.0.[7]

Since the 1960s rare-earth applications gradually expanded to electronics and the petroleum industry.[7] Therefore, global rare-earth production and consumption started to increase significantly in the next decades (Figure 1). When China began exporting rare-earth materials in the 1970s, it was limited to crude minerals only.[8] In the 1990s, China also started to isolate and produce inorganic phosphors, magnets, and polishing powders leading to a significant increase of rare-earth output worldwide. Nowadays, China is not just producing resources; it is also researching, developing, and launching finished products containing rare-earth materials like electric motors, batteries, LCDs, LEDs, mobile phones, and so on.[8]

The primary producer for rare-earth materials in 2015 was China itself with 84 % (Figure 2). One reason for that is the distribution of the global amount of rare-earth resources, mainly located in China with 35 %. Major demands in the same year were magnets (23 %) and catalysts (24%).[7] Next, to the production values strong restrictions for export, mining, trading as well as high export taxes up to 27 were set by the Chinese government in 2015, impacting the prices and accessibility of these materials culminated in involvement to the trade war of China and the United States of America in 2019.[9,10]

If new supplies or alternatives do not come up within the next decade, a global shortage will affect science and industries, especially in the electric vehicle and electronics productions.[8] A regaining procedure has been evaluated for neodymium, dysprosium, terbium, and erbium used in different magnetic applications, but there is no practicable recycling method known for rare-earth materials in optoelectronic devices like LCD, LED where rare-earth phosphors are implemented steadily.[11]

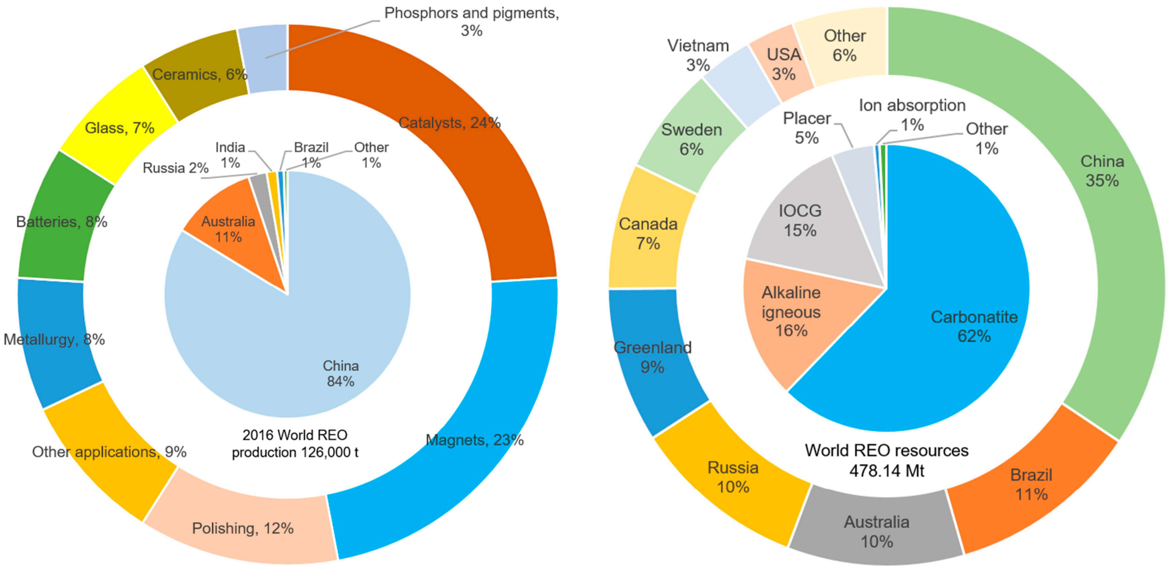

Figure 2. The distribution of global rare earth production and consumption in 2015 and the distribution of global rare earth resources by principle deposit type and country. Reprinted from Zhou, B., Li, Z. & Chen, C., Minerals 7, 203 (2017), licensed under CC-BY 4.0.[7]

The reduction or even the substitution of rare-earth-containing components for LED applications and the associated development of new siloxane-based host materials for the new components are the main objects of the research presented in this thesis. The most promising candidates for this purpose on the one side are organic perylene based fluorescence dyes.[12] They can be synthesized by classical organic chemistry on a ton scale, are non-toxic, not harmful for any environment, and their efficiency is equal to most of the inorganic rare-earth counterparts. However, their limited chemical and physical stability in optoelectronic applications must be enhanced significantly, especially for the use in LED applications. On the other side, siloxane-based host materials must be found which can solve the organic dyes and protect it against degradation by photophysical and thermal expositions. Especially in high power applications, the conditions are rough, and the continuous treatment with short-wavelength excitation light and high temperatures lead to a decreased stability of a pure organic LED device. The organic dye and its siloxane-based encapsulation need to withstand thousands of operating hours without losing performance relevant properties like quantum efficiency, transparency, brightness, and color.[13] A suitable and longtime stable dye-polymer combination can also enhance the efficiency of other optoelectronic devices for renewable energy applications like the luminescent solar collectors.

2. Theoretical Backgrounds

2.1. Light Emitting Diode

Common Solid-State LEDs

The white light impression of a commercially available LED is generated by multiple concerted physical processes of different materials. The main parts of a LED are placed in a polymeric and high reflective titania filled polyphtalamide package attached to a silver-coated baseplate called lead frame (**Figure 3**). The main component is made from one or more semiconductor chips emitting narrowband light of specific wavelength by recombination of electrons and holes in the material's structure. The most common semiconductors are based on p- and n-doped $In_{1-x}Ga_xN$. It is doped with Mg^{2+} to create p-semiconducting properties, whereas the n-semiconducting properties are caused by doping with Si^{4+}.[3] The chip is attached to high conductive noble metal bond wire transferring electric current from the baseplates' point of contact to the chip's surface. By applying a potential in the forward direction, the p-n junction is biased, and the electrons can move from the p- to the n-junction generating positively charged holes. Recombination of electrons and holes leads to the emittance of photons. The photons energy is directly correlated to the bandgap of the semiconducting material, which allows partly an adjustment of the wavelength emitted by the semiconductor. In $In_{1-x}Ga_xN$, for example, the wavelength can be adjusted between 370 and 580 nm with increasing Indium concentration.[3]

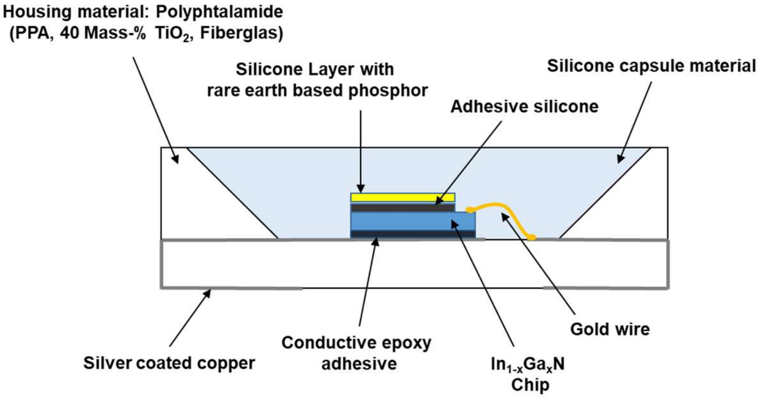

__Figure 3.__ General LED device with the main parts assigned.

The efficiency of these materials is categorized in an internal and an external part. The internal efficiency is defined by the number of photons emitted from the chip per second divided by the number of electrons injected per second. The external efficiency is defined by the number of photons emitted to the free space per second divided by the number of photons emitted from the chip per second. A higher external efficiency results an increased light output at the same amount of input.[13] The highest external efficiency of $In_{1-x}Ga_xN$ is observed at a wavelength of

450 nm. This is the main reason why this wavelength is used for most white light LED devices known. The chip is typically covered or layered with an inorganic phosphor encapsulated in a polymeric material like silicone. These phosphors consist of inorganic metal oxide microparticles doped with divalent or trivalent rare-earth ions called the activator. The integration of an activator ion leads to the addition of optical-electronic states to the lattice. The rare-earth ions show optical transitions and luminescence, respectively. Typical examples for such phosphors are $Y_3Al_5O_{12}:Ce^{3+}$, $Lu_3Al_5O_{12}:Ce^{3+}$, $CaAlSiN_3:Eu^{2+}$, $(Ba,SrCa)_2Si_5N_8:Eu^{2+}$ and β-sialon:Eu^{2+}.[2–5,12,14–17] Most of the integrated divalent rare-earth metal ions like Eu^{2+}, Sm^{2+}, and Tm^{2+} and the trivalent Ce^{3+} show optical allowed f-d-transitions, which cause a high-efficiency light output and a broadband emission.

When the semiconductor $In_{1-x}Ga_xN$ chip emits light, it is partially transmitted through the phosphor layer and partially absorbed by the phosphor leading to additional light emission of a wavelength with lower frequency. $Y_3Al_5O_{12}:Ce^{3+}$, for example, shows a very broad f-d emission from 500 to 750 nm.[18] The sum of the emitted light from the chip and the phosphor results in a cold white light impression (**Figure 5**). The high efficiency, the broadband emission and the fact that the excitation maximum of the rare-earth-doped oxides is located at the semiconductor chips emitted a wavelength of 450 nm, are the reasons for the general use of this material combination in white light LEDs. Nevertheless, the use of rare-earth materials is still challenging. The commonly used $Y_3Al_5O_{12}:Ce^{3+}$, for example, shows a strong dependence of the color rendering on the working conditions of the LED.[3] The reason for this is the missing red part of the spectrum leading to a more pleasant warm white impression, which is nowadays compensated by mixtures of different rare-earth phosphors.

Next, to the white light LEDs, there have been many monochromatic LEDs investigated in the last decades, which are used especially in scientific applications and devices where monochromatic light is needed.[19–21]

Figure 4. Golden Dragon high power white light LED. Copyright ©2019, OSRAM Opto Semiconductors GmbH.[22]

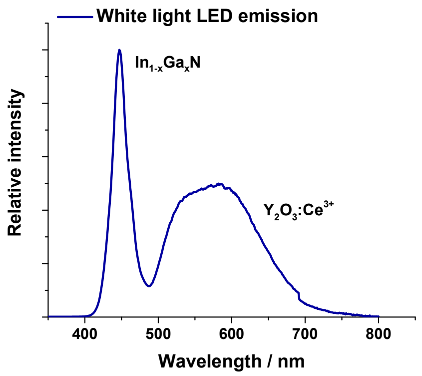

Figure 5. *The emission spectrum of white light LED with an $In_{1-x}Ga_xN$ chip covered with a YAG:Ce^{3+} phosphor*

Organic Hybrid LED

Organic light-emitting diodes (OLEDs) and quantum dot light-emitting diodes (QLED) are recently the most suitable alternatives for the replacement of classical LEDs in low-performance applications like display illumination.[23,24] Their low external quantum efficiencies, their limited lifetime and the use of toxic cadmium compounds (QLED only) confine their use in a lot of ambient lightning or high power application.[25] Whereas OLED technology is based on semiconducting dyes that are directly excited by a current leading to electroluminescence, QLED technology is based on a classical rare- earth-containing white light LED backlight that excites quantum dot-containing layers. A more sustainable variation are hybrid LEDs consisting of the classical LED setup using a blue light emitting semiconductor chip and an organic phosphor substituting the inorganic rare-earth containing one.[26] This organic dye is also able to be excited by the chips emitted wavelength of 450 nm. Due to the fact, that it is not able to emit light in the solid-state it has to be solved completely in a host material protecting it from expositions and pollutions and preserving an optimized emission behavior. Therefore, these dyes are often directly solved in the encapsulation material. It can be cast and cured in the LEDs package leading to an on-chip configuration of a hybrid LED (**Figure 6**a).

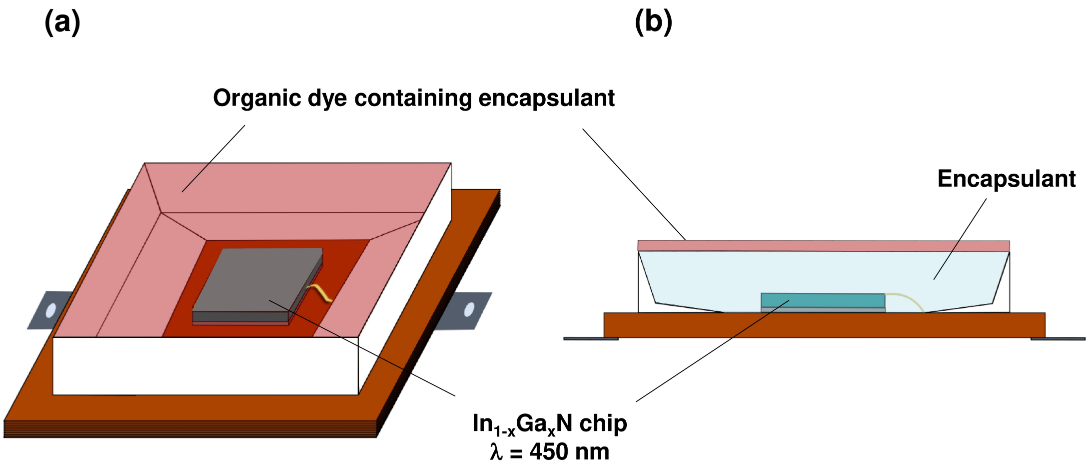

__Figure 6.__ Organic hybrid LED design scheme with an on-chip configuration (A) and a remote configuration (B).

In this configuration, the stress for the dye is maximized due to the direct contact to the semiconductor chips surface. The local heat generation of the chip up to 200 °C and the high radiation exposure up to 1000 mW/cm^2 is directly affecting the dyes and the devices lifetime, respectively. This stress is massively reduced by an increased distance between the solved dye molecules and the excitation source. A first low power approach with organic converters in epoxy resins has already been realized earlier, forming red and green organic hybrid LEDs.[12] The so-called remote phosphor configuration considers these circumstances by separating the dye molecules from the chip (**Figure 6**b). The pure encapsulants are cast and cured in the

LED package first. Afterward, the second layer of a dye-containing encapsulants is cast on the encapsulated package.[27–29] The excitation light produced from the chip is transmitted through the package to the dye molecules leading to excitation and fluorescence respectively. This remote phosphor configuration is also known for classical inorganic solid-state LEDs.[30–32] Another type of remote phosphor configuration of an organic hybrid LED is made of a blue light-emitting LED covered with an organic dye-containing polymer dome. This configuration of is already used in commercially available LED light bulb from Wellypower™ and The BASF SE (**Figure 7**a).[27–29]

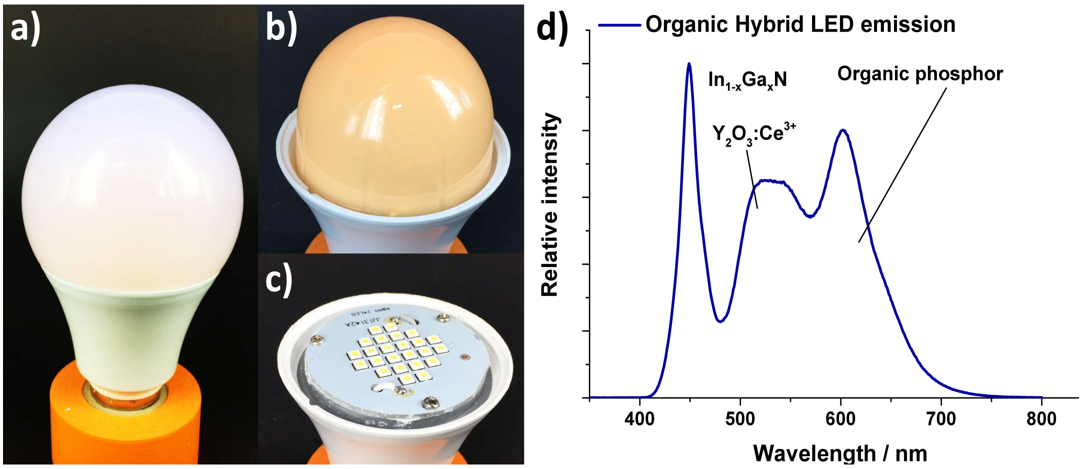

Figure 7. *Commercially available remote phosphor hybrid LED bulb (A), with a dye-containing polymer dome (B) in which the dye is excited by the blue part of a white regular white light, LED board (C) leading to a warm white light expression shown by the emission spectrum of the bulb.*

The main emission is based on classical rare-earth-containing cold white LEDs mounted on a baseplate with the classic rare-earth-containing cold white light LED arrangement. The polymer dome is made from polystyrene or polycarbonate containing organic dyes able to emit green and red light by excitation with the LEDs. By covering the baseplate with this polymer dome, the red and green light is added to the emission spectrum and a warm white light impression is obtained. Due to this configuration, no additional red light-emitting rare-earth-containing components are required leading to a more sustainable device for ambient lighting. Additionally, the lifetime of the organic dye is enhanced significantly by the separation from the LED package. A comparison of perylene dyes in polycarbonate, for example, shows an extinguished fluorescence after 1000 h within an on-chip configuration, whereas a remote setup with 3 cm distance to the excitation source leads to a loss of only 15 % after 2870 h.[33]

Reliability

The lifetime of a LED can vary massively depending on the type and the application it is used for. The LEDs performance like the light output and the light color should not change significantly within 2000 – 70000 h.[13] It is quantified by the measurement of the light intensity and color over time. Therefore, the color rendering index (CRI) and the efficiency in lumen/watt are measured under different working conditions. The main features of a common LED are an initial CRI of >80 and external efficiency of 87 lm/W.[22] For the display industry, the lifetime is defined by the time the light output is decreased by 50 % of the initial intensity (L50). For the lightening industry, it is defined by 20 – 30 % (L70/L80). The individual devices lifetime is strongly affected by intrinsic and extrinsic causes. The semiconductor, the interconnects and the package, including polymeric encapsulations and lenses, are subject to thermal, mechanical, electrical and photophysical stress leading to several possible failure and degradation mechanisms respectively.[13] External expositions like high humidity, temperatures and pollutants like hydrogen sulfide can also cause a lifetime decrease.[34–36] Internal failures can also reduce the devices lifetime significantly. The sedimentation of the inorganic phosphor particles on and around the semiconductor chips, for example, is always linked to a formation of a composite with the encapsulation material. After the curing procedure, the phosphor particles are fixed to this encapsulation resulting in an increased Young's modulus, reduced strength, and elongation of the encapsulation material.[37] At the same time, delamination and cracks are nucleated around the settled particles promoting failure by external expositions penetration into the package. The right choice of an appropriate encapsulation material and the implementation of a highly efficient thermal management can lead to a significant reduction of failure.[38] Materials with low thermal expansion and high thermal conductivity are therefore needed and subject to recent research projects.[39–43] Due to these requirements, the manufacturer has to perform a variety of tests before market launching a new type of LED. Therefore more than twenty different methods are established. The LEDs are always tested a two sequence procedure with defined working conditions like the forward voltage, reverse current and luminous flux. In the environmental and the operational sequence up to 100 temperature cycles and temperature shock cycles as well as longtime high and low-temperature storage experiments between -40 and 100 °C and relative humidity of 90 % are performed.

2.2. Siloxane Chemistry

Synthesis of Siloxanes and their Monomers

Polysiloxanes (silicones) and polysilsesquioxanes are linear or cross-linked polymers with a Si-O-Si backbone and pendant functionalities. The polysiloxane structure is based on repeating difunctionalized Si-O-Si units, whereas polysilsesquioxanes consist of trifunctionalized cross-linked units. Both siloxane type polymers have organic pendant groups **R** like methyl, ethyl, vinyl or phenyl, etc. or other functional groups like hydrides, giving the materials their hybrid character (**Scheme 1**).

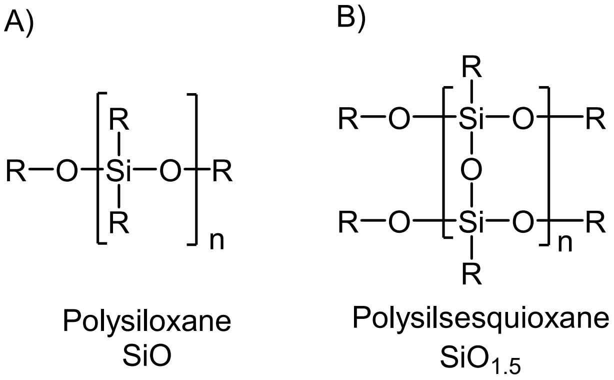

Scheme 1. *(A) Structure of a polysiloxane, (B).structure of a polysilsesquioxane.*

The polymer structure and properties can be varied with the choice of monomers and the applied subsequent synthetic procedure. In an industrial scale, the monomers for the siloxane production are synthesized by a two-step process. First elemental silicon is reacted with methylchlorosilane (Müller-Rochov reaction) applying a copper catalyst to produce mainly dichlorodimethylsilane and other chlorosilane derivatives.[44] The chlorosilanes can be subsequently functionalized by Grignard reactions or by addition reactions. Hydrolysis or alcoholysis leads to the silanol or alkoxysilane derivatives. Afterward, these derivatives can be functionalized by platinum catalyzed hydrosilylation, a palladium catalyzed heck reaction, a Barbier reaction or with organolithium compounds.[45–48] Cyclic side products of the condensation reaction of difunctionalized siloxane monomers like hexaalkyltrisiloxanes (D^3) or octaalkyltetrasiloxanes (D^4) can be separated from the main condensation products and used for ring opening polymerizations, for example.[49–52] Their hydride ($D_{3/4}^H$) and vinyl ($D_{3/4}^V$) derivatives can also be used for hydrosilylations.[53]

The most often used method for the preparation of functionalized polysiloxanes and polysilsesquioxane in laboratory scale is the polycondensation or sol-gel reaction (**Scheme 2**). These reaction types are segmented in a two-step procedure. First organoalkoxysilane monomers are hydrolyzed in an acid or base-catalyzed reaction forming the corresponding silanol species. Second these reactive species condensate with other alkoxysilane monomers by alcohol elimination or with another silanol by water elimination. The structures and properties of the obtaining reaction products can be varied and tuned by several parameters like the alkoxysilane type, the pH and the organic substituents.[54]

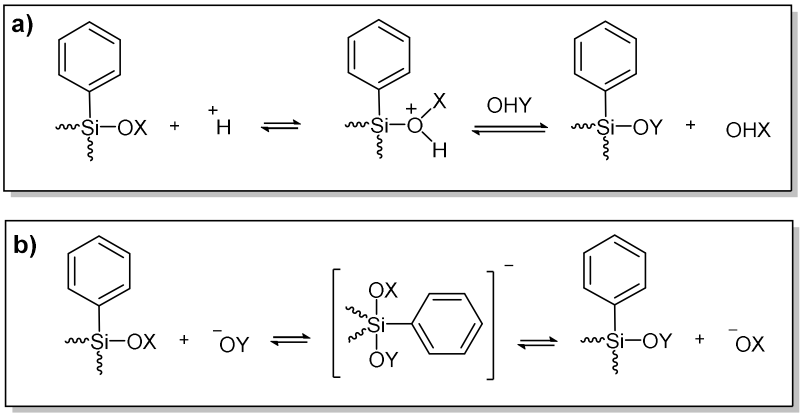

Hydrolysis reaction: X = Me, Y = H
Condensation reation: X = Me or H, Y = $PhSi(OR)_3$

Scheme 2. *Reaction mechanism of the condensation of a phenyltrialkoxysilane or a polyphenylsilsesquioxane under acidic and basic conditions.*

A condensation of diorganodialkoxysilanes, for example, leads to linear or cyclic structures resulting in polysiloxane oils or gels, whereas organotrialkoxysilanes can be condensed to completely and partially cross-linked polysilsesquioxanes with the general composition $RSiO_{1.5}$. Using tetraalkoxysilanes a complete condensation leads to the formation of SiO_2. With mixtures of different alkoxysilanes, the proportion of organic groups as well as the structures and properties of the obtained materials can be adjusted.

In the acid-catalyzed reaction, oxygen atoms are rapidly protonated, forming a good leaving group. The connected silicon atom is donating electrons to the oxygen atom, increasing its own electrophilicity and making it vulnerable for water or silanol groups (**Scheme 2**a). The positively charged transition state is stabilized when the electron density of the silicon atom is increased. Chain-like networks are formed due to an increased electron density on terminal alkoxy or silanol containing silicon atoms. Under basic conditions, an S_N2-type nucleophilic attack of hydroxides or deprotonated silanols takes place (**Scheme 2**b). The less electrophilic central silicon atoms are favored for such a reaction resulting in more branched structures. Hydrolysis and condensation are competing with each other resulting in different intermediates and products. At pH <5 hydrolyses is favored, and condensation is the rate-determining step at pH >5 hydrolyzed species are immediately involved in a condensation reaction.[54] Under highly basic conditions mainly anionic species are formed causing Si-O-Si bond cleavage or redissolution of already cross-linked species and structures.

The rate of hydrolysis is also related to the steric situation of the alkoxy and the organic groups.[55] A longer or more branched alkoxy group is less reactive than a shorter one. Methoxysilanes, for example, hydrolyzes up to 10 times faster than comparable ethoxysilanes. And an increased number of organic substituents enhances the hydrolysis also alkoxysilanes > dialkoxysilanes > trialkoxysilanes. The type of organic substituent (methyl, phenyl) is slightly affecting the reactivity of the monomers.

The strong dependence of the pH and the monomers to the network forming process during the condensation is used to prepare different kinds of siloxane-based materials.

In basic media, often particle shaped materials are observed. Tetraalkoxysilanes, for example, are used to prepare nanostructured silica by the so-called Stöber reaction.[56,57] Linearly functionalized oligosiloxanes and polysiloxanes can be prepared by an acid-catalyzed polycondensation.[58] Whereas partially cross-linked polysiloxanes are often prepared under basic conditions.[59,60] A sequence of pH is also often used for the synthesis of silsesquioxane nano and microparticles, hydrolyzing the monomers first under acidic conditions and performing a condensation under basic conditions.[61]

^{29}Si NMR Spectroscopy

For the investigation of the siloxane structure, the most used method is the ^{29}Si NMR spectroscopy. The resonance of functionalized silicon atoms inside silica, polysilsesquioxane or polysiloxane based materials generate separated chemical shifts in the ^{29}Si NMR spectrum, which can be used for qualitative and quantitative investigations of different units and groups. With a higher occupation of the Si(3p)-orbitals, which are part of the s-bonding system the ^{29}Si-nucleus shielding increases leading to decreased $\delta(^{29}\text{Si})$ values.[62,63] Therefore, minor changes in the total charge density lead to distinct shifts of the NMR signals. The $\delta(^{29}\text{Si})$ value decreases with the number of oxygen bridged bonds to the silicon atom in the order of mono- (M), di- (D), tri- (T) und tetra- (Q) functionalized silicon. Every Si-O-Si bond formed further decreases chemical shift. The number of Si-O-Si bonds can be assigned to the type of group by a superscript number (**Figure 8.**). When a trialkoxysilane reacts in an acid-catalyzed condensation, for example, the signal intensity of the chemical shifts of the T^0 monomer starts to decrease whereas the T^1 for an end group, the T^2 for a linearly linked unit, and the T^3 for a cross-linked unit increase. By integrating the respective chemical shift signals the degree of cross-linking can be calculated and related to the condensation products properties.

Also, changes in organic substituents lead to distinct shifts of the NMR signals. The substitution of a methyl group by a phenyl group leads to a high field shift of 10 – 12 ppm due to the higher p-orbital interactions with the phenyl ring and have to be considered for the NMR spectra interpretation.

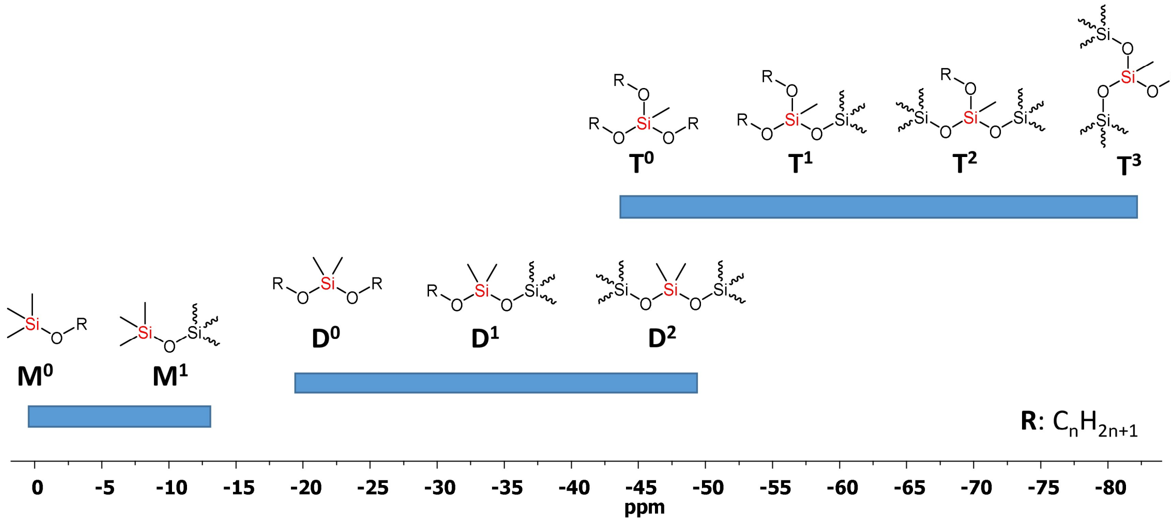

Figure 8. Range of chemical shifts for Mono- (M), di- (D), tri- (T) und tetra (Q) functionalized silicon.

2.3. LED Encapsulations

Common Materials and Requirements

The polymeric encapsulation protecting all parts of the LED from external expositions is at the same time, the most claimed material. It covers the semiconductor chip, which is producing high temperatures up to 200 °C locally and it is exposed to the high-intensity light output at the same time (**Figure 3** and **Figure 6**).[64–67] The fluctuation of temperature by turning the device on and off, additionally causes stress to the encapsulation. Epoxy resins are the most commonly used thermosetting polymers for low-power LED applications due to their low cost, ease of processing, and good thermal, electrical, mechanical, and moisture-barrier properties.[67]

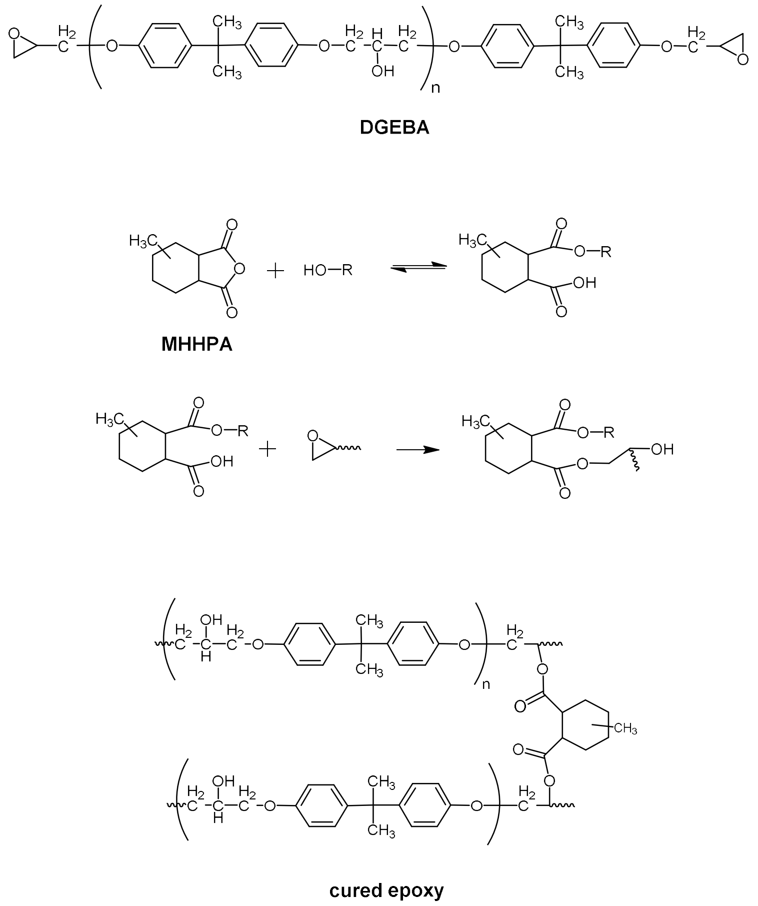

Scheme 3. The curing procedure of a DGEBA with an MHHPA hardener and an alcohol accelerator.

The diglycidyl ether of bisphenol-A (DGEBA) is the most often used epoxy resin due to its tunable molecular weight and viscosity.[68,69] It is combined with a curing agent like methyl hexahydrophthalic anhydride (MHHPA) to form a polymeric structure. The anhydride is not reacting directly with the epoxy group. Therefore it has to be opened in a first step by accelerators like Lewis acids, alcohols, metal salts or tertiary amines (**Scheme 3**).[70–72]

However, the cured epoxy resins are usually hard and brittle and start to degenerate under the exposure of high radiation and temperatures as they are present in high-power applications. The caused thermo-oxidative cross-linking leads to discoloration and yellowing of the material.[13,67,69] The use of antioxidants can reduce these discoloration effects.[73] Thermoplastics like bisphenol-A polycarbonate show similar degradation phenomena at LED working conditions but are also widely used for encapsulation purposes (**Scheme 4**).[74]

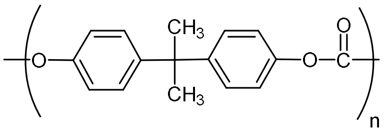

Scheme 4. Structure of bisphenol-A polycarbonate

Polysiloxanes (silicones) are the most suitable material for the replacement of the known polymeric systems. They reveal much better heat stability, high transparency, and tunable refractive indices.[75,76] Because of the combination of organic groups like methyl or phenyl with an inorganic Si-O-Si backbone, polysiloxanes exhibit additional unique properties such as stronger stress absorbing, better high and low-temperature stabilities and more excellent biocompatibility than other polymers.[67] Most of the silicone resins used for encapsulation purposes are supplied as two-component polysiloxane copolymers, which are able to be cured by a thermal initiated and platinum-catalyzed hydrosilylation reaction (**Scheme 5**).

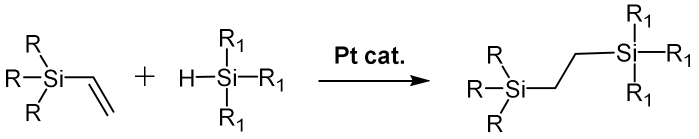

R, R_1 = siloxan, alkyl, aryl, alkenyl, alkoxy

Scheme 5. Hydrosilylation reaction of a vinyl-containing and hydride-containing siloxane component.

One component consists of a mixture of a polysiloxane copolymer containing pendant and terminated vinyl or allyl functional groups and a platinum catalyst. The other component consists of a polysiloxane copolymer containing pendant and terminated hydride groups. The catalysts used are chosen by the given purpose and can initiate the cross-linking reaction at different temperatures. The concentration of the catalyst used is affecting the reaction time and the properties of the materials. An excessive concentration can lead to the formation of platinum (nano)particles and thus to discoloration of the complete silicone.[77] The platin carbonyl cyclovinylmethylsiloxan catalyst (Ossko), is most often used for a curing procedure offset at temperatures >60 °C. The platin-divinyltetramethyldisiloxan catalyst (Karstedt), initiates the curing procedure already at room temperature (**Scheme 6**). The number of vinyl and hydride groups also influences the cross-linking degree and the final thermal and mechanical properties of the cured resin.

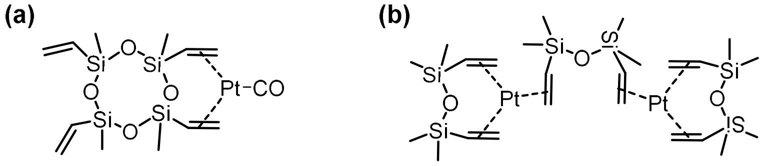

Scheme 6. *(a) Platin carbonyl cyclovinylmethylsiloxan (Ossko), (b) platin-divinyltetramethyldisiloxan (Karstedt) (c) chloroplatinic acid (Speyer's catalyst).*

More important for the optical properties are the organic groups of the polysiloxane. Especially in optoelectronic applications, high transparency and a high refractive index (RI) of the encapsulation and lenses are required. High transparency is particularly required for wavelengths that must be passed through the encapsulation material, whereas a high refractive index is required to reduce total internal reflection phenomena at the interfaces of the encapsulation materials to chip and/or phosphor. The light emitted by the semiconductor chip or the phosphor, for example, is incident on the encapsulation interfaces. The incident angle of the light must be larger than the critical angle that can be calculated by Snell's law where n_1 is the RI of the light-emitting materials, and n_2 is the RI of the encapsulation

$$\Theta = sin^{-1}\left(\frac{n_2}{n_1}\right)$$

Otherwise, the emitted light is partially or totally reflected back in the light-emitting medium.[6] Therefore, the RI of the encapsulation must be maximized to reduce the amount of reflected light and ensure an increases light decoupling and efficiency, respectively. The refractive index of the LED chip is between 2.5 and 3.5.[6] The refractive index of commercially available silicones is between 1.38 and 1.57, depending on the organic groups attached to the silicon atoms.[78–80] Methyl groups lead to a RI of ≤1.41. The commercially available polydimethylsiloxanes (PDMS) for example, are therefore called low refractive index encapsulants (LRI). The introduction of phenyl groups increases the electron density in the silicon structure and the refractive index respectively leading to high refractive index encapsulants with a RI >1.50.[80,81] Thermally curable two-component silicone HRI resins with a high amount of phenyl groups are the most often used encapsulation materials for high performance LED applications. For the stated reasons, the material developed within this thesis needed to have a refractive index of >1.48 to enhance the efficiency of the organic hybrid LED. Therefore, phenyl groups have to be part of the materials to be developed.

Dye Compatibility

The requirements for the incorporation of organic dyes solved in the encapsulation material are different from the requirements for the common inorganic phosphors. They are versatile and can be divided into the requirements of the polymer and those of the phosphor. The polymer requirements are the same as for the classical LED encapsulation materials, but additionally, it must be able to dissolve the incorporating organic substances completely without any negative influence on its properties. Some matrix materials promote stacking effects or even precipitation of the dye, leading to scattering effects and a significant loss of efficiency.[82] A high solubility is therefore also very important for other optoelectronic applications using polymer encapsulations like luminescent solar collectors (LSC). Here, the incorporated dye is excited by sunlight, and its emitted light is channeled by its polymeric host material to solar cells producing an electric current. Increased dye concentration can enhance LSCs efficiency significantly.[83,84] Other polysiloxanes promote dye degradation just by their composition. Some perylenes, for example, solved in polysiloxanes start to bleach without any further exposition, even if stored in dark environment.[33] This can happen when the dye reacts with commonly used additives like adhesion agents.

Therefore the influence of the polymer matrix structure to the solubility and the degradation of the dyes used for the given purpose must be tested and evaluated to prevent concentration induced quenching effects, precipitation, or bleaching.

2.4. Encapsulants – Research and Development

Siloxanes

The major objective of the research and development of siloxane-based encapsulations for optoelectronic applications is the increase of lifetime, refractive index, and external efficiency, respectively, as explained before by the stated reasons.

The most common and easy way to increase the refractive index of a polymeric matrix is the increase in the amount of phenyl containing units.[85] Therefore precursor polymers were synthesized by a polycondensation reaction using phenyl- or diphenyl alkoxysilanes. Adding vinyl or hydride containing alkoxysilanes to the reaction leads to polymer precursors that can be cross-linked by hydrosilylation afterward. A phenyl containing encapsulation, for example, was synthesized by the group of Kim et al., preparing a phenylvinyloligosiloxane precursor by a base-catalyzed polycondensation using vinylrtrimethoxysilane and diphenylsilandiol monomers.[60] A subsequent hydrosilylation with phenyltris(dimethylsiloxy)silane leads to a transparent and flexible elastomer with a RI of 1.5597 and hardness of 70 Shore-D (**Scheme 7**). After a thermally aging process at 200 °C for 1152 hours, the material was discolored, resulting in a decreased transparency.

A more densely crosslinked polysiloxane could be synthesized by a similar synthesis procedure preparing one vinyl and one hydride containing precursor oligomer made of phenyltrialkoxysilanes and diphenyldialkoxysilanes followed by a hydrosilylation. This procedure results in a maximized RI of 1.532.[86] Because the amount of phenyl groups incorporable to such cross-linked polysiloxanes is limited the increase of the refractive is limited as well.

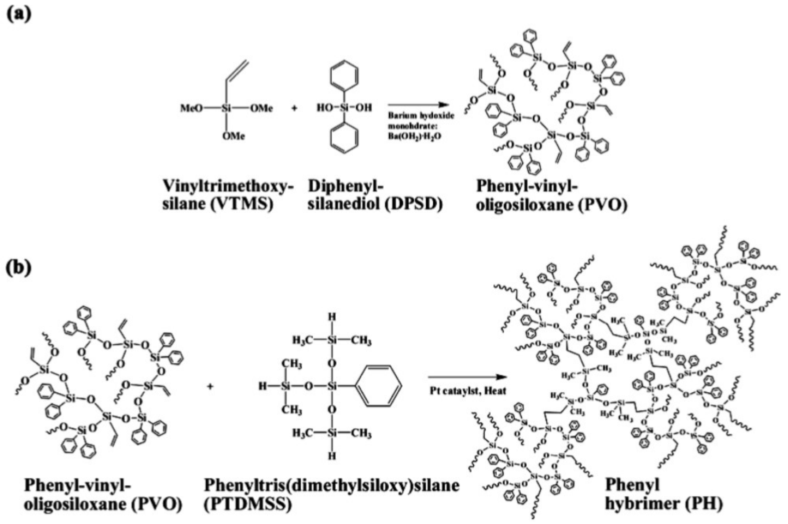

Scheme 7. *(a) Synthesis of Phenyl-vinyl-oligosiloxane (PVO) by sol-gel condensation of vinnyltrimethoxysilane (VTMS) and diphenylsilanediol (DPSD) and (b) fabrication of a phenyl hybrimer (PH) by a hydrosilylation reaction of PVO and phenyltris(dimethylsiloxy)silane (PTDMSS). Reprinted with permission from Kim, J. S., Yang, S. & Bae, B. S., Chem. Mater. 22, 3549–3555 (2010). Copyright ©2010 American Chemical Society.*[60]

Other possibilities were investigated like the incorporation of sulfur or polyaromatic groups. Mercaptoalkylalkoxysilanes, for example, can be used to introduce sulfur with an allylic spacer to a linear hydride and phenyl-containing siloxane polymer backbone leading to an increased RI.[85,87] The resulting precursor polymer can be modified by click chemistry to introduce additional RI increasing groups like biphenyl allyl derivatives before hydrosilylation with a second vinyl-containing component. The combination of sulfur and biphenyl unit results in a high RI with a maximum of 1.65.[87] The procedure can also be turned over by introducing thiol derivatives by click chemistry to allyl or vinyl functionalized polysiloxanes.[88] Anyway, sulfur-containing compounds are not able to be implemented to most of the commercially available light-emitting diodes. The reaction with silver-coated components is leading to degradation caused by the precipitation of silver sulfide.[89–91] Therefore, the devices lifetime would be decreased for the benefit of a high refractive index encapsulation. HRI polysiloxanes with polyaromatic side groups have also been synthesized sulfur-free with RIs up to 1.627 but have not been tested for LED applications yet.[92]

Polymer hybrids

Hybrid materials are also attractive to LED research due to their possible combination of materials advantages. Epoxy-containing alkoxysilanes, for example, can be integrated into polycondensation or sol-gel processes (**Scheme 8**).[93,94] The obtained epoxy-silicone polymer can be subsequently used to be cross-linked by a chemical or photoinitiated reaction.[73,93] They show enhanced properties concerning their thermal and photophysical stability compared to pure epoxy encapsulants.

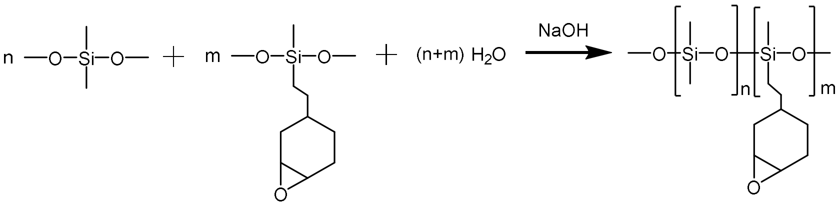

Scheme 8. Synthesis of a silicone-epoxy resin by polycondensation.

Another approach is the integration of pendant alkoxysilane groups into epoxy-based materials for the preparation of an epoxy composite partially cross-linked by a polycondensation reaction.[95] Due to its low transparency in the UV/Vis region and a strong discoloration, these materials are also not suitable for optoelectronic applications. Another known option for enhancing the refractive index and the external efficiencies are composites containing high refractive index components. Particles or structural units of titania (TiO_2) and zirconia (ZrO_2) for example can be integrated into PMMA, epoxy, and silicones to enhance the RI to a maximum of 1.630.[42,96–98] TiO_2 was also be integrated by adding a titanium alkoxide to the finished polycondensation of alkoxysilanes.[99]

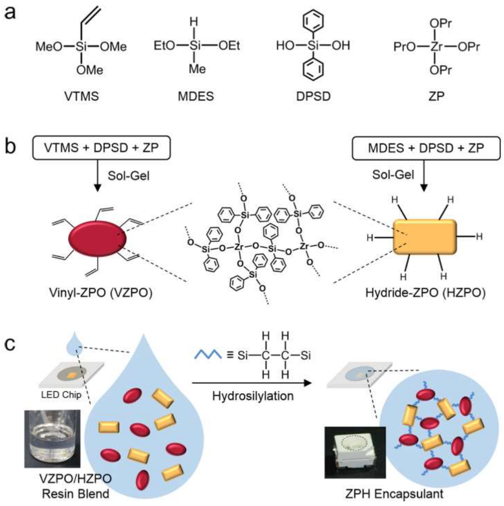

Scheme 9. *Fabrication of zirconium-phenyl siloxane LED encapsulant: (a) chemical structures of the precursors used for synthesizing VZPO and HZPO resin; (b) schematic illustration of the synthesis of VZPO and HZPO resin; VZPO and HZPO are multifunctional oligosiloxanes containing Zr−O−Si heterometallic phase that are functionalized with vinyl and hydride groups, respectively; (c) hydrosilylation-derived curing of VZPO/HZPO resin blend to fabricate the ZPH encapsulant; Inset photographs are the VZPO/HZPO resin blend (left) and the ZPH-encapsulated LED Chip (right). Reprinted with permission from Kim, Y. H., Bae, J. Y., Jin, J. & Bae, B. S., ACS Appl. Mater. Interfaces 6, 3115–3121 (2014). Copyright ©2014 American Chemical Society.*[98]

Curing and Hybrid Glasses

Whether a siloxane-based polymeric material is liquid or solid at room temperature depends on the chain length and the value of linearly or cross-linked sections inside its structure. Polydimethylsiloxanes, for example, are liquid or gel-like materials not able to be cured to a solid cross-linked sample by any chemical or physical treatment. By mixing hydride and vinyl functionalized polydimethylsiloxane copolymers and adding a platinum catalyst, a thermally curable gel is generated, leading to transparent and elastomeric materials with low glass transition temperatures by hydrosilylation usable for several applications.[59,60] By introducing thiol or epoxy functionalities to the polysiloxanes, also photo or UV-curable materials can be synthesized. Epoxy materials made by polycondensation of di-, tri- or tetraalkoxysilanes with already cross-linked structures and alkoxy or hydroxy groups left can also be solid at room temperature without any further curing process. The material's flexibility is decreased by the already existing siloxane network leading to solid samples or particles, for example.[61]

Another possible curing process can be initiated by thermal treatment of partially cross-linked polysilsesquioxanes, synthesized by acid-catalyzed condensation of trialkoxysilanes. Remaining hydroxy and alkoxy groups are still able to be hydrolyzed and condensed by a thermal treatment, leading to a solid material. One example of these materials are hybrid glasses (**Figure 9**). They can be prepared by an acid catalyzed polycondensation reaction of trialkoxysilanes followed by the removal of reaction products and solvents. Their properties, like the consolidation temperature, can be adjusted by adding dialkoxysilanes in a second condensation step.[100–105] The obtained materials are solid, transparent, and rigid. Due to their partially cross-linked structure they can be softened or even melted at temperatures >80 °C reversibly. An additional heat treatment >150 °C leads to further hydrolysis of remaining alkoxy groups by air moisture followed by condensation and irreversible consolidation.

Figure 9. *Consolidated coatings of melting gels on glass: (left) undoped and (right) with 2 ml of 10 nM Au-nanospheres solution added during the purification step. Gel composition is 65 mol% Methyltriethoxysilane −35 mol% Dimethyldiethoxysilane. Reprinted with permission from Klein, L. C. et al., J. Sol-Gel Sci. Technol. 89, 66–77 (2018), Copyright ©2018 Springer.*[102]

Many different methyl and phenyl containing hybrid glasses have been synthesized already. The structure of the materials was studied by 2D solid-state NMR spectroscopy, for example, showing a partially cross-linked polysilsesquioxane structure by the presence of T^3, T^2 and D^2 units only.[106] The T^3 and T^2 units are connected, forming highly cross-linked domains. These domains are interconnected by D^2 units. This structural feature is caused by the synthesis route in which the trialkoxysilanes are hydrolyzed first before the dialkoxysilanes are added. Interestingly, these materials can also be synthesized by phenyltrimethoxysilane only, having the same properties with T^t and T^2 units only.[103] The high cross-linking degree of this polyphenylsilsesquioxane leads to the formation of cracks of a consolidated coating.

2.5. Organic Fluorescence Dyes for Optoelectronics

Selection and Requirements

The phosphors used in organic white light hybrid LEDs are based on organic fluorescence dyes. The most important requirement for the selection of the dye is the absorption maximum, the emission spectrum, and the quantum yield. The quantum yield is measured in a integration sphere setup and is defined by the ratio of emission and excitation spectra values E

$$QY = \frac{Em_B - Em_A}{Ex_A - Ex_B}$$

where E_m and E_x are the areas of the emission and excitation spectra values. A represents the values of the empty sphere B for a sample in the sphere.[107,108] E is calculated from the sum of the product of the photon count rate and the wavelength E respectively

$$E = \sum E(\lambda)\Delta\lambda$$

The quantum yield of the dye used in LED applications is therefore directly correlated to the efficiency of the device. As explained before the excitation wavelength of the commonly used excitation light source, the $In_{1-x}Ga_xN$ semiconductor chip is at 450 nm, based on its increased external efficiency.[3,13] As a result, an organic dye for LED purpose needs to show at least a local absorption or excitation maximum around this wavelength. At the same time, it needs to show broadband emission over the visible spectrum of light, from 500 – 800 nm and a high photophysical and thermal stability. Due to the small Stokes shift of organic fluorescence compounds and the intense prevailed expositions, only a few molecules are suitable to meet these requirements. Perylene diimides are the most common, highly photostable organic dyes with a tunable excitation and emission behavior by substitution.[109] Substituents can be mainly introduced in the shoulder (R_1), bay (R_2) and imide (R_3) position (**Scheme 10**).

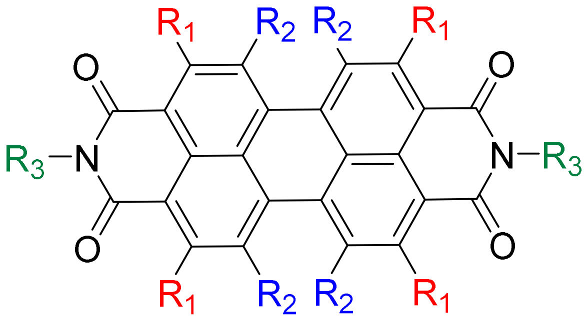

Scheme 10. *Perylene diimide core with substitution pattern, showing the shoulder (R_1), bay (R_2) and imide (R_3) positions.*

Most of the common perylene diimide derivatives were synthesized by a three-step procedure. The imide is often introduced by a condensation reaction of perylene-3,4,9,10-tetracarboxylicadic (PTCDA) with primary amines or anilines catalyzed by molten imidazole or quinolone, leading to symmetrically N,N'-perylene-3,4,9,10-tetracarboxylic diimides.[109] A subsequent acid-catalyzed halogenation of the perylene diimides with bromide or chloride results in a mixture of all possible shoulder and bay derivatives with a yield of around 20 % for the 1,6,7,12- tetrabrominated product.[110] Nucleophilic substitutions and metal-catalyzed reactions can be used for further functionalization (**Scheme 11**).[109–111]

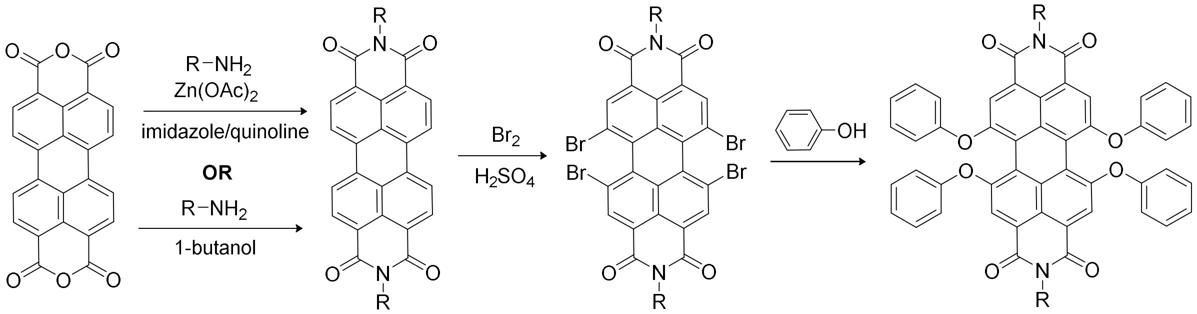

Scheme 11. *Synthesis of dialkyl perylene diimide from PTCDA with amines.*

By introducing different organic substituents to the imide position of the perylene core without other substituents, an excitation maximum is located at around 525, 490 and 460 nm and emission from 510 to 650 nm is observed in solution. The absorption maximum can be assigned to the $S_o \rightarrow S_1$ transition described as a HOMO→LUMO excitation caused by the π-conjugated perylene diimide core structure.[109,112] Other energy allowed electronic transitions had been theoretically predicted a HOMO-1, HOMO-2 and HOMO-3 transition to the LUMO by DFT calculations.[112] The imide substituents have negligible influence to the absorption and emission properties because of nodes of the HOMO and LUMO orbitals at the imide nitrogen atoms (**Scheme 12**).[113]

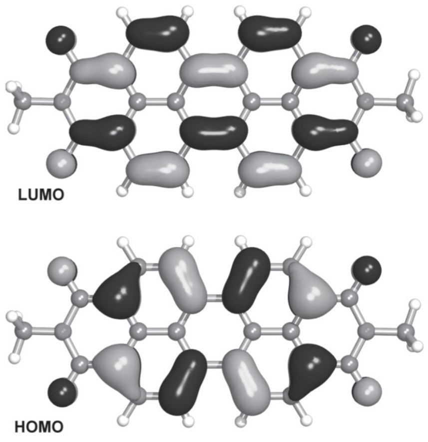

Scheme 12. *Frontier orbitals of N,N'-dimethyl perylene diimide, according to DFT calculations. Reprinted with permission from Huang, C., Barlow, S. & Marder, S. R., J. Org. Chem. 76, 2386–2407 (2011). Copyright ©2011 American Chemical Society.*[109]

The S_1-S_0 remains unaltered by the imide substituent. Introducing electron donating groups like phenoxy substituents at the bay position by of the molecule the π-conjugation is enhanced leading to an energy decrease of the π → π* transition and to a bathochromic shift of the excitation and emission respectively (**Scheme 13**).[114] An increase of phenoxy groups to the core increases the shift. Simultaneously a new local absorption maximum is measurable in hypochromic position to the absolute absorption maximum caused by this substitution.[115] An introduction of polyaromatic groups like pyrenes to the bay position can also generate a new absorption maximum, which is not affecting the perylene core fluorescence due to separated π-conjugated systems.[116]

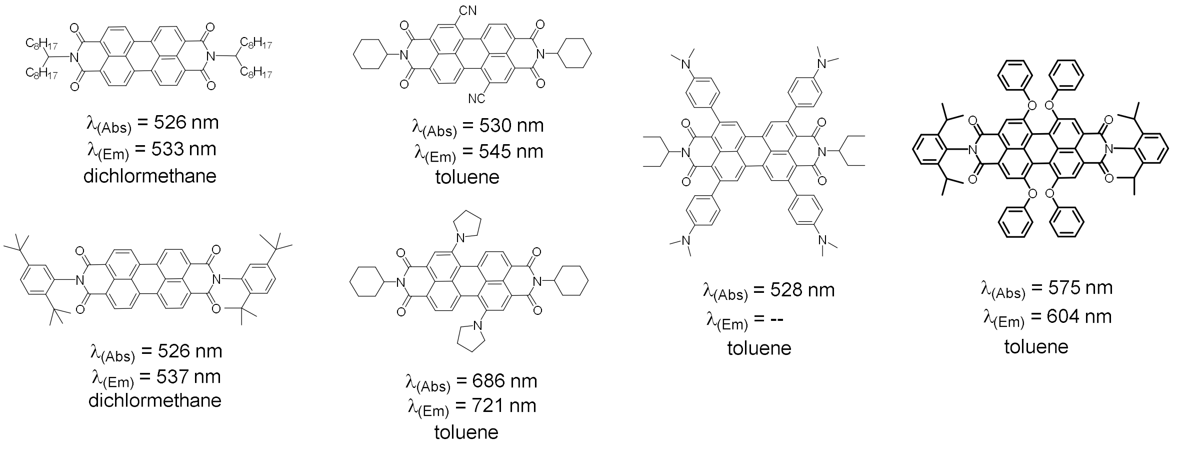

Scheme 13. *Absorption and emission maxima of different substituted perylene diimides.*[109]

The perylene diimide Lumogen®F Red 305 (LG305, BASF SE) is an N,N'-2,6-diisopropylphenyl perylene diimide with phenoxy groups at all four bay positions (**Scheme 14**). It is commercially available and is therefore produced in ton scale for many different purposes.

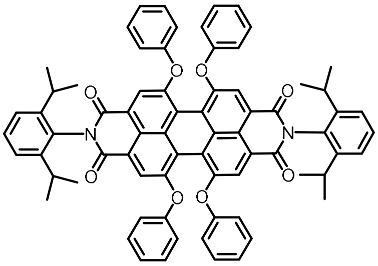

Scheme 14. *Structure of Lumogen®F 305 Red*

Its absorption maxima in toluene are located around 575, 531, 491, and 445 nm with emission from 550 to 725 nm caused by the four phenoxy groups (Figure 10). The bulky diisopropylphenyl groups attached to the imides of the perylene additionally enhance the absolute quantum efficiency and photostability of LG305. The bulky isopropyl rests on the phenyl groups inhibit a non-radiative deactivation pathway by a rotational or torsional vibration around the C-N bond.[117] Furthermore, π-π interactions of two or more molecules and resulting quenching effects are less probable by this sterically hindering additionally increases the quantum yield even at higher concentrations respectively.[118] A further advantage of LG305 is its high solubility in organic solvents and polymeric materials like PMMA and PC.[119,120] Nevertheless, positive solvatochromism of perylene dyes leads to a red shift of the absorption and emission maxima with increasing solvent polarity.[116,121,122] Its properties, especially its locations of the excitation and emission maxima, makes LG305 highly suitable for the integration in organic hybrid LEDs for the stated reasons and a lot of other applications.

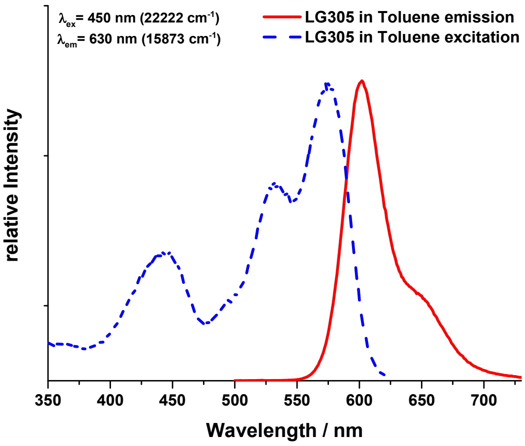

Figure 10. *Emission and excitation spectra of diluted solutions (5 mmol L^{-1}) of Lumogen® F Red 305 (LG305) and FC546 in toluene with an emission wavelength of 630 nm (15 873 cm^{-1}) and with an excitation wavelength of 450 nm (22 222 cm^{-1}).*

Quenching and Spectral Shifts

Due to their distinct conjugated π-system core, some molecules can promote dye-dye aggregation by π- π stacking interactions among these molecules.[123,124] This interaction can lead to specific quenching effects, like decreased quantum yields caused by changes in the absorption and emission mechanism. The aggregation can mainly be characterized and distinguished by a spectral shift of the absorption bands as compared to the monomeric species, measurable with UV/Vis and fluorescence spectroscopy. The molecules can form sandwich-like H-aggregates generating to a bathochromic shift of the absorption maximum, whereas a head to tail-like J-aggregation of the molecules leads to a hypsochromic shift. Due to the interaction of the dyes transition dipoles the excited state S_1 of the aggregate splits into to levels S_1^+ and S_1^- (**Figure 11**). For parallel transition dipoles of a molecular dimer, a transition from the ground state S_0 to the excited state S_1^+ is allowed, whereas the transition from the ground state S_0 to the excited state S_1^- is forbidden, thus generating a blue-shifted absorption band in H-aggregated molecules.[123] In case of J-aggregated molecules the S_0 to S_1^- transition is allowed, leading to a red-shifted absorption band.

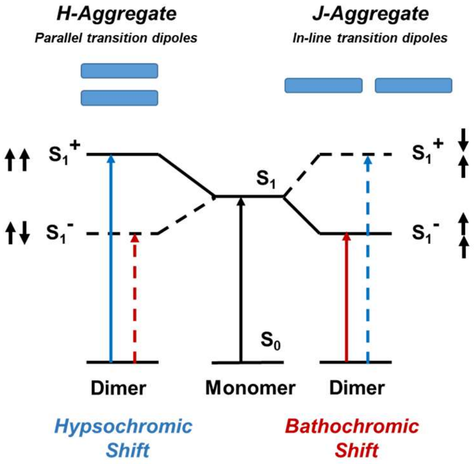

Figure 11. Model of the change of excited states caused by dye-dye interactions and the resulting interactions of the transition dipoles excited states for the H-Aggregate and the J-Aggregate. Adapted with permission from Mishra, A., Behera, R. K., Behera, P. K., Mishra, B. K. & Behera, G. B., Chem. Rev. 100, 1973–2011 (2000). Copyright ©2000 American Chemical Society.[124]

Another kind of dye-dye interaction is the formation of excited dimers (excimers). The excited state of a molecule and the ground state of another molecule can interact due to an attractive potential caused by the interaction between resonance and excited states.[123] The excimer formation leads to unstructured and bathocromically shifted fluorescence emission maxima as compared to the monomeric species. It also causes an increased excited state lifetime and a decreased quantum yield depending on the dyes structure, concentration, and solvent, respectively.[125] The quantum yield for the monomeric emission of perylene based dyes is often high with >90 %.[109] Whereas the quantum yield decreases significantly to <20% for excimer emission phenomena.[125] As described before, the main reason for aggregation and a decreased quantum yield is the dyes structure. Bulky substituents can promote a dye separation and prevent an excimer induced fluorescence quenching. Perylene diimides with different sized substituents introduced to the dyes imide position, for example, were integrated into a PMMA matrix with a concentration of 10 to 120 mM. The unsubstituted perylene diimide show a strong blue shift of the absorption maxima caused by the formation of H-aggregates and a strong redshift of the fluorescence emission caused by excimer formation. The highest quantum yield at the lowest dye concentration was 20 %. The perylene diimide dyes with bulky substituents show high quantum yields of >90 % and almost no shift of the absorption and emission maxima.[118] Another reason for decreased quantum yields or shifted spectra are self-absorption, non-radiative deactivation, and reflection phenomena.[126] When the emission maximum of a molecule is only slightly shifted from the absorption, which is often the case for singlet excitation in organic semiconductors, reabsorption can occur.[107] The reabsorption also leads to a red-shifted emission. The probability of reabsorption increases with the dye concentration and the sample thickness, due to an increased path length of the emitted light through a sample. This is also the reason for an angular dependent redshift of the emission for unsymmetrical samples.[108] The concentration and angular dependent redshifts can be illustrated by a simple concentration series of a dye in a solvent and by fluorescence measurement at different angles (**Figure 12**). A redshift of emission is therefore, not always correlated with an aggregate or excimer formation only. Reabsorption has to be considered and evaluated.

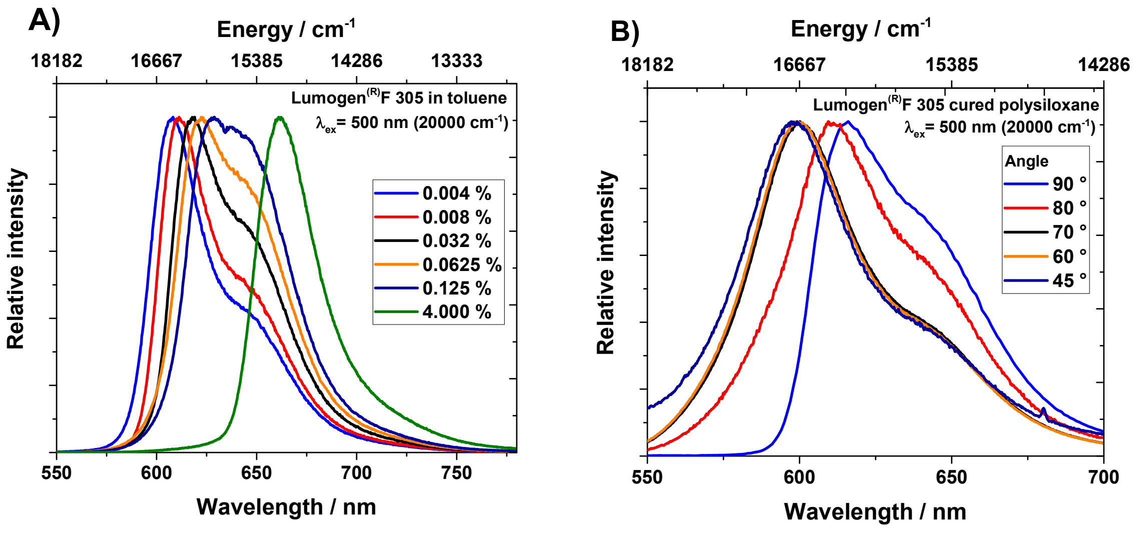

Figure 12. *(A) Concentration dependence of the emission spectra of Lumogen®F 305 Red in toluene measured with an excitation wavelength of 500 nm. The spectrum is red shifted with increased concentration. (B) Angular dependence of the emission spectra of 1000 ppm Lumogen®F 305 Red in a cured polysiloxane resin measured with an excitation wavelength of 500 nm. A redshift occurs when the sample is turned.*

Applications

Due to their high accessibility and solubility in polymeric materials, substituted perylenes have already been used and tested for several optoelectronic applications. As mentioned before, a first low power approach has been prepared with perylene based Lumogen® dyes. Solved in an epoxy resin and excited by an InGaN chip, green (LG083) and red (LG300) colored organic hybrid LEDs has been prepared called luminescence conversion LEDs (LUCO).[12] Low quantum/power conversion efficiencies have been found for both dyes with 0.57/0.46 for the green (LG083) and 0.80/0.57 for the red (LG300) version of the LED.[127] Other similar low power LEDs prepared with other dyes like 1,8-naphthalimide derivative converters showed significant degradation of the dyes in epoxy resins and PMMA.[128] The initial light output of the epoxy-based LED decreased rapidly by 80 % after 3.5 h of operation time at 200 mA.

Figure 13. *Blue LED and three LUCOLEDs emitting green, red, and white light. Reprinted with permission from Schlotter, P., Schmidt, R. & Schneider, J., Appl. Phys. A Mater. Sci. Process. A 64, 417–418 (1997). Copyright ©1997 Springer.*[12]

This degradation was slightly reduced by using PMMA, leading to a decreased light output of 33 % after 19 d under the same conditions. A proposed reason for that is the more properly protection from the environment. Another approach for the integration of a perylene based dye into a LED device was the functionalization by styrene and subsequent synthesis of polystyrene with N-(10-nonadecyl)-perylene-3,4,9,10-tetra-carboxylic diimide pendant groups attached (**Scheme 15**).[26,129]

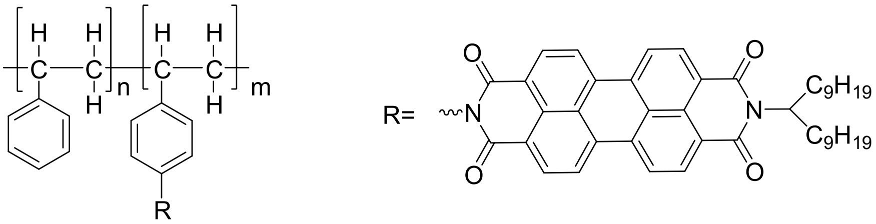

Scheme 15. *Polystyrene with pendant perylene diimide groups attached to the polymer chains.*

The obtained material was transformed by different methods to microparticles and fibers that could be implemented into a polydimethylsiloxane host material. With a quantum efficiency of 0.57 and an intensity loss of 10 % after 220 minutes under working conditions, optimization is still required for suitable reliability. One more setup mentioned before, were yellow, green and red perylene dyes were incorporated in a polycarbonate matrix show a significant photodegradation of the dyes using an on-chip configuration of a hybrid LED after 1000 h. Remote setup of this material combination increases the lifetime but is still not reliable enough for an application with a 15 % loss of fluorescence intensity after 2870 h of illumination.[33]

In other optoelectronic applications using polymer encapsulations like the luminescent solar collectors (LSC) perylenes are the most often used organic dyes for the stated reasons like high solubility, high quantum yield, high photostability and excitation maxima around 575, 531, 491 and 445 nm with emission from 550 to 725 nm.[130] The LSC setup was developed to increase the efficiency of photovoltaic cells by a down-conversion of the incoming sunlight before channeling it to the cell by a high refractive index polymer. Therefore an organic fluorescence dye has to be dissolved completely in a polymeric host material to prevent quenching effects, which is afterward cured and framed by solar cells (**Figure 14**). The incident solar light is absorbed by the fluorescence dye which emits bathochromic shifted light isotopically. Up to 80 % of this emitted light is trapped in the LSC due to total internal reflection (@RI=1.51) resulting in the theoretical photovoltaic conversion efficiency of 24 %.[131] The emitted wavelength photons equal the bandgap and the sensitivity of the attached solar cell to ensure high quantum yields and power conversion efficiencies (**Figure 15**).[115]

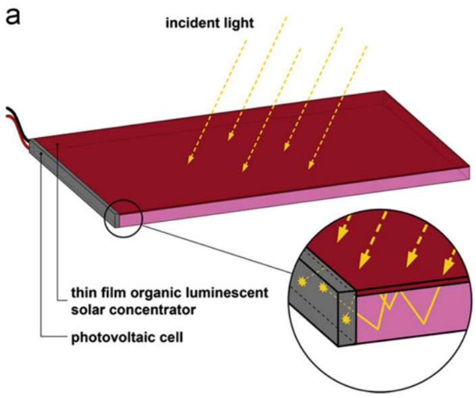

Figure 14. (a) Schematic representation of an LSC device under illumination. Reprinted with permission from Griffini, G., Brambilla, L., Levi, M., Del Zoppo, M. & Turri, S., Sol. Energy Mater. Sol. Cells 111, 41–48 (2013). Copyright ©2013 Elsevier.[115]

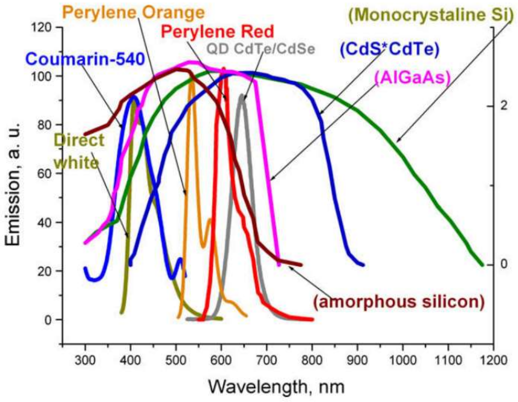

Figure 15. Emission spectra of a number of dyes and sensitivity curves of several solar cells, as specified in the figure. Reprinted with permission from Reisfeld, R., Opt. Mater. (Amst). 32, 850–856 (2010).Copyright ©2010 Elsevier.[131]

For the performance and lifetime of the LSC, the same requirements are needed to be met as for a LED device. In particular, the thermal and photophysical degradation of the polymeric host material and the luminescent organic dyes are also the most common degradation pathways and had to be optimized for enhanced performance of the LSC. The only difference between the two mentioned applications are the irradiance conditions. While the irradiance in LEDs can be larger than 500 mW/mm^2, materials in photovoltaics and LSCs have only to withstand 100 mW/cm^2 under standard testing conditions.[132,133] Furthermore, the efficiency of the LSC is increased with the dye concentration, whereas a stacking or even precipitation of the dye decreases the efficiency significantly.[83] The high solubility of the dye in the host material has, therefore, be ensured for LSC and LED applications. As a result, the development of a new dye-matrix combination for LEDs is suitable for LSC applications as well. Other optoelectronics like organic photovoltaics, where perylenes are used as n-type semiconductors and other physical properties are needed also common but not discussed within this thesis.[134–137]

Degradation

The most important property for an organic fluorescence dye in LED applications is outstanding stability against the exposition of the excitation light under the environmental conditions of an LED. Two different methods have been used yet for the quantification of the dye stability. In both methods, the dye-containing samples are irradiated by a given excitation wavelength. In the first method, the relative fluorescence intensity change is determined directly by fluorescence spectroscopy.[26] The results obtained by this method are directly correlated to the performance of a device under real conditions, but not correlated to the absolute dye concentration.

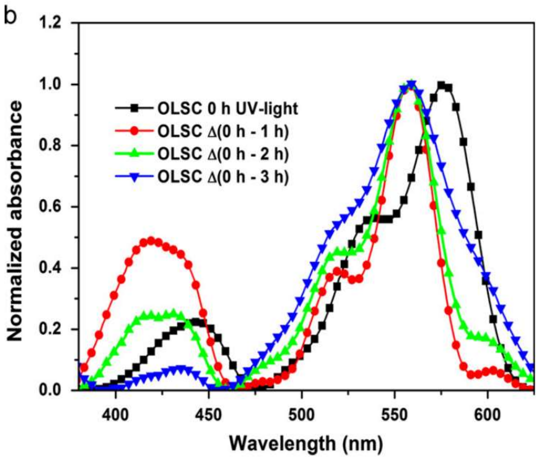

Figure 16. (b) Normalized UV/Vis subtraction spectra of OLSC thin films at increasing UV-exposure time (each subtraction spectrum was obtained by subtracting the spectrum of the degraded sample from the spectrum of the unexposed sample). Reprinted with permission from Griffini, G., Brambilla, L., Levi, M., Del Zoppo, M. & Turri, S., Sol. Energy Mater. Sol. Cells 111, 41–48 (2013). Copyright ©2013 Elsevier.[115]

In the second method, the absorbance of the sample is periodically measured externally by UV/Vis spectroscopy during the exposition to determine the relative change in absorbance.[115] Caused by the direct correlation of absorbance and dye concentration at low concentrations the dye degradation can be quantified directly. Nevertheless, there is no general defined mechanism for the degradation process of the dye molecules during light exposition yet. Even with more detailed methods on the molecular scale-like ESR or NMR spectroscopy, there are just a few proposals trying to understand what happens when organic fluorescence dyes in polymer host materials start to degrade.[138]

The photodegradation of Lumogen®F Red 305 under UV light (500W, Mercury vapor) has been studied in more detail in a PMMA host material, originally prepared for LSC applications, by UV/Vis, FTIR and fluorescence spectroscopy as well as GC-MS.[115] After 1 h of light exposition a strong decrease of 30 % and after 5 h a decrease of 99 % of the initial absorbance was measurable. The normalized subtraction spectra indicate a strong dependence of the different local absorption maxima to the degradation (**Figure 16**). The absorbance at 445 nm caused by the phenoxy groups attached to the perylene core at the four-bay positions starts to decrease earlier and more strongly than the rest of the absorbance maxima that are caused by the perylene core only. Supported by the FTIR and GC-MS data, a two-phase degradation mechanism is proposed. In the first phase, lateral phenyl ring substituents undergo abstraction from the perylene core via homolytic cleavage of the oxygen-phenyl bond generating benzene. In the second phase, an abstraction of the diisopropylphenyl groups by homolytic cleavage of the nitrogen-phenyl bond was detected.

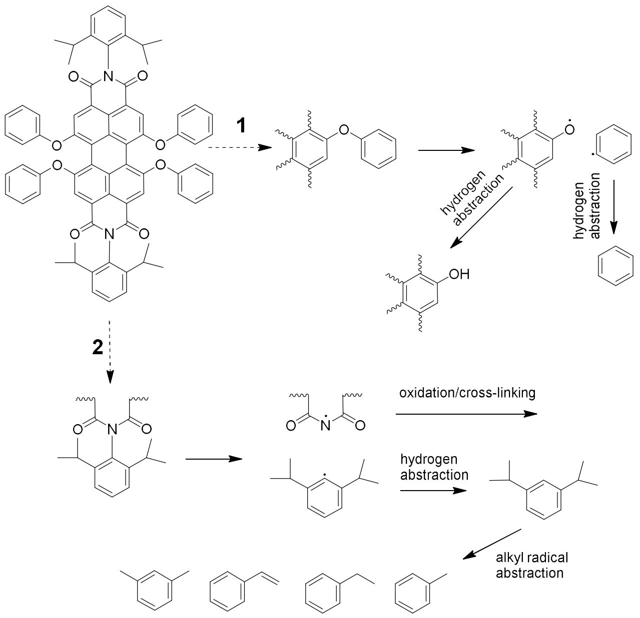

Scheme 16. *The first and second phase of the degradation mechanism of LG305 molecules in PMMA LSC thin films. Adapted with permission from Griffini, G., Brambilla, L., Levi, M., Del Zoppo, M. & Turri, S., Sol. Energy Mater. Sol. Cells 111, 41–48 (2013). Copyright ©2013 Elsevier.*[103]

This intrinsic degradation mechanism indicates that there are no other species involved in the degradation process then the dye itself. Protection of the dye with a suitable encapsulation material would not have any significant influence on the longtime photostability. On the other hand, the conditions used in these experiments are not comparable to that in an LED application, due to the use of high energy UV light.

Another conceivable process able to initiate degradation is the formation of triplet states followed by an interaction with other species. The formation and interaction of triplet states with oxygen and polymer substrates have been studied by ESR and time-resolved oxygen infrared phosphorescence spectroscopy. Triarylmethane dyes, crystal violet, and malachite green were incorporated and cured in a polydimethylsiloxane substrate and excited by an Nd:YAG laser with 532 nm wavelength (3 kHz, 2 ns).[138] Four of five dyes show a massive concentration of triplet states caused by intersystem crossing (ISC) induced by the laser excitation. The authors propose two possible types of electron transfer or photo-oxidation from the triplet state to another species, besides the possibility of phosphorescence. Type I assumes an electron transfer to the polymer host material, whereas in a type II transfer the electron is donated to oxygen. The resulting measurements indicate a direct correlated of the formation of singlet oxygen and the triplet states, leading to the conclusion that a type II energy transfer process is more predominant over type I.

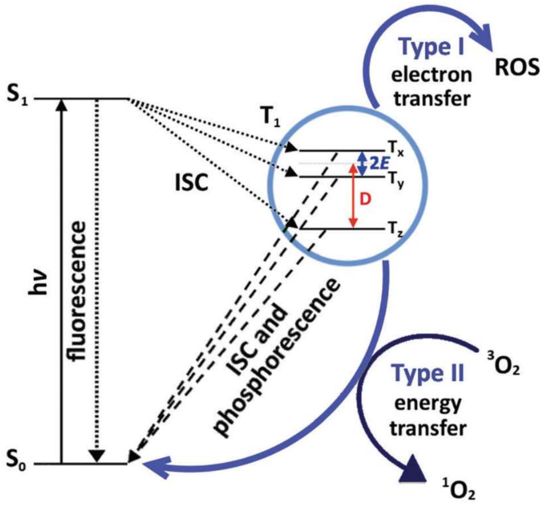

Figure 17. Jablonski diagram and accompanying photochemical processes subsequent to photoexcitation of a photosensitizer. The ground state molecule (S_0) absorbs a photon of energy and is promoted to an excited singlet state (S_1). The excited singlet state molecule can release energy radiatively (fluorescence), via internal conversion or can undergo ISC to the excited triplet state (T_1) which has three sublevels: T_x, T_y, T_z. D and E are the zero-field splitting parameters, which describe the magnetic dipolar interaction between the two unpaired electrons. The triplet state molecule can release energy as radiation (phosphorescence) or transfer its energy to surrounding molecules by either Type I or Type II photo processes and return to the ground state. A Type I photo process involves electron transfer between the triplet state and a substrate, whereas a Type II photo process involves the quenching of the triplet state by molecular oxygen. Reprinted from Noimark, S. et al., Phys. Chem. Chem. Phys. 18, 28101–28109 (2016).Published by the PCCP Owner Societies under CC-BY-3.0.[138]

Nevertheless, Malachite Green was the only dye without generating measurable triplet state or singlet oxygen concentrations, which was explained by low ISC efficiencies or a more isotropic ISC process.[138]

A similar quenching effect of the triplet states by oxygen has been reported for perylene based dyes in different media. N,N'-bis(dicarboximide) perylene diimides, for example, has been investigated in solution, making it also a suitable photosensitizer for the generation of singlet oxygen.[139] But compared to other dyes, a very low ISC efficiency is proposed. As a result, a more appropriate polymer with oxygen barrier properties should be needed to protect the dye from a photodegradation process initiated by a triplet state-oxygen interaction.

Lumogen®F Red 305 has also been studied in PMMA and polyester host materials under vacuum and defined oxygen pressure conditions by ESR, fluorescence and time-resolved oxygen infrared phosphorescence spectroscopy using an Nd:YAG laser with 532 nm wavelength.[140] Due to the measurement under anaerobic conditions, other conclusions were made regarding oxygen interferences then reported before. The samples measured under vacuum showed a highly increased photo degradation of LG305 compared to the samples exposed to air. Additionally, the samples show a recovery of the fluorescence after the irradiation was stopped and oxygen was air was added to the samples. This phenomenon is proposed to be caused by a reversible type II photo-reduction of the perylene dye.

Nevertheless, a decreased photodegradation was also determined for increased oxygen partial pressure. The presence of the high electron affinity oxygen suppresses the photoreduction by reducing the excited state by a type II photo-oxidation as reported before. Two different mechanisms are proposed from the authors for the degradation of perylenes in polymers. The oxygen-free device fabrication of organic dye-containing encapsulations for optoelectronics is suggested to be not suitable since the exclusion of oxygen would facilitate the photo-reduction mechanism.[140]

From another application-related point of view, most of the common OLEDs show enhanced photostabilities by using polymer laminations, protecting the containing organic emitters from oxygen and other pollutions.[141–143]

As a result, for the development of a new siloxane based host material for organic hybrid LEDs, the influence of oxygen and the oxygen barrier properties of the encapsulation to the dyes photostability had to be determined and evaluated for further optimization steps.

Polymers

Introducing reactive substituents to the imide or bay positions of a perylene dye can possibly lead to a product, which can be used as a monomer in polymerization reactions. Polymerized perylenes or copolymers with an incorporated defined dye concentration can be used several applications, and their properties can differ significantly from the molecular species. The perylene molecules can, therefore, be integrated ladder-like, pendant or in the polymer backbone. By reacting a 1,6,7,12-tetra-*tert*-butylphenoxyperylene diimide with an aminopropyl alkoxysilane, a derivative was synthesized can be implemented into a subsequent acid-catalyzed polycondensation reaction (**Scheme 17**).[144] The ladder-like perylene polysiloxane shows a good solubility, a wide absorption region, higher thermal stabilities and proper LUMO energy levels in contrast to its precursor monomers, making it suitable as n-type semiconducting material for photovoltaics for example. Due to its self-assembly properties by hydrogen bonding and π-π-stacking a periodic crystal-like structure of the monomers has been determined by XRD. Simultaneously the fluorescence is quenched by this phenomenon, why this material is not suitable for other light-emitting applications.

The synthesis of a copolymer with pendant perylene units attached to the polymer backbone was discussed before for polystyrene fibers, and particles for LED applications.[26] The synthesis of the monomer was carried out by a condensation reaction of an N-(10-nonadecyl)-3,4,9,10-tetracarboxylic acid dianhydride with 4-aminostyrene. A subsequent nitrogen mediated radical polymerization with styrene resulted in a polystyrene perylene co-polymer.[129]

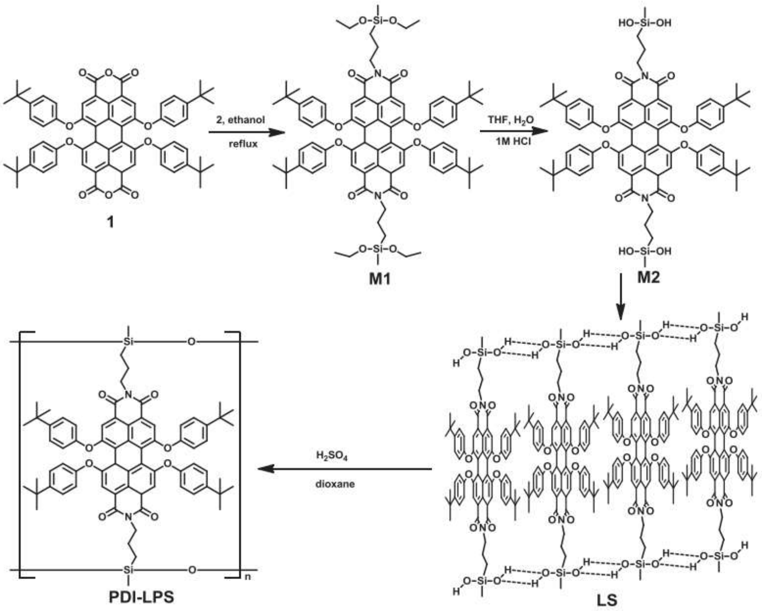

Scheme 17. Synthesis route of a perylene diimide ladder polysiloxane by polycondensation. (1) 1,6,7,12-Tetra-tert-butylphenoxyperylene diimide, (M2) reaction product of the condensation with an aminopropyl alkoxysilane, (M2) hydrolyzed species of M1, (LS) proposed ladder like self-assembly by hydrogen bonding and π-π stacking, (PDI-LPS) perylene polysiloxane product. Reprinted with permission from Fu, W. et al., Macromolecules 44, 203–207 (2011). Copyright ©2011 American Chemical Society.[144]

The main feature, which is needed to be realized in this case is the unsymmetrical substitution of the perylene dye by a reactive group, making it suitable for polymerization. This unsymmetrical substitution can be carried out by partial condensation of PTCDA with an amine or by decarboxylation.[145–148] The implementation of this polystyrene perylene co-polymer into an LED setup leads to a rather good CRI of 83, poor efficiency of 5 % or 28 lm/W and a cold bluish light with a color correlation temperature of 6600K (**Figure 18**, left). A commercially available inorganic warm white LED from OSRAM™ has 87 lm/W, a CRI of 80, and a color correlation temperature of 2700 – 4500 K.[22] Additionally, the light intensity of this organic hybrid LED is decreasing significantly during the operation by 50 % of the initial value in 100 minutes (**Figure 18**, right).[129] The dye itself, the pendant integration of the dye and the choice of the polymer host material did not improve the stability, and the performance of this organic hybrid LED device, respectively.

Examples for a polymer where the perylene dyes were already successfully incorporated into the polymers' backbone are polystyrenes and polydimethylsiloxanes, synthesized for corrosion protection or photo-functional devices.[149–151] Both polymer types have been synthesized by condensation of aminopropyl terminated polystyrene or polydimethylsiloxane with PTCDA respectively. The polydimethylsiloxane was isolated as a gel and was not curable to obtain a solid sample. The fluorescence intensity is quenched due to aggregation. The perylene containing polystyrene also show aggregation and a strong quenching of the fluorescence. The characterization of the materials resulted in a higher solubility of the dyes with lower probability of precipitation, but aggregation, quenching, and the liquid state of the polydimethylsiloxane are not appropriate for an application or device.

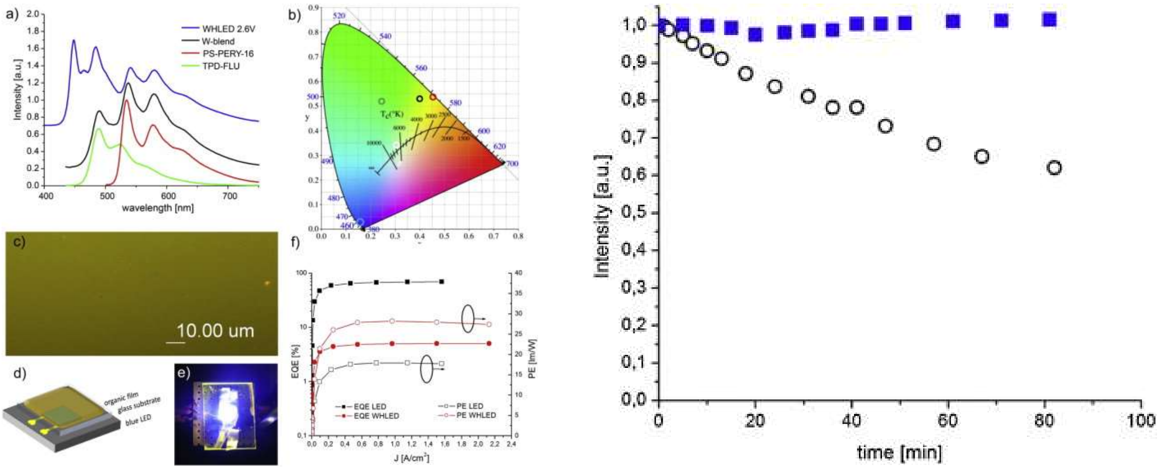

__Figure 18.__ Left: (a) Spectrum of the LEDs. (b) CIE coordinates of the LEDs. (c) Fluorescence microscopy image of W-blend film. (d) Schematic representation of the device. (e) Picture of the turned on device. (f) External quantum efficiency and power efficiency of a blue LED and white hybrid device. Right: Integrated emission intensity of blue LED (blue square) and W-blend (circles) under constant 2.6 V bias. Reprinted with permission from Kozma, E., Mróz, W. & Galeotti, F., Dye. Pigment. 114, 138–143 (2015). Copyright ©2015 Elsevier.[129]

2.6. Siloxane-based Particles

In the last decades, the synthesis of polymeric micro- and nanoparticles have been investigated and optimized for a variety of applications.[152] The synthesis of carbon-based materials like epoxy, polyurethane, or polystyrene have been optimized and characterized already extensively.[152–155] The most commonly used method for preparing those carbon-based microspheres is the emulsion polymerization with or without the use of emulsifiers. The resulting particles can be used for example for sensing, medical or imaging applications.[156–158] The investigation of silicon-based particles of polysilsesuqioxanes or polysiloxanes is also in great demand due to the interesting combination of tunable properties and accessibility. Just by hydrolyzing organotrialkoxysilanes with an acid, forming the respective silanols followed by a base-catalyzed condensation uniform particles with tunable properties can be prepared.[159–162] The particle shape and properties can be adjusted by the organic groups of the monomers used, the reaction conditions or even by assisted methods like an ultra-sonic treatment or the use of continuous methods like the micro-jet approach.[61,163] The pure siloxane-based particles can also be used for the preparation of polymer-derived ceramics or carbide-derived carbon, for toughening of other polymers by integration into the polymer, or for drug delivery, for example.[164–168]

One example for the preparation of several different particles like methyl, ethyl, vinyl, and phenylsilsesquioxane, and silica by the same sol-gel based method has been reported using a micro-jet reactor (**Figure 19**).[61] The different trialkoxysilanes monomers were hydrolyzed and subsequently mixed with ammonia solution in a gas supported reactor leading to a very fast condensation reaction, producing up to 23 g of particles per minute. All particles synthesized show a narrow size distribution and particle sizes <2µm.

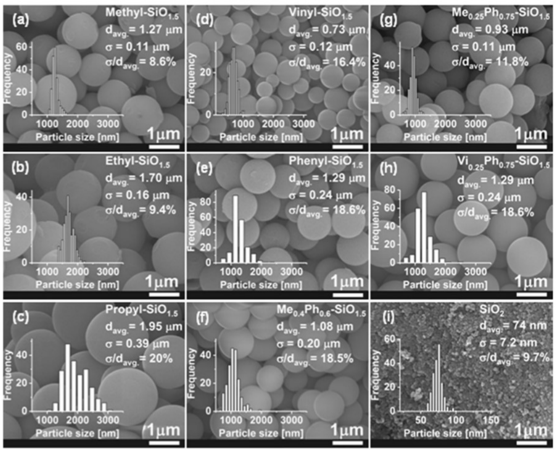

*__Figure 19.__ SEM images of (a) Methyl-, (b) Ethyl-, (c) Propyl-, (d) Vinyl-, (e) Phenyl-, (f) $Me_{0.4}Ph_{0.6}$-, (g) $Me_{0.25}Ph_{0.75}$-, (h) $Vi_{0.25}Ph_{0.75}$- $SiO_{1.5}$, and (i) SiO_2 with size distribution curves, average particle diameters (davg.), standard deviations (σ), and polydispersities (100*σ/davg.) of the prepared particles (250 ml min^{-1}, 20 °C). Reprinted with permission from Odenwald, C. & Kickelbick, G., J. Sol-Gel Sci. Technol. 89, 343–353 (2019). Copyright ©2019 Springer.*[61]

The structure of the particles has also been studied by solid-state ^{29}SI NMR spectroscopy showing the presence of partially condensed T^2 and fully-condensed T^3 units with a maximum degree of cross-linking of 91 % for the polyvinylsilsesquioxane particles. The lowest cross-linking degree was found for the polyphenylsilsesquioxane particles with 60 %, proposed to be caused by the bulky substituents leading to a more polymer-like behavior. As a consequence, the obtained particles dissolve in various organic solvents, e.g., toluene, tetrahydrofuran, and dichloromethane. In addition, the particles typically melt, to form a dense film during a thermal treatment. This behavior has also been reported for partially cross-linked polysilsesquioxane hybrid glasses as described before.[100–105]

For a functionalization of those particles, trialkoxysilanes with functional groups are added to the synthesis route. Thiol-functionalyzed polysilsesquioxane microspheres, for example, were prepared by a surfactant-free emulsion-based method by hydrolyzing 3-mercaptopropyltrimethoxysilane followed by a base-catalyzed condensation.[159] The obtained particles show a narrow size distribution with a minimum average particle size of 3.04±0.89 µm. With the variation of the time of hydrolysis, the particle size could be varied from 2.5 – 5 µm. The structure of the particles has been studied by solid-state ^{29}Si NMR spectroscopy showing the presence of partially condensed T^2 and fully-condensed T^3 units with a degree of cross-linking of 83 %. There is no reason given for this incomplete cross-linking.

The siloxane based particles can also be synthesized by non-hydrolytic sol-gel methods using different techniques. Phenyl-, ethyl- and methylsilsquioxane microspheres, for example, can also been synthesized by a non-hydrolytic sol-gel reaction using the respective trichlorsilane monomers and dimethylsulfoxide.[169] The particles are less regularly shaped, exhibit a great degree of aggregation with a particle size from 0.1 – 2 µm. Different to most of the sol-gel reactions in aqueous solutions, a high concentration of T^1 end groups was detected by NMR spectroscopy, indicating a very low degree of cross-linking. The highest degree of cross-linking was calculated for the phenyl modified particles. In another non-hydrolytic approach, extraordinary bowl-shaped polysilsesquioxane particles of methyltriethoxysilane and phenyltrimethoxysilane were made by an emulsion of the monomers in a toluene water mixture.[170] The morphology of particles can be fine-tuned by judiciously adjusting the amount of two organoalkoxysilane precursors.

Organic dyes can also be incorporated or labeled to the microparticles by adding them to directly to the synthesis or by a post-synthetic reaction with the microparticles.[159–162]

Whereas ionic dyes can be easily integrated into polysilsesquioxane particles, the integration of hydrophobic dyes like perylene diimides is difficult to realize. Due to their insolubility in aqueous solutions, the integration of hydrophobic dyes is mostly performed by a previous functionalization, making them accessible to be integrated into a condensation reaction.[160,171–

[173] For a complete integration of Rhodamin(B) into a sol-gel like synthesis of poly(3-mercaptopropylsilsesquioxane) particles for example, the dye can easily been added to a trialkoxysilane solution during the hydrolization step (**Figure 20**).[160] The dye is integrated to the partially cross-linked particles structure, showing a slightly higher photostability compared the pure dye solution.

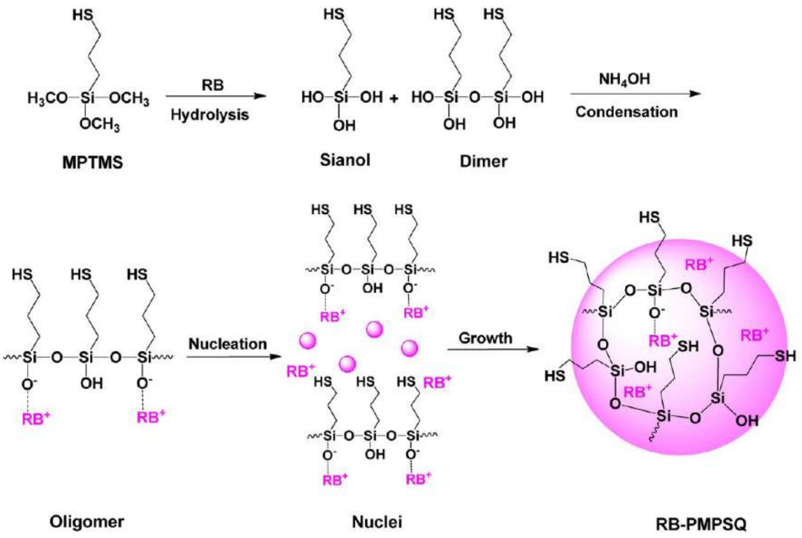

Figure 20. The mechanism for the formation process of Rhodamine B-doped poly(3-mercaptopropylsilsesquioxane) fluorescent microspheres. Reprinted with permission from Lu, X., Hou, Y., Zha, J. & Xin, Z., Ind. Eng. Chem. Res. 52, 5880–5886 (2013). Copyright ©2013 American Chemical Society.[160]

In another approach rhodamine(B)isothiocyanate has been labeled to the thiol groups after the synthesis of poly(3-mercaptopropylsilsesquioxane) microparticles. Confocal microscopy images show a complete distribution of the dye inside the particle structure and not just an attachment to the surface of the particles, which indicates a high mobility of the dye molecules through the partially cross-linked structure (**Figure 21**). No further characterizations regarding the dyes properties have been made.

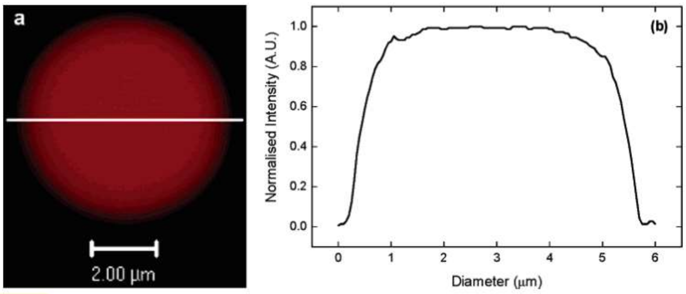

Figure 21. (a) Confocal image of a rhodamine B isothiocyanate labeled organosilica microsphere and (b) normalized fluorescence intensity profile through the center of the microsphere. Reprinted with permission from Trau, M. et al., Langmuir 21, 9733–9740 (2005). Copyright ©2005 American Chemical Society.[159]

For the integration of hydrophobic perylenes into polymeric particles, they are mostly functionalized by using polyhedral oligomeric silsesuqioxanes (POSS). [171–174] The POSS functionalized perylenes can been prepared by reacting amino functionalized POSS with PTCDA for example (**Figure 22**).[174]

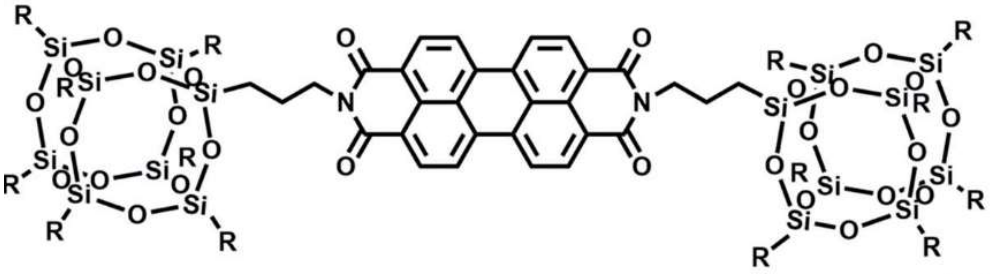

Figure 22. POSS functionalized perylene diimide. Reprinted with permission from Chen, J. et al., RSC Adv. 8, 35534–35538 (2018), licensed under CC-BY-NC 3.0.[173]

By the preparation of polystyrene and poly(3-hydroxylbutyrate-co-3-hydroxyvalerate) micro particles by an electrostatic spray method, POSS-perylene diimides have been used to generate highly fluorescent particles.[173] The emission spectra of the 8 – 25 µm sized particles show bathochromic shifts compared to the pure POSS-perylene diimide in solution, caused by dye aggregation. At the same time a massive decrease of quantum yield was detected for dye to polymer rations >1/1000, also caused by the aggregation, which is more probable at high dye concentrations. In all of the previously described methods the alkoxysilane precursor used were in the monomeric state. The particles are formed during the condensation reaction of the trialkoxysilane monomers under basic conditions. Additionally the structural investigations by spectroscopic methods, most commonly resulting in partially cross-linked structures indicated by the presents of T^2 units in the siloxane network. By using already partially cross-linked polysiloxanes, reacted by hydrosilylation it is also possible to prepare microspheres.

A polyhydromethylsiloxane was reacted with a 1,3-divinyltetramethyldisiloxane in THF, using a Karstedt catalyst. When the mixture started to get viscous it was transferred into a solution of n-eicosane in *iso*-propanol, and water containing polyvinyl alcohol was added forming an emulsion. After the isolation the microspheres with a diameter of 90 to 220 µm. Due to the preparation a lot of the former Si-H groups from the olyhydromethylsiloxan units were hydrolyzed by water, forming Si-OH groups, which were functionalized by (3-aminopropyl)triethoxysilane, (3-glycidyloxypropyl)trimethoxysilane, and dimethylvinylchlorosilane.

3. Research Goals

This work aims to improve the solubility, quantum yield, as well as the thermal and photophysical stability of perylene based fluorescence dyes by investigating and find new siloxane-based host-materials, protecting the incorporated dye from precipitation, degradation, and quenching effects. This dye-containing siloxane-based materials shall be compared to the known polymer-dye combinations and meeting all requirements for implementation in an organic hybrid LED application. That means, the preparation of liquid, workable and thermally curable or/and solid and particle shaped cross-linked siloxanes with high thermal and photophysical stabilities, high transparencies and significant protective properties for the integrated dyes.

In detail, the following studies were carried out:

- **Perylene dyes in Polysiloxane Matrices**

  A perylene based fluorescence dye and a vinyl functionalized derivative of this dye, both with a local absorption maximum at the excitation wavelength of a classical LED (450 nm), were incorporated in one commercially available and thermally curable polydimethylsiloxane and one polyphenylmethylsiloxane. Due to the vinyl functionalization of the perylene derivative, it can be involved in the curing procedure by hydrosilylation and therefore covalently bonded to the structure of the polymers, whereas the other dye is only physically integrated. By preparing concentration series of each dye in each polysiloxane the influence of the different organic groups (phenyl, methyl) and the influence of the covalent and non-covalent integration to the optical, thermal and chemical properties were studied by performing fluorescence, FTIR and UV/Vis spectroscopy, absolute quantum yield and microscopic measurements as well as leaching, swelling and longtime thermal and photostability experiments (results published).

- **Liquid Perylene polysiloxane Copolymers**

  The perylene based and vinyl functionalized fluorescence dye was used to be covalently integrated into the backbone of linear polyphenylmethylsiloxane chains by hydrosilylation forming a liquid perylene polyphenylmethylsiloxane. In a second approach, the dye was used as a network agent between polyphenylmethylsiloxane chains forming a liquid but partially cross-linked perylene polyphenylmethylsiloxane. Afterward, these liquid dye-containing precursors were added to the previously used and cured subsequently to solid and flexible materials. The influence of each polymer, the dye concentration, the chain length, and the integrated precursor polymers concentration to the optical, thermal, mechanical and chemical properties were studied by performing NMR, fluorescence, FTIR and UV/Vis spectroscopy, absolute quantum yield, SEC, hardness, DSC and TG measurements as well as longtime photostability experiments (results published).

- **Platinum free but curable Siloxanes**
  By performing an acid-catalyzed condensation reaction of different trialkoxysilanes, dialkoxysilanes, and a methoxy terminated oligosiloxane platinum-free, but thermally curable polysiloxanes were synthesized. The influence of the polymers compositions on the optical, thermal, mechanical and chemical properties was studied by performing NMR, FTIR and UV/Vis spectroscopy, rheology, hardness, DSC and TG measurements as well as longtime thermal and photostability experiments (results published).

- **Fluorescent Polyphenylsilsesuqioxane Microspheres**
  A perylene based fluorescence dye was integrated into the synthesis of a polysilsesquioxane based hybrid glass material synthesized by an acid-catalyzed condensation reaction. Used this fluorescent material as a precursor, fully-crosslinked polyphenylsilsesquioxane microspheres were synthesized by a new surfactant assistant hot emulsion procedure, which allows the integration of hydrophobic organic molecules like the perylene dyes to polysilsesquioxane particles. This procedure was optimized regarding to the particle size, and the influence of a subsequent thermal treatment to the microspheres integrity, morphology and structure, their solubility and leaching behavior, as well as their surface coating, were studied by performing NMR, CP-MAS-NMR, fluorescence, FTIR and UV/Vis spectroscopy, absolute quantum yield, TG-FTIR measurements as well as longtime photostability experiments (*results are part of the thesis but **unpublished yet***).

4. Results and Discussion

In this chapter, three already published publications on the topic of the thesis are presented. An addition chapter named *Fluorescent polyphenylsilsesuqioxane Microspheres* of unpublished results is also included. These results have been formatted in a paper manuscript style with a preceding short introduction to previous results.

4.1. Effect of Polysiloxane Encapsulation Material Compositions on Emission Behavior and Stabilities of Perylene Dyes

Published as an article:

Nils Steinbrück, Martin Könemann, and Guido Kickelbick, *RSC Adv.*, **2018**, *8*, 18128-18138

https://doi.org/10.1039/c8ra01700j

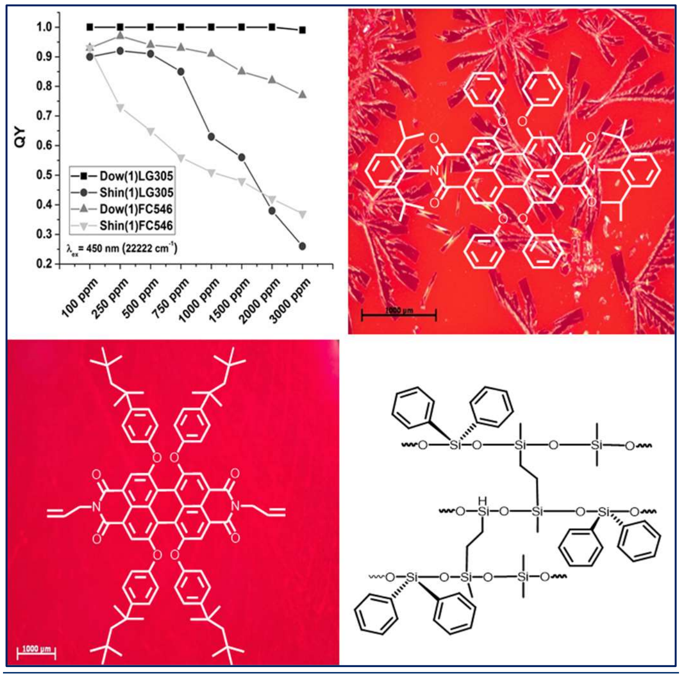

Contributions of the Authors to the Manuscript:

Nils Steinbrück wrote the complete draft of this manuscript that was acknowledged by all named authors. Nils Steinbrück performed the synthesis of the dye integrated polymer resins as well as the FTIR, NMR, fluorescence, quantum yield, UV/Vis, hardness, and microscopic measurements, the swelling behavior, heat and photostability experiments and the calculation of the self-absorption coefficients. He also performed the key part of the data and results interpretation.

Dr. Martin Könemann synthesized the organic fluorescence dyes used for the sample preparation.

Prof. Dr. Guido Kickelbick gave the input to this project, supervised and discussed it, and optimized the manuscript to its final form.

In the **first part “*Effect of polysiloxane encapsulation material compositions on emission behavior and stabilities of perylene dyes*”** the chemical and physical properties of a non-covalent and a covalent incorporable perylene based dye integrated into curable polydimethylsiloxane and polyphenylmethylsiloxane resins were studied. Low solubility and decreased efficiency of non-covalent bonded LG305 integrated into polydimethylsiloxanes were already reported for LSC applications.[83] Using the pure methyl containing polymer resin resulted in dye precipitation at concentrations >500 ppm causing a significant decrease of the quantum yield. The covalent integration of an allyl functionalized perylene dye (FC546) prevents this precipitation but did not prevent a decrease of quantum yield. Due to a less sterically hindered structure, compared to LG305, the affinity of the dye for dye-dye interactions is increased, causing quenching effects. Furthermore, the pure methyl containing polymer resin enhances the degradation of the dyes incorporated significantly. This degradation is even more enhanced by an additional heat treatment at 200 °C, simulating the working conditions in LEDs.

A quiet positive influence of the covalent integration of the dye in the phenyl group containing matrix to the dyes solubility and lifetime has been ascertained. LG305 and FC546 were soluble up to 3000 ppm without precipitation and without a significant decrease of the quantum yield. We consider a direct interaction of the phenyl groups with the integrated dyes leading to a separation of the dye molecules and a decreased probability of dye-dye interactions. The self-absorption coefficients of all samples were calculated from the absolute quantum yield emission spectra showing that there is no correlation between self-absorption phenomena and the quantum yield. To simulate real LED irradiation conditions photostability experiments under an inert nitrogen atmosphere and under air at 450 nm light exposure were performed, showing that the degradation of the dye is significantly enhanced in polydimethylsiloxanes and in the presence of oxygen. An increased radical formation in polydimethylsiloxanes as reported for LG305 in PMMA or an increased probability of photo-oxidation is conceivable.[115,138] As a result of this first study, phenyl substituents in the siloxane-based materials are required to increase the perylene dyes solubility, quantum yield and thermal as well as photophysical stability. Furthermore, a separation of the dye molecules by a covalent-integration increases the amount of dye incorporable to the siloxane.

RSC Advances

PAPER

View Article Online
View Journal | View Issue

Cite this: *RSC Adv.*, 2018, **8**, 18128

Effect of polysiloxane encapsulation material compositions on emission behaviour and stabilities of perylene dyes†

Nils Steinbrück,[a] Martin Könemann[b] and Guido Kickelbick *[a]

The replacement of inorganic conversion dyes with their organic counterparts in LED application bears a large potential for the reduction of rare earth elements in these devices. A major challenge of this substitution is the emission and stability of organic dyes, which is more sensitive to the composition of the polymer matrix they are embedded in than inorganic systems. In this study we systematically investigated the influence of the composition and structure of a low refractive index (LRI) polydimethylsiloxane (PDMS) and a high refractive index (HRI) polymethylphenysiloxane (PMPS) based encapsulation material on the optical properties of two different embedded perylene diimide dyes. Both dyes show low solubility in the PDMS matrix, which also fosters the heat- or light-induced degradation of the incorporated dyes. Contrary phenyl containing polysiloxane encapsulation materials enhance dye solubility, improve quantum yields, and promote heat and radiation resistance. Bulky *N*-aryl substituents at the dye structure decrease the probability of dye–dye interaction and increase the absolute quantum yields additionally. Increased photostability and no leaching was observed when the dye was covalently attached to the polymer matrix. Additionally covalent bonding to and improved solubility of the organic dyes in the polysiloxanes allow for a solvent free processing of such dye-matrix combinations. In conclusion a good matching between the matrix and the dye is crucial for a substitution of inorganic conversion dyes by organic ones in LED devices.

Received 26th February 2018
Accepted 5th May 2018

DOI: 10.1039/c8ra01700j

rsc.li/rsc-advances

Introduction

Most of the commonly used phosphors in LED applications consist of inorganic oxides doped with rare earth ions. Typical examples are $Y_3Al_5O_{12}$:Ce^{3+}, $Lu_3Al_5O_{12}$:Ce^{3+}, $CaAlSiN_3$:Eu^{2+}, $(Ba,SrCa)_2Si_5N_8$:Eu^{2+} and β-sialon:Eu^{2+}.[1–9] Due to the geopolitical dependence of the supply of rare earth compounds and the high prices of those materials, alternative organic compounds are an object of recent research projects.[10–13] The limited chemical and physical stability in LED applications is a major challenge of organic phosphors. High temperatures, oxygen, moisture and the continuous exposure to short wavelength visible light radiation promotes chemical and structural changes in organic dyes.[10–13] Because of the low heat and photostability of most of the common dyes, the integration in high power LEDs requires specific precautions.[10–14] Remote applications, in which the dye is embedded in a polymer matrix that is located in distance to the excitation light source and thus decomposition processes are minimized, are already commercially available.[15–18] But a direct integration of the dye into the encapsulation material is preferred due to light performance and efficiency. The primary used epoxy based encapsulation materials show a heat- or light-initiated change in optical properties, which prevented their use in high power LEDs.[19,20] Polysiloxane based encapsulation materials reveal a much better heat stability, high transparency, and tunable refractive indices by side group substitution.[20,21] The chemical inertness of this polymer class in combination with the possibility for a covalent incorporation of an organic fluorescence dye makes them to an excellent material for an optimization focusing on dye stability. Polysiloxane matrices for LED applications can be categorized in two main groups: low (LRI) and high refractive index polymers (HRI).[22] The main difference in their chemical composition is the quantity of phenylmethyl- or diphenylsiloxane units, which increase the refractive index due to the much higher electron density.[23,24] The influence of the polysiloxane structure on the fluorescence properties of a matrix incorporated dye system is not studied yet. One of the most commonly used fluorescence dyes is the commercial available, perylene-based Lumogen® F Red 305 dye by BASF SE.[25–29] This dye can only be non-covalently embedded in the polysiloxane matrix. In

---

[a] *Saarland University, Inorganic Solid State Chemistry, Campus Building C4 1, 66123 Saarbrücken, Germany. E-mail: guido.kickelbick@uni-saarland.de*

[b] *BASF SE, 67056 Ludwigshafen, Germany*

† Electronic supplementary information (ESI) available: Including measured and corrected quantum yield, self-absorption coefficient calculations and fit functions, infra-red spectroscopy data, UV/VIS spectra of the bleaching experiments and the ^{1}H NMR spectra of the Lumogen®F 305 Red and FC546 dyes. See DOI: 10.1039/c8ra01700j

our study we present the synthesis of a new dye, which allows a covalent attachment to the polymer matrix. We investigated the influence of the matrix structure on quantum yields, heat- and photostability, as well as the crosslinking behaviour of polysiloxane matrices. The obtained results should lead to an optimized dye incorporated emitting encapsulation system for LED application.

Experimental

Materials

Two commercially available polysiloxane matrices were used in our study: ShinEtsu KJR9022E [Shin(1)], which is a low refractive index (LRI) polydimethylsiloxane (PDMS), and Dow Corning OE6630 [Dow(1)], which is a high refractive index (HRI) polymethylphenylsiloxane (PMPS) (Scheme 1). They were used as received. Both are two component polymers containing Si–H and Si–vinyl groups, respectively. The curing process is based on a platinum catalysed hydrosilylation reaction. After crosslinking applying standard curing conditions the polymers revealed high transparency and high temperature stability up to temperatures above 200 °C. The main differences in the structure of the two systems are the phenyl groups, which are responsible for the increased refractive index of the Dow(1) polymer. In addition to the phenylmethylsiloxane units, diphenylsiloxane groups are a structural motive in the Dow(1) polymer. All components can additionally contain unknown additives like catalyst inhibitors, coupling or crosslinking agents.

BASF SE provided the two organic dyes that were used in our studies Lumogen® F Red 305 (LG305) and FC546 (Scheme 2).[30]

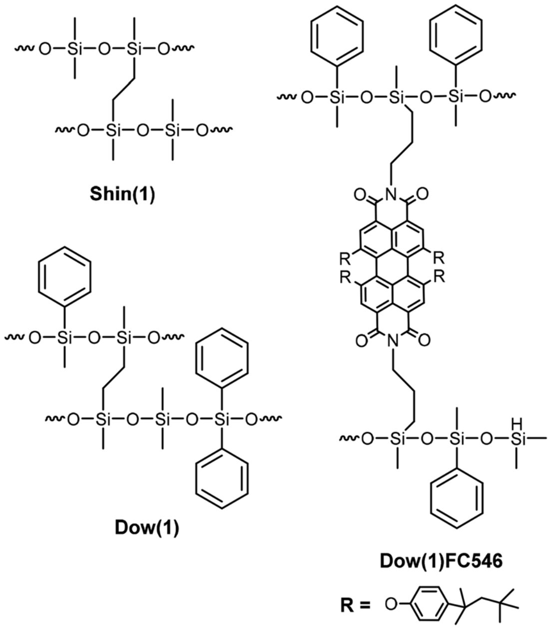

Scheme 1 Scheme of possible structures of the cured Dow(1) and Shin(1) matrices and the covalent bonded FC546 dye in the Dow(1) matrix.

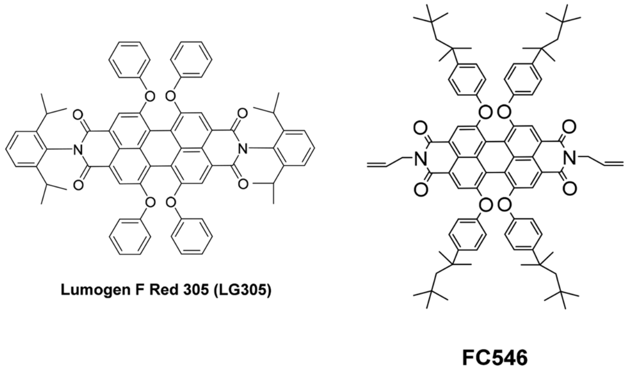

Scheme 2 Structure of Lumogen® F Red 305 (LG305) and FC546.

The synthesis of FC546 is reported in the ESI,† Lumogen® F Red 305 (LG305) is a commercially available dye. Both dye structures are based on a perylene-3,4,9,10-tetracarboxylic acid diimide framework. LG305 contains four phenoxy units in bay position and N,N′-2,6-diisopropylphenyl units that lead to an increased solubility, a very high quantum yield of 1, and emission maxima around 600 nm. The best known common solvent for this dye is toluene.[31] Covalent integration of LG305 in polysiloxane matrices can be excluded due to the lack of reactive groups. The novel dye FC546 contains N,N′-diallyl units which allow a covalent integration into the polysiloxane network *via* hydrosilylation. Due to the missing N,N′-2,6-diisopropylphenyl units, the solubility in toluene is decreased compared to LG305. Four 2,4,4-trimethylpentan-2-yl phenoxy units in bay position were introduced to offset this decrease. It is known that addition of bulky substituents to the imide position can change the intermolecular interactions by maintaining the perylene core's photo physical properties and improving the absolute quantum yield massively.[32] Additionally a non-radiative deactivation caused by a rotation vibration of the N–R-bond is prevented,[14] which also enhances the quantum yield. The missing bulky substituents on the FC546 molecule could lead to a decrease of quantum yield due to the mentioned reasons. At the same time, the covalent bonding of the dye to the polysiloxane structure could reduce the π-stacking probability by molecular separation.

Instrumentation

Fourier transformed infrared spectra (FTIR) were recorded in total reflectance mode on a Vertex 70 spectrometer (Bruker, USA) from 4500–400 cm^{-1} with a 4 nm increment and by averaging 10 scans. The absolute photoluminescence quantum yields and the emission spectra were measured in a Quantaurus C11347-11 integration sphere setup (Hamamatsu Photonics, Japan) with a xenon high-pressure lamp and a multichannel analyzer at 450 nm excitation wavelength. UV-VIS transmission and reflectance measurements were performed on a Lambda 750 instrument (Perkin Elmer Inc., USA) equipped with a 100 mm integration sphere from 700–320 nm with a 2 nm increment and 0.2 s integration time in transmission or reflectance mode. Fluorescence spectroscopy was performed applying a FluoroMax 4 Spectrofluorometer (Horiba Scientific, Japan) with an excitation wavelength of 450 nm and an emission wavelength of 630 nm. A fibre coupled, collimator equipped UHP-T-LED 450 nm wavelength system with 780 mW was used as irradiation source for photobleaching experiments (Prizmatix Ltd., Israel). NMR spectra were recorded with an Avance III 300 MHz spectrometer (Bruker, USA) applying a frequency of 300.13 MHz for ^{1}H NMR-spectra. For the visualization of sub millimetre structures an Axioskop 50 transmitted light/fluorescence microscope with an AxioCam MRc (1388 × 1040 pixel) was used. Sample thickness was determined with a FMD12TB precision dial gauge (Käfer Messuhrenfabrik GmbH & Co. KG, Germany) with an accuracy of 1 μm.

Preparation and sample denotation

The two components of the different polysiloxane were premixed as specified by the respective manufacturer (Dow Corning OE6630: 4/1; ShinEtsu KJR9022E: 10/1). A stock solution was used (0.1 wt%, $CHCl_3$) to add a defined amount of dye to the mixtures. Physical dissolved gases and solvent were removed under reduced pressure (4 mbar, >30 min) before casting the samples into PTFE molds (30 × 10 × 1 mm). The mixtures were cured for 4 h at 150 °C. The resulting mean sample thickness is 1.11 ± 0.09 mm. The samples are denoted by the polymer and dye type abbreviations and the final dye concentration in ppm by weight (Table 1). Sample concentrations of 100, 250, 500, 750, 1000, 1500, 2000, and 3000 ppm dye in the matrix were prepared for each polymer.

Swelling and leaching behaviour

Investigations of the degree of crosslinking and dye mobility in the cured polymers were performed in swelling experiments. If there is any influence of the crosslinking behaviour due to the dye molecules the swelling behaviour should be different compared to the pristine matrix. In the swelling experiments, a weighted, small sample was placed in toluene for 24 h at room temperature. Excess of surface adsorbed solvent was removed by a filter paper before mass determination. The degree of swelling (SD) was calculated applying eqn (1).

$$\mathrm{SD} = \frac{m_\mathrm{s} - m_\mathrm{d}}{m_\mathrm{d}}\,100\% \tag{1}$$

Table 1 Nomenclature and composition of the prepared samples[a]

Sample designation	Polymer	Dye
Dow(1)LG305-X	Dow Corning OE6630	Lumogen® F Rot 305
Dow(1)FC546-X	Dow Corning OE6630	FC546
Shin(1)LG305-X	ShinEtsu KJR9022E	Lumogen® F Rot 305
Shin(1)FC546-X	ShinEtsu KJR9022E	FC546

[a] X is the dye concentration by weight with 100, 250, 500, 750, 1000, 1500, 2000 and 3000 ppm.

where m_s and m_d are the masses of the swollen and the dry sample.[33,34] The experiment was repeated twice for standard deviation determination. A higher crosslinking degree leads to a lower uptake of solvent depending on the solvent type and its polarity. Toluene was used because of the high solubility of the perylene dyes in this solvent. Leaching behaviour was investigated by UV-VIS measurements of the solvents after this procedure. The measurement was performed for the pristine matrices and for 100 ppm and 3000 ppm incorporated dye sample, repectively.

Quantum yield (QE) measurement and self-absorption coefficient (SA-coefficient) calculation

For a quantification of the dye stability and reabsorption phenomena absolute quantum yield measurements were implemented. An alteration in quantum yield due to a physical treatment should be directly related to the dye concentration. The self-absorption coefficient a can be calculated from the emission spectra recorded with the photoluminescence quantum yield measurement.[35,36] It can be used for quantum yield correction procedure and as a measure for self-absorption effects. From raw spectral data the sum of the product of photon count rate and the wavelength E are calculated applying eqn (2).

$$E = \sum E(\lambda)\Delta\lambda \tag{2}$$

The quantum yield is calculated from eqn (3).

$$\mathrm{QY} = \frac{\mathrm{Em_B} - \mathrm{Em_A}}{\mathrm{Ex_A} - \mathrm{Ex_B}} \tag{3}$$

where Em and Ex are the areas of the emission and excitation spectra values. A represents the values of the empty sphere and B for a sample in the sphere. The corrected quantum yield $\mathrm{QY_{Corr.}}$ can be calculated applying eqn (4).

$$\mathrm{QY_{Corr.}} = \frac{\mathrm{QY}}{1 - a + a\,\mathrm{QY}} \tag{4}$$

The self-absorption coefficient a is calculated by the ratio of the areas of the emission spectra of a regular sample F_sample and a very low concentrated sample with virtually zero self-absorption F_0 (15 ppm dye by weight) using eqn (5).

$$a = \frac{\sum F_\mathrm{sample}(\lambda)\mathrm{d}\lambda}{\sum F_0(\lambda)\mathrm{d}\lambda} \tag{5}$$

The spectra F_sample are scaled to match the spectrum F_0 that is not effected by self-absorption. The scaling is linked to a fitting of the spectra at longer wavelength and leads to a normalization in an area, which is not influenced by self-absorption (Fig. 1). The fit quality was verified by Pearson's chi squared test.

Heat and photostability experiments

Long-time stability of and matrix influence to the different dyes was examined after the main curing procedure by heat and

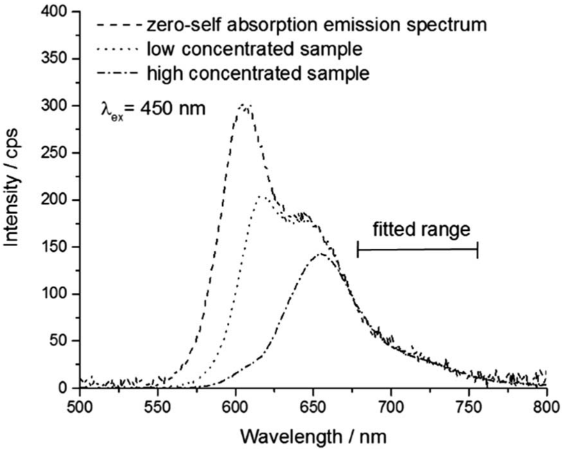

Fig. 1 Exemplarily shown scaled and matched emission spectra of a low concentrated sample with LG305 integrated and two samples with higher concentrations from quantum yield measurement. After fitting the tales of the spectra at 675–775 nm wavelengths the emission spectra are scaled. The quotient of the scaled area integral of the measured sample and the area integral of the zero self-absorption sample spectra results in the self-absorption coefficient *a*.

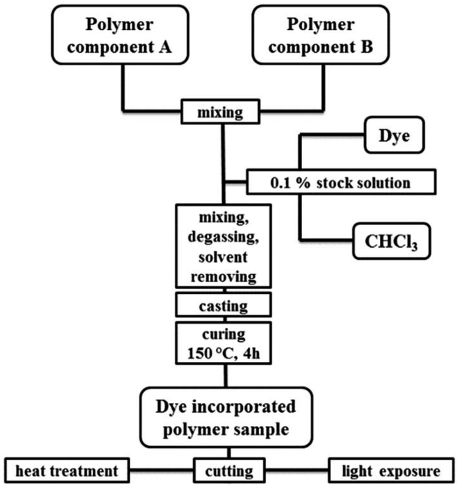

Fig. 2 Schematic preparation process of dye incorporated polysiloxane samples from two components and a dye containing chloroform stock solution.

irradiation exposure experiments to simulate the operation conditions in high performance LED applications. The samples were heat treated for 48 h and another 72 h at 200 °C (summed up 120 h). After every heating step the absolute quantum yield was measured. Despite the curing for 4 h at 150 °C a post-curing process was initialized by the additional heat treatment. Therefore, the samples got more rigid due to a higher cross-linking density after the main curing procedure. For photostability experiments a mask sample (5 × 7 mm) with a dye concentration of 100 ppm was fixed to the UV-VIS sample holder and light was exposed under air or nitrogen applying a 450 nm LED with 800 W cm^{-2}. Exposure was carried out for at least 60 h or until a decrease of absorbance of at least 50% was observed. The absorbance was determined by UV-VIS spectroscopy with an integration sphere setup in transmission mode periodically.

Results and discussion

The two perylene dyes were incorporated in two different cured polysiloxane matrices to investigate the influence of the matrix on the stability and optical properties of the dyes. Dow(1) is a phenyl containing HRI PMPS and Shin(1) is a non-phenyl containing LRI PDMS type polymer, which are regularly used as encapsulation materials of high performance LEDs. Both polymeric systems were used as received. The two components containing Si–H and Si–vinyl groups were mixed and thermally cured by platinum catalysed hydrosilylation. LG305 is a commercially available perylene based dye and not suitable for a covalent inclusion in the matrix. FC546 was synthesized with *N*-allyl groups to force a covalent attachment to the polymer structure by hydrosilylation with Si–H groups in the polymer backbone.

Dye incorporation into the matrix was carried out by mixing the polymer components according to the suppliers' specifications and addition of a stock solution of a chosen dye concentration between 15 and 3000 ppm by weight. This covers a range in which concentration quenching effects can occur. Before curing at 150 °C for 4 h the mixtures were degassed, the solvent was removed by reduced pressure, and the samples were casted in Teflon molds. After the curing procedure, the samples were cut into pieces for the different experiments and measurements (Fig. 2).

Fluorescence spectroscopy of dilute solution

The fluorescence of the two pure dyes was determined in toluene to obtain a qualitative comparison of excitation and emission maxima. The emission as well as the excitation spectra of LG305 and FC546 in toluene are similar referring to the

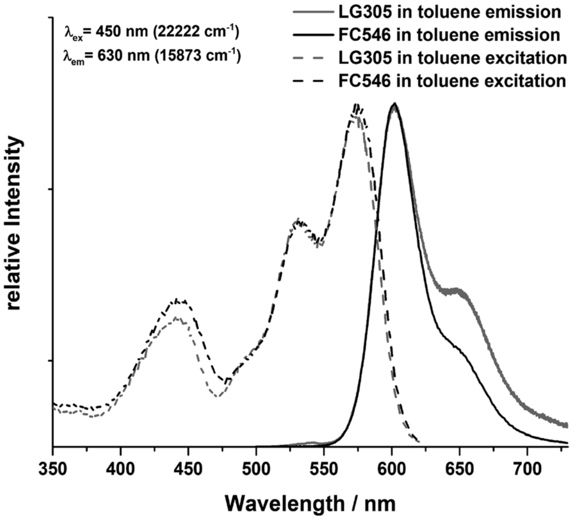

Fig. 3 Emission and excitation spectra of diluted solutions (5 μmol L^{-1}) of Lumogen® F Red 305 (LG305) and FC546 in toluene with an emission wavelength of 630 nm (15 873 cm^{-1}) and with an excitation wavelength of 450 nm (22 222 cm^{-1}).

location of the maxima (Fig. 3). The emission maximum is located at 604 nm (16 556 cm^{-1}) with an excitation wavelength of 450 nm (22 222 cm^{-1}). The excitation maximum is located at 575 nm (17 391 cm^{-1}) with an emission wavelength of 630 nm (15 873 cm^{-1}). The third local excitation maximum is detected at 444 nm (22522 cm^{-1}) which is the most important one concerning LED applications, due to the 450 nm emission wavelength of the blue LED chip. It is caused by the lateral substituents on the perylene core and is not detectable in molecules without bay substituents.[13]

Solubility

The two dyes were incorporated into the matrices by adding a chloroform stock solution to the premixed polymer components. After removing the solvent from the prepared but still liquid polymer mixtures, the dye precipitated in all samples with a concentration ≥750 ppm of the Shin(1) series independent of the used dye. The casted mixtures turned dark red and opaque, while the Dow(1) mixtures remained transparent and bright red without any visible precipitation (Fig. 4). Due to its structures the perylene diimide based dyes were highly soluble in the more phenyl groups containing Dow(1) mixture, most likely due to the ability of π–π-stacking interactions. The solubility in the non-phenyl containing Shin(1) matrix is very low. After curing at 150 °C for 4 h the Shin(1) series of both dyes showed a significant change in colour from dark red to bright red for samples with a concentration ≥750 ppm. The colour of the Dow(1) sample did not change (Fig. 5), which can be explained by the high curing temperatures resulting in an increased solubility of the dyes in the Shin(1) matrix.

Every sample was evaluated with light microscopy to investigate potential inhomogeneous distributions of the dye in the matrix. Samples of the Shin(1)LG305 series showed crystallization of the dye at concentrations ≥750 ppm after the curing process. There was no crystallization detected for all Dow(1) LG305 samples and for all samples with FC546 dye independent of the concentration. The LG305 dye was soluble in Dow(1) up to 4 wt% without any crystallization. The main reason for the prevention of crystallization of the FC546 dye in the Shin(1) matrix is most likely the covalent bonding between the molecules and the matrix. Similar to LG305, precipitation occurs for every sample with a concentration ≥750 ppm in the liquid polymer mixture. After the curing process no crystallites were detectable up to 3000 ppm. The high temperature curing process leads to an increase of dye solubility and mobility in the matrix. In addition the FC546 molecules can covalently attach to the polymer matrix by hydrosilylation, which prevents diffusion of the dye in the matrix and thus crystallization. This leads to the result, that FC546 can be incorporated into non-phenyl or phenyl containing polysiloxanes without any solvent. The covalent bonding was also verified by FTIR spectroscopy (see ESI†). An indirect prove was obtained by the leaching experiments described in the next paragraph.

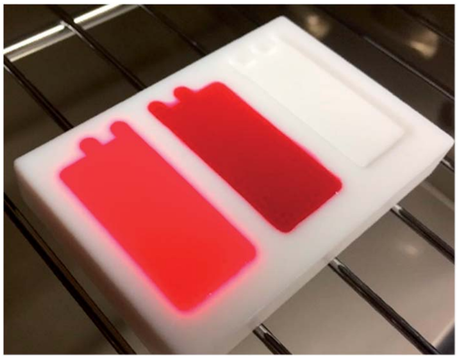

Fig. 4 Image of the casted solvent free liquid mixtures of the Dow(1) components (left) and the Shin(1) components (right) with a LG305 concentration of 1000 ppm. The Dow(1)LG305 1000 mixture is transparent and bright red. The dye is solvated very well without any precipitation. The Shin(1)LG305 1000 mixture is dark red and opaque. The dye precipitated after solvent removal.

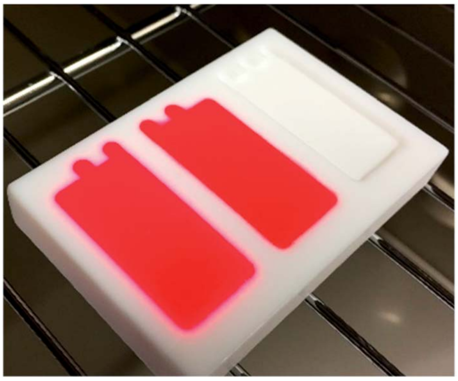

Fig. 5 Image of cured solid samples of the Dow(1) components (left) and the Shin(1) components (right) with a LG305 concentration of 1000 ppm. The Dow(1)LG305 1000 sample did not change its colour. The Shin(1)LG305 1000 sample changed its colour from dark red to bright red. A part of the precipitated dye resolved in the matrix due to the high temperature curing process, but there are still crystallites visible.

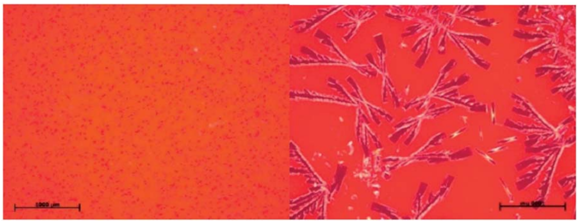

Fig. 6 Microscopic images of Shin(1)LG305 2000 ppm (100× optical magnification). After the curing process (150 °C, 4 h) small crystallites were detected (left). An additional heat treatment of the cured sample (200 °C, 120 h) resulted in a crystal growth in the cured, solid matrix.

A second heat treatment of the already cured samples showed the high mobility of the non-bonded LG305 in the solid matrix. The additional heat treatment at 200 °C for 120 h benefits a crystal growth process, which could be detected by light microscopy (Fig. 6). The crystallization of LG305 in the

Shin(1) matrix is supported by FTIR and UV-VIS data (see related chapters).

Swelling and leaching

Contrary to FC546 the LG305 dye is not covalently connected to the polymer structure. During swelling studies of the samples in toluene LG305 is entirely leached out of the crosslinked matrices while FC546 completely remained in the matrix (Fig. 7).

The visual impression was supported by UV-VIS spectroscopy of the diluted toluene solution after the leaching experiments. Only Shin(1)LG305 100 and Dow(1)LG305 100 show the typical dye absorption bands at 575 nm (Fig. 8). Differences in absorbance were due to variations in sample sizes which leads to deviations in the dye concentrations after leaching. As a result the leaching experiment can give an indirect indication of the covalent linkage of the dye to the matrix.

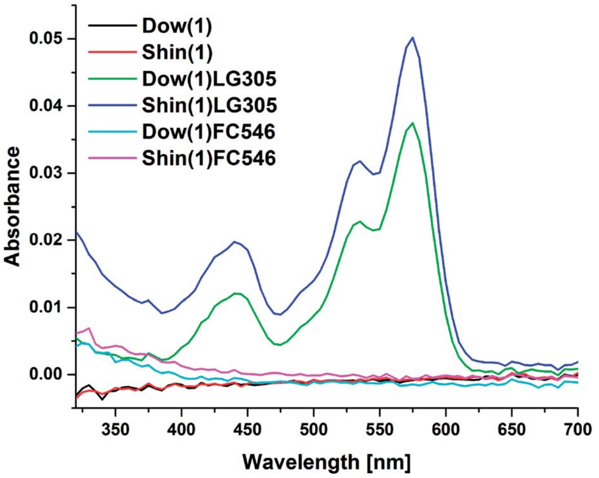

Fig. 8 Absorbance spectra of the diluted toluene solution after the leaching experiments of the isolated pure matrices Dow(1) and Shin(1) and of the dye incorporated samples Dow(1)LG305, Shin(1)LG305, Dow(1)FC546 and Shin(1)FC546 with 100 ppm dye, respectively.

The swelling degree is a measure for the crosslinking degree of a polymer system (eqn (1)). A high swelling degree indicates a less crosslinked polymer. The high mobility of the polymer chains increase the permeation of solvent molecules. A higher crosslinked system decreases this permeation and the swelling degree, respectively. The swelling degree of the isolated Shin(1) matrix is 117.9 ± 0.9%. The Dow(1) samples show a similar swelling behaviour of 80.4 ± 1.9% irrespective of the incorporated dye molecule, which indicates a much higher crosslinked system. There was no significant change in swelling behaviour due to the dye incorporation. This means, no macroscopic influence to the crosslinking of the matrix can be detected by incorporation of the dyes (Fig. 9).

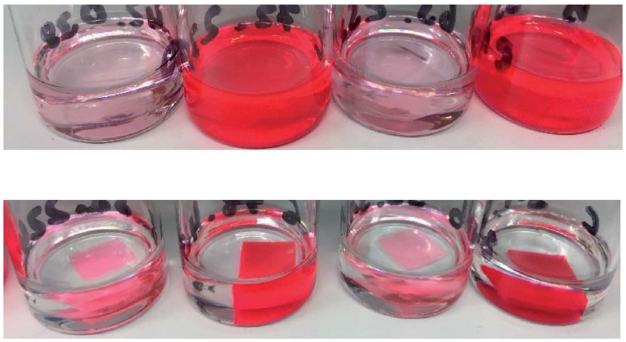

Fig. 7 Top: Image of Dow(1)LG305 100 and 3000 ppm (left) and Shin(1)LG305 100 and 3000 ppm (right). The solvent leached the incorporated dye entirely out of the matrix after 24 h. Bottom: Image of Dow(1)FC546 100 and 3000 ppm (left) and Shin(1)FC546 100 and 3000 ppm (right). No leaching was observed due to the covalently bonded dye molecules.

ATR-FTIR spectroscopy

The FTIR spectra of the isolated components and cured matrices reveals the anticipated vibration bands for the two polysiloxane type polymers (see ESI†).[37–40] The B components of the Dow(1) and Shin(1) show additional vibration bands due to the Si–H bond respectively at 2129/2159 cm^{-1} [ν(Si–H)] and 896/906 cm^{-1} [ρ(Si–H)], which disappeared after curing. The Dow Corning OE6630 spectra shows specific aromatic vibration bands due to phenyl side groups at 3049, 3072 [ν(C–H)$_{AR}$]; 1490, 1430 [ν(C=C–C)$_{AR}$] and 726, 694 [δ(C–H)$_{AR}$] cm^{-1}. The FTIR spectra of the polymers containing FC546 and the Dow(1)LG305 samples present no substantial differences to the isolated polymer. Heat treatment has no significant influence on the vibration spectra of these samples. The spectrum of Shin(1) LG305 3000 ppm displays an additional increase of sharp vibration bands between 1750 and 1250 cm^{-1}. These bands can be assigned to the Lumogen® F Red 305 chemical groups at 3030, 3064 [ν(C–H)$_{AR}$]; 2960, 2925 [ν(C–H)]; 1705, 1672 [ν(C=O)]; 1583, 1485 [ν(C=C–C)$_{AR}$]; 1407, 1338 [ν(C–N)] and 1309, 1282, 1193 [ν(C–O–C)] cm^{-1}.[28] As previously mentioned the LG305 dye

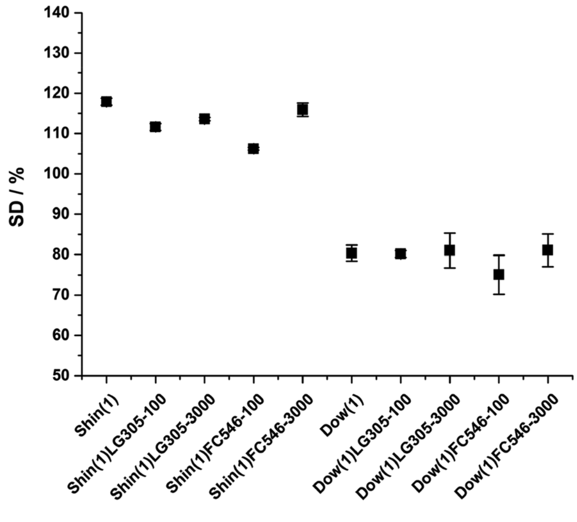

Fig. 9 Swelling degree of Shin(1), Dow(1) and the dye incorporated samples with 100 and 3000 ppm dye concentration, respectively.

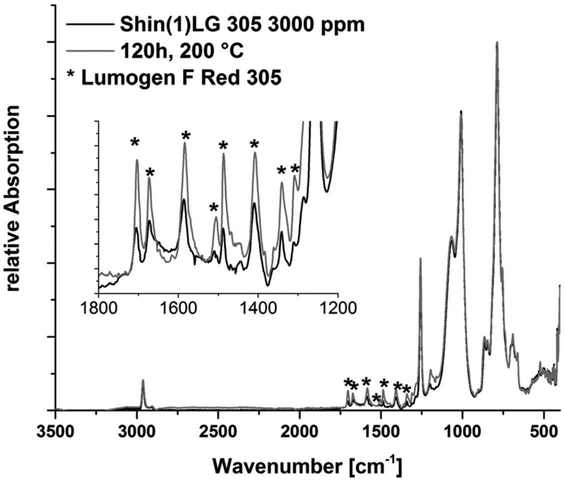

Fig. 10 FTIR spectra of Shin(1)FC546 3000 before and after the heat treatment at 200 °C for 120 h. An increase of LG305 vibration bands occurs due to the heat treatment.

precipitates in the Shin(1) polymer at concentrations ≥750 ppm. The ATR-FTIR measurement is limited in its penetration depth. The samples with 3000 ppm concentration show crystallized dye on the sample surface as well. This leads to detectable signals from dye vibrations (Fig. 10). The intensity of the vibrations increases after the heat treatment at 200 °C for 120 h. All measured spectra are part of ESI.†

UV-VIS spectroscopy

The absorption of the samples was measured by transmission UV-VIS spectroscopy. A comparison of the absorption values at 450 nm is plotted below (Fig. 11). All samples show a direct relationship between the increase of dye concentration and the increase of absorption until saturation is reached. Sample Shin(1)LG305 deviates the most from the a theoretical Lambert–Beer function calculated by eqn (6).

$$A = 1 - 10^{-\varepsilon c d} \tag{6}$$

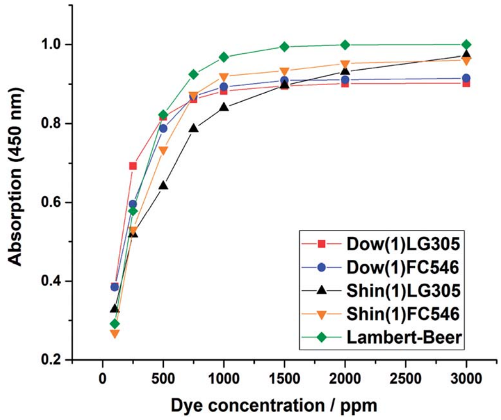

Fig. 11 Absorption of the Dow(1)LG305, Shin(1)LG305, Shin(1)FC546, and Dow(1)FC546 concentration series. A theoretical Lambert–Beer function calculated using eqn (6) is included for reasons of comparison.

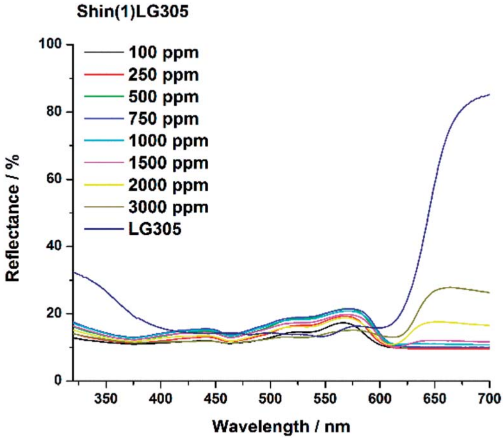

Fig. 12 Reflectance spectra of the Shin(1)LG305 concentration series and the isolated dye as solid powder.

where A is the absorption, ε is the constant absorption coefficient, d is the constant path length and c is the dye concentration.[41]

Due to the saturation a concentration optimum can be determined for any dye matrix combination. For example the Dow(1)LG305 absorption is saturated at 1000 ppm, thus a higher concentration is unnecessary from the perspective of absorbance. The unexpected trend in the Shin(1)LG305 absorption can be explained by the crystallization process which changes the absorption values due to the solid phase inside the polymer matrix. This crystallization of the LG305 dye in the Shin(1) matrix can be detected by reflectance measurement as well (Fig. 12). The reflectance from 615–700 nm is increasing at concentrations larger than 750 ppm. This increase is caused by the reflectance of the crystalline dye, which generates a strong reflectance edge in this area of the VIS spectrum. This is verified by the reflectance spectrum of the isolated pure dye.

Despite the high absorption values an efficiency increase of solar cell concentrators was determined in solution for Lumogen® F Red 305.[41] Because total LED efficiency also depends on emission efficiency, absolute quantum yield measurement were performed as well. All UV-VIS spectra are part of the ESI.†

QE and SA-coefficient

Quantum yield was measured from all untreated samples, after 48 and 120 h heat treatment at 200 °C and after the light exposure experiments (Fig. 13). The incorporated dyes in the Dow(1) polymer reveal much higher quantum yields compared to the Shin(1) system. The quantum yield of the Dow(1)LG305 series is 1 and not influenced by an increase of dye concentration. An absolute absence of quenching effects due to the matrix dye combination is observed. A similar result is known for LG305 in a PMMA matrix for concentrations smaller than 1600 ppm.[36] The Dow(1)FC546 series quantum yield increases slightly from 0.93 to 0.97 at 100 and 250 ppm then decreases slowly but constant to 0.77 at 3000 ppm. The Shin(1)LG305 series quantum yield also increases slightly from 0.90 to 0.92 at

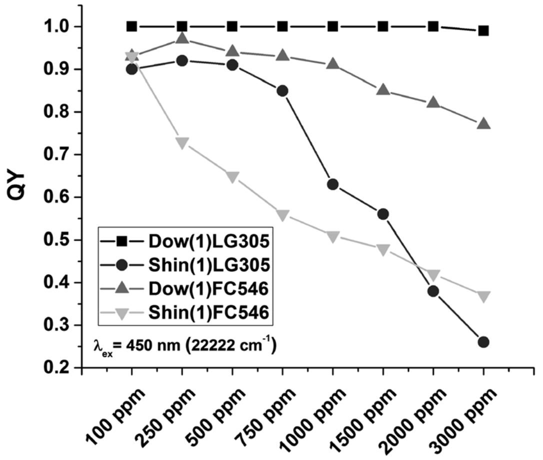

Fig. 13 Absolute quantum yield of the Dow(1)LG305, Shin(1)LG305, Shin(1)FC546, and Dow(1)FC546 concentration series.

100 and 250 ppm then decreases fast to 0.26 at 3000 ppm. The Shin(1)FC546 series quantum yield is decreasing very fast from 0.93 to 0.37 at 100 and 3000 ppm samples, but it shows higher quantum yields at 2000 and 3000 ppm than Shin(1)LG305 samples with similar concentrations.

The calculated SA-coefficient is increasing with the increase of concentration for all samples (Fig. 14). The lowest concentrated samples with 100 ppm dye are starting with the same SA-coefficient for each matrix.

The SA-coefficient of the Dow(1)LG305 and the Dow(1)FC546 100 samples are 0.27 and 0.28. The SA-coefficient of the Shin(1) LG305 and the Shin(1)FC546 100 samples are 0.24, respectively. These values are much lower compared to LG305 in PMMA.[36] The largest increase of the SA-coefficient with increasing dye concentration is observed for the Shin(1)FC546 series. At 3000 ppm dye concentration, the SA-coefficient is 0.71. The Dow(1)LG305 3000 sample shows an enlargement up to 0.56.

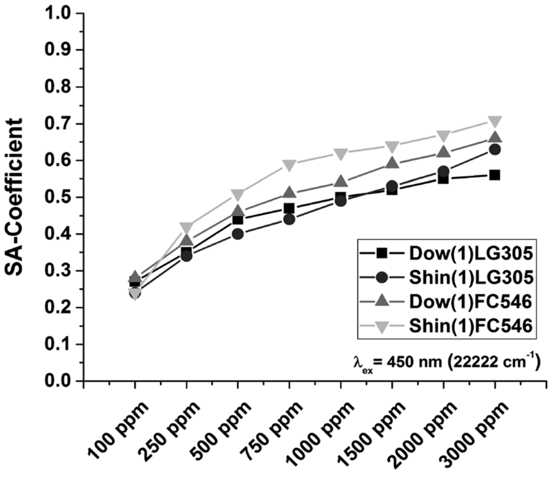

Fig. 14 Calculated SA-coefficient of the Dow(1)LG305, Shin(1)LG305, Shin(1)FC546, and Dow(1)FC546 concentration series (eqn (5)).

The Dow(1) polymer contains a high number of aromatic phenyl units able to interact with the planar perylene core of the dyes. As a consequence a sterically blocking of the dye–dye π–π-stacking is conceivable.[32,42] Additionally the structure of the LG305 dye is sterically affecting the π–π-stacking due to its bulky imide substituents.[14,32] Hence, a high quantum yield independent of the dye concentration is observed. The Shin(1) polymer contains no aromatic units. Its weak solvation due to its structure benefits a dye–dye interaction and causes crystallization. The quantum yield of the Shin(1)LG305 series is lowered by this interaction and starts decreasing massively with the crystallization process at concentration of 750 ppm. A decrease of quantum yield by concentration for the FC546 series is caused by the dye structure. Certainly the missing bulky imide substituents benefit a quenching effect due to dye–dye interactions.[32] Comparable results are known for different perylene diimide compounds in PMMA.[32] A sterically blocking of the dye–dye π–π-stacking due to the phenyl units of the Dow(1) structure is supported by the Dow(1)FC546 quantum yield results compared to the Shin(1)FC546 series. If the dye–dye π–π-stacking of the FC546 occurs first in the process of sample preparation a separation by covalent bonding is not necessarily probable. This is supported by the Shin(1)FC546 series quantum yield, which decreases constantly by increasing concentration in the non-heat treated samples. After heat treatment and thus a covalent connection of the FC546 dye to the matrix, the quantum yield shows not such a high concentration dependency. The samples with matrix dye combination Dow(1)LG305 in any concentration and Dow(1)FC546 100–500 ppm display the highest quantum yields and are most suitable for the application in LED devices.

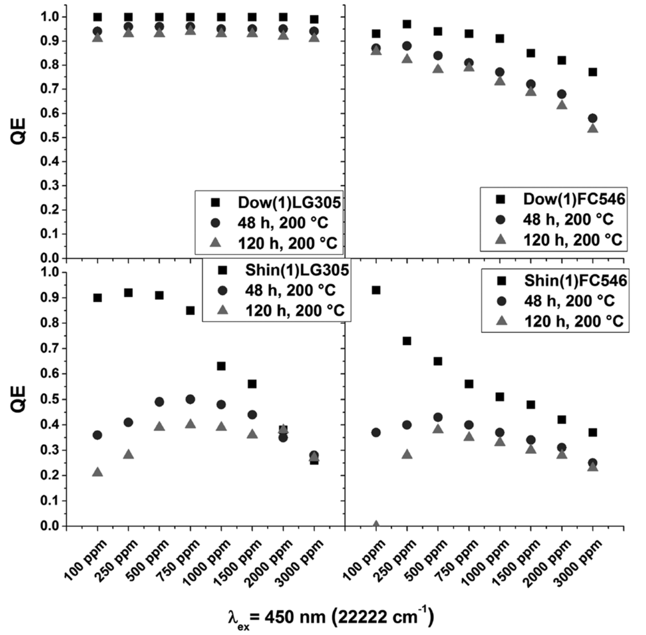

Fig. 15 Absolute quantum yields of the Dow(1)LG305, Shin(1)LG305, Shin(1)FC546, and Dow(1)FC546 concentration series before and after a heat treatment for 48 and 120 h at 200 °C.

Heat treatment results

In LED applications usually a post-curing process is carried out by reheating the polymer samples. After heating the samples to 200 °C for 48 h a decrease of QY occurs (Fig. 15). This indicates a direct influence of the post-curing process to the dye–dye interaction or to the structural integrity of the dye molecules.

The quantum yields of the Dow(1)FC546 series decreases with an increasing dye concentration. Higher dye concentration leads to a larger and systematic decrease in quantum yield. A rearrangement of the dye molecules due to the post-curing at high temperatures is possible. Compared to the Shin(1) we do not assume a heat induced decomposition of the dye molecules. The Shin(1)LG305 100 sample bleaches under heat treatment and the quantum yield decreases from 0.9 to 0.2, which is both a strong hint for dye decomposition. At significantly higher concentrations, a constant quantum yield is measured. This is caused by the high concentration of temperature stable crystalline dye aggregates (>200 °C).[43] The LG305 dye is precipitated due to the low solubility in the Shin(1) matrix, as described in detail in the previous chapters. The quantum yield of the low concentrated Shin(1)FC546 decreases massively as well. Contrary to the Dow(1)FC546 series the decrease is smaller at higher dye concentrations. This indicates a very fast decomposition of the dye due to the high temperatures, promoted by the structure of the Shin(1) matrix. The decrease at higher concentrations caused by some destructive processes is not significant compared to the low concentrated sample values. The main difference in the matrix structure is the methyl to phenyl group ratio. The Shin(1) matrix contains no phenyl groups. This leads to the conclusion that the phenyl groups are protecting the dye from physical decomposition or chemical reactions with the matrix. This is supported by the results of the Dow(1)LG305 series, which is barely influenced by the heat treatment. At temperatures above 200 °C different decomposition mechanisms are reported for PDMS, PMPS and PDMDPS.[44–49] In PDMS a homolytic cleavage of the Si–CH_3 bond is described by forming radicals.[45–47] A second mechanism is described by forming cyclic oligomers from a condensation reaction with terminal hydroxyl groups.[47] A third possible decomposition mechanism describes the cyclic oligomer formation by an intramolecular reaction of the silicone backbone by forming four membered ring transition states.[47,49] In phenyl containing systems the decomposition causes a benzene or cyclic oligomer formation. The proposed decomposition mechanisms are similar to the PDMS mechanisms.[44,48,49] The main difference in decomposition is the chemical bonding in the main chain. The electron withdrawing phenyl groups increase the strength of the Si–O bonds due to inductive effects. The formation of cyclic oligomers is hindered which leads to an increase of degradation temperature.[49] A radical formation in Shin(1) at 200 °C is conceivable and a possible reason for the massive decomposition of the incorporated dye. The calculated SA-coefficient is increasing for all samples (Fig. 16). Due to the crystallization of the LG305 dye in the Shin(1)LG305 series the value of the SA-coefficient stays constant for samples with dye concentrations larger than 750 ppm after 48 h.

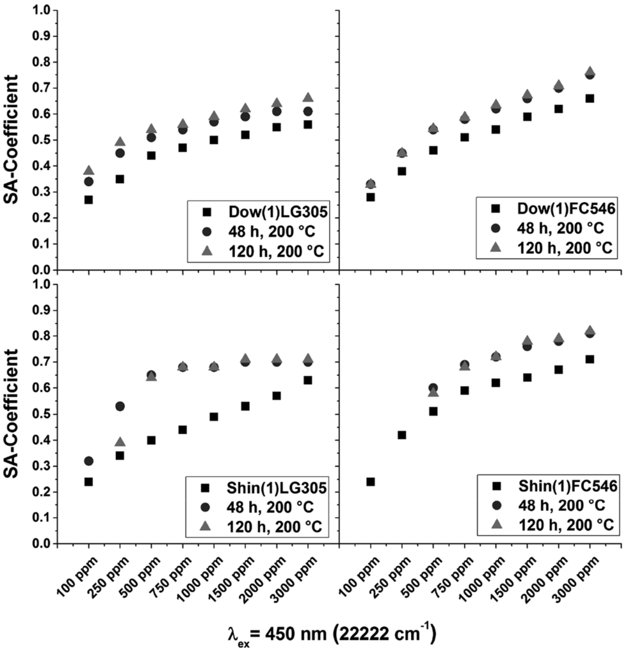

Fig. 16 SA-coefficient of the Dow(1)LG305, Shin(1)LG305, Shin(1)FC546, and Dow(1)FC546 concentration series before and after a heat treatment for 48 and 120 h at 200 °C.

Caused by the very intense weak emission spectra of the samples Shin(1)LG305 100 and the samples Shin(1)FC546 100 and 250 a calculation of the SA-coefficient was not possible. As a result the Dow(1) matrix is capable to protect the incorporated dyes from heat initiated decomposition while the Shin(1) matrix promotes their decomposition. The use of an isolated polymethylsiloxane matrix for dye protection is inappropriate.

All results of the fitted quantum yield emission spectra, the calculated SA-coefficients and the corrected quantum yield values for each concentration series are reported in the ESI.†

Photostability

The photostability of the incorporated dyes is correlated to the change in absorbance. Samples with equal dye concentration of 100 ppm were exposed to a high power density 450 nm light source. For all samples a decrease of absorbance occurs. The absorbance of Shin(1)LG305 decreased about 57% in 1375 min. The absorbance of the FC546 dye in the same matrix in the same period decreased just by 21%. The absorbance of Dow(1)LG305 decreased 19% in 1380 min and just 10% in the same period for Dow(1)FC546 (Fig. 17).

This indicates a much higher photostability of the covalent bonded FC546 dye. Possible photodegradation phenomena are more ineffective due to its structure. It is already known that *N*-alkyl substituted perylene diimide dyes in solution are generally more photostable than *N*-aryl substituted.[14] There is no mechanism described, which explains this promotion due to a 450 nm light exposure yet. It is reasonable that a radical initiated decomposition takes place, as proposed for UV radiation experiments of LG305 in PMMA.[13] In these literature described studies a decomposition is initiated by the disruption

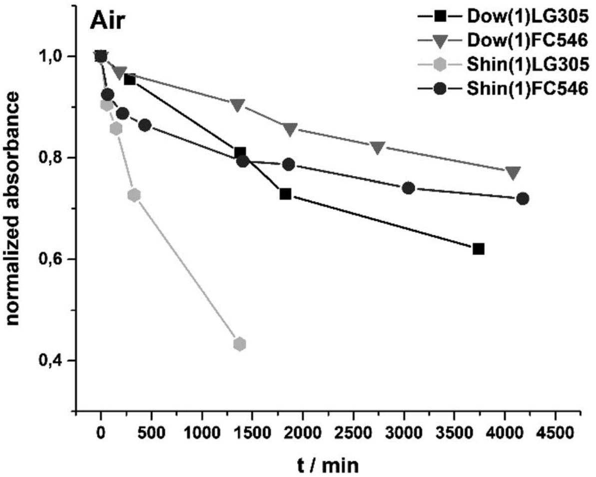

Fig. 17 Normalized absorbance of Dow(1)LG305, Shin(1)LG305, Shin(1)FC546, and Dow(1)FC546 100 ppm at different times measured during a light exposure with a 450 nm light source of 800 mW cm^{-2} light intensity.

of the lateral phenoxy substituents as radicals followed by a homolytic cleavage of the N–R bond.[13] A second possible explanation is an oxygen caused photo-oxidation as described for Lumogen® F Red 300 and Lumogen® F Orange 240 in polyester and PMMA.[50]

A second photostability experiment was carried out to investigate an oxygen influence. After 2500 min of light exposure under nitrogen atmosphere, the samples were exposed to air. The absorbance of all samples decreased under nitrogen atmosphere and the Shin(1)LG305 revealed the highest decrease in absorbance (Fig. 18). This indicates a matrix promoted degradation as described above.

In an air atmosphere the photostability decreases much more pronounced particularly for the Shin(1)LG305 sample. One reason for this behaviour might be the high oxygen permittivity of the Shin(1) matrix. An additional oxygen barrier layer could protect the encapsulation against this influence.[51] The results show a strong influence of oxygen and of the matrix structure on the photodegradation process of the perylene diimide dyes in polysiloxane matrices. Independent of the extrinsic reasons for the degradation, the FC546 dye is the most stable investigated sample in combination with the Dow(1) matrix. But its loss of 33% absorbance in 4000 h is still considerable less than the lifetime of a commercially available LEDs containing inorganic conversion phosphors.

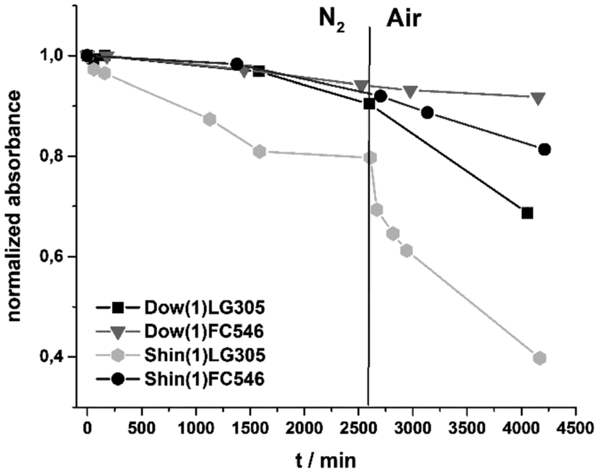

Fig. 18 Normalized absorbance of Dow(1)LG305, Shin(1)LG305, Shin(1)FC546, and Dow(1)FC546 100 ppm at different times measured during a light exposure with 450 nm light source with 800 mW cm^{-2} light intensity in nitrogen and air atmosphere.

Conclusions

The influence of a LRI polydimethylsiloxane (ShinEtsu KJR 9022 E [Shin(1)]) and a HRI polymethylphenysiloxane (Dow Corning OE6630 [Dow(1)]) on the properties of two different incorporated perylene diimide based dyes was investigated. Heat- and photostability were measured and evaluated for both dyes in both matrices. Shin(1) showed a weak solubility for both dyes, which was increased by the curing procedure due to an increase of temperature. Crystallization of the LG305 dye in Shin(1) was observed after curing and crystal growth appears after an additional heat treatment. This indicated a high mobility of dissolved molecules caused by a temperature increase. There was no crystallization detected for the other samples due to covalent bonding or higher solubility of the dyes in the Dow(1) matrix. As a result, a solvent free incorporation of FC546 is achievable due to the covalent bonding and the increased solubility at curing conditions. High quantum yields ≥0.9 were detected for low concentrated samples of all kind. The Dow(1) LG305 series showed no decrease in quantum yield with an increase in concentration. A π–π-stacking is blocked due to the high amount of aromatic phenyl units in Dow(1), which are able to interact with the planar perylene core. A decrease of quantum yield for the FC546 series is caused by the dye structure, which favours dye–dye interaction. The Shin(1) series quantum yield decreases constantly with an increase of concentration. The low solubility benefits a dye–dye interaction that even leads to a crystallization process in the matrix. Dye incorporation is not influencing the polymer structure, shown by swelling experiments in toluene. Furthermore, no leaching occurs for covalent bonded FC546. Heat treatment for 120 h at 200 °C results in a decrease in quantum yield due to a post-curing process or dye decomposition. The Shin(1) matrix benefits the decomposition process massively. The highest photostability was observed for the FC546 dye. Shin(1) also favors a photo initiated decomposition of the dyes. Overall, a phenyl containing polysiloxane matrix with a low concentrated, covalently bonded perylene-based dye is a promising combination for LED application.

Conflicts of interest

There are no conflicts to declare.

Note added after first publication

This article replaces the version published on 17th May 2018, which contained an error in eqn (3) in the pdf version.

Acknowledgements

This research has been funded by the Federal Ministry of Education and Research (BMBF, Germany) in the project ORCA – Organic and rare earth reduced conversion materials for LED-based lightning (project number 03XP0050). We would like to thank Prof. Gregor Jung for granting access to the Quantaurus instrument and for fruitful discussions, Dr Patrick Wenderoth and Dennis Meier for experimental, and Silvia Beetz for technical support.

References

1 Z. Xia and Q. Liu, *Prog. Mater. Sci.*, 2016, **84**, 59–117.

2 T. Jüstel, H. Nikol and C. Ronda, *Angew. Chem., Int. Ed.*, 1998, **37**, 3084–3103.

3 C. Feldmann, T. Jüstel, C. R. Ronda and P. J. Schmidt, *Adv. Funct. Mater.*, 2003, **13**, 511–516.

4 C. R. Ronda, *J. Alloys Compd.*, 1995, **225**, 534–538.

5 S. Ye, F. Xiao, Y. X. Pan, Y. Y. Ma and Q. Y. Zhang, *Mater. Sci. Eng., R*, 2010, **71**, 1–34.

6 M. Born and T. Jüstel, *Chem. Unserer Zeit*, 2006, **40**, 294–305.

7 P. Schlotter, R. Schmidt and J. Schneider, *Appl. Phys. A Mater. Sci. Process.*, 1997, **64**, 417–418.

8 Y. N. Arukawa, I. N. Iki, K. I. Zuno, M. Y. Amada, Y. M. Urazaki and T. M. Ukai, *Jpn. J. Appl. Phys.*, 2002, **41**, 371–373.

9 R.-J. Xie, N. Hirosaki, H.-L. Li, Y. Q. Li and M. Mitomo, *J. Electrochem. Soc.*, 2007, **154**, J314.

10 D. Di Martino, L. Beverina, M. Sassi, S. Brovelli, R. Tubino and F. Meinardi, *Sci. Rep.*, 2014, **4**, 4400.

11 H. J. Kim, J. Y. Jin, Y. S. Lee, S. H. Lee and C. H. Hong, *Chem. Phys. Lett.*, 2006, **431**, 341–345.

12 L. Zhang, B. Li, B. Lei, Z. Hong and W. Li, *J. Lumin.*, 2008, **128**, 67–73.

13 G. Griffini, L. Brambilla, M. Levi, M. Del Zoppo and S. Turri, *Sol. Energy Mater. Sol. Cells*, 2013, **111**, 41–48.

14 A. Rademacher, S. Märkle and H. Langhals, *Chem. Ber.*, 1982, **115**, 2927–2934.

15 G. Wagenblast, M. Könemann, S. Ivanovici, G. de Keyzer, R. Send and M. Pepers, *Novel Illumination Devices*, *US Pat.*, US20160084477 A1, 2016.

16 G. Wagenblast, M. Könemann, S. Ivanovici, G. de Keyzer and R. Send, *Color Converters*, *US Pat.*, US9711665 B2, 2017.

17 M. Könemann, G. Wagenblast, S. Ivanovici, G. de Keyzer and R. Send, *Novel Color Converters*, *US Pat.*, US20140076397 A1, 2014.

18 M. Könemann, G. Wagenblast, S. Ivanovici, G. de Keyzer and R. Send, *Novel Color Converter*, *US Pat.*, US20160284947 A1, 2016.

19 Y. Yang, G. Xian, H. Li and L. Sui, *Polym. Degrad. Stab.*, 2015, **118**, 111–119.

20 R. Wen, J. Huo, J. Lv, Z. Liu and Y. Yu, *J. Mater. Sci.: Mater. Electron.*, 2017, **28**, 1–14.

21 J. E. Mark, *Acc. Chem. Res.*, 2004, **37**, 946–953.

22 T. Higashihara and M. Ueda, *Macromolecules*, 2015, **48**, 1915–1929.

23 J. Wang, M.-L. Du, C.-S. Xu, H. Zhu and Y.-Q. Fu, *J. Macromol. Sci., Part B: Phys.*, 2012, **51**, 2462–2472.

24 J. S. Kim, S. Yang and B. S. Bae, *Chem. Mater.*, 2010, **22**, 3549–3555.

25 I. A. Lei, D. F. Lai, T. M. Don, W. C. Chen, Y. Y. Yu and W. Y. Chiu, *Mater. Chem. Phys.*, 2014, **144**, 41–48.

26 M. Buffa and M. G. Debije, *Springer Ser. Mater. Sci.*, 2014, **190**, 247–266.

27 L. Y. Tyng, M. R. Ramli, M. B. H. Othman, R. Ramli, Z. A. M. Ishak and Z. Ahmad, *Polym. Int.*, 2013, **62**, 382–389.

28 G. Maggioni, A. Campagnaro, S. Carturan and A. Quaranta, *Sol. Energy Mater. Sol. Cells*, 2013, **108**, 27–37.

29 C. Huang, S. Barlow and S. R. Marder, *J. Org. Chem.*, 2011, **76**, 2386–2407.

30 M. Könemann, S. Ivanovici, H. S. Mangold, G. Kickelbick and N. Steinbrück, EP18151250.0 (patent pending), 2018.

31 BASF AG, Lumogen(R)F – Technical Information, TI/P 3201 e (9125), 1997.

32 B. Zhang, H. Soleimaninejad, D. J. Jones, J. M. White, K. P. Ghiggino, T. A. Smith and W. W. H. Wong, *Chem. Mater.*, 2017, **29**, 8395–8403.

33 C. Feldgitscher, H. Peterlik, M. Puchberger and G. Kickelbick, *Chem. Mater.*, 2009, **21**, 695–705.

34 N. Stafie, D. F. Stamatialis and M. Wessling, *Sep. Purif. Technol.*, 2005, **45**, 220–231.

35 T. S. Ahn, R. O. Al-Kaysi, A. M. Müller, K. M. Wentz and C. J. Bardeen, *Rev. Sci. Instrum.*, 2007, **78**, 2007–2009.

36 L. R. Wilson and B. S. Richards, *Appl. Opt.*, 2009, **48**, 212.

37 P. J. Launer, *Silicon Compd. Regist. Rev.*, 1987, pp. 100–103.

38 J. H. Lady, G. M. Bower, R. E. Adams and F. P. Byrne, *Anal. Chem.*, 1959, **31**, 1100–1102.

39 J. Coates, *Encycl. Chem. Technol.*, 2000, 10815–10837.

40 N. B. Sanches, S. N. Cassu, R. De Cássia and L. Dutra, *Polimeros*, 2015, **25**, 247–255.

41 Z. Krumer, W. G. J. H. M. van Sark, R. E. I. Schropp and C. de Mello Donega, *Sol. Energy Mater. Sol. Cells*, 2017, **167**, 133–139.

42 M. Mitsui, H. Fukui, R. Takahashi, Y. Takakura and T. Mizukami, *J. Phys. Chem. A*, 2017, **121**, 1577–1586.

43 Y. Nagao, *Prog. Org. Coat.*, 1997, **31**, 43–49.

44 G. Deshpande and M. E. Rezac, *Polym. Degrad. Stab.*, 2002, **76**, 17–24.

45 G. Camino, S. M. Lomakin and M. Lageard, *Polymer*, 2002, **43**, 2011–2015.

46 C. Camino, S. M. Lomakin and M. Lazzari, *Polymer*, 2001, **42**, 2395–2402.

47 N. Grassie and I. G. Macfarlane, *Eur. Polym. J.*, 1978, **14**, 875–884.

48 N. Grassie, I. G. Macfarlane and K. F. Francey, *Eur. Polym. J.*, 1979, **15**, 415–422.

49 N. Grassie, K. F. Francey and I. G. Macfarlane, *Polym. Degrad. Stab.*, 1980, **2**, 67–83.

50 N. Tanaka, N. Barashkov, J. Heath and W. N. Sisk, *Appl. Opt.*, 2006, **45**, 3846–3851.

51 G. H. Kim, J. Oh, Y. S. Yang, L. M. Do and K. S. Suh, *Thin Solid Films*, 2004, **467**, 1–3.

4.2. Perylene Polyphenylmethylsiloxanes for Optoelectronic Applications

Published as an article:

Nils Steinbrück and Guido Kickelbick, *J. Pol. Sci. B.*, **2019**, *57*, 1062-1073

https://doi.org/10.1002/polb.24861

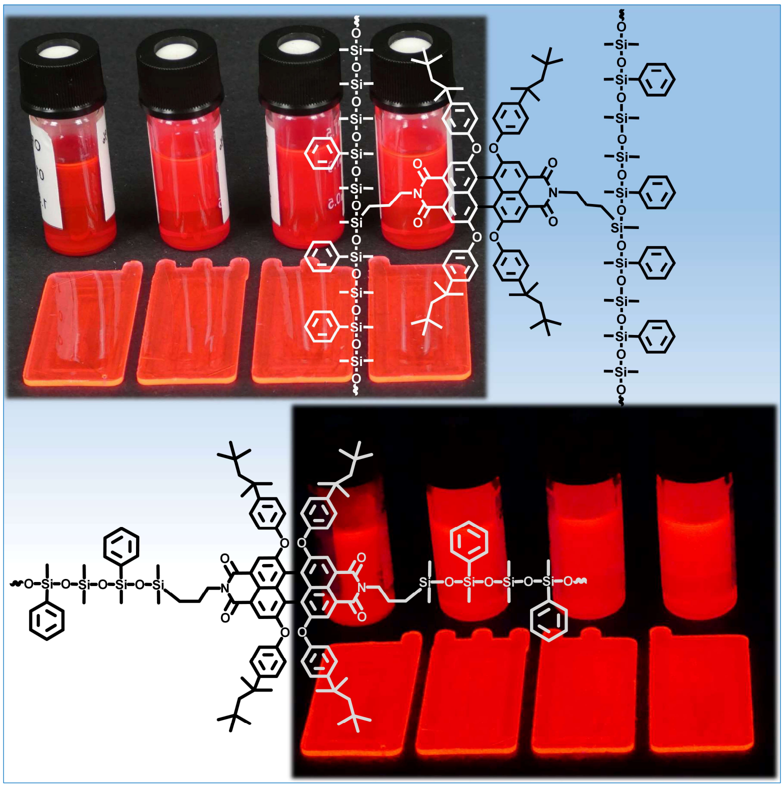

Contribution of the Authors to the Manuscript:

Nils Steinbrück wrote the complete draft of this manuscript that was acknowledged by all named authors. Nils Steinbrück performed the synthesis and characterization of all Perylene Polysiloxanes and their samples as well as the FTIR, NMR, TG, TG-IR, DSC, UV/Vis, hardness and microscopic measurements and the heat and photostability experiments. He also performed the key part of the data and results interpretation.

Prof. Dr. Guido Kickelbick gave the input to this project, supervised and discussed it, and optimized the manuscript to its final form.

Based on the results and conclusions of the previous part of this thesis, novel liquid perylene polyphenylmethylsiloxanes were synthesized in which the allyl functionalized FC546 dye is integrated covalently by hydrosilylation linearly in the polymer backbone and as a cross-linking agent between polymer chains. The results of the subsequent characterization and evaluation of the perylene polymers properties before and after adding them to another thermally curable polymer resin were summarized in the **second part** of this thesis called ***"Perylene Polyphenylmethylsiloxanes for Optoelectronic Applications".*** In the first approach, linear hydride- and vinyl-terminated polyphenylmethylsiloxanes were mixed in different ratios, and 0.1 wt% of FC546 was added. Linear perylene polymers with different chain length could be synthesized with M_w between 5600 and 8400 g mol^{-1}. By holding the hydride to the vinyl ratio of the polymers constant and change the concentration of the dye from 0.025 to 1.0 % no systematic variation in chain length could be detected. In a second approach, a polymethylhydrosiloxane-phenylmethylsiloxane copolymer with pendant and terminal hydride atoms was cross-linked by up to 8 wt% of FC546, leading to still liquid perylene polyphenylmethylsiloxanes with a significantly high concentration of dye incorporated.

Afterward, these perylene polymers were incorporated in a curable polyphenylmethylsiloxane resin. Due to unreacted hydride functionalities, the perylene polymers are also covalently bonded to the structure of the resin. This type of preparation separates the dye molecules even more than by just integrating the pure dye, leading to less dye-dye interactions. At the same time, the phenyl content in the final samples was increased, and oxygen permeability should be decreased.[80] Furthermore, due to this preceding formation of the perylene polysiloxanes, the incorporated dye concentration could be enhanced significantly. A second feature could be introduced by change of the perylene polysiloxane concentration inside the curable polysiloxane resin. The hardness of the material got tunable without changing the properties of the dye. The perylene polymers added to the resin lower the glass transition temperature of the cured resin structure and therefore lower the cross-linking degree, which was verified by DSC and TG measurements. An increased perylene polyphenylmethylsiloxane concentration leads to softer samples. The variety of flexibility makes this material combination also suitable for other optoelectronics. They are especially interesting for luminescent solar collectors, in which a more flexible polymer host material can improve the number of possible applications.[83] Summarized, the perylene polymers properties implemented to the thermally curable polysiloxane resin, like quantum yield and thermal stability, were as same as good as the ones from the pure dye incorporated into the resin. The photostability could also not be improved enough for the use in hybrid-LEDs. Whereas the use in low power applications like luminescent solar collectors is conceivable.

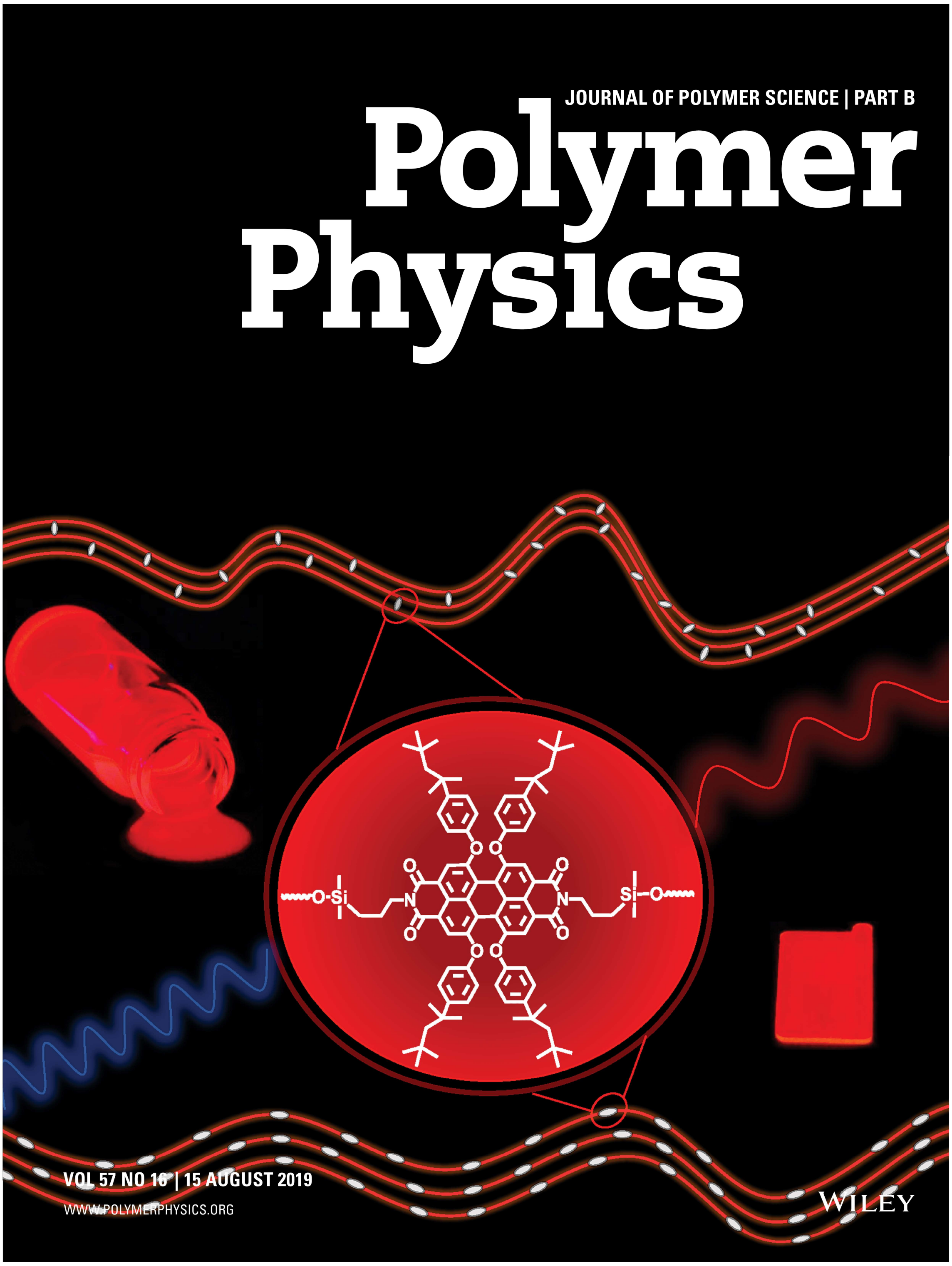

JOURNAL OF POLYMER SCIENCE | PART B

Polymer Physics

VOL 57 NO 16 | 15 AUGUST 2019

WWW.POLYMERPHYSICS.ORG

WILEY

On page 1062, Steinbrück and Kickelbick report the preparation of perylene polysiloxanes and their embedding into an LED HRI encapsulation resin. An allyl functionalized perylene diimide was covalently integrated linearly into a polyphenylmethylsiloxane backbone and as a cross-linking agent between polyphenylmethylsiloxane chains by hydrosilylation reactions forming liquid and highly fluorescent polymer gels. The applied synthetic methods avoid dye aggregation, leading to enhanced incorporable dye concentrations. Added to a thermally curable polysiloxane resin, fluorescent encapsulants with a solid and flexible consistency, uniform dispersion of the dyes, adjustable mechanical properties, and steady quantum yields can be formed, stabilizing the dye molecules ideal for the use in optoelectronic applications such as LEDs or LSCs.

Perylene Polyphenylmethylsiloxanes for Optoelectronic Applications

Nils Steinbrück, Guido Kickelbick

Inorganic Solid State Chemistry, Saarland University, 66123, Saarbrücken, Germany
Correspondence to: G. Kickelbick (E-mail: guido.kickelbick@uni-saarland.de)

Received 1 May 2019; revised 5 July 2019; accepted 12 July 2019; published online 25 July 2019
DOI: 10.1002/polb.24861

ABSTRACT: The incorporation of fluorescent organic dyes in an encapsulating matrix represents a route to generate stable and processable materials for optoelectronic devices. Here, we present a method to embed perylene dyes into a high refractive index (HRI) polysiloxane matrix applying an allyl functionalized perylene dye and hydrosilylation chemistry. In a first approach, the dye molecules were covalently integrated into the backbone of linear polyphenylmethylsiloxane chains. The fluorescent and liquid polymers were synthesized with molecular weights from 5660 up to 8400 g mol^{-1}. In a second approach, the dye itself was used as a cross-linking agent between linear polyphenylmethylsiloxane chains. These preformed fluorescent batch polymers are liquids with dye concentrations between 0.025 and 8 wt %. The applied synthetic methods incorporated the dye covalently into the polymer structure and avoided the crystallization of the dye molecules and thus the formation of excimers, which would reduce the optical emission. The resulting products can be easily incorporated into curable commercially available HRI polyphenylmethylsiloxane resins. The formed materials are ideal LED encapsulants with a solid and flexible consistency, a uniform dispersion of the dyes, and adjustable mechanical properties, realized by changing the amount of perylene polymers. Further properties of the obtained materials are thermal stabilities up to 478 °C, quantum yields larger than 0.97, and high photostabilities. Thus, the covalent integration of dyes into polyphenylsiloxane structures represents a possible route for the stabilization of the organic dyes against the extreme irradiance and thermal conditions in LED applications. © 2019 The Authors. *Journal of Polymer Science Part B: Polymer Physics* published by Wiley Periodicals, Inc. J. Polym. Sci., Part B: Polym. Phys. **2019**, *57*, 1062–1073

KEYWORDS: LED; optoelectronics; perylene; polysiloxane; silicone

INTRODUCTION Organic alternatives for inorganic rare earth containing conversion materials in light emitting diodes (LEDs) are an object of present research.[1–4] In these applications, the organic dyes should substitute traditional rare earth containing conversion compounds, such as $Y_3Al_5O_{12}$:Ce^{3+}, $Lu_3Al_5O_{12}$:Ce^{3+}, $CaAlSiN_3$:Eu^{2+}, $(Ba,SrCa)_2Si_5N_8$:Eu^{2+}, or β-sialon:Eu^{2+}.[5–13] One of the major challenges in the targeted materials is the solubility and stability of the organic dyes in the matrix, which can be improved by a tailored design of the matrix polysiloxane. Organic dye-based converters are also attractive for clean and renewable energy generating applications, such as new efficient materials for photovoltaics and luminescent solar collectors (LSC). Quite stable and promising candidates for both types of applications are perylene diimide derivatives.[14–20] The difference in the two mentioned applications are the irradiance conditions. While the irradiance in LEDs can be larger than 500 mW mm^{-2}, materials in photovoltaics and LSCs have only to withstand 100 mW cm^{-2} under standard testing conditions.[21,22] Requirements for organic dyes and their matrices in these optoelectronic applications are high quantum yields as well as high thermal and photophysical stabilities, which are both necessary for improved lifetimes of the devices.[2–4,23–29] Often used substrates for the integration of perylene dyes are poly(methyl methacrylates) and epoxy-based polymer materials.[21,30–33] The physical or covalent integration of perylene diimide derivatives into various types of polymers can lead to improved materials properties.[15,17,18,34–37] Examples for matrices in which the fluorescent dyes were already successfully incorporated are polystyrene and polydimethylsiloxanes.[38–43]

The chemical inertness of polysiloxanes, their high thermal stabilities, high transparencies, and tunable refractive indices by side group substitution in combination with an incorporation of organic fluorescence dyes makes them excellent materials for an optimization with focus on dye stability.[31–33] The integration of the commercially available perylene dye Lumogen®F Red

Additional Supporting Information may be found in the online version of this article.

305 (LG305) into low refractive index (LRI) polysiloxanes for LSC applications revealed that the integrated light output of the samples correlates with an increased dye concentration up to 0.01 wt %.[30] At concentrations larger than 0.05 wt % the efficiency decreases significantly. The same results were found for the quantum yield (QY) of LG305 in another LRI polysiloxane for LED applications.[1] The QY started to decrease at LG305 concentrations ≥0.05 wt % due to the low solubility and consequent precipitation of LG305 in polydimethylsiloxanes. In our previous work, we were able to show that curable phenyl group containing high refractive index polysiloxanes (HRI) allow higher concentrations (≥0.3 wt %) of the dyes with constant high quantum yields and extended stabilities of covalently and non-covalently bonded perylene-based dyes.[1] One of the main reasons for this constant quantum yield and dramatically reduced crystallization is the separation of dye molecules due to the sterically demanding polymer matrix structure and due to the direct covalent bonding of the dye molecules to this structure.

An integration of organic dye molecules into a linear polyphenylsiloxane backbone or cross-linked between polyphenylsiloxane chains separates the molecules locally. A subsequent covalent incorporation of these liquid perylene containing polymers into a heat curable polysiloxane resin leads to a solid and flexible material in which high dye concentrations can be incorporated and crystallization is inhibited. Additionally, increasing the phenyl group concentration or incorporating cross-linked siloxanes to a curable polymer resin can lead to enhanced gas barrier properties and thus decreases oxygen caused degradation phenomena.[1,44,45] While linear and cross-linked polymers with perylene derivatives incorporated have already been published, the resulting materials are not suitable for a subsequent covalent integration into a curable matrix system by hydrosilylation.[39,40,46,47]

In the presented study, the allyl group containing perylene diimide dye FC546 was used to synthesize two different perylene polysiloxanes with various dye concentrations in the backbone of a polymethylphenylsiloxane (PMPS) and cross-linked to the pendant hydride groups of a methylhydrosiloxane-phenylmethylsiloxan copolymer. Both polymer classes were synthesized by a platinum catalyzed hydrosilylation reaction. By changing the ratio of the hydride and vinyl terminated PMPS precursors the chain length was modified systematically. Subsequently, the liquid perylene polymers were covalently integrated in a thermally curable phenyl containing HRI polysiloxane resin.

EXPERIMENTAL

Materials

Polyphenylmethylsiloxane hydride terminated (*PMS-H03*, Gelest Inc., Morrisville, PA). polyphenylmethylsiloxane vinyl terminated (*PMV-9925*, Gelest Inc.), (45–50% methylhydrosiloxane)-phenylmethylsiloxan copolymer hydride terminated (*HPM-502*, Gelest Inc.), the platinum carbonyl cyclovinylmethylsiloxane complex (*Ossko-Catalyst*, 1.85–2.1% Pt in vinylmethylcyclosiloxane, Gelest Inc.) and the commercially available, curable *OE6630* polysiloxane resin [Dow(1), Dow Corning Inc., Midland, MI] were used as received without any further purification (Scheme 1). The Dow(1) two component resin contains a Si-H and a Si-vinyl component.[1] It is thermally curable by thermal treatment of the mixed components. The curing process is a platinum catalyzed hydrosilylation. The allyl functionalized organic dye FC546 was provided by BASF SE and was also used as received. The synthesis of FC546 was already published in a previous work.[1] FC546 contains *N,N′*-diallyl units which permit a covalent integration into the polysiloxane backbone or network *via* hydrosilylation. Four 2,4,4-trimethylpentan-2-yl phenoxy units in *bay position* were introduced to increase the solubility in the phenyl containing polymers and in organic solvents like toluene (Scheme 1). The emission maximum is detected at 602 nm (16,611 cm^{-1}), the excitation maximum is detected at 574 nm (17,421 cm^{-1}) in toluene (Fig. S1). A local excitation maximum is detected at 450 nm (22,222 cm^{-1}) caused by the substituents in bay position. The precursor's purity was characterized by NMR and FTIR spectroscopy (Figs. S2-S10).

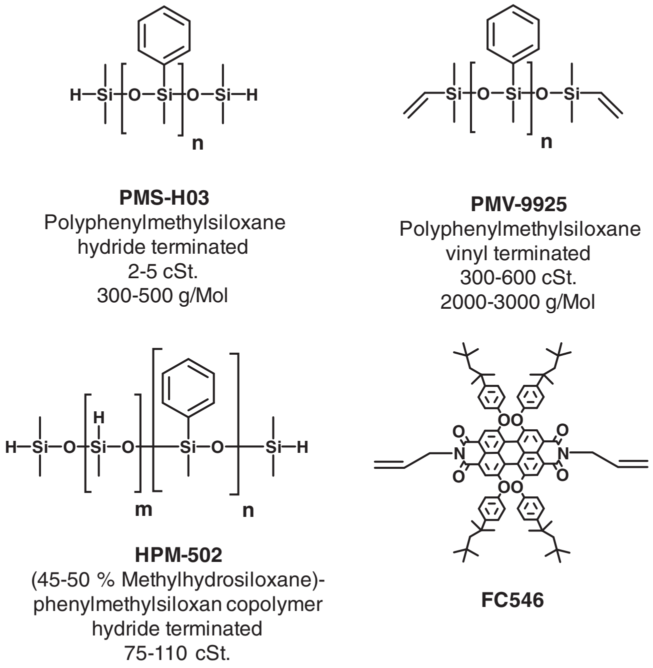

SCHEME 1 Structures, names, abbreviations, and important properties of the polymer and dye precursors.

Instrumentation

Fourier transformed infrared spectra (FTIR) were recorded in total reflectance mode on a Vertex 70 spectrometer (Bruker Corporation, USA) from 4500–400 cm^{-1} with a resolution of 4 cm^{-1} increment and 10 scans averaged. UV–vis transmission measurements were performed on a Lambda 750 instrument (Perkin Elmer Inc., USA) equipped with a 100 mm integration sphere from 700 to 350 nm with a 2 nm increment and 0.2 s integration time. Fluorescence spectroscopy was performed applying a FluoroMax 4 Spectrofluorometer (Horiba Scientific, Japan) with an excitation wavelength of 450 nm and an emission wavelength of 630 nm. The absolute photoluminescence quantum yields and the emission spectra were measured in a Quantaurus C11347-11 integration sphere setup (Hamamatsu Photonics, Japan) with a xenon high-pressure lamp and a multichannel analyzer at 450 nm excitation wavelength. NMR spectra were recorded with an Avance III 300 MHz spectrometer and an Avance III HD 400 MHz spectrometer (Bruker Corporation, USA) at 300.13/400.13 MHz for ^{1}H NMR and at 59.63/79.49 MHz for ^{29}Si NMR. All NMR samples were prepared in chloroform-D ($CDCl_3$). SEC measurements were performed with concentrations of 2 g l^{-1} sample in THF applying a PSS-SDB-1000 Å and a PSS-SDB-100000 Å column with 1 ml min^{-1} and a RI-Shodex and a UV-Waters 2487 detector. In a further experiment, we applied a setup with sample concentrations of 4 g l^{-1} in THF using a PSS-SDV-1000 Å or a PSS-SDV-10000 Å column with 1 ml min^{-1} and a RI-SECurity^2 and a UV-SECurity^2 detector. Thermogravimetric measurements were carried out with a TG209 F1 Libra thermomicrobalance (Netzsch-Gerätebau GmbH, Germany) applying a heating rate of 10 K min^{-1} up to 250 or 800 °C with gas flux of N_2/O_2 of 20 ml min^{-1} each. Differential scanning calorimetry was performed with a Netzsch DSC 204 F1 Phoenix calorimeter with aluminum crucibles with pierced lids under nitrogen (100 ml min^{-1}) with a heating rate of 5 K min^{-1} from −40 to 400 °C. Hardness measurements were performed using a Sauter HBA-100 Shore A durometer (Sauter GmbH, Germany). A self-constructed fiber coupled 450 nm wavelength illumination system with 710 mW LEDs (6 × LDW5SN) was used as irradiation source for photostability experiments.

Quantum Yield and Self-Absorption Coefficients

For the quantification of dye stability and efficiency after the integration of the perylene polymers to a curable polysiloxane resin the absolute quantum yield of all solid samples has been measured before and after curing, as well as after a post-curing procedure. In these experiments, solid samples (7 × 7 × 1 mm) were measured in an integration sphere setup in reflectance mode with an excitation wavelength of 450 nm. From the quantum yield emission spectra the self-absorption coefficients were determined. Therefore, a cured sample of Dow(1) with a very low concentration of FC546 (15 ppm dye by weight) with virtually zero self-absorption was prepared. The emission spectra of the samples were scaled by a fit to the zero self-absorption spectrum leading to a normalization in an area, which is not effected by self-absorption. The quality of the fit was verified by Pearson's chi squared test. The procedure was already described in literature in more detail.[1,48,49]

Preparation

The covalent integration of FC546 into the polymer backbone (P-FC546 series) was performed by mixing phenylmethylpolysiloxane PMS-H03 and PMV-9925 in variable ratios before adding the dye (Scheme 1). The cross-linking integration of FC546 into HPM-502 (OPSB-FC546 series) requires no premixing (Scheme 2). A stock solution of FC546 was used (0.1 wt %, toluene) to add a defined amount of dye to the polymers (m(polymer +dye) = 500 mg for each sample). Toluene was added to increase the total volume of solvent to 5 ml. Ossko-catalyst was diluted (0.18% Pt in xylene) and added (2 ppm Pt[0] referred to the product mass) to the mixture which was stirred at 100 °C for 24 h. Afterwards the solvent was removed under reduced pressure. The liquid products are denominated P-FC546 for the linear polymers and OPSB-FC546 for the cross-linked polymers.

For the subsequent integration of P-FC546 or OPSB-FC546 into the Dow(1) resin the two Dow(1) components A and B were premixed as specified by the manufacturer (4/1). The perylene containing polymers were added to the mixture respectively and gas was removed under reduced pressure (4 mbar, >30 min) before casting the mixture into PTFE (30 × 10 × 1 mm) or aluminum molds (8 × 2 mm). The samples are denoted by the name of the commercial resin Dow(1), the respective dye integrated perylene polysiloxanes and the final dye concentration in the perylene polysiloxanes in % and in the cured resin in ppm by weight.

RESULTS AND DISCUSSION

New polysiloxanes were synthesized by covalent attachment of the perylene dye to different polymer precursors. In the first precursor, the allyl-modified dye molecules were integrated linearly into the polymer by hydrosilylation with α,ω-Si-H-group containing polysiloxanes. The second precursor polymer was prepared by cross-linking the polysiloxane chains with the dye molecules by hydrosilylation of pendant Si-H groups in the linear polymer chains. Both methods result in liquid polymer structures in which the integrated dye molecules are separated from each other, which cause a reduced possibility of stacking phenomena, excimer formation, and solubility problems in the final polysiloxanes matrix. The influence of the various bonding modes as well as the final polymer structure on the dye properties was studied.

Linear Perylene Polysiloxanes

The linear polysiloxanes were prepared by using a hydride terminated polyphenylmethylsiloxane (PMS-H03) and a vinyl terminated polyphenylmethylsiloxane (PMV-9925). Applying a

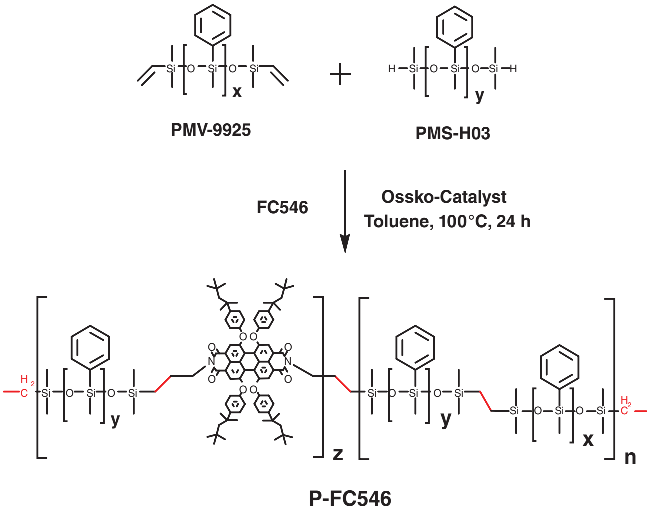

SCHEME 2 Synthesis of P-FC546 perylene polysiloxane by hydrosilylation of a vinyl and a hydride terminated precursor. The FC546 dye is part of the polymer backbone due to missing pendant hydride groups. [Color figure can be viewed at wileyonlinelibrary.com]

platinum catalyst the terminated Si-H and Si-vinyl groups start to form C-C single bonds leading to longer chains. By adding small amounts of the FC546 dye, the dye can also react in the hydrosilylation reaction and thus, was also incorporated into the formed polymer backbone (Scheme 2).

Cross-linked Perylene Polysiloxanes

We investigated a second route to incorporate the FC546 dye covalently in a liquid polysiloxane. In this case, a polymethylhydrosiloxane-phenylmethylsiloxane copolymer with pendant and terminal hydride atoms was used as precursor (HPM-502). Applying a platinum catalyst the Si-H groups start to form C-C single bonds with the dye molecules (Scheme 3).

Due to the pendant Si-H groups, the precursor polymer chains can be cross-linked with each other. The resulting products are still liquid and denoted as OPSB-FC546. In these studies, only one polymer precursor was used and allowed the systematic investigation of the effect of dye concentration. The synthesized polymers are denoted with OPSB-FC546 X% with X = 0.05, 0.1, 1, and 8. The highest concentrated sample with 8 wt % dye covalently incorporated was only prepared for a better detection in IR and NMR spectroscopy.

Precursor Incorporation in Curable Polysiloxane Resin

The synthesized perylene polysiloxanes are not suitable for a direct use in optoelectronics because they are still liquids. Optoelectronic suitable solid materials were obtained by a subsequent addition of the polymers to a thermally curable, two component polysiloxane resin incorporating 100 ppm dye in the final cured sample (Fig. 1). In applications in which high temperatures are predominant at working conditions, polysiloxane resins are subject to post-curing processes.

This is the reason why the absolute quantum yield and the hardness (Shore A) of the samples were determined for both cases, directly after preparation of the samples and after a post-curing process (200 °C, 48/120 h). The corrected quantum yields and the self-absorption coefficients were calculated from the absolute quantum yield emission spectra, respectively (see Supporting Information).[1,48,49]

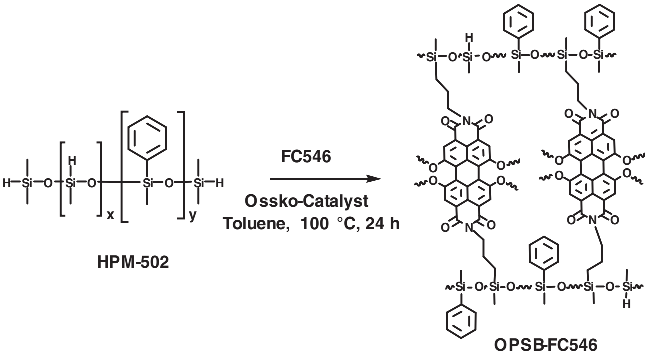

SCHEME 3 Synthesis of OBSB-FC546 perylene polysiloxane by hydrosilylation of a polysiloxane with hydride pendant and terminated groups with FC546. The FC546 dye is cross-linking the polymer chains.

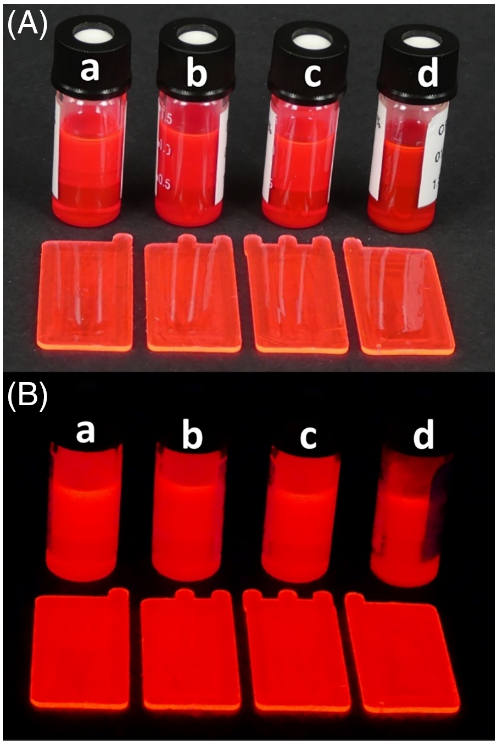

FIGURE 1 (A) Image of the liquid perylene polysiloxanes (a) P2-FC546, (b) P3-FC546, (c) P4-FC546, and (d) OPS-B FC546 0.1% and casted specimen of the same precursor polymers mixed with the OE6630 resin and cured subsequently for 4 h at 150 °C below. (B) Samples shown in (A) excited with a 450 nm light source. [Color figure can be viewed at wileyonlinelibrary.com]

Under working conditions, the local temperature at the light emitting InGaN chip of a LED for example can reach up to 150 °C and the irradiance can reach values >500 mW mm^{-2} (at λ = 450 nm). The dye-incorporated matrices need to withstand these extreme conditions to ensure a long and stable performance. For a simulation of these working conditions a variety of cured samples was exposed to light (450 nm, 710 mW LEDs (6 × LDW5SN) and other samples were exposed to high temperature (200 °C, air) for several hours. Transparency measurements by optical spectroscopy can detect a change in color, which is usually caused by dye degradation due to light exposition. The influence of the thermal treatment was determined by measuring changes in quantum yield. Additionally changes in the cured polymer resin structure due to the incorporation of the perylene polymers were investigated by thermogravimetric (TG) and differential calorimetric measurements (DSC).

Chain Length Variation Chain Length Variation of Linearly Incorporated Dye Polymer with Constant Dye Concentration

By changing the hydride to vinyl ratio of the precursors with a constant dye concentration of 0.1 wt % chain length of the perylene polymers were modified. The nomenclature of the samples was chosen to differentiate between the samples

TABLE 1 Composition of the different samples with the FC546 dye in the PX-FC546 polymer

PX-FC546 0.1%	n(PMS)/ n(PMV)	m(PMS)/g	m(PMV)/g	c(FC546)/wt %
5	1/1	0.0689	0.4310	0.1
4	1/0.8	0.0833	0.4166	0.1
3	1/0.6	0.1052	0.3947	0.1
2	1/0.5	0.1212	0.3788	0.1

(Table 1). SEC, FTIR, and ^{1}H NMR spectra were measured directly after the synthesis. The FTIR spectra show the anticipated vibration bands for phenyl containing polysiloxane type polymers (Fig. 2).[50–53]

Specific aromatic vibration bands due to phenyl side groups at 3045, 3070 [ν(C-H)$_{AR}$]; 1488, 1429 [ν(C=C-C)$_{AR}$]; and 725, 694 [δ(C-H)$_{AR}$] cm^{-1} can be detected next to the silicon oxygen vibrations at 1014, 1048, and 1120 cm^{-1} [ν(Si-O-Si)].

Two additional vibration bands according to the Si-H bond at 2125 cm^{-1} [ν(Si-H)] and 905 cm^{-1} [ρ(Si-H)] are also present. These bands can be used to differentiate between the samples. At a PMS/PMV ratio of 1/1 no Si-H vibrations can be detected while a decreasing vinyl concentration leads to an increasing number of unreacted Si-H groups. This agrees with the assumption that a higher concentration of the hydride terminated PMS-H03 leads to a higher concentration of Si-H terminated reaction products and to lower chain lengths.

An increase of molecular weight (M_w) compared with the precursor polymers are caused by the hydrosilylation reaction. The stepwise increase of the ratio of the hydride and vinyl terminated precursor polymers leads to an increase of M_w as expected (Table 2). The product elugrams show that there are still traces of unreacted polymeric educts. The polydispersity is larger than 1.7 but very similar for all measured samples and in the same range like other polysiloxanes synthesized by hydrosilylation or ring-opening polymerization with values from 1.2 to 3.5.[54–57]

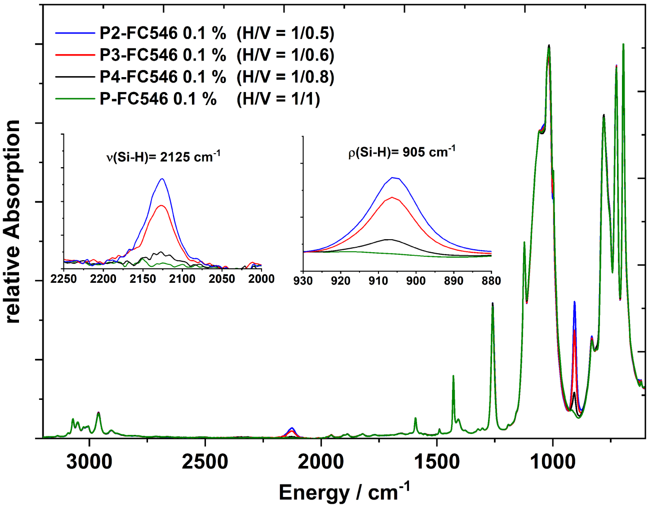

FIGURE 2 FTIR spectra of P-FC546 and the PX-FC546 - 0.1% series with x = 2, 3, 4. [Color figure can be viewed at wileyonlinelibrary.com]

TABLE 2 Molecular weight M_w and polydispersity index D for various polymers

Sample	M_w/g mol^{-1}	D
PMS-03	420/400[a]	1.1
PMV-9925	2500/2500[a]	2.4
P4-FC546 0.1%	8400	1.9
P3-FC546 0.1%	6080	1.7
P2-FC546 0.1%	5660	1.7

[a] M_w taken from the manufacturer data sheet.

The ^{1}H NMR spectra show all anticipated chemical shifts of the polymers at 7.86–6.88 (m, Phenyl-H) and 0.62 – −0.26 ppm (m, Si-CH$_3$) (Fig. S11). Additionally, small signals of the incorporated dye can be detected at 1.37 (s, FC546) and 0.79 ppm (s, FC546) next to impurities at 2.00 (s), 1.55 (s, water), and 1.27 ppm (s). The intensity of the chemical shift at 4.76 ppm according to the hydrogen atom in the Si-H group is decreasing from P2-FC546–0.1% to P5-FC546–0.1% due to the decrease of unreacted Si-H groups. This result corresponds with the FTIR data shown before. The spectroscopic data and chromatographic data prove the successful synthesis of linear polymers with different chain length and the covalent integration of FC546.

Variation of Dye Concentration in Linear Dye Incorporated Polymers with Equal Chain Length

The influence of the polymer chain length and the covalent bonding of the dye was investigated by maintaining the hydride to vinyl ratio of the precursors constant (1/0.5 [P2-FC546]) and increase the dye concentration from 0.025 to 1 wt % stepwise (Table 3). The FTIR spectra show the anticipated vibration bands for phenyl containing polysiloxane type polymers as described and assigned in the section before (Fig. 3).[50–53]

The two vibration bands according to the Si-H bond at 2125 cm^{-1} [ν(Si-H)] and 905 cm^{-1} [ρ(Si-H)] show a decrease of intensity, which is an indication of the covalent incorporation of

TABLE 3 Composition of the different samples with the FC546 dye in the P2-FC546 polymer

P2-FC546 X %	m(FC546)/mg	n(FC546)/μmol	c(FC546)/%
0.025	0.125	0.097	0.025
0.05	0.25	0.194	0.05
0.1	0.4	0.388	0.1
0.25	1	0.971	0.25
0.5	2.5	1.941	0.5
1.0	5	3.883	1.0

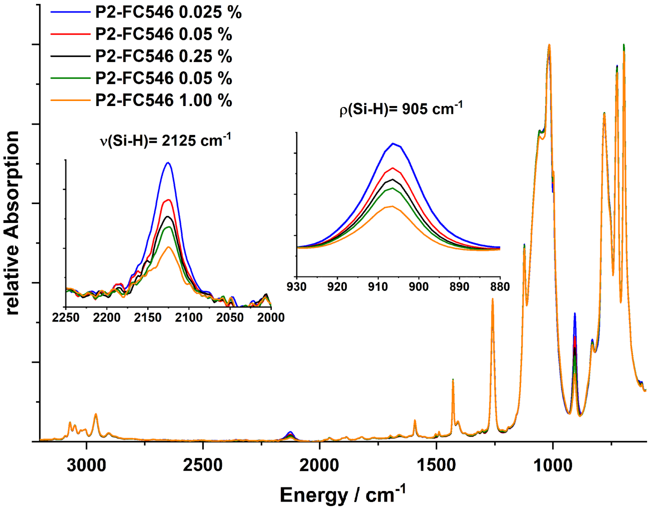

FIGURE 3 FTIR spectra of the P2-FC546 - X% series with X = 0.025, 0.05, 0.25, 0.5, and 1.0. [Color figure can be viewed at wileyonlinelibrary.com]

the FC546 dye molecules into the polymer backbone by the hydrosilylation reaction. If there were no attachment to the polymer, the intensity would be equal for every sample.

The decrease of hydride vibration bands intensity is directly correlated to the increase in dye concentration. As a result, a higher dye concentration should also lead to slightly longer polymer chains if the dye is not attached as an end group. By comparing the SEC data, no systematic changes in chain lengths can be detected due to the change of dye concentration (Table S9), which is most likely based on the low concentration of the dye and the possibility of attaching it as a polymer end group. Due to the high concentration of 1% dye in the sample P2-FC546 all chemical shifts of the incorporated FC546 dye can be detected in a much better resolution than in the lower concentrated sample P2-FC546 0.1% discussed before. FC546 shows two specific chemical shifts for the allyl functionalization caused by the methylene (5.12 ppm, 2H) and methine protons (5.93 ppm, 4H) (Fig. S10). Due to the covalent integration by hydrosilylation these shifts are not detectable in the perylene polymer anymore, which also verifies the covalent bonding to the polymer backbone (Fig. S12).

Cross-linking of Polymer Chains by Variations in Dye Concentration

By reacting the allyl groups FC546 with polymers with pendant hydride groups a cross-linked perylene polymer is formed (Table 4). The total mass of the polymer and the added dye was 500 mg for each sample, except for the high concentrated sample OPSB-FC546–8.0%, where the dye was weighted and directly added to the polymer instead of using a stock solution (see section 2). The FTIR spectra reveal the anticipated vibration bands for phenyl containing polysiloxane type polymers as described and assigned in the section before.[50–53] The two vibration bands according to the Si-H bond at 2160 cm^{-1} [ν(Si-H)] and 900 cm^{-1} [ρ(Si-H)] show no change of intensity at lower dye concentrations. At the highest concentration of 8% a significant increase occurs, due to the covalent attachment of the dye to the polymer structure (Fig. 4).

TABLE 4 Composition of the different samples with the FC546 dye in the OPSB-FC546 polymer

Sample	m(FC546)/mg	n(FC546)/μmol	c(FC546)/%
OPSB-FC546 - 0.1%	0.5	0.38	0.10
OPSB-FC546 -1.0%	5.0	3.88	1.00
OPSB-FC546 -8.0%	40.0	31.06	8.00

This missing intensity change of the Si-H vibration at low dye concentrations according to a covalent integration of FC546 is caused by the very high concentration of Si-H units in the polymer chain. In the synthesis of the P-FC546 polymers, the hydride terminated PMS-H03 contains two Si-H units per molecule. In the HPM-502 that is used for the OPSB-FC546 synthesis contains 45–50% of the polymer's silicon atoms attached to a pendant hydride atom. A reaction with a small amount of FC546 does not change the signal intensity significantly and measurable.

The ^{1}H NMR spectra of the sample OPSB-FC546–8.0% shows every anticipated chemical shifts of the polymer and the FC546 dye except the methylene and methine protons of the allyl groups of the dye. As described before, FC546 shows two specific chemical shifts for the allyl functionalization caused by the methylene (5.12 ppm, 2H) and methine protons (5.93 ppm, 4H). The HPM-502 polymer reveals no chemical shifts in this area. By just mixing an unspecific amount of FC546 and HPM-502, the sum spectrum of the corresponding chemical shifts can be observed (Fig. 5). After the hydrosilylation reaction of 8 wt % of FC546 with HPM-502 (OPSB-FC546 8% is formed), the methylene and methine proton chemical shifts of FC546 allyl groups disappeared and a new shift for the formed methylene proton of the C-C single bond is observed (1.49 ppm, 4H).

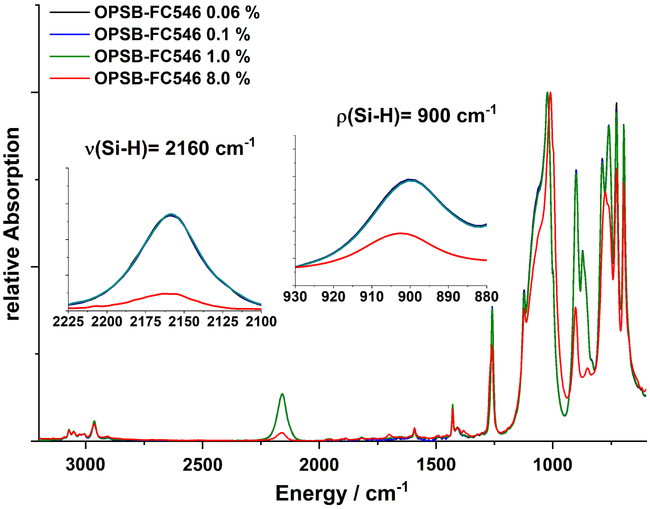

FIGURE 4 FTIR spectra of the OPSB-FC546 - X% series with X = 0.06, 0.1, 1.0, and 8.0. [Color figure can be viewed at wileyonlinelibrary.com]

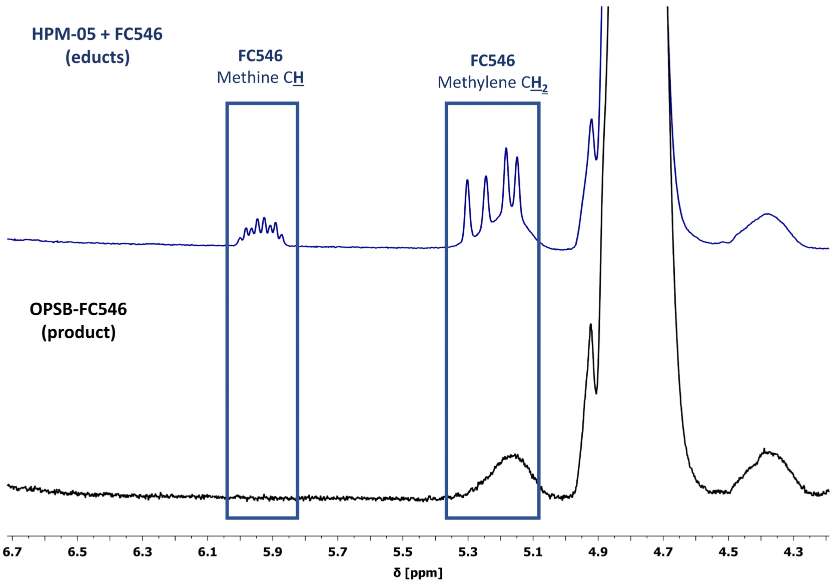

FIGURE 5 ^{1}H NMR spectra of OPS-B-FC546 8% before and after the hydrosilylation reaction measured in chloroform-D. [Color figure can be viewed at wileyonlinelibrary.com]

From the ^{1}H NMR spectra the percentage of phenyl groups was calculated for a quantitative comparison. Compared with the P-FC546 series with 38% phenyl groups the OPSB-FC546 samples contain only 29%. This is also caused by the high concentration of methylhydrosiloxane units of 45–50% in the OPSB-FC546 samples.

The SEC is calibrated with linear polystyrene standards. This leads to a significant inaccuracy by determining cross-linked polysiloxanes. Nevertheless, we tried to determine the M_w of one of the OPSB-FC546 samples exemplarily. The SEC of the linear OPSB precursor polymer shows M_w values of 1400 g mol^{-1} and a polydispersity index of 4.1. The OPSB-FC546–0.1% sample shows an M_w value of 13,470 g mol^{-1} and a polydispersity of 3.1 (SEC data and elugrams are part of the Supporting Information). The M_w of this OPSB-FC546–0.1% sample increases significantly (~10 times). This is another indirect proof of the expected cross-linking properties of FC546 when it is reacted to polymers with pendant hydride groups.

Integration of Perylene Polysiloxanes to a Curable Resin

A selection of the prepared perylene polysiloxanes were added to a commercially available, two component polysiloxane resin (Dow Corning OE6630 [Dow(1)]). Subsequently, the mixtures were cured according to the supplier's temperature profile to form solid samples containing 100 ppm dye, respectively. For the Dow(1)PX-FC546 0.1% - 100 ppm series with a constant dye concentration the amount of perylene polysiloxane added to the resin is 10 wt %. For the other perylene polymers with different dye concentrations incorporated the amount was adjusted to get 100 ppm dye in the cured samples (Table 5). The perylene polymers are completely mixable with the two Dow(1) components without any haze or precipitation. At working conditions in optoelectronic devices, especially in LEDs, high temperatures up to 200 °C affecting cured polysiloxane resin and the incorporated dyes by inducing a post-curing process. This is why the absolute quantum yield and the hardness (Shore A) of the samples were determined directly after preparation of the samples and after a post-curing process (200 °C, 48/120 h). For a further characterization of changes in

TABLE 5 Composition of the cured polymers from Dow(1) component A and the perylene polysiloxane precursors

Sample	m(Dow(1)-A)/g	m(Dow(1)-B)/g	m(Peryl. Polys.)/g	Phosphor conc./ppm
Dow(1)PX-FC546 0.1% - 100 ppm (X = 2, 3, 4, 5)	0.720	0.180	0.10	100
Dow(1)P2-FC546 0.025% - 100 ppm	0.480	0.120	0.40	100
Dow(1)P2-FC546 0.05% - 100 ppm	0.640	0.160	0.20	100
Dow(1)P2-FC546 0.25% - 100 ppm	0.768	0.192	0.04	100
Dow(1)P2-FC546 0.5% - 100 ppm	0.784	0.196	0.02	100
Dow(1)P2-FC546 1.0% - 100 ppm	0.792	0.198	0.01	100
Dow(1)OPSB-FC546 0.05% - 100 ppm	0.664	0.166	0.17	100
Dow(1)OPSB-FC546 0.1% - 100 ppm	0.720	0.180	0.10	100
Dow(1)OPSB-FC546 1.0% - 100 ppm	0.792	0.198	0.01	100

TABLE 6 The degradation temperatures T$_{95}$ of the samples

Sample	T$_{95}$/°C
Dow(1)	465
Dow(1)FC546 - 100 ppm	468
Dow(1)P2-FC546 0.025% - 100 ppm	433
Dow(1)P2-FC546 0.05% - 100 ppm	450
Dow(1)P2-FC546 0.1% - 100 ppm	474
Dow(1)P2-FC546 0.5% - 100 ppm	472
Dow(1)P2-FC546 1.0% - 100 ppm	470
Dow(1)P3-FC546 0.1% - 100 ppm	469
Dow(1)P4-FC546 0.1% - 100 ppm	472
Dow(1)OPS-B-FC546 0.1% - 100 ppm	478

the resin structure due to the incorporation of the perylene polymers FTIR spectra were measured and thermogravimetric as well as calorimetric measurements were performed.

Quantum Yield and Heat Treatment

The Dow(1)PX-FC546 0.1% - 100 ppm and the Dow(1)P2-FC546 X% - 100 ppm samples show no significant changes in the quantum yield (QY) compared with the quantum yield of the prepolymer samples (Fig. 6). This was expected because the dye concentration is low (100 ppm) and equal in every cured sample.

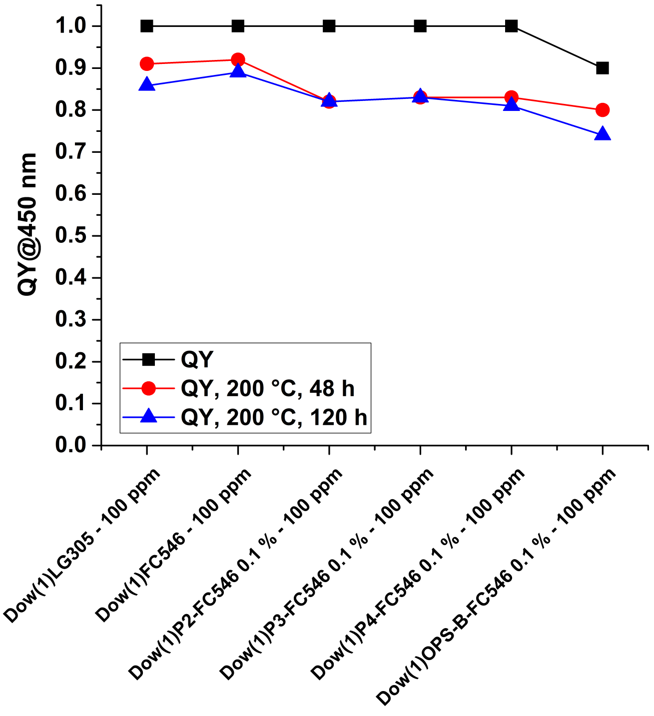

FIGURE 6 Absolute quantum yield of the cured Dow(1) samples with the PX-FC546 0.1% or the pure dye incorporated measured with an excitation wavelength of 450 nm directly after the synthesis, as well as after a first (200 °C, 48 h) and a second heat treatment (200 °C, 72 h). [Color figure can be viewed at wileyonlinelibrary.com]

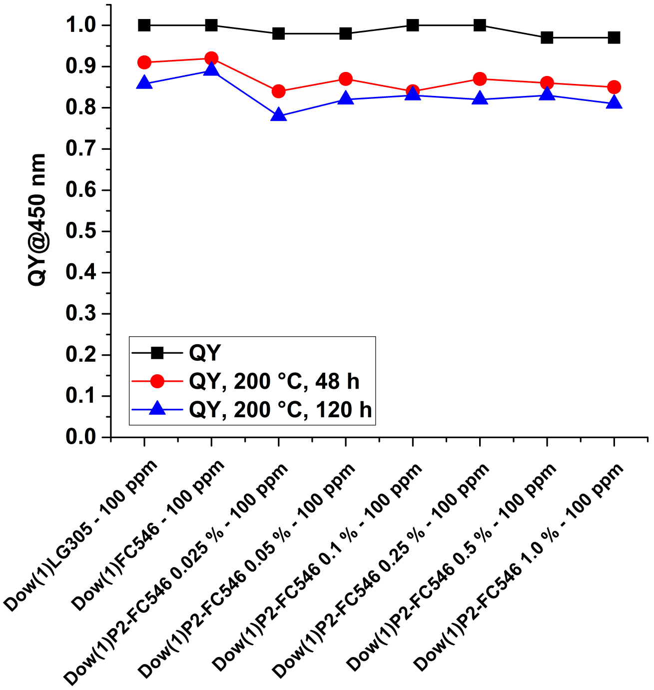

FIGURE 7 Absolute quantum yield of the cured Dow(1) samples with the P2-FC546 X% series or the pure dye incorporated measured with a excitation wavelength of 450 nm directly after the synthesis, as well as after a first (200 °C, 48 h) and a second heat treatment (200 °C, 72 h). [Color figure can be viewed at wileyonlinelibrary.com]

The differences in dye concentrations of the perylene polymer precursors do not affect the final QY either. In previous results, we already showed that the influence of the dye concentration to the QY in phenyl containing polysiloxanes is insignificant compared with only methyl containing polysiloxanes. This can be explained by the high solubility of the dye caused by a closer physicochemical compatibility of sterically demanding perylene molecules to phenyl containing polymers.[1]

The QY is above 0.97 for all samples. Neither the chain length of the perylene polysiloxane nor the concentration of the bonded dye molecules shows significant influences to the QY (Fig. 7).

The Dow(1)OPSB-FC546 X% - 100 ppm samples show a decrease in QY correlated to the increase of dye concentration from 0.95 (X = 0.05%) to 0.875 (X = 1%). In the P-FC546 compounds polymer chains separate the dye molecules. π-π-Interactions of dye molecules leading to quenching effects are less probable in these samples. Furthermore, the high concentration of phenyl side groups leads to a sterically shielding and of the dye units as shown in a previous paper.[1]

In the OPSB-FC546 polymers, the separation of the FC546 dye molecules is influenced by distribution of silicon hydride units. The molecules can be attached to directly neighboring silicon atoms, which would increase the possibility of dye–dye interactions. This is more probable with an increasing dye concentration as reported for perylene bridged ladder polysiloxane, synthesized by polycondensation, where an increased π-π stacking interaction at high concentrations is caused by the direct localization of the molecules next to each other.[47] As a consequence, a decrease in quantum yield is possible.

Again, we believe that the phenyl groups in the Dow(1) matrix decrease the π-π stacking probability of single dye molecules.[1,58,59] The phenyl units are able to interact with incorporated dyes core. The separation of the dye molecules and the dilution leads to a quantum yield increase. The QY of the isolated OPSB-FC546 1.0% (QY = 0.452) is 1.93 times lower compared with the diluted Dow (1)OPSB-FC546 1.0% - 100 ppm (QY = 0.875) sample. The QY of all measured samples decreased after the first post curing heat treatment (48 h, 200 °C). The highest decrease was detected for the Dow(1)PX-FC546 0.1% - 100 ppm series ≥18%.

After the second heat treatment (72 h, 200 °C) the decrease of QY is not significant for all samples. The slightly higher methyl group concentration of the OPSB-FC546 polymers has no impact on the temperature stability. The influence of the post-curing heat treatment to the dye–dye interaction or to the structural integrity of the dye molecules and the significantly higher dye stability in the Dow(1) matrix compared with the covalently or non-covalently bonded perylene dyes in curable non-phenyl containing polydimethylsiloxanes was discussed in former studies.[1]

The incorporation of the FC546 dye in a perylene polysiloxane before adding it to a curable polysiloxane resin does not change the dyes properties responsible for the high QY compared with a direct integration. The measured QY, the corrected QY, the self-absorption coefficients, and the emission spectra from the QY-measurements (λ_{ex} = 450 nm) are part of the Supporting Information. The self-absorption coefficient was calculated by using the emission spectra of a very low concentrated sample with virtually zero self-absorption (Dow(1)FC546–15 ppm) as described in literature.[1,48,49]

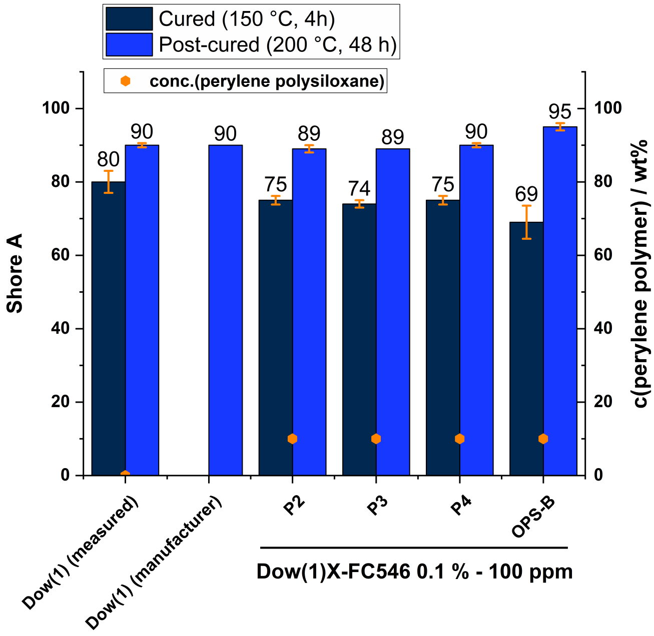

FIGURE 8 Shore A values of the cured Dow(1) samples with the linear perylene polymers PX-FC546 0.1% and OPS-B FC546 0.1% incorporated compared to the pure cured Dow(1) resin. [Color figure can be viewed at wileyonlinelibrary.com]

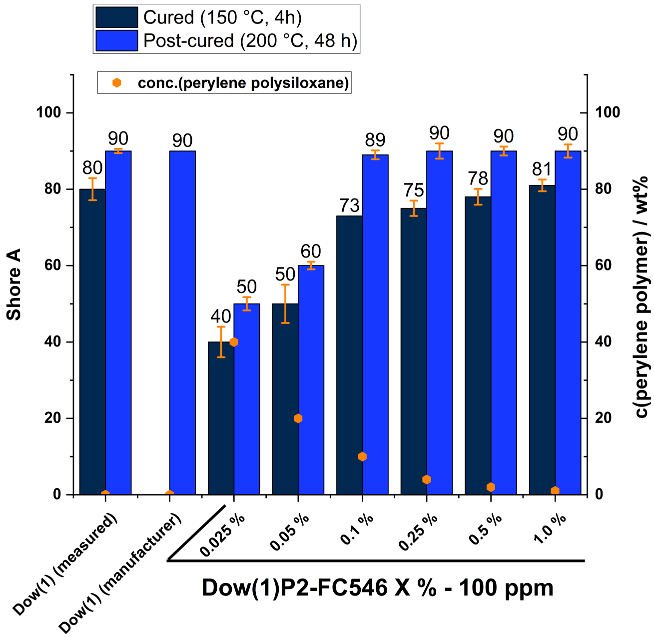

FIGURE 9 Shore A values of the cured Dow(1) samples with the linear perylene polymers P2-FC546 X% incorporated compared with the pure cured Dow(1) resin. [Color figure can be viewed at wileyonlinelibrary.com]

FTIR, Hardness, Thermal, and Calorimetric Investigations

Due to the addition of the perylene polysiloxane to the Dow (1) resins components a change in structure, respectively, material properties are expected. The stability of the cured materials was studied by detecting the T_{95} value in the TGA. To evaluate the different materials state of degradation the temperature at which the samples possess 95% of their original mass is defined as T_{95} value. Therefore, larger T_{95} values reveal higher thermal stability of the materials.

The mixing proportions, given by the manufacturer were retained, but the total number of polymer chains and reactive groups is increased by the perylene polysiloxane addition. By measuring the hardness of the cured samples directly after the curing procedure and after the additional post-curing process (120 h, 200 °C), conclusions about mechanical changes can be made (Fig. 8). The hardness of the Dow(1)PX-FC546 0.1% - 100 ppm series is not affected by the addition of 10 wt % of perylene polysiloxane compared with the pure Dow(1) sample (Shore A = 90). The Dow(1)OBSB-FC546 1% - 100 ppm sample shows a slight increase of hardness (Shore A = 95). The Dow(1) P2-FC546 X % - 100 ppm series show an increase of hardness with an increase of perylene polymer concentration (Fig. 9). The trend in hardness directly correlates with the thermogravimetric data and the degradation temperatures of the post-cured samples, respectively (Table 6).

All samples show a high T_{95} degradation temperature above 433 °C. The T_{95} of all samples with dye concentrations larger than 0.1 wt % dye in the perylene polysiloxane slightly higher than the pure Dow(1) matrix with an insignificant deviation of 6 °C (468–474 °C).

The lowest T_{95} values were measured for the Dow(1) P2-FC546 0.025% - 100 ppm (433 °C) and Dow(1)P2-FC546 0.05% - 100 ppm (450 °C) samples. The highest T_{95} value was observed for the Dow(1)OPS-B-FC546 0.1% - 100 ppm sample (478 °C). Comparable cross-linked structures like perylenediimide-bridged ladder polysiloxanes show lower T_{95} values of 430 °C.[47] The increases of hardness and degradation temperatures are not caused by the higher dye concentration but by the higher amount of perylene polysiloxane added to the Dow(1) matrix.

The hydride and vinyl terminated Dow(1)P2-FC546 polymers widen the actually closer-meshed network of the pure Dow (1) matrix (>10 wt %), which leads to a more flexible and less stable structure. Whereas the already cross-linked OBSB-FC546 perylene polysiloxane, with its additional pendant hydride atoms, is cross-linking the Dow(1) matrix furthermore, even in small amounts, which explains the increase of hardness and thermal stability. Additionally, due to the increased polymer and hydride concentration in the Dow(1)P2-FC546 X % - 100 ppm samples, respectively, the manufacturers curing conditions are insufficient, which makes a post-curing process necessary. This can be shown by FTIR of the samples. The vibration bands according to the Si-H bond at 2125 cm^{-1} [ν(Si-H)] and 905 cm^{-1} [ρ(Si-H)] are still present in the cured samples. No Si-H vibrations can be detected in the post-cured samples. The polymers are completely integrated into the resins structure (Figs. S16-S17).

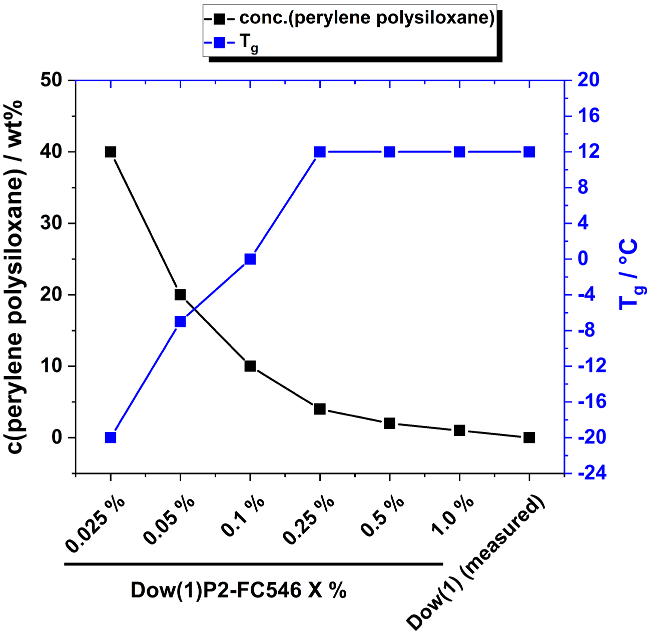

FIGURE 10 T_g values of the of the cured Dow(1) samples with the perylene polymers or the pure dye incorporated. [Color figure can be viewed at wileyonlinelibrary.com]

This interpretation agrees with the DSC data of the post-cured samples. The glass transition temperature (T_g) is directly correlated to the cross-linking degree of the polymer structure. Less cross-linked polymer chains lead to a decrease of the T_g value.[60–63] The lowest T_g and the lowest cross-linking degree consequently was measured for the Dow(1)P2-FC546 0.0025% - 100 ppm sample in which the highest amount of perylene polysiloxane is incorporated. A decrease of perylene polysiloxane concentration leads to an increase of T_g and cross-linking as expected (Fig. 10). All DSC measurements and T_g values are part of the Supporting Information.

As a result, the incorporation of the linear perylene containing polymers to a curable polysiloxane resin can be used to incorporate high concentration of organic dyes to the resin. At the same time, the hardness of the cured material, predefined by the manufacturer can be tuned and adjusted to a given purpose by changing the amount of linear polymer added to the resin without losing the high thermal stability of >400 °C. The change in hardness and T_{95} is a consequence of a decrease of cross-linking caused by the incorporation of the perylene polymers to the resin and was verified by DSC measurements. The high thermal stability and the adjustable flexibility make these materials very interesting for different molding, grafting, or dispensing methods valid for manufacturing optoelectronics or LSCs.

Photostability

The photostability of the FC546 dye is directly correlated to the decrease in absorbance caused by irradiation. Therefore, five samples were exposed to a high power density 450 nm light source with 710 mW LEDs (6 × LDW5SN, 0.45 mA [max.: 0.7 mA]) in a remote setup to evaluate their photostability under LED working conditions. The absorbance of the samples was

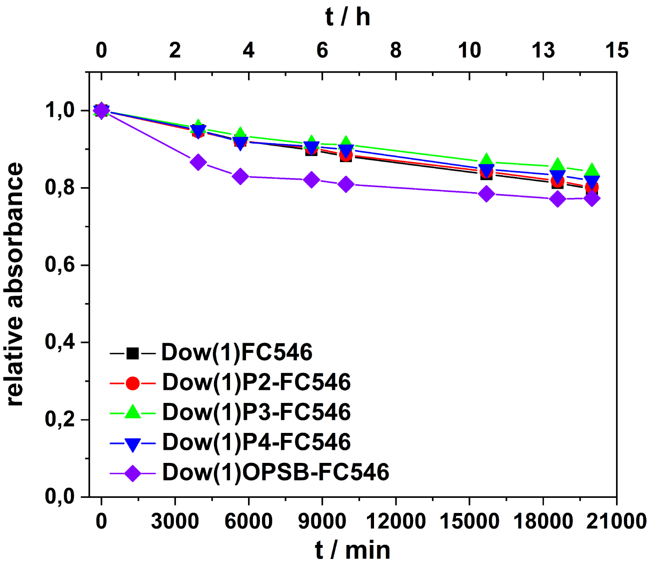

FIGURE 11 Relative absorbance of Dow(1)FC546 - 100 ppm, the Dow(1)PX-FC546 0.1% - 100 ppm series (X = 2, 3, 4) and Dow(1) OPSB-FC546 at different times measured during a light exposure with 450 nm light source. [Color figure can be viewed at wileyonlinelibrary.com]

determined periodically during the light exposure for 14 days by UV–vis spectroscopy with an integration sphere setup. Related to the absorbance at 450 nm the relative absorbance was calculated. A direct correlation between the dye degradation due to the exposure can be illustrated and compared by these values. The complete absorbance spectra for all measured samples are part of the Supporting Information (Figs. S43-S47).

For all samples, a decrease of absorbance occurs (Fig. 11). The decrease of the Dow(1)PX-FC546 0.1% - 100 ppm series is equal to the decrease of the Dow(1)FC546–100 ppm reference sample with the dye directly incorporated to the Dow(1) resin. Whereas the absorbance of the Dow(1)OPSB-FC546 0.1% - 100 ppm sample shows a larger decrease in the beginning of the irradiation. After a few days of irradiation, it approximates to the other samples relative absorbance. These results reveal that the photostability of the synthesized perylene polysiloxanes is not increased compared with a direct incorporated pure dye into a curable phenyl containing silicone resin. The slightly larger decrease of the absorbance of the cross-linked OPSB-FC546 sample at the beginning of the irradiation is not representative. The total number of methyl groups in this polymer is increased (Table 5) but the change in absorbance is not so significant compared with pure methyl containing polysiloxanes with equal dyes incorporated.[1]

Assuming a further linear decrease of absorbance for all samples a decrease of 50% of initial absorbance is expected after 40 days. This is still considerably less than the lifetime of commercially available high performance LEDs with inorganic conversion phosphors. For other optoelectronic applications, the irradiance, respectively, the power density of the exposed light is lower. For example, in solar cells a total irradiance of 100 mW cm^{-2} is used under standard testing conditions.[21,22] Considering the experimental setup for the irradiation the estimated irradiance is ~700 mW cm^{-2}. Because the degradation of the dye directly correlates with the irradiance a much higher photostability for LSCs or solar cell applications is expected. A further investigation of the applicability in these kinds of applications is not part of this publication for operational reasons.

CONCLUSION

The *N,N'*-diallyl functionalized perylene diimide FC546 was used to synthesize two different classes of perylene polysiloxanes for a subsequent integration in a curable phenyl containing polysiloxane resin. First, the dye was incorporated into the polymer backbones of phenylmethylpolysiloxanes forming P-FC546 compounds. By changing the ratio of the hydride and vinyl terminated PMPS precursors and holding the dye concentration constant (0.1 wt %) samples with different chain length were synthesized. A second series with different dye concentrations was realized as well. Another polymer was prepared with the dye cross-linked to pendant hydride groups of a methylhydrosiloxane-phenylmethylsiloxane copolymer called OPSB-FC546. Both polymers were synthesized by a platinum catalyzed hydrosilylation reaction. The highest dye concentration covalently incorporated was 8 wt %. The formation of different polymers and the covalent integration of the dye were proven by spectroscopic methods. Much higher dye concentrations can be realized compared with other polysiloxane substrates without precipitation and without using organic solvents due to the integration of the dye into the polymer structure. The perylene polysiloxanes were integrated into a phenyl containing HRI polysiloxane resin. The absolute quantum yield of the derived samples is >0.97 and is decreased slightly by a subsequent post-curing process. The hardness of the samples does not change for small amounts of the linear P-FC546 polymers added to the resin. An increased amount causes a tunable decrease of hardness, due to a widened network. At the same time the thermal stability decreases quantified by the T_{95} degradation temperature, which is still very high with >430 °C for all samples. These changes in hardness and degradation temperature are a consequence of a decrease of cross-linking caused by the incorporation of the perylene polymers to the resin and was verified by DSC measurements. Applying the cross-linked OPSB-FC546 polymer as a batch polymer in the final resins leads to a slightly increase of hardness and thermal stability, due to the higher cross-linking ability caused by pendant Si-H groups. The measured photostability of the dye is very high for a radiation with an estimated radiance of ~700 mW cm^{-2} at 450 nm wavelength compared with other organic fluorescence materials but still considerably less than the lifetime of commercially available high-performance LEDs with inorganic conversion phosphors. For significantly lower radiance applications like LSCs or solar cells a high application potential is expected.

ACKNOWLEDGMENTS

This research has been funded by the Federal Ministry of Education and Research (BMBF, Germany) in the project ORCA–Organic and rare earth reduced conversion materials for LED-based lightning (project number 03XP0050D). We would like to thank Svenja Pohl for experimental, Silvia Beetz and Stefan Blank for technical support, and Blandine Boßmann for SEC measurements.

REFERENCES

1 N. Steinbrück, M. Könemann, G. Kickelbick, *RSC Adv.* **2018**, *8*, 18128.

2 H. J. Kim, J. Y. Jin, Y. S. Lee, S. H. Lee, C. H. Hong, *Chem. Phys. Lett.* **2006**, *431*, 341.

3 L. Zhang, B. Li, B. Lei, Z. Hong, W. J. Li, *Luminescence* **2008**, *128*, 67.

4 G. Griffini, L. Brambilla, M. Levi, M. Del Zoppo, S. Turri, *Sol. Energy Mater. Sol. Cells* **2013**, *111*, 41.

5 Z. Xia, Q. Liu, *Prog. Mater. Sci.* **2016**, *84*, 59.

6 T. Jüstel, H. Nikol, C. Ronda, *Angew. Chem. Int. Ed.* **1998**, *37*, 3084.

7 C. Feldmann, T. Jüstel, C. R. Ronda, P. J. Schmidt, *Adv. Funct. Mater.* **2003**, *13*, 511.

8 C. R. Ronda, *J. Alloys Compd.* **1995**, *225*, 534.

9 S. Ye, F. Xiao, Y. X. Pan, Y. Y. Ma, Q. Y. Zhang, *Mater. Sci. Eng. R. Rep.* **2010**, *71*, 1.

10 M. Born, T. Jüstel, *Chem. Unser Zeit* **2006**, *40*, 294.

11 P. Schlotter, R. Schmidt, J. Schneider, *Appl. Phys. A Mater. Sci. Process.* **1997**, *A 64*, 417.

12 Y. N. Arukawa, I. N. Iki, K. I. Zuno, M. Y. Amada, Y. M. Urazaki, T. M. Ukai, *Jpn. J. Appl. Phys.* **2002**, *41*, 371.

13 R.-J. Xie, N. Hirosaki, H.-L. Li, Y. Q. Li, M. Mitomo, *J. Electrochem. Soc.* **2007**, *154*, J314.

14 D. Zaremba, R. Evert, J. Kielhorn, F. Jakobs, R. Caspary, W. Kowalsky, H.-H. Johannes, *Polym. Int.* **2018**, *67*, 1179.

15 J. Sol, V. Dehm, R. Hecht, F. Würthner, A. Schenning, M. Debije, *Angew. Chem. Int. Ed.* **2017**, *57*, 1030.

16 D. Pintossi, A. Colombo, M. Levi, C. Dragonetti, S. Turri, G. Griffini, *J. Mater. Chem. A* **2017**, *5*, 9067.

17 Y. Li, J. Olsen, K. Nunez-Ortega, W. J. Dong, *Sol. Energy* **2016**, *136*, 668.

18 X. Liu, Y. J. Kim, Y. H. Ha, Q. Zhao, C. E. Park, Y.-H. Kim, *ACS Appl. Mater. Interfaces* **2015**, *7*, 8859.

19 B. Balaban, S. Doshay, M. Osborn, Y. Rodriguez, S. A. Carter, *J. Lumin.* **2014**, *146*, 256.

20 G. Horowitz, *Adv. Mater.* **1996**, *8*, 242.

21 A. H. A. S. I. Ibrahim, S. Khyoon, A. Alrda, *Int. J. Curr. Eng. Technol.* **2015**, *5*, 2439.

22 M. Manikandan, N. Deepa Arun, P. Sivaranjini, M. Suresh, R. Ashok Kumar, *Int. J. Adv. Res. Electr. Electron. Instrum. Eng.* **2015**, *4*, 7628.

23 D. Di Martino, L. Beverina, M. Sassi, S. Brovelli, R. Tubino, F. Meinardi, *Sci. Rep.* **2014**, *4*, 4400.

24 M. Meneghini, L.-R. Trevisanello, G. Meneghesso, E. Zanoni, *IEEE Trans. Device Mater. Reliab.* **2008**, *8*, 323.

25 S. I. I. Chan, W. S. S. Hong, K. T. T. Kim, Y. G. G. Yoon, J. H. H. Han, J. S. S. Jang, *Microelectron. Reliab.* **2011**, *51*, 1806.

26 C. W. Hsu, C. C. M. Ma, C. S. Tan, H. T. Li, S. C. Huang, T. M. Lee, H. Tai, *Mater. Chem. Phys.* **2012**, *134*, 789.

27 Hang, C., Fei, J., Tian, Y., Zhang, W., Wang, C., Zhao, S., Caers, J. Proceedings of the 14th International Conference Electronic Packaging Technology (ICEPT), Dalian, China, August 11–14, **2013**, 1126–1129.

28 T. Li, J. Zhang, H. Wang, Z. Hu, Y. Yu, *ACS Appl. Mater. Interfaces* **2013**, *5*, 8968.

29 J. Kim, S. Yang, S. Kwak, Y. Choi, *J. Mater. Chem.* **2012**, *22*, 7954.

30 M. Buffa, S. Carturan, M. G. Debije, A. Quaranta, G. Maggioni, *Springer Ser. Mater. Sci.* **2014**, *190*, 247.

31 J. E. Mark, *Acc. Chem. Res.* **2004**, *37*, 946.

32 R. Wen, J. Huo, J. Lv, Z. Liu, Y. Yu, *J. Mater. Sci. Mater. Electron.* **2017**, *28*, 1.

33 Y. Yang, G. Xian, H. Li, L. Sui, *Polym. Degrad. Stab.* **2015**, *118*, 111.

34 V. Kamm, G. Battagliarin, I. A. Howard, W. Pisula, A. Mavrinskiy, C. Li, K. Miillen, F. Laquai, *Adv. Energy Mater.* **2011**, *1*, 297.

35 J. Van Herrikhuyzen, A. Syamakumari, A. P. H. J. Schenning, E. W. Meijer, *J. Am. Chem. Soc.* **2004**, *126*, 10021.

36 F. Würthner, Z. Chen, F. J. M. Hoeben, P. Osswald, C. C. You, P. Jonkheijm, J. V. Herrikhuyzen, A. P. H. J. Schenning, P. P. A. M. Van Der Schoot, E. W. Meijer, E. H. A. Beckers, S. C. J. Meskers, R. A. J. Janssen, *J. Am. Chem. Soc.* **2004**, *126*, 10611.

37 E. Kozma, M. Catellani, *Dyes Pigments* **2013**, *98*, 160.

38 F. Galeotti, W. Mróz, M. Catellani, B. Kutrzeba-Kotowska, E. Kozma, *J. Mater. Chem. C* **2016**, *4*, 5407.

39 M. Cazacu, A. Vlad, A. Airinei, A. Nicolescu, I. Stoica, *Dyes Pigments* **2011**, *90*, 106.

40 E. Dahan, P. R. Sundararajan, *Eur. Polym. J.* **2015**, *65*, 4.

41 Z. Ren, X. Cao, P. Xie, R. Zhang, Y. Ma, *Chem. Commun.* **2009**, 4079.

42 S. Wang, W. C. Lee, J. Y. Lee, S.-H. Hwang, *New J. Chem.* **2018**, *42*, 5059.

43 Z. Ren, P. Xie, S. Jiang, S. Yan, R. Zhang, *Macromolecules* **2010**, *43*, 2130.

44 M. Velderrain, In SPIE 8280, Advances in Display Technologies II **2012**; vol. *82800O*.

45 X. X. Shang, S. Duan, M. Zhang, X. Y. Cao, K. Zheng, J. N. Zhang, Y. M. Ma, R. B. Zhang, *RSC Adv.* **2018**, *8*, 9019.

46 D. Yao, B. Tuteja, P. R. Sundararajan, *Macromolecules* **2006**, *39*, 7786.

47 W. Fu, C. He, S. Jiang, Z. Chen, J. Zhang, Z. Li, S. Yan, R. Zhang, *Macromolecules* **2011**, *44*, 203.

48 T. S. Ahn, R. O. Al-Kaysi, A. M. Müller, K. M. Wentz, C. J. Bardeen, *Rev. Sci. Instrum.* **2007**, *78*, 2007.

49 L. R. Wilson, B. S. Richards, *Appl. Optics* **2009**, *48*, 212.

50 P. J. Launer, In *Silicon Compounds Register and Review*; B. Arkles (Ed.); Petrarch Systems, Inc.: Levittown, NY, USA, **1987**; pp. 100–103.

51 J. H. Lady, G. M. Bower, R. E. Adams, F. P. Byrne, *Anal. Chem.* **1959**, *31*, 1100.

52 J. Coates, In *Encyclopedia of Analytical Chemistry*; R. A. Meyers, Ed.; John Wiley & Sons Ltd.: Chichester, **2000**, pp. 10815-10837.

53 N. B. Sanches, S. N. Cassu, R. De Cássia, L. Dutra, *Polímeros* **2015**, *25*, 247.

54 J. Wang, M.-L. Du, C.-S. Xu, H. Zhu, Y.-Q. Fu, *J. Macromol. Sci. Part B* **2012**, *51*, 2462.

55 N. Stafie, D. F. Stamatialis, M. Wessling, *Sep. Purif. Technol.* **2005**, *45*, 220.

56 L. Y. Tyng, M. R. Ramli, M. B. H. Othman, R. Ramli, Z. A. M. Ishak, Z. Ahmad, *Polym. Int.* **2013**, *62*, 382.

57 S. N. Yahya, C. K. Lin, M. R. Ramli, M. Jaafar, Z. Ahmad, *Mater. Des.* **2013**, *47*, 416.

58 B. Zhang, H. Soleimaninejad, D. J. Jones, J. M. White, K. P. Ghiggino, T. A. Smith, W. W. H. Wong, *Chem. Mater.* **2017**, *29*, 8395.

59 M. Mitsui, H. Fukui, R. Takahashi, Y. Takakura, T. Mizukami, *J. Phys. Chem. A* **2017**, *121*, 1577.

60 L. C. Klein, B. McClarren, A. Jitianu, *Adv. Mater. Res.* **2014**, *783–786*, 1432.

61 L. C. Klein, A. Jitianu, *J. Sol-Gel Sci. Technol.* **2011**, *59*, 424.

62 A. Jitianu, G. Gonzalez, L. C. Klein, *J. Am. Ceram. Soc.* **2015**, *98*, 3673.

63 A. Jitianu, K. Lammers, G. A. Arbuckle-Kiel, L. C. Klein, *J. Therm. Anal. Calorim.* **2012**, *107*, 1039.

4.3. Platinum free thermally curable Siloxanes for Optoelectronic Application

Published as an article:

Nils Steinbrück, Svenja Pohl, and Guido Kickelbick, *RSC Adv.*, **2019**, *9*, 2205–2216.

https://doi.org/10.1039/C8RA09801H

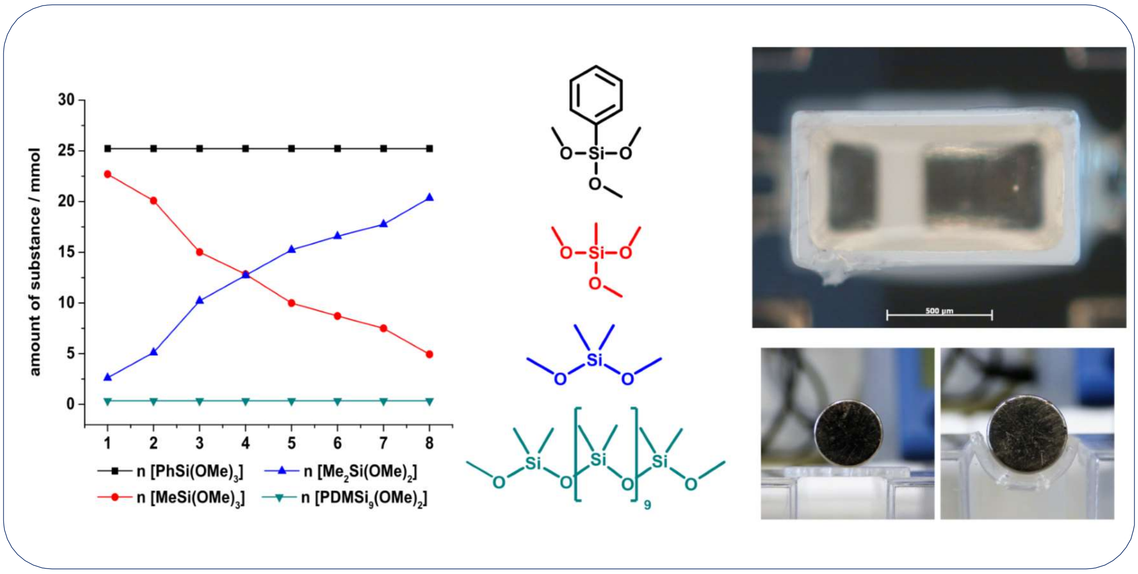

Contribution of the Authors to the Manuscript:

Nils Steinbrück wrote the complete draft of this manuscript that was acknowledged by all named authors. Nils Steinbrück performed the synthesis of platinum-free curable siloxanes and their samples as well as the FTIR, NMR, TG, TG-IR, DSC, UV/Vis, hardness and microscopic measurements and the heat and photostability experiments. He also performed the key part of the data and results interpretation.

Svenja Pohl reproduced the synthesis and performed all viscosity measurements during her course as a research assistant.

Prof. Dr. Guido Kickelbick gave the input to this project, supervised and discussed it, and optimized the manuscript to its final form.

All results and conclusions made in the previous parts of the thesis were obtained by experiments carried out in polysiloxane resins curable by platinum-catalyzed hydrosilylation. In an additional approach, we used the preparation of platinum-free curable siloxanes, able to be used as stand-alone encapsulation or as a host material for organic fluorescence dyes.

After the reconsideration of the curing process of polysiloxanes without metal-based catalysts, we discovered another route to synthesize this new platinum-free thermally curable polysiloxanes with tunable properties. By performing a stepwise acid-based catalyzed polycondensation reaction of different di- and trialkoxysilanes, liquid but partially cross-linked polysiloxane gels were prepared. The research and development of these materials committed to writing in the **third part** of this thesis called ***"Platinum free thermally curable siloxanes for optoelectronic application – synthesis and properties"***.

Due to unreacted alkoxy groups, a thermal condensation or curing reaction can be initiated by a heat treatment at >150 °C for >72 h. An addition of a small amount of an inorganic base like NaOH or an organic base like DABCO can catalyze the condensation reaction and therefore the curing procedure significantly, as shown by rheology. The resulting elastomers are transparent, elastic, and their high refractive index (1.494 – 1.505), as well as their hardness (50 - 90 Shore A), can be tuned by changing the ratio of trialkoxy and dialkoxasilane monomers used. The change in hardness could be related to the change in the cross-linking degree also, verified by increasing glass transition temperatures as described for other thermally curable polysilsesquioxanes and by thermogravimetric data.[104] All samples are temperature stable up to minimum 360 °C. A long-time heat treatment at 200°C, as well as long-time irradiation of the gels with 450 nm light, does not change the properties of the material, making it stable and reliable as encapsulation, also for high power applications. Due to its properties, especially its tunable refractive index and its sustainable platinum-free curing process, this material is remarkably interesting for any optoelectronic application that needs transparent encapsulation.

RSC Advances

PAPER

View Article Online
View Journal | View Issue

Cite this: *RSC Adv.*, 2019, **9**, 2205

Platinum free thermally curable siloxanes for optoelectronic application – synthesis and properties†

Nils Steinbrück, Svenja Pohl and Guido Kickelbick *

Received 28th November 2018
Accepted 5th January 2019

DOI: 10.1039/c8ra09801h

rsc.li/rsc-advances

Polysiloxanes for applications in the area of optical devices are usually based on two-component platinum catalysed cross-linked materials. Here we report the synthesis and properties of a novel one-component siloxane that can be thermally cured showing similar tailorable properties like commercially available encapsulation systems without using a noble metal catalyst. The pre-curing material is formed by an acid catalysed condensation reaction of trialkoxysilanes (TAS), dialkoxysilanes (DAS) and alkoxy-terminated polysiloxanes. NMR analysis of the formed polymeric compounds reveal that the materials are partially cross-linked gels. The obtained compounds can be thermally cured and consolidated at temperatures between 160 and 200 °C. Depending on the composition a tuneable hardness in between 50–90 Shore A, refractive indices of 1.494–1.505, as well as high temperature stabilities up to 443 °C were obtained. The high thermal- and photostability, the high transparency, as well as the tailorable refractive index makes these materials to ideal systems for optoelectronic applications. Investigations under increased temperatures and high-density illumination reveal that the material can withstand conditions, which are typical for high-performance light emitting diodes (LED).

Introduction

The developments in optoelectronic research lead to an increasing interest in new packaging materials suitable for high-performance applications. For instance light emitting diode (LED) curable encapsulations require excellent processability and have to reveal high stability under various conditions to ensure steady optical efficiencies and lifetimes.[1–8] The thermal stability required in this context is defined as a resistance against discolouration and changes in transparency caused by the temperatures prevailed at the LED parts which are usually around 120–150 °C.[9,10] Beside thermal aging, light initiated photo degradation can occur caused by the constant exposure to high light radiation densities with wavelength between 200–500 nm.[10–12] The two most common used packaging materials for optoelectronic applications are two-component polysiloxane elastomers, thermally curable by platinum catalysed hydrosilylation (Scheme 1), or irradiation curable epoxy systems.[7,13–17]

The commercially used two-component polysiloxanes are suitable for many different applications and meet all the important requirements for conventional LEDs with inorganic converters. However, new applications like rare earth reduced LEDs containing converters based on organic dyes have additional requirements. The lifetime of the components in these organic converters often depends on oxygen permeability and the composition of the matrix material.[18,19] Platinum traces and reactive hydride groups can potentially interact with the organic dyes and result in a reduced performance of the device. From an ecological and economical point of view, non-recyclable noble metal compounds should be avoided in modern materials. Epoxy based polysiloxanes are a known alternative but a heat- or light-initiated change in properties, like a colouration often occurs.[5,20,21] Thiol-en curable polysiloxanes are also potential alternatives.[22–24] But sulphur containing systems are not suitable for devices with silvered parts used in common LED technology, due to the formation of silver sulphides colouring the encapsulation.[25] Other alternative materials like hybrid sol–gel

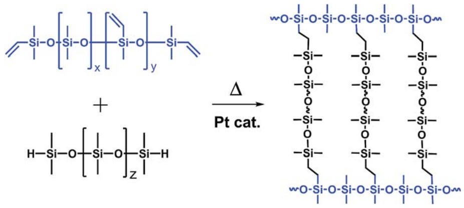

Scheme 1 Example of a platinum catalysed hydrosilylation cross-linking reaction of a two-component polydimethylsiloxane resin containing Si–vinyl and Si–H reactive pendant and end groups.

Saarland University, Inorganic Solid State Chemistry, Campus Building C4$_1$, 66123 Saarbrücken, Germany. E-mail: guido.kickelbick@uni-saarland.de

† Electronic supplementary information (ESI) available: Including NMR and FTIR data and a LED packaging demonstration section. See DOI: 10.1039/c8ra09801h

glasses are often hard and rigid in the consolidated state.[26] For applications that require a high flexibility at high temperatures these materials are also not suitable. Variations in the coefficients of thermal expansion of the lead frames, chips, wires, and other device components demand a high elasticity of the packaging material, especially under working conditions. This is one reason why silicone elastomers are currently the most often used encapsulation materials in LEDs.[27,28]

The development of new platinum free curable polysiloxanes with a high degree of elasticity but also suitable properties for optoelectronic applications was the main goal of our studies. For this reason, new materials were produced by an acid catalysed condensation reaction of different trialkoxysilanes (TAS), dialkoxysilanes (DAS), and alkoxy-terminated polysiloxanes. Heat treatment of the obtained partially cross-linked gel precursor leads to a curing process, which consolidates the material by further condensation reactions of the alkoxysilane groups. The viscosity of the liquid precursor as well as its refractive index can be tailored by its composition, which also influences the properties of the consolidated materials (CM), such as hardness and elasticity.[29] Finally we investigated the properties of the resulting materials with respect to applications as packaging materials for optoelectronic devices.

Experimental

Materials

Dimethyldimethoxysilane (97%), methyltrimethoxysilane (97%), phenyltrimethoxysilane (97%) and methoxy terminated polydimethylsiloxane (5-12 cst.) were all purchased from ABCR (Germany). 1,4-Diazabicyclo[2.2.2]octane (98%) was purchased from Alfa Aesar (Germany). Hydrochloric acid was provided from Bernd Kraft GmbH (Germany) and potassium hydroxide (85%) from Grüssing GmbH Analytica (Germany). All chemicals were used as received (Scheme 2). The hydrochloric acid was diluted to pH = 2.5 with demineralised water. Potassium hydroxide was dissolved in methanol (0.11 mol l^{-1}). The purity of all precursors and the averaged chain length of the methoxy-terminated polydimethylsiloxane were characterised by ^{1}H and ^{29}Si NMR spectroscopy (see ESI Fig. ESI1–8†).

Instrumentation

Fourier transformed infrared spectra (FTIR) were recorded in total reflectance mode on a Vertex 70 spectrometer (Bruker Corporation, USA) from 4500–400 cm^{-1} with a resolution of 4 cm^{-1} increment and 10 scans averaged. UV-VIS transmission measurements were performed on a Lambda 750 instrument (Perkin Elmer Inc., USA) equipped with a 100 mm integration sphere from 700–350 nm with a 2 nm increment and 0.2 s integration time. NMR spectra were recorded on an Avance III 300 MHz spectrometer and an Avance III HD 400 MHz spectrometer (Bruker Corporation, USA) with 300.13/400.13 MHz for ^{1}H NMR spectra and 59.63/79.49 MHz for ^{29}Si NMR spectra. All NMR samples were prepared in methanol-d_4 ($MeOD_4$) or chloroform-d ($CDCl_3$). CP-MAS NMR spectra were recorded on an Avance III HD – Ascend 400WB spectrometer (Bruker Corporation, USA) with 13 KHz rotation, 100.65 MHz for ^{13}C and 79.53 MHz for ^{29}Si NMR spectra. The absolute value of viscosity was determined applying a MCR-301 rheometer with a CTD-450 convection heating system (Anton Paar GmbH, Austria) in oscillatory mode with a plate–plate geometry using a 25 mm PP25 measuring plate, an amplitude of 5%, a frequency of 1 Hz and a normal force value of 0. The refractive index was measured using an AR4 Abbé refractometer with a PT31 Peltier thermostat (A. Krüss Optronic GmbH, Germany) at 20 °C and 590 nm LED illumination. Thermogravimetric measurements were carried out applying a TG209 F1 Libra thermo-microbalance (Netzsch-Gerätebau GmbH, Germany) at a heating rate of 10 K min^{-1} to 250/800 °C with a gas flow of N_2/O_2 of 20 ml min^{-1} each. Differential scanning calorimetry was performed with a Netzsch DSC 204 F1 Phoenix calorimeter in aluminium crucibles with pierced lids under nitrogen (100 ml min^{-1}) applying a heating rate of 5 K min^{-1} from −40 to 400 °C. An Axioskop 50 transmitted light/fluorescence microscope (Carl Zeiss Microscopy GmbH, Germany) with an AxioCam MRc (1388 × 1040 pixel) was used for the visualization of sub millimetre structures. A quadruple film applicator Model-360 (Erichsen GmbH & Co. KG, Germany) was applied to produce 13 × 0.12 mm polymer films on glass object slides (VWR International GmbH, Germany) for transmission measurements. The thickness of the samples was determined applying a FMD12TB precision dial gauge (Käfer Messuhrenfabrik GmbH & Co. KG, Germany) with an accuracy of 1 μm. Hardness measurements were performed using a Sauter HBA-100 Shore-A durometer (Sauter GmbH, Germany). A self-fabricated fibre coupled 450 nm wavelength illumination system with 710 mW LEDs (6 × LDW5SN) was applied as irradiation source for photostability experiments.

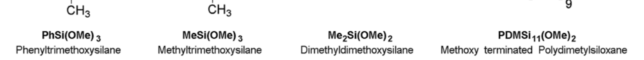

Scheme 2 Structures, names and abbreviations of the monomers used in the synthesis.

Preparation

A certain amount of phenyltrimethoxysilane [$PhSi(OMe)_3$], methyltrimethoxysilane [$MeSi(OMe)_3$], dimethyldimethoxysilane [$Me_2Si(OMe)_2$], and hydrochloric acid (1.5× n[alkoxysilanes]) were stirred in a sealed vial (45 °C, 3 h, 320 rpm). Methoxy terminated polydimethylsiloxane [$PDMSi_{11}$-$(MeO)_2$] (0.7% of n[alkoxysilanes]) was added under further stirring (45 °C, 18 h, 320 rpm). The mixture was transferred into a beaker (100 ml) and stirred until gelation occurred (25 °C, 0.5–1 h, 150 rpm). Gelation was detected by homogenous distributed remaining gas bubbles and significant increase of viscosity. The beaker was transferred into a compartment drier to interrupt the gelation by removing water, hydrochloric acid, and methanol (110 °C, 1 h). The observed transparent gels were

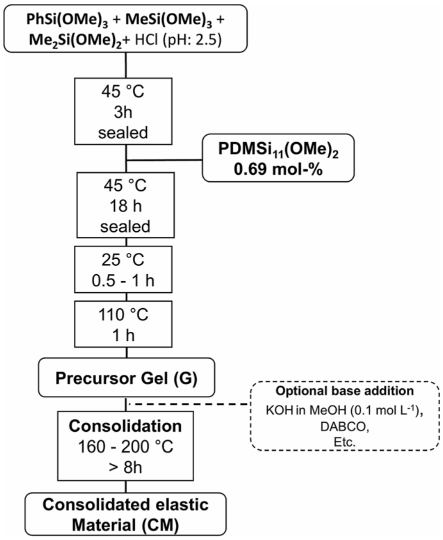

Fig. 1 Schematic procedure for the synthesis of a platinum free, thermally curable polysiloxane based material.

isolated and cooled to room temperature (Fig. 1). The concentrations used in the synthesis of the different samples are presented in Table 1.

Curing procedure

The material was consolidated by heating in a mould or cavity (150–200 °C, 8–72 h). The consolidation time was depending on the materials' composition, the sample thickness, and the consolidation temperature. The consolidation process was terminated when the sample was not sticky anymore at the surface. Addition of small amounts of base (1–20 mmol g^{-1}) to the gel resulted in reduced consolidation times and temperatures (≤60 min). The consolidated materials were crack-free and depending on the chemical composition flexible and elastic (Fig. 2A). The unconsolidated gels were either cast into PTFE (30 × 10 × 1 mm) or aluminium moulds (8 × 2 mm), or films were prepared on glass slides (13 × 0.12 mm) for the mechanical or optical measurements. Samples 1 and 2 were heated for a better processability (110 °C). The prepared samples were consolidated in a compartment drier (160 or 200 °C, 72 h). The observed transparent materials (CM) were cooled to room temperature and isolated. To demonstrate the processability of the precursor polysiloxanes a polyphtalamide LED lead frame (1.4 × 0.7 × 4.0 mm) was cast with samples 4 and 6 by hand. The filled lead frames were heat-treated to cure the polymers (160 °C, 20 h) (Fig. 2B). Further images of the cast lead frames are presented in the ESI.†

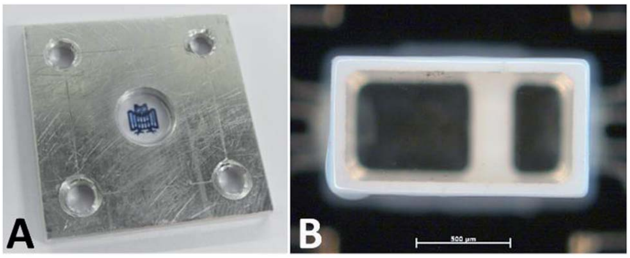

Fig. 2 (A) Sample 4 cast in an aluminium frame and consolidated for 72 h at 200 °C. The cured, flexible and crack free material shows a high transparency. (B) Sample 4 cast in polyphtalamide LED lead frame (1.4 × 0.7 × 4.0 mm).

Base catalysis

Exemplarily one sample was studied to investigate the effect of base catalysis on the curing behaviour. To study this effect potassium hydroxide (0.093 g, 1.65 mmol) was dissolved in methanol (14.949 ml, 0.369 mol, 0.11 mol l^{-1}). Different amounts of this solution (0.0, 1.0 and 2.5 µl) were added and mixed to a portion of a 60 day aged sample 4 (0.2 g) each. The change of viscosity was measured isothermal at 110 °C with the given parameters.

Heat and photostability experiments

Long-time stability of the cured polymers was tested after the main curing procedure by heat and irradiation exposure experiments to simulate the operation conditions in high performance LED applications. The sample films on glass substrate were heat treated for 1177 h at 200 °C. After the heat

Table 1 Quantities of substances used for the synthesis of sample 1–8, percentage of phenyl groups, trialkoxysilane monomers (TAS), dialkoxysilane monomers (DAS) and methoxy-terminated polydimethylsiloxane (PDMS)

Sample	$n[PhSi(OMe)_3]$, mmol	$n[MeSi(OMe)_3]$, mmol	$n[Me_2Si(OMe)_2]$, mmol	$n[PDMSi_{11}\text{-}(MeO)_2]$, mmol	Ph[calc.]/Ph[^{1}H NMR][a], %	TAS[b], %	DAS[b], %	PDMS[b], %
1	25.23	20.02	3.23	0.35	42.5/42.5	92.68	6.61	0.71
2	25.27	17.71	6.31	0.36	39.9/39.9	86.58	12.72	0.70
3	25.23	13.24	12.59	0.35	35.4/34.9	74.84	24.48	0.68
4	25.21	11.33	15.69	0.35	33.4/33.1	69.50	29.84	0.66
5	25.06	8.81	18.78	0.35	31.7/31.3	63.90	35.44	0.66
6	25.21	7.69	20.44	0.37	31.0/30.3	61.28	38.07	0.65
7	25.23	6.61	21.89	0.35	30.3/29.9	58.87	40.48	0.64
8	25.21	4.35	25.10	0.35	28.8/28.8	53.73	45.63	0.63

[a] Percentage of phenyl groups regarding to the total number of alkyl and aryl groups Ph[calc.]: calculated from the weighted portions; Ph[^{1}H NMR]: calculated from the integration of ^{1}H NMR signals (NMR spectra see ESI). [b] Mole percentage of the summed amount of substance of trialkoxysilanes (TAS), dialkoxysilanes (DAS), and polydimethylsiloxanes (PDMS), respectively.

treatment the transmission of the samples was determined. For photostability experiments the aluminium mould cast and cured samples were radiated on a self-prepared fibre coupled 450 nm wavelength illumination system with 710 mW LEDs (6 × LDW5SN) for 692 h. The transmission of the samples was determined at different times during the experiment.

Results and discussion

Platinum free cross-linked polyphenylmethylsiloxanes with tailorable properties for optoelectronic applications were synthesised by an acid catalysed hydrolysis and condensation reaction from alkoxysilanes. In the first reaction step trialkoxysilane (TAS) and dialkoxysilane (DAS) monomers were added to diluted hydrochloric acid, hydrolysed and condensed forming oligomer and polymer chains as well as partially cross-linked structures (Fig. 3). After three hours of reaction a methoxy-terminated oligodimethylsiloxane ($PDMSi_{11}(OMe)_2$) was added, which should lead to an additional but less closed-meshed cross-linking of the network (Scheme 3). After further stirring, the reaction was stopped by heating the mixture to 110 °C, which removes the excess of formed methanol and water. The resulting compounds were transparent polymer gels. Phenyltrimethoxysilane [$PhSi(OMe)_3$] was applied as a precursor to increase the refractive index.[7] The amounts of $PhSi(OMe)_3$ and methoxy-terminated oligomer [$PDMSi_{11}$-$(MeO)_2$] were kept constant in the reaction mixture. The quantity of trimethoxysilane [$MeSi(OMe)_3$] was stepwise substituted by dimethyldimethoxysilane [$Me_2Si(OMe)_2$]. This exchange of trifunctional T unit monomers by difunctional D units leads to a less cross-linked structure. At the same time, the percentage of phenyl- compared to methyl-groups decreases, which causes a simultaneous decrease of the refractive index.

The isolated polymers were cured without any further catalytic activation by simple heat treatment of the gels at temperatures above 150 °C remaining water and methanol were removed and a further network forming process was started. In this step, the previous gel-like materials formed solid but elastic cross-linked polymers (Scheme 3b).

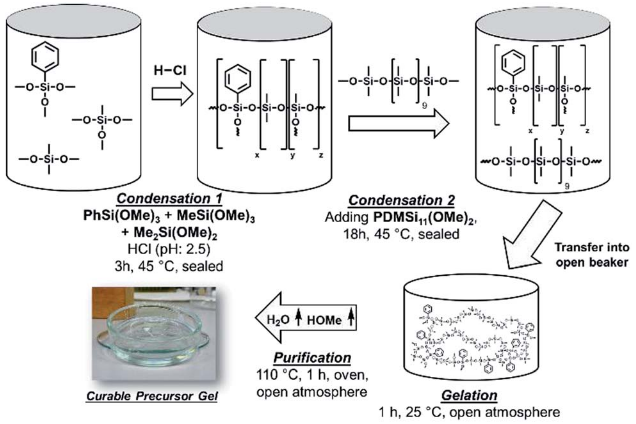

Fig. 3 Scheme of the preparation of the polysiloxane gels. After the condensation of DAS and TAS monomers a methoxy-terminated polysiloxane was added to the reaction. The reaction vessel was opened to form a gel due to the loss of water and methanol. The reaction was interrupted by a heat treatment to remove excess of water, methanol, and hydrochloric acid from the products.

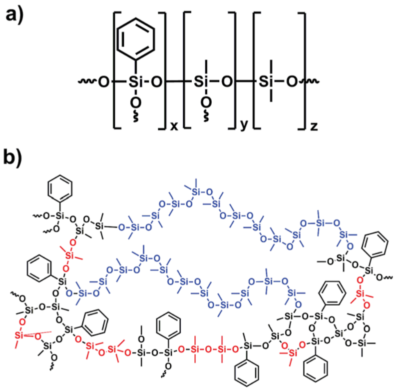

Scheme 3 Schematic formula (a) and structure of a consolidated sample (b). TAS (black), DAS (red) and PDMS (blue) are highlighted in the given colours.

Eight gel compositions were synthesised containing different ratios of $MeSi(OMe)_3$ to $Me_2Si(OMe)_2$ (Table 1). Addition of small amounts of base to the gels before curing reduces the consolidation time and temperature due to the pH dependency of the condensation reaction.[30–33] The unconsolidated gels are also subject to an ageing process, in which the viscosity of the gels increases with storage time at room temperature.

NMR studies of the condensation behaviour

Two-dimensional ^{29}Si–^{1}H HMBC NMR spectroscopy was used to follow the condensation reaction of the different monomers exemplarily for the syntheses of four samples (Fig. 5). Samples 1, 2 and 3 with a stepwise increasing amount of DAS and sample 8 with the highest amount of DAS were chosen. We did not observe any significant differences in the data of samples 3 and 8, therefore no further samples were studied. Small samples were withdrawn from the reaction mixture after 3 h of hydrolysis (before adding $PDMSi_{11}$-$(MeO)_2$) and after the completed synthesis. Due to the high concentration of the different molecules (hydrolysed and non-hydrolysed, monomers, oligomers, polymers, rings, *etc.*) the ^{29}Si NMR chemical shifts are very broad which results in a poor resolution of the spectra. Therefore, a range is given for the measured chemical shifts of the different functional groups. The recorded spectra are part of the ESI.† The spectra of sample 1, 2, 3 and 8 show all possible signals of the trifunctional T units except T^0 (Table 2). Therefore it can be concluded that all phenyltrimethoxysilane [$PhSi(OMe)_3$], and methyltrimethoxysilane [$MeSi(OMe)_3$] monomers reacted at least with one additional molecule or are part of a linear or cross-linked structure. Furthermore, it appears that all T signal couple with the methoxy groups except T^3. Hence, not all methoxy groups of the trialkoxysilanes were hydrolysed before reacting with other molecules. The signals caused by difunctional D units of [$Me_2Si(OMe)_2$] show a different behaviour. In sample 1 and 2 with the lowest concentration of $Me_2Si(OMe)_2$ no D^0 signals of unreacted

Table 2 Ranges of the cross peaks measured with the ^{29}Si–^{1}H HMBC 2D correlation NMR spectroscopy of sample 1, 2, 3 and 8[a]

^{29}Si [Ph**Si**(OR)$_{3-x}$]	^{1}H [**Ph**Si(OMe)$_{3-x}$]	^{1}H [PhSi(O**Me**)$_{3-x}$]	Functional Group	Sample 1	Sample 2	Sample 3	Sample 8
−78…−80	7.82…7.4	—	T^3	+	+	+	+
−71…−74	7.82…7.4	3.65…3.28	T^2	+	+	+	+
−66…−69	7.82…7.4	3.65…3.28	T^2	+	+	+	+
−59…64	7.82…7.4	3.65…3.28	T^1	+	+	+	+

[a] Corresponding atoms are highlighted; di- or trifunctional groups are classified. Detected cross peaks are assigned with a "+", not detected cross peaks are assigned with a "−".

^{29}Si [Me**Si**(OR)$_{3-x}$]	^{1}H [**Me**Si(OMe)$_{3-x}$]	^{1}H [MeSi(O**Me**)$_{3-x}$]	Functional group	Sample 1	Sample 2	Sample 3	Sample 8
−62…−68	0.36…−0.26	—	T^3	+	+	+	+
−56…−60	0.36…−0.26	3.65…3.28	T^2	+	+	+	+
−52…−56	0.36…−0.26	3.65…3.28	T^2	+	+	+	+
−44…−50	0.36…−0.26	3.65…3.28	T^1	+	+	+	+

^{29}Si [Me$_2$**Si**(OR)$_{2-x}$]	^{1}H [**Me$_2$**Si(OMe)$_{2-x}$]	^{1}H [Me$_2$Si(O**Me**)$_{2-x}$]	Functional group	Sample 1	Sample 2	Sample 3	Sample 8
−18…−22	0.36…−0.26	—	D^2	+	+	+	+
−15…−18	0.36…−0.26	—	D^2	+	+	+	+
−9.5…−12	0.36…−0.26	—	${D_1}^1$	+	+	−	−
−9.5…−12	0.36…−0.26	3.65…3.28	${D_0}^1$	−	−	+	+
2… −5	0.36…−0.26	3.65…3.28	D_0	−	−	+	+

dialkoxysilane monomers are detected (Fig. 4), which means that all monomers reacted at least once with a second molecule or are part of a linear or cross-linked structure. This argument is supported by the detected D^1 and D^2 signals. Additionally the D^1 signals can be separated in ${D_0}^1$ and ${D_1}^1$. The indexed number gives the amount of hydroxyl groups attached to the molecule. A ${D_0}^1$ signal is caused by a monomer with no hydroxyl group; a ${D_1}^1$ signal is caused by a monomer with one hydroxyl group. In the spectra of sample 3 and 8 with an intermediate and high concentration of $Me_2Si(OMe)_2$ the D^1 signals of end groups and D^2 signals of linear or cross-linked units are observed. D^0 signals are also detectable in both samples, which belong to the unreacted monomers. We can conclude from these observations that the reactions of the DAS monomers seem to be not completed in the first three hours of stirring. Examining the condensation behaviour of the precursors, we can conclude that TAS reacts with each other and with the DAS forming linear and cross-linked structures. By increasing the DAS concentration, the number of unreacted DAS monomers increases, while no unreacted TAS can be detected in any measured sample. Our synthetic procedure resembles literature known procedures in which the resulting materials are solid, hard, and rigid. However in these studies TAS is condensed first for several hours before DAS is added dropwise.[26,34–37] This leads to highly cross-linked structures, mainly consisting of regions with full condensed T^3-T^3 units with D^2, T^2 and D^1 groups connecting the

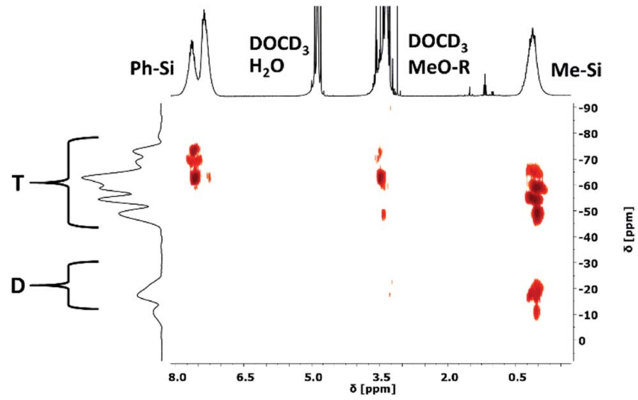

Fig. 4 ^{29}Si–^{1}H HMBC 2D NMR spectrum of the reaction mixture of sample 1 after 3 h of condensation reaction before addition of methoxy-terminated polydimethylsiloxane. Chemical shifts: T: trifunctional units, D: difunctional units, Ph–Si: phenyl groups, $DOCD_3$: methanol-d$_4$, Me–OR (R = H, Me): methanol and methoxy groups, Me–Si: methyl groups.

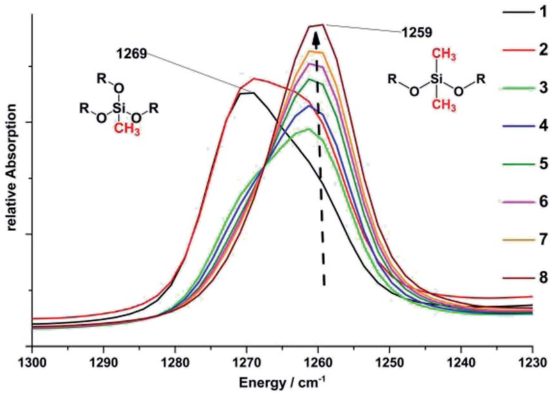

Fig. 5 Enlarged segment of the FTIR spectra of sample 1–8. The spectra show the decrease of the vibration band at 1269 cm^{-1} [δ(C–H[Si–CH_3])] caused by the decreasing concentration of $MeSi(OMe)_3$ and an increase of the vibration band at 1259 cm^{-1} [δ(C–H[Si–CH_3])] caused by the increasing concentration of $Me_2Si(OMe)_2$ in the final product.

edges of this regions.[38] In our studies the addition of DAS directly to the condensation reaction of TAS units leads to a less cross-linked and flexible structure with T^1, T^2 and T^3 units. After completion of the reaction the D^0 signals are not detectable anymore but D^1 end groups. All measured NMR spectra are part of the ESI (Fig. ESI7–28).†

FTIR spectroscopy of the unconsolidated gels

Directly after removing methanol and water at 110 °C for 1 h the freshly prepared gels were cooled to room temperature and characterised by FTIR spectroscopy. All samples show the expected vibration bands of phenylmethylpolysiloxane networks indicated by the very broad ν(Si–O) vibration bands at 1052, 1016, 806 cm^{-1} and the vibration bands of the methyl and phenyl side groups at 1259, 1269 [δ(C–H[Si–CH$_3$])]; 1130 δ(Si–C)$_{AR}$, 726 cm^{-1} [ρ(C–H[Si–(CH$_3$)$_2$])], and 694 cm^{-1} [ν(Si–C)] (Fig. ESI29†).[35] All other vibration bands at 3380 ν(O–H), 2840 [ν(C–H[O–CH$_3$])], and 846 [δ(Si–O–CH$_3$)] are caused by the pendant and terminal methoxy groups as well as unreacted monomers, methanol, or water (Fig. 6). The vibration δ(C–H[Si–CH$_3$]) bands at 1259 and 1269 cm^{-1} prove the stepwise substitution of methyltrimethoxysilane [MeSi(OMe)$_3$] by dimethyldimethoxysilane [Me$_2$Si(OMe)$_2$] from sample 1 to 8. The vibration band at 1259 cm^{-1} is caused by the CH$_3$ groups of the MeSi(OR)$_3$ (R = Si, Me, H) units. The vibration band at 1269 cm^{-1} belongs to the CH$_3$ groups of the Me$_2$Si(OR)$_2$ (R = Si, Me, H) units (Fig. 5). As a result of the substitution the intensity of the band at 1269 cm^{-1} decreases while the intensity of the band at 1259 cm^{-1} increases.

HCl was used as a catalyst in the hydrolysis and condensation reactions for the preparation of the precursor polysiloxanes. Residues of HCl can be harmful for materials in optoelectronic devices. Therefore, we investigated the presence of HCl after the synthesis of the precursor polymers and were not able to detect any HCl after the heating step in the polysiloxane synthesis by TG-FTIR experiments.

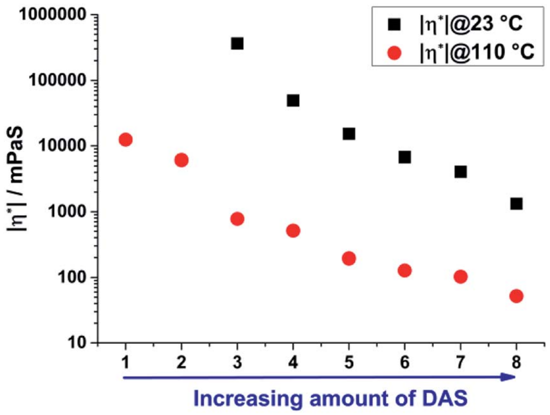

Fig. 6 Averaged absolute value of viscosity of sample 1–8 measured isotherm at 23 and 110 °C for 10 min. The increase of DAS leads to a decrease of viscosity, due to less cross-linked and more linear structure motives.

Viscosity of unconsolidated gels

The absolute value of viscosity was determined at 23 and 110 °C directly after the synthesis of the unconsolidated materials using a rheometer in oscillatory mode with a plate–plate geometry to determine the temperature dependent processing range for the materials. Due to the stepwise substitution of TAS by DAS units from sample 1 to 8 a simultaneous decrease of cross-linking respectively of viscosity is expected.[16] The viscosity of sample 1 and 2 was too high for a determination at room temperature. An increase in temperature to 110 °C results in a significant decrease of the absolute value of viscosity of the samples from 1 to 8 (Fig. 6). As expected, a decrease of TAS/DAS ratio leads to a decrease of viscosity from 362 079 to 1324 mPa s. This trend was also reported in literature for vinylphenylpolysiloxane (22 658 to 3928 mPa s).[16] Comparable non vinyl containing but also curable sol–gel based materials are solid and cannot be processed at room temperature but also soften at higher temperatures.[26,34–38] Generally viscosities of 10 000–300 000 mPa s respectively 3000–15 000 mPa s are required for the manufacturing of optoelectronic devices by moulding or dispensing processes.[27,28]

Ageing experiment

All prepared samples show an increasing absolute value of viscosity with long storage times at room temperature. This ageing process is caused by the loss of excess of reaction products like water and methanol and by further condensation reactions induced by Si–OMe and Si–OH groups.[30,32] The ageing of the gels was studied exemplarily on sample 4 by measuring the absolute value of viscosity isothermally at 30 °C for 260 h. Subsequently the sample was heated to 110 °C to evaluate the processability and to 200 °C to evaluate the curing process after the ageing. The absolute value of viscosity of sample 4 increases during the heat treatment at 30 °C from 32 000 to 142 800 mPa s (Fig. ESI32†). A fast increase of viscosity was observed in the first 20 h, afterwards there is only a slow but steady increase up to 260 h. The sample is still liquid and gel like after the ageing. Heating the sample to 110 °C results in a strong decrease of the absolute value of viscosity from 142 800 to 270 mPa s (Fig. ESI33†), which confirms that the processability of the gel is not influenced by the ageing experiment.

Refractive index of unconsolidated gels

Polymeric encapsulation materials in optoelectronic devices require a defined and preferably high refractive index.[27,28]

Especially in applications in which light is uncoupled from a device like LEDs a high refractive index is mandatory to prevent total internal reflection phenomena.[8] Commercially used high refractive index (HRI) polysiloxanes often contain aromatic side groups to increase the refractive index. Low index polydimethylsiloxane based systems (LRI) usually reveal an RI of 1.40 while polyphenylmethylsiloxanes show a value of 1.54 (Table 3).[7,39,40]

In our materials we used a similar approach. The percentage of phenyl groups decreases from sample 3 to 8 from 37 to 32%

(Fig. 7), which decreases the refractive index from 1.505 to 1.494. Based on the gradual substitution of $MeSi(OMe)_3$ by $Me_2Si(OMe)_2$ the overall concentration of phenyl groups, which also influences the refractive index.[16] The refractive index of sample 1 and 2 could not be determined by Abbé refractometry due to its very high viscosity at 20 °C. By extrapolation we expect the RI of these materials to be in the range of 1.508–1.510.

Curing behaviour investigated by ^{29}Si and ^{13}C CP-MAS NMR and TG-FTIR

CP-MAS NMR spectroscopy was applied for further characterization of the consolidated materials. The amount of DAS increases from the consolidated samples 1, 3, and 5. We were not able to prepare CP-MAS NMR samples with a higher amount of DAS (sample 6–8) because these compounds were too elastic for grinding. The main objective of this study are the changes in D or T signals caused by the consolidation process. A completely cross-linked structure would be distinguished by T^3 and D^2 signals only. ^{29}Si and ^{13}C NMR spectra of three samples with different compositions were measured. In the ^{29}Si NMR spectra we detected eight signals for individual Si groups (Table 4). The $Me_2Si(OSi)(OMe)$ end groups generate a very weak, barely assignable signal in the D^1 range from −5 to −12 ppm (Fig. 8). A second very strong signal can be assigned in the D^2 range of −15 to −25 ppm. It indicates a nearly complete linkage of DAS monomers to $Me_2Si(OSi)_2$ chain parts or side products like cyclosiloxanes.[43] The more high field shifted T signals at −52 to −85 ppm show a splitting in T^1, T^2 and T^3 of the $PhSi(OR)_3$ and $MeSi(OR)_3$ groups. The presence of the different T^1 and T^2 signals shows that the material is not completely cross-linked. Comparable results were obtained for the inorganic–organic hybrid glasses obtained by the so-called melting gel approach.[38] Due to the fact that the very broad chemical shifts of the $[PhSi(OR)_{3-x}]$ and $[MeSi(OR)_{3-x}]$ units were superimposed a quantitative determination was not expedient. The T^2 chemical shifts of $[PhSi(OR)_{3-x}]$ are located in the region of −66…−69 ppm. The T^3 chemical shift of $[MeSi(OR)_{3-x}]$ are located at −62…−68 ppm. There is no indication for a reasonable separation of the peak areas. Therefore a degree of condensation cannot be calculated accurately. A correlation between the samples composition and the cross-linking degree is given by the systematically decrease of viscosity and hardness and by the increase glass transition temperatures shown in a following chapter.

Table 3 Refractive indices of published high refractive index (HRI) and low refractive index (LRI) packaging materials[a]

nd_{20} (LED encapsulant)	Reference
1.505	This work (S3)
1.53	41
1.40	41
1.41	42
1.53	42
1.5402	16
1.5597	9

[a] All materials reported in literature are polysiloxane based and were thermally cured applying a platinum catalysed hydrosilylation reaction. The value of S3 was determined in unconsolidated state.

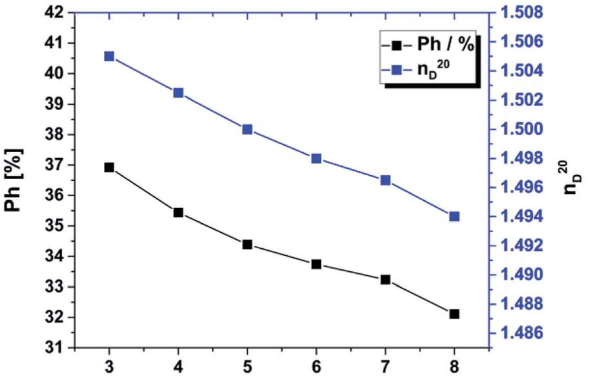

Fig. 7 Refractive indices and calculated percentage of phenyl groups for sample 3–8. The refractive index is directly correlated to the phenyl content. A higher phenyl content leads to a higher refractive index.

The ^{13}C CP-MAS NMR spectra are in good agreement with the ^{29}Si results showing a not entirely cross-linked structure (Fig. ESI34†). The expected chemical shifts of the carbon atoms at 120 to 140 ppm (Si–Ph), 51 to 47 ppm ($-O-CH_3$), 2 to −2 ($-(O)_2-Si-(CH_3)_2$) and −2.5 to −8.5 ($-(O)_3-Si-CH_3$) of the structure were detected. The chemical shift of $-O-CH_3$ is caused by D^1, T^1, and T^2 units and indicates the not complete hydrolysis of the methoxy groups in these units during the reaction. Related materials described in literature reveal a significant loss of DAS monomers or side products caused by the curing procedure shown by quantitative analysis of the ^{13}C MAS NMR data.[38]

In the condensation process six and eight membered cyclosiloxanes can be formed and can evaporate at elevated temperatures.[38] Because these ring forming reactions are independent of the compositions used, we studied the evaporation gases of the precursor gel of sample 5 exemplarily by TG-FTIR coupling methods. Isothermal heating at 250 °C for 4 h revealed a significant mass loss immediately after raising the temperature (Fig. ESI36†). Additionally, sample 15 was heated to 100 °C and the evaporated gases were directly transferred into a solvent ($CDCl_3$) for further NMR investigations.

The slope of the TG mass curve decreases and approximates a constant value. After 306 minutes at 250 °C the overall mass loss of the sample was 10%. In the IR spectra of the evolved gases the first absorption bands appear at 1350–1600 cm^{-1} [δ(O–H[H_2O])], which indicates the loss of water and at 1268 [δ(C–H[Si–(CH_3)])] and 1083, 1033, 808 cm^{-1} [ν(Si–O–Si)], which indicates the loss of siloxane units at temperatures ≥74 °C (Fig. 9). At 220 °C new vibration bands at 1066, 1033 and 1000 cm^2 [ν(C–O)] appear caused by the loss of methanol, which is one reaction product of the condensation reactions. The methanol and DAS signal intensities decrease during the isothermal treatment and disappear completely afterwards. The water signal intensity increases steadily.

These results show the presence of DAS units in the evaporated gases as well as a significant mass loss of the precursor gel

Table 4 ^{29}Si CP-MAS NMR chemical shift range and corresponding building units in the consolidated material

	δ ^{29}Si/ppm [$Me_2Si(OR)_{2-x}$]	δ ^{29}Si/ppm [$PhSi(OR)_{3-x}$]	δ ^{29}Si/ppm [$MeSi(OR)_{3-x}$]
D^1	−5…−12	—	—
D^2	−15…−25	—	—
T^1	—	−59…64	—
$T_a^{\ 2}$	—	−66…−69	−52…−56
$T_b^{\ 2}$	—	−71…−74	—
T^3	—	−78…−85	−62…−68

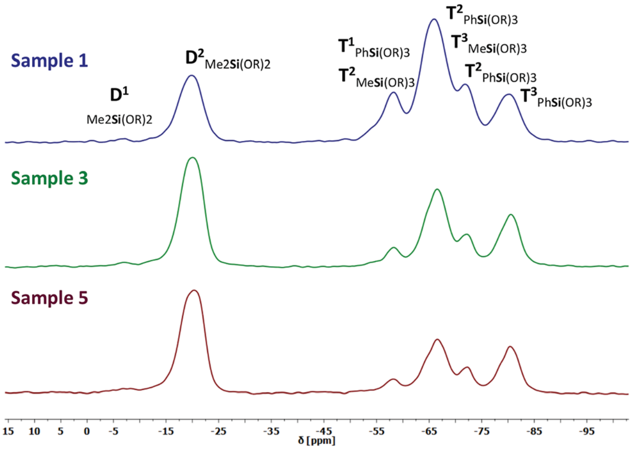

Fig. 8 ^{29}Si CP-MAS NMR spectra of sample 1, 3, and 5. The detected chemical shifts can be aligned to the di- or trifunctional D^1, D^2, T^1, T^2, and T^3 structure units, which are superimposed in some cases shown by the annotations.

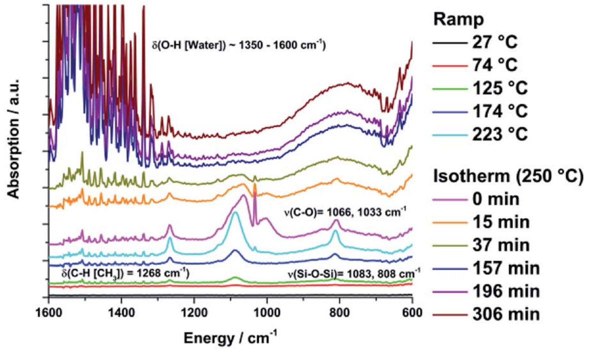

Fig. 9 FTIR spectra of the evaporated gasses from sample 5 during the isothermal thermogravimetric measurement at 250 °C for 250 min.

in the first hours of curing. The collected evaporation gases, which were transferred into a NMR solvent were measured with ^{29}Si–^{1}H 2D HMBC NMR experiment (Fig. 10). The ^{1}H NMR spectrum shows three main chemical shifts at 1.53 ppm, caused by water, and 0.09, 0.08 and 0.07 ppm caused by CH_3 units at a silicon atom. The only detectable cross peaks with the CH_3 units are observed between −17 and −22 ppm can be assigned to D^2 structural motifs of $(Me_2SiO)_x$ molecules.[44] This observation proofs the presence of small, fully condensed, and volatile dimethylcyclosiloxanes in the precursor gel and explains the former reported loss of DAS units.[38] The formation of these side products during the polycondensation reaction cannot be prevented as long as $Me_2Si(OMe)_2$ monomers are involved in the reaction.

These cyclosiloxanes can be formed by DAS monomers and the methoxy-terminated polydimethylsiloxanes during the condensation reactions.[30,31] However, the mass loss in the final materials based on formed dimethylcyclosiloxanes is low compared to the mass loss of the excess of water. The properties of the cured material are not influenced by these side products.

Hardness of the consolidated materials

After the liquid gels were cast and consolidated in PTFE moulds the hardness was measured at room temperature with a Shore A durometer. For this purpose the specimen were stacked to get the minimum of thickness required (6 mm). The substitution of $MeSi(OMe)_3$ by $Me_2Si(OMe)_2$ enables a tuneable hardness of the consolidated materials. Similar to the viscosity of the unconsolidated gels the hardness can be correlated with the TAS/DAS ratio (Fig. 11). Sample 7 and 8 were too soft for hardness determination. The increase of $Me_2Si(OMe)_2$ leads to longer and less cross-linked polymer chains, which directly correlates with the consolidated materials' hardness (Fig. 12).[26,45]

Differential scanning calorimetry

Differential scanning calorimetry (DSC) was used to determine the glass transition temperature (T_g) of the cured samples to

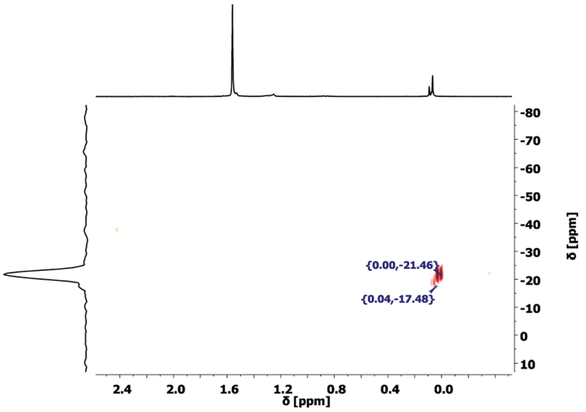

Fig. 10 ^{29}Si–^{1}H 2D HMBC NMR spectrum of the evaporated gases of sample 5 after heating it to 100 °C. Cross-peaks are only detected for the coupling of Si and CH_3 (−17 and −22 ppm), which can be assigned to D^2 structural motifs of $(Me_2SiO)_x$ molecules formed during the condensation reaction.

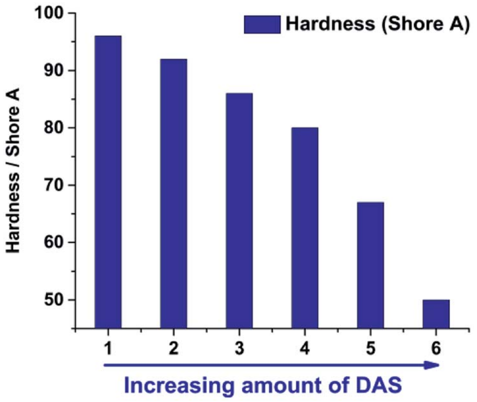

Fig. 11 Shore-A values of the samples 1–6 measured after consolidation at 200 °C for 72 h in PTFE moulds. The increase of DAS leads to a decrease of Shore-A hardness, due to less cross-linked and more linear structure motives.

verify systematic changes in the cross-linking behaviour (Fig. 14). The T_g is directly correlated to the cross-linking of the silica network and indicated by a inflection in the DSC curve of a sample.[46] An increase of T_g indicates an increase of cross-linking between the silicon atoms. The DSC was measured from −40 to 400 °C with 5 K min^{-1} under N_2 atmosphere (100 ml min^{-1}).

The DSC curves of samples 3–8 show a consistent decrease of the T_g caused by a decrease of cross-linking as already expected from the hardness measurements (Fig. 13). The substitution of $Me_2Si(OMe)_2$ by $MeSi(OMe)_3$ leads to less cross-linked polymer chains and a softer more flexible material resulting in the decrease of T_g.[26,35,46,47] The signal intensity of sample 1 and 2 is very weak, which makes the T_g determination less accurate (ESI37†). The T_g of sample 1–3 seems to be equal and not influenced by a further increase of TAS. The degree of cross-linking seems to be constant and maximized.

Base catalysed consolidation

The thermal consolidation of the liquid polymers is a time consuming process dependent of the thickness of the cast sample and the consolidation temperature. Even at high temperatures up to 200 °C a sufficient consolidation state is only reached after 72 h indicated by the loss of stickiness on the samples surface. Addition of acids or bases to the liquid precursor polymers can catalyse the cross-linking reactions.[30] Using a base leads to the deprotonation of hydroxy groups in the main structure which can attack other silicon atoms undergoing a S_N2 type reaction. The reaction rate is increased for lowered electron density silicon atoms (ED: Si–O–Si < Si–OH < Si–OR). This catalytic effect was studied by adding small amounts of KOH to one sample exemplarily. For a qualitative demonstration the change in viscosity a 60 days aged sample 4 was determined at 110 °C after adding different amounts of KOH.

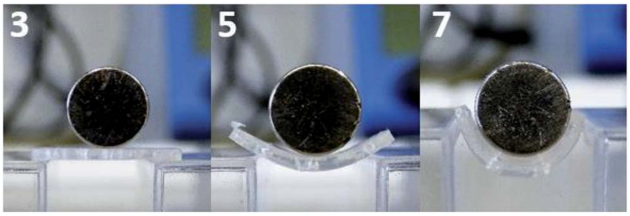

Fig. 12 Images of a small piece of sample 3, 5 and 7 deformed by the weight of a metal cylinder (1.9 g) for hardness demonstration. The increase of DAS from sample 1–8 leads to a decrease of sample hardness.

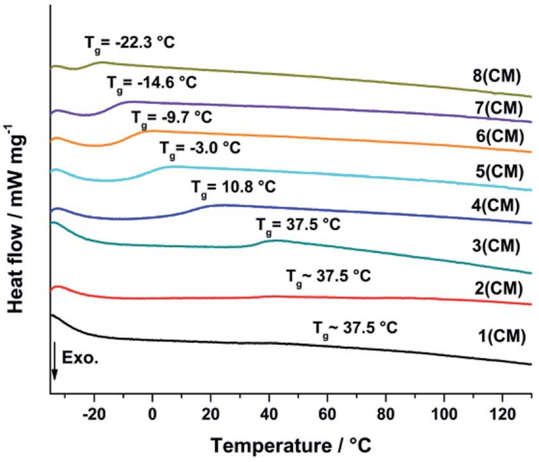

Fig. 13 DSC measurements of the consolidated samples 1–8 measured from −40 to 400 °C with 5 K min^{-1} under N_2 atmosphere (100 ml min^{-1}). The substitution of $Me_2Si(OMe)_2$ by $MeSi(OMe)_3$ leads to less cross-linked polymer chains resulting in a decrease of the glass transition temperature T_g.

During the initial heating step all samples showed a decrease of viscosity (Fig. 14). The KOH treated samples showed a significant increase of viscosity at 110 °C, while the viscosity of KOH free sample kept nearly constant. The increase can be

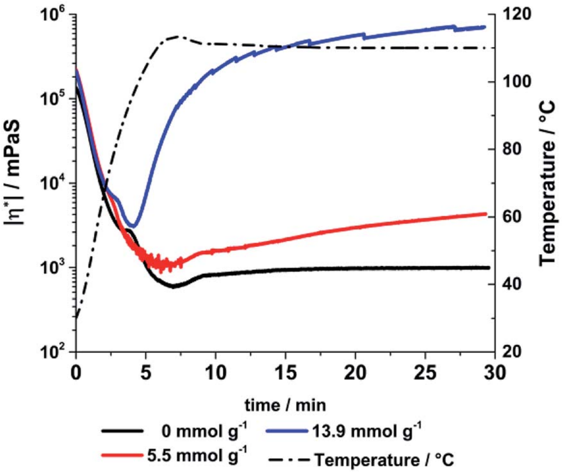

Fig. 14 Absolute amounts of viscosity of the aged sample 4 after adding different amounts of KOH measured with oscillation rheometry (5 K min^{-1} ramp, 110 °C).

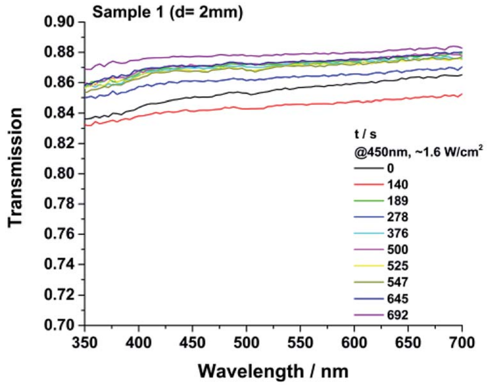

Fig. 15 Transmission spectrum of the consolidated sample 1 after the given time of irradiation at 450 nm with ~1600 mW cm^{-2} and 60 °C. There is no systematically change in transparency and no yellowing due the light exposition.

directly correlated with the amount of KOH added to the samples. A higher KOH concentration leads to more deprotonated hydroxyl species and increases the reaction and condensation rate respectively. Therefore, the consolidation time and temperature can be tailored by adjusting the amount of added base and it leads to an exemplary reduction of consolidation time from around 72 h to 30 minutes. The consolidation temperature program must be optimised for each composition to avoid bubble formation due to methanol or water evaporation. If the material hardens too fast small gas bubbles remain in the final material. A pre-treatment under reduced pressure before casting is suggested to remove solvent traces or gases. By using small amounts of a weaker base like DABCO (pK_b = 5.2) bubble formation can prevented as well.

Transmission, heat and light treatment

For a comparable transmission measurement all samples have to be smooth, without any inclusions or bubbles and homogeneous in thickness. For this reason, a polymer film of the gel (G) was prepared with a film applicator (13 × 0.12 mm) on glass slides for each sample. The as prepared samples were consolidated in a compartment drier (200 °C, 72 h). Shrinkage occurs, caused by the consolidation process indicated by the thickness change from liquid (0.12 mm) to solid thickness (see ESI†). The actual film thickness was determined at three different spots for each consolidated sample before measuring UV/VIS.

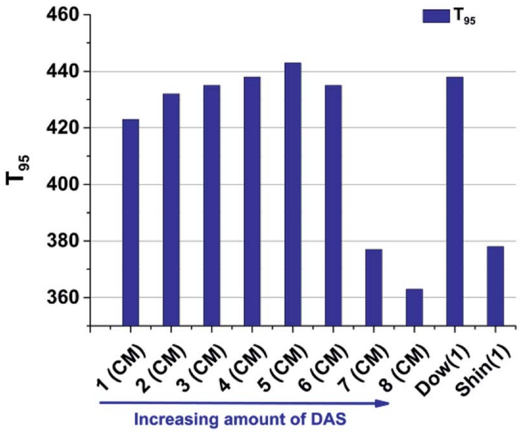

Fig. 16 T_{95} value of sample 1–8. It is >360 °C for all samples, which makes it suitable for high power applications with high temperature working conditions.

All samples show transmission values of >0.98 between 350 and 730 nm immediately after the consolidation procedure (Fig. 16). An additional heat treatment for 1170 h at 200 °C was performed to investigate changes in transparency (Fig. ESI39†). After the heat treatment, no significant change in colour or UV/VIS spectra were detected for samples 3–8. The more cross-linked and very hard materials 1 and 2 were pealed off from the glass slides after the heat treatment. No yellowing of the material was detected. Optical grade epoxy resins and commercial available HRI silicones show a much higher loss of transparency even at 120 °C.[8] Non-commercial, literature known platinum catalysed curable polysiloxanes also can show a decrease of transparency causing a discoloration due to a high temperature or light treatment.[9,21] Under working conditions of a LED the local temperature at the light emitting parts of a LED for example can reach up to 150 °C and the irradiance can reach values >500 mW mm^{-2} usually at 450 nm. Therefore a high temperature- and photostability of the packaging materials is required.[1–6] The samples 1, 3 and 8 were additionally cast in aluminium moulds (d = 2 mm) to test the irradiation stability at 450 nm as well. After 690 h of irradiation small but unsystematic changes in transparency were detected for the tested samples (Fig. 15). The spectra of sample 3 and 8 are shown in the ESI (Fig. ESI38).† The lower value of transparency of the irradiated samples compared to the heat-treated ones is caused by the higher sample thickness of 2 mm and the slightly structured and unpolished surface of the samples. All measured samples show unsystematic changes. The transparency of sample 1 and 3 increases slightly.

Changes in transparency of sample 8 show no trend. The highest decrease in transparency detected is about 0.04. Compared to the reported decrease of transparency of 0.05 for a commercially HRI silicone and over 0.25 for an epoxy resin due to a 480 h UV light treatment the here reported materials show a high photostability.

Thermogravimetric studies

For a further characterization of the heat stability the consolidated materials were heated up to 800 °C with 10 K min^{-1} and under N_2/O_2 with a gas flow of 20 ml min^{-1} to investigate the degradation behaviour respectively (Fig. ESI35†). To evaluate the degradation behaviour of the samples the temperature at which 5% of mass is lost is defined as T_{95} value.

For a comparison of the obtained stabilities, two cured reference encapsulation materials were also measured. The platinum curable silicone resin ShinEtsu KJR9022E [Shin(1)], which is a low refractive index (LRI) polydimethylsiloxane (PDMS), and Dow Corning OE6630 [Dow(1)], which is a high refractive index (HRI) polymethylphenylsiloxane (PMPS). Their components were mixed as specified by the respective manufacturer [Dow(1): 4/1; Shin(1): 10/1] and cured for 4 h at 150 °C.

Generally the T_{95} of all samples is larger than 360 °C (Fig. 16). No degradation is caused by temperatures lower than 200 °C. This indicates a very high thermal stability for the materials. The reference materials show large differences in their thermal stability. The T_{95} value of Dow(1) is 438 °C and 378 °C for Shin(1). In general more branched, platinum cured polysiloxane shows higher T_{95} values compared to less cross-linked or linear systems.[48,49] The same result is shown for the reference polymers, where the Dow(1) system is harder (Shore A $\sim$ 90) and more cross-linked compared to the Shin(1) polymer (Shore A = 42). Also the hybrid glasses show a decrease in degradation temperature caused by a decrease of TAS units, which leads to an decrease of crosslinking and stiffer polymers.[47] In our case, the hardness of the material decreases from sample 1 to 8 but the degradation temperature increases at the same time from sample 1 to 5. Sample 6–8 show a decrease of T_{95}. Grassie and others have shown that the degradation reaction of methyl and phenyl containing polysiloxanes depend on the type of the terminal group. Terminal hydroxyl groups can initiate a back-biting process liberating benzene and cyclosiloxanes.[50,51] Impurities like water and acid can also influence the rate of degradation.[50,52] One possible reason for the increase of degradation temperature from sample 1 to 8 is the increased lability of phenyl groups adjacent to cross-linking T^3 units in branched polymer chains.[51] By substitution of TAS by DAS units the possibility of phenyl groups next to a T^3 unit is reduced. In platinum curable polysiloxane systems this is not a common structural motif. The cross-linking is based on C–C single bonds formed by the hydrosilylation reaction. The decrease from sample 6 to 8 can be explained by the higher concentration of D^1 end groups and higher mobility of polymer chains leading to a higher appearance of a back biting degradation mechanism.

Conclusion

A series of platinum free curable polysiloxane based materials were synthesised by an acid catalysed condensation reaction of phenyltrimethoxysilane, methyltrimethoxysilane, dimethyldimethoxysilane, and an alkoxy-terminated polysiloxane. The material properties could be controlled substituting the amount of methyltrimethoxysilane by dimethyldimethoxysilane, which was proven by NMR and FTIR spectroscopy measurements. Two-dimensional ^{29}Si–^{1}H HMBC NMR spectroscopy (2D NMR) was used to characterise the first three hours of condensation reaction. An increasing amount of dimethyldimethoxysilane leads to unreacted monomers in the reaction solution. Therefore, it seems that a reaction of DAS with TAS monomers is more preferred then a dimerization of the DAS monomers. A direct relation between the substitution and a decrease of viscosity was found as well as a correlation between the corresponding decrease of percentage of phenyl groups and a decrease of refractive indices. Due to its gel state the viscosity was low enough for a processing at room temperature for most of the samples. The viscosity of the samples increases slightly due to long time storage verified by rheology. Similar to the precursor's viscosity the hardness of the samples after the curing procedure decreases when methyltrimethoxysilane is substituted by dimethyldimethoxysilane. The consolidated materials show no cracks, bubbles or changes in transparency due to the curing procedure. ^{29}Si and ^{13}C CP-MAS NMR spectroscopy revealed the presence of T^2 and T^1 signals in the ^{29}Si spectra and the presence of methoxy group signals in the ^{13}C spectra. This indicates an incomplete cross-linked structure. The glass transition temperature of the consolidated samples decreases with the amount of DAS, which verifies the correlated decrease of cross-linking. The loss of DAS units during the consolidation was investigated by TG-FTIR and ^{29}Si–^{1}H 2D HMBC NMR spectroscopy. The presence of volatile dimethylcyclosiloxanes in the precursor gels was proven and mainly responsible for the reported DAS loss. The main mass loss of >10% during the consolidation was caused by the loss of water and methanol.

Conflicts of interest

There are no conflicts to declare.

Acknowledgements

This research has been funded by the Federal Ministry of Education and Research (BMBF, Germany) in the project ORCA – Organic and rare earth reduced conversion materials for LED-based lightning (project number 03XP0050D). We would like to thank Dr Michael Zimmer for the CP-MAS NMR measurements, Dr Patrick Wenderoth and Dennis Meier for experimental, and Silvia Beetz for technical support.

References

1 M. Meneghini, L.-R. Trevisanello, G. Meneghesso and E. Zanoni, *IEEE Trans. Device Mater. Reliab.*, 2008, **8**, 323–331.
2 S. I. I. Chan, W. S. S. Hong, K. T. T. Kim, Y. G. G. Yoon, J. H. H. Han and J. S. S. Jang, *Microelectron. Reliab.*, 2011, **51**, 1806–1809.
3 C. W. Hsu, C. C. M. Ma, C. S. Tan, H. T. Li, S. C. Huang, T. M. Lee and H. Tai, *Mater. Chem. Phys.*, 2012, **134**, 789–796.
4 C. Hang, J. Fei, Y. Tian, W. Zhang, C. Wang, S. Zhao and J. Caers, *Proc. - 2013 14th Int. Conf. Electron. Packag. Technol.*, ICEPT, 2013, vol. 2013, pp. 1126–1129.
5 T. Li, J. Zhang, H. Wang, Z. Hu and Y. Yu, *ACS Appl. Mater. Interfaces*, 2013, **5**, 8968–8981.
6 J. Kim, S. Yang, S. Kwak and Y. Choi, *J. Mater. Chem.*, 2012, **22**, 7954–7960.
7 X. Yang, Q. Shao, L. Yang, X. Zhu, X. Hua, Q. Zheng, G. Song and G. Lai, *J. Appl. Polym. Sci.*, 2013, **127**, 1717–1724.
8 Y. H. Lin, J. P. You, Y. C. Lin, N. T. Tran and F. G. Shi, *IEEE Trans. Compon. Packag. Technol.*, 2010, **33**, 761–766.
9 J. S. Kim, S. Yang and B. S. Bae, *Chem. Mater.*, 2010, **22**, 3549–3555.
10 M. H. Chang, D. Das, P. V. Varde and M. Pecht, *Microelectron. Reliab.*, 2012, **52**, 762–782.
11 J. Y. Bae, Y. H. Kim, H. Y. Kim, Y. B. Kim, J. Jin and B. S. Bae, *ACS Appl. Mater. Interfaces*, 2015, **7**, 1035–1039.

12 N. Narendran, Y. Gu, J. P. Freyssinier, H. Yu and L. Deng, *J. Cryst. Growth*, 2004, **268**, 449–456.

13 Z. Ren and S. Yan, *Prog. Mater. Sci.*, 2016, **83**, 383–416.

14 I. A. Lei, D. F. Lai, T. M. Don, W. C. Chen, Y. Y. Yu and W. Y. Chiu, *Mater. Chem. Phys.*, 2014, **144**, 41–48.

15 J. Y. Bae, Y. Kim, H. Kim, Y. Kim, J. Jin and B. S. Bae, *ACS Appl. Mater. Interfaces*, 2015, **7**, 1035–1039.

16 J. Chen, Z. Fu, H. Huang, X. Zeng and Z. Chen, *RSC Adv.*, 2016, **6**, 71924–71933.

17 M. Zhao, Y. Feng, G. Li, Y. Li, Y. Wang, Y. Han, X. Sun and X. Tan, *Polym. Adv. Technol.*, 2014, **25**, 927–933.

18 N. Steinbrück, M. Könemann and G. Kickelbick, *RSC Adv.*, 2018, **8**, 18128–18138.

19 M. Könemann, S. Ivanovici, H. S. Mangold, G. Kickelbick and N. Steinbrück, EP18151250.0, 2018.

20 Y. Yang, G. Xian, H. Li and L. Sui, *Polym. Degrad. Stab.*, 2015, **118**, 111–119.

21 R. Wen, J. Huo, J. Lv, Z. Liu and Y. Yu, *J. Mater. Sci.: Mater. Electron.*, 2017, **28**, 1–14.

22 Y. Gan, X. Jiang and J. Yin, *J. Mater. Chem. C*, 2014, **2**, 5533.

23 S. D. Bhagat, J. Chatterjee, B. Chen and a E. Stiegman, *Macromolecules*, 2012, **45**, 1174–1181.

24 Y. Zuo, Z. Gou, J. Cao, X. Li and S. Feng, *RSC Adv.*, 2016, **6**, 45193–45201.

25 G. Mura, G. Cassanelli, F. Fantini and M. Vanzi, *Microelectron. Reliab.*, 2008, **48**, 1208–1211.

26 L. C. Klein and A. Jitianu, *J. Sol-Gel Sci. Technol.*, 2011, **59**, 424–431.

27 Wacker Chemie AG, *Silicone Solutions for High-Performance LEDs - Brochure 6875*, 2013.

28 Wacker Chemie AG, *Silicone Solutions for High-Performance LEDs - Brochure 6875*, 2017.

29 T. Higashihara and M. Ueda, *Macromolecules*, 2015, **48**, 1915–1929.

30 U. Schubert, *The Sol-Gel Handbook: Synthesis, Characterization, and Applications*, Wiley-VCH, 2015, vol. 1.

31 B. Arkles, J. R. Steinmetz, J. Zazyczny and P. Mehta, *Silanes and Other Coupling Agents: Factors contributing to the stability of alkoxysilanes in aqueous solutions*, 1992.

32 C. J. Brinker and G. W. Scherer, *J. Non-Cryst. Solids*, 1985, **70**, 301–322.

33 C. J. Brinker, *J. Non-Cryst. Solids*, 1988, **100**, 31–50.

34 A. Jitianu, G. Amatucci and L. C. Klein, *J. Am. Ceram. Soc.*, 2009, **92**, 36–40.

35 A. Jitianu, G. Gonzalez and L. C. Klein, *J. Am. Ceram. Soc.*, 2015, **98**, 3673–3679.

36 A. Jitianu, J. Doyle, G. Amatucci and L. C. Klein, *J. Sol-Gel Sci. Technol.*, 2010, **53**, 272–279.

37 L. C. Klein, S. Kallontzi, L. Fabris, A. Jitianu, C. Ryan, M. Aparicio, L. Lei and J. P. Singer, *J. Sol-Gel Sci. Technol.*, DOI: 10.1007/s10971-018-4599-9.

38 A. Jitianu, S. Cadars, F. Zhang, G. Rodriguez, Q. Picard, M. Aparicio, J. Mosa and L. C. Klein, *Dalton Trans.*, 2017, **46**, 3729–3741.

39 D. Corning, OE6630, http://www.dowcorning.com.

40 ShinEtsu, KJR9022, http://www.shinetsu-encap-mat.jp/e/.

41 Dow Corning Corporation, *LED Packaging - Advanced silicone technology for LED applications*, http://www.ellsworth.com/globalassets/literature-library/manufacturer/dow-corning/dow-corning-brochure-silicone-technology-for-led-packaging.pdf.

42 Shin-Etsu Chemical Co. Ltd., *Encapsulation materials for optical devices*, http://www.shinetsu-encap-mat.jp/e/product/k_l/lds/.

43 S. Yoshiyuki, O. Seigo, K. Kazuyuki and K. Chuzo, *J. Non-Cryst. Solids*, 1992, **139**, 25–34.

44 Z. Zhang, B. P. Gorman, H. Dong, R. A. Orozco-Teran, D. W. Mueller and R. F. Reidy, *J. Sol-Gel Sci. Technol.*, 2003, **28**, 159–165.

45 J. Kunz and M. Studer, *Kunstst. Int.*, 2006, **6**, 1–3.

46 L. C. Klein, B. McClarren and A. Jitianu, *Adv. Mater. Res.*, 2014, **783–786**, 1432–1437.

47 A. Jitianu, K. Lammers, G. A. Arbuckle-Kiel and L. C. Klein, *J. Therm. Anal. Calorim.*, 2012, **107**, 1039–1045.

48 W. Zhou, H. Yang, X. Guo and J. Lu, *Polym. Degrad. Stab.*, 2006, **91**, 1471–1476.

49 X. Zhan, H. Liu, J. Zhang, J. Cheng and X. Lin, *Ind. Eng. Chem. Res.*, 2014, **53**, 4254–4262.

50 N. Grassie and I. G. Macfarlane, *Eur. Polym. J.*, 1978, **14**, 875–884.

51 N. Grassie, I. G. Macfarlane and K. F. Francey, *Eur. Polym. J.*, 1979, **15**, 415–422.

52 S. A. Visser, C. E. Hewitt and T. D. Binga, *J. Polym. Sci., Part B: Polym. Phys.*, 1996, **34**, 1679–1689.

4.4. Lifetime Measurements of Dye incorporated Polysilsesquioxanes

The platinum-free thermally curable polysilsequioxane encapsulations were not just prepared for the encapsulation of the LED package; they also should enhance the lifetime of organic dyes significantly and protect them from degradation. For the evaluation of the lifetime, samples, including different dyes and concentrations were prepared and send to the BASF SE test laboratory. The samples were irradiated at 450 nm with an irradiance of 160 mW/cm^2 while following the development of fluorescence intensity was measured (**Figure 23**). The blue curve shows the decrease of intensity of the Lumogen®F Red 305 (LG305) dye, assigned with FC01. Due to confidentiality agreements, the properties of the other dyes FC430 and FC739 have to stay unspecified.

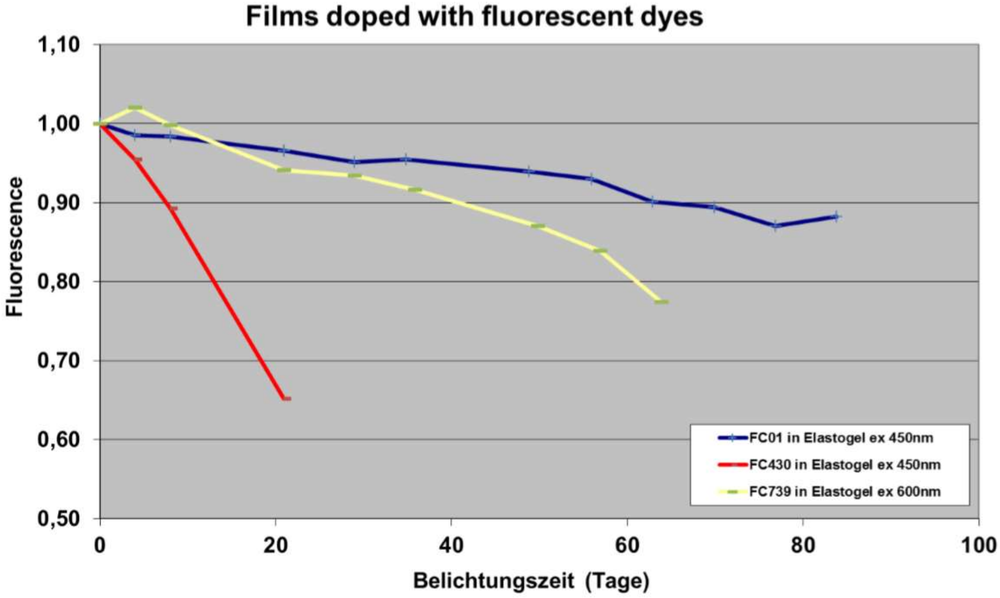

Figure 23. Fluorescence intensity of a platinum-free thermally polysilsequioxane encapsulation with three different dyes incorporated irradiated by 450 nm light source with 160 mW/cm^2 at the BASF SE laboratory.

The fluorescence intensity of LG305 (FC01) decreases only by 10 % after 90 days of irradiation at the given conditions. In the first place, the platinum-free thermally curable elastomer encapsulations presented in chapter 4.3 enhance the photostability of the dye significantly (**Figure 25**). The related publication stated out that this material is also a sustainable and quite outstanding alternative to the conventional two-component platinum-catalyzed encapsulations. Another contemplated approach, which was not discussed before, is the preparation of polysilsesquioxanes, which consists of trialkoxysilane units only. A partially, but highly cross-linked polysilsesquioxane hybrid glass was therefore prepared by a synthetic route known from the literature.[103] Phenyltrialkoxysilane was reacted by an acid-catalyzed condensation reaction followed by gelation and a two-step temperature treatment. The transparent, rigid, and hard materials are solid at room temperature and meltable at temperatures >80 °C. By a further temperature increase, it consolidated irreversibly by further condensation (see chapter 2.3). By introducing the reference dye LG305 to the materials synthesis procedure, a fluorescent hybrid glass was synthesized. The highly cross-linked structure can result in hermetic oxygen barrier properties that are probably able to protect the incorporated dyes from degradation.[102,175]

The material was cast, consolidate, and has also been tested at the BASF SE laboratory with by radiation with a 450 nm light source with an irradiance o 160 mW/cm^2 at different conditions (**Figure 24**).

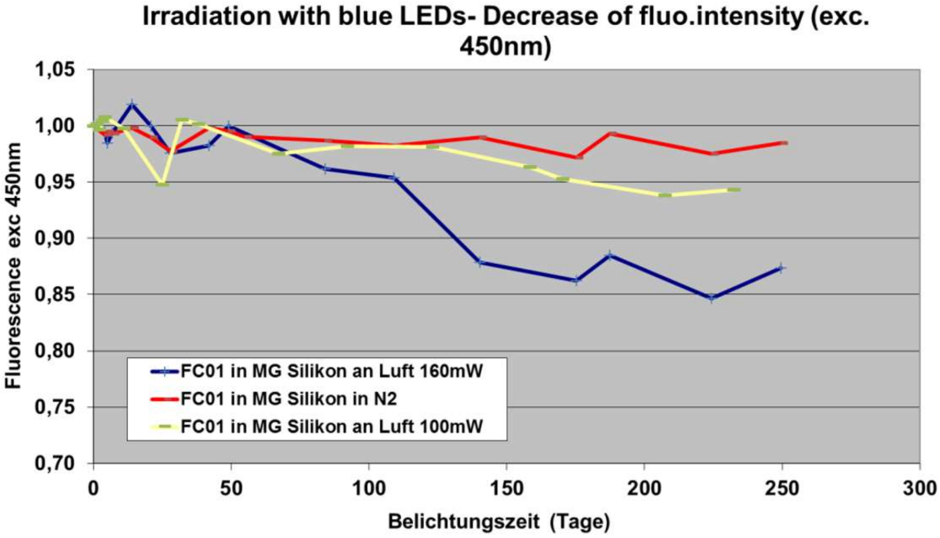

Figure 24. *Fluorescence intensity of the hybrid glass encapsulation with Lumogen®F Red 305 incorporated and irradiated by 450 nm light source with 160 mW/cm^2 at the BASF SE laboratory.*

The photostability of LG305 increases significantly due to this hybrid glass matrix. After 250 d of irradiation at 160 mW/cm^2 under N_2 and at 100 mW/cm^2 under ambient conditions, the initial fluorescence intensity decreased slightly by 1-5 %. At 160 mW/cm^2 under ambient conditions, the increase in intensity was less than 15 %.

Due to the massive enhancement of the photostability further tests were carried out with the LG305 incorporated platinum-free elastomer and the hybrid glass under more powerful conditions in our laboratory and the results were compared to those from longtime stability tests of LG305 in the commercially available, two-component, and platin containing polymer resins used before, Dow Corning OE6630 [Dow[(1)] and ShinEstu KJR9022E [Shin(1)] (**Figure 25**). Incorporated in Dow(1) the dyes initial absorbance was decreased by 10 % after 25 hours of irradiation at 450 nm and 850 mW/cm^2. Incorporated in the platinum-free elastomers and in the hybrid glass, the initial absorbance decreased by 10 % after 928 h (~39 d) of irradiation at the same conditions. Using the platinum-free elastomer or the hybrid glass as an encapsulation for the dye a lifetime increase of 3700 % can be realized.

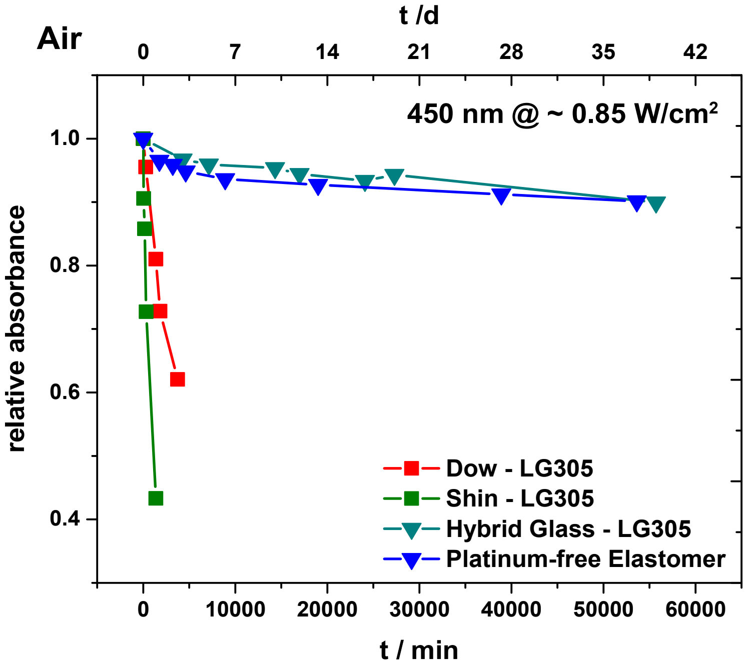

Figure 25. *Relative absorbance of Dow(1)LG305, Shin(1)LG305, platinum-free elastomer with LG305 and hybrid glass with LG305 at different times measured during a light exposure with 450 nm light source with 800 mW/cm^2.*

Crack and bubble formation started during the consolidation procedure when casting the dye-containing hybrid glasses in different molds and cavities. The material is too hard and rigid for casting it without getting any surface or sample destruction because of large differences of the hybrid glasses and molds coefficient of thermal expansion. To make use of the hybrid glasses features concerning the protection of the dye, another possibility had to be found to make this host-dye-combination suitable for implementation in an LED package without casting it.

The industrial used inorganic rare-earth phosphors are always used in a particular morphology. The YAG:Ce^{3+} phosphor, for example, is produced and used as a powder consisting of spherical oxide particles with a diameter of < 25 µm. Considering the idea of fluorescent hybrid glass microparticles able to be implemented in an LED package as a powder, a surfactant mediated synthesis route was developed and optimized. The synthesis procedure leads to highly fluorescent, thermally stable and fully cross-linked hybrid glass particles with narrow size distributions, which can be implemented in optoelectronic applications like the organic hybrid LED without using rare-earth or platinum-containing components.

4.5. Fluorescent Polyphenylsilsesquioxane Hybrid Glass Microspheres

Unpublished Results

Nils Steinbrück, Svenja Pohl, Guido Kickelbick*

Saarland University, Inorganic Solid State Chemistry, Campus, Building C4 1, 66123 Saarbrücken, Germany.

The platinum-free curable siloxanes were modified with Lumogen®F Red 305. The fluorescent materials were exposed to 450 nm light for several days showing the highest lifetimes and lowest dye degradation measured within this thesis and our studies. Due to confidentiality agreements, some experiments and results were not allowed to be published in paper form. This is the reason why the lifetime measurements are shown in a short research summary preceded the fourth and last chapter.

The hybrid glass material was prepared by an acid-catalyzed polycondensation of phenyltrimethoxysilane. After the consolidation of this material in all casts, it started to crack. This formation of cracks and destruction of the material in molds or cavities is caused by the high cross-linking degree and hardness respectively, and the low thermal coefficient of expansion. However, the improvement of the photostability of the integrated dye was so significant, that a preparative way had to be found to make this material dye combination suitable for implementation into optoelectronic applications.

In the **fourth and last chapter,** a new preparation method of ***Fluorescent Polyphenylsilsesquioxane Hybrid Glass Microspheres*** is presented in the form of an unpublished paper manuscript. A pure polyphenylsilsesquioxane hybrid glass with LG305 incorporated was prepared and transformed into microparticles by a novel surfactant mediated hot emulsion technique. The hybrid glass was melted and stirred in an aqueous solution of a surfactant (Triton X-405) forming an emulsion. Addition of NaOH leads to condensation and hardening of the particle surface. The solid and spherical particles were isolated, dried, and post cured at 200 °C. An optimization with regard to the particle size distribution leads to small size distributions with an averaged particle size of 3 µm by using a disperser tool. Thermogravimetric and spectroscopic data show that the surfactant used in the synthesis is still located on the surface of the particles after isolation, creating a hydrophobic surface. After the post-curing process at 200 °C the surfactant is completely removed, making the surface hydrophilic. During this heat treatment, the cross-linking degree of the particles increases to 100 %, which was not reported for this type of hybrid glasses or any other polyphenylsilsesquioxane particles prepared by sol-gel chemistry yet.[61,176,177] Due to the formation of this completely cross-linked $PhSiO_{1.5}$ structure, the particles turn insoluble in organic solvents. The quantum yield of the dye incorporated in the particles decreased slightly from 1.0 to 0.87, caused by morphology and size effects. Such a decrease has also been reported by other silica and polymeric particles, and can also be explained by scattering effects .[108,156,178,179]

This synthesis procedure can also be used to incorporate other hydrophobic organic dyes and substances into the polysilsesquioxane matrix without changing the polarity of the organic molecules. Therefore, the formed microparticles are also suitable as containers in other fields like medicine or biology.

Abstract

Polysilsesquioxane based micro- and nanoparticles are often synthesized by facile sol-gel methods using trialkoxysilanes precursor or by platinum assisted hydrosilylation. By performing an acid-catalyzed condensation reaction of phenyltrimethoxysilane a partially cross-linked but solid polyphenylsilsesquioxane hybrid glass was synthesized, able to be melted at >80 °C and consolidated at >150 °C without any platinum catalyst. A hydrophobic perylene dye can be added to this polymeric precursor during the synthesis. Triton™ X-405 emulsifier was used as a surfactant in the preparation of an emulsion of this precursor in water for the preparation of fluorescent polyphenylsiloxane microspheres with an emission maximum at 647 nm. The size of the microspheres can be varied in the range of 3.09 – 7.50 µm.

By using NMR and FTIR spectroscopy as well as thermogravimetric analysis of the polyphenylsilsesquioxane precursors and the microspheres revealed that the hydrophilic untampered microspheres are partially cross-linked and soluble in organic solvents. An additional heat treatment leads to a complete cross-linking of the microspheres' structure and the removal of the surface attached surfactant. The obtained microspheres are hydrophobic and insoluble in organic solvents

Introduction

Most of the known synthetic procedures for silica or polysilsesquioxane particles are based on the sol-gel process. Applying a base catalyzed the sol-gel process, organotrialkoxysilanes or tetraalkoxysilanes can be used for the formation of spherical particles with narrow size distribution.[159–162] The particle shape and properties can be adjusted by the selection of the organic substituents of the monomers, the reaction conditions, or by assisted methods like an ultrasonic treatment or the use of continuous methods.[61,163] The integration of hydrophobic dyes into the particle structure without a previous functionalization of the dye is difficult to realize due to their insolubility in the continuous phase like water or ethanol. Ionic dyes can be integrated easily whereas hydrophobic dyes like perylenes required a previously functionalization as described for example for perylene containing polyhedral oligomeric silsesquioxanes particles (POSS).[160,171–173] Another approach is the functionalization of the outer and inner particles surfaces by surfactants, before incorporating hydrophobic or hydrophilic dyes selectively in a second step.[180] Additionally, structural investigations of the silica or polysilsesquioxane networks by spectroscopic methods usually show that the materials are only partially cross-linked structures.[61,159,176,177]

In our work, we present a new approach for the synthesis of fully-crosslinked polyphenylsilsesquioxane microspheres by a two-step procedure in which the microspheres are synthesized by an already partially cross-linked polyphenylsilsesquioxane hybrid glass. This precursor was synthesized by performing an acid-catalyzed condensation reaction of phenyltrimethoxysilane. The synthetic procedure is based on the published hybrid glass polysiloxane materials.[103] A hydrophobic highly fluorescent perylene dye was mixed with the precursor. The subsequent addition of a base to the emulsion starts a condensation reaction of the particles resulting in partially cross-linked but unmeltable microspheres. An additional heat treatment enforces the removal of the surfactant from the particle surface and leads to a further cross-linking of the particle network resulting in a complete $PhSiO_{1.5}$ structure. By performing spectroscopic investigations like ^{1}H, ^{13}C and ^{29}Si (CP-MAS)-Nuclear magnetic resonance (NMR), infrared spectroscopy (FTIR) and fluorescence spectroscopy as well as thermogravimetric methods (TG, TG-FTIR) the structural changes of the polyphenylsilsesquioxane network and its surface was studied and correlated to the materials properties like solubility, heat stability and hydrophobia. The presents and removal of the surfactant on the surface of the microspheres were also investigated and proven by the given methods. Additionally, the fluorescence properties of the integrated dye were characterized, and the synthesis procedure was optimized with regard to the microspheres mean size by increasing the stirring velocity.

Experimental

Materials

Phenyltrimethoxysilane (97 %, ABCR GmbH, Germany), polyoxyethylene(40)isooctylphenylether solution (Triton X-405, 70 % in water, Sigma-Aldrich/Merck KGaA, Germany), hydrochloric acid (Bernd Kraft, GmbH) and potassium hydroxide (85 %, Grüssing GmbH Analytica, Germany) were used as received. The hydrochloric acid was diluted with demineralized water (pH = 2.5). Potassium hydroxide was dissolved in water (3 mol l^{-1}). The commercially available, curable *OE6630* polysiloxane resin [Dow(1), Dow Corning Inc., USA] were used as received without any further purification. The perylene dye Lumogen®F Red 305 was also used as received without any further purification. The precursor's purity was characterized by ^{1}H and ^{29}Si NMR spectroscopy (see ESI).

Instrumentation

NMR spectra were recorded with an Avance III 300 MHz spectrometer and an Avance III HD 400 MHz spectrometers (Bruker Corporation, USA) applying 300.13/400.13 MHz for ^{1}H NMR spectra, 59.63/79.49 MHz for ^{29}Si NMR spectra and 75.47/100.61 MHz for ^{13}C NMR spectra. All NMR samples were prepared in methanol-d_4 ($MeOD_4$, Ref.: 3.310 ppm) or Chloroform-d ($CDCl_3$, Ref.: 7.260 ppm). CP-MAS-NMR spectra were recorded with an Avance III HD – Ascend 400WB spectrometer (Bruker Corporation, USA) using 13 KHz rotation and 100.65 MHz for ^{13}C as well as 79.53 MHz for ^{29}Si NMR spectra. For the visualization of submillimeter structures, an Axioskop 50 transmitted light/fluorescence microscope with an AxioCam MRc (1388x1040 pixel) was used. Thermogravimetric measurements were carried out with a TG209 F1 Libra thermo-microbalance (Netzsch-Gerätebau GmbH, Germany) with 10 K/min to 250/800 °C with the gas flux of N_2/O_2 of 20 ml/min each. Fourier transformed infrared spectra (FTIR) were recorded in total reflectance mode on a Vertex 70 spectrometer (Bruker Corporation, USA) from 4500 – 400 cm^{-1} with a 4 nm increment and 10 scans averaged. A self-made fiber-coupled 450 nm wavelength illumination system with 710 mW LEDs (6 x LDW5SN) was used as an irradiation source for photostability experiments. UV/Vis transmission measurements were performed on a Lambda 750 instrument (Perkin Elmer Inc., USA) equipped with a 100 mm integration sphere from 700 – 350 nm with a 2 nm increment and 0.2 s integration time. Fluorescence spectroscopy was performed applying a FluoroMax 4 Spectrofluorometer (Horiba Scientific, Japan) and the absolute photoluminescence quantum yields were measured in a Quantaurus C11347-11 integration sphere setup (Hamamatsu Photonics, Japan) with a xenon high-pressure lamp and a multichannel analyzer at 450 nm excitation wavelength.

Preparation

The hybrid glass microspheres were synthesized in a two-step procedure. First, a polyphenylsilsesquioxane-like hybrid glass was prepared inspired by a literature synthesis route.[103] During the synthesis, a specific perylene diimide dye was added for incorporation into the material. The dye used in this work was Lumogen®F Red 305, which is physically integrated into the hybrid glass.

Synthesis of precursor hybrid glass (MG)

Phenyltrimethoxysilane (25 g, 126.07 mmol, [$PhSi(OMe)_3$]) and hydrochloric acid (pH=2.5, 3.41 g, 189.12 mmol) was stirred in a sealed vial at 45 °C for 6 h. Absolute methanol (1.80 g, 56.18 mmol) was added dropwise while further stirring at 40 °C for 2 h. The solution was transferred into a 100 ml beaker, a certain amount of one of the perylene diimide dyes were added (18 mg, n(LG305) = 16.68 µmol). The mixture was stirred until gelation was completed (25 °C, 18 h). The beaker was transferred into a compartment drier and to interrupt reactions by removing water, hydrochloric acid, and methanol in two steps. Hence the material was heated at 70 °C for 24h and afterward at 110 °C for a further 24 h. The red materials were cooled to room temperature to obtain solid hybrid glass materials (15.24 g, 1200 ppm/1.09 µmol g^{-1} LG305). The hybrid glasses soften reversible at temperature > 80 °C. At temperatures > 150 °C the materials consolidate irreversibly. The unconsolidated materials were denoted with **MG (LG305)**. The consolidated materials were denoted with **MG Cons. (LG305)**

Synthesis hybrid glass microspheres (MGP)

Polyoxyethylene(40)isooctylphenylether solution (90 mg, Triton™ X-405, 70 wt% in water [~0.356 mmol/g]) was added to water (14 ml, 0.77 mol) and stirred at 100 °C with 500 rpm. The 100 mg of the hybrid glass precursor was added to the hot solution. The emulsion formed due to the melting of the precursor was further stirred for 0.4 – 2 h at 100 °C. Sodium hydroxide solution was added to the emulsion (1 ml, 3 mol L^{-1}). After further stirring with 500 rpm for 0.4 h at atemperature of 100 °C the emulsion was cooled in an ice-water bath. The obtained hybrid glass microspheres were isolated and washed by centrifugation 4 times with water and dried in a compartment drier under reduced pressure at 80 °C and 5 mbar. The obtained products are denoted **MGP (LG305)**. Subsequent heat treatment of the particles was also performed for a comparison with the untampered ones. The heat-treated particles were denoted **MGP-T (LG305)**.

Stirring variation

Five experiments were made with different stirring to investigate the influence of the stirring to the particle morphology. By using an Ultra-Sonic finger (150 W) and an Ultra-Turrax™ dispenser (10,000 rpm) after stirring at 500 rpm for 10 min we investigated the influence of high energy processes to the particle morphology as well. The given stirring rate and time are related to the experimental part before adding sodium hydroxide. After adding sodium hydroxide the stirring rate was 500 rpm for all samples. The particle size and distribution was determined by measuring and counting particles from microscopy images

Post-curing

For further investigations of temperature-induced changes in structure or heat stabilities, the **MGP** microspheres were additionally heat treated in a post-curing process at 200 °C for 4h. The so obtained tampered particles were denoted with **MGP-T**.

Particle integration to a Polyphenylmethylsiloxane Resin

The particles have been added to Dow Corning OE6630. The two Dow(1) components A and B were premixed as specified by the manufacturer (4/1). The particles were added to the mixture respectively, and gas was removed under reduced pressure (4 mbar, >30 min) before casting the mixture into PTFE (30 x 10 x 1 mm) or aluminum molds (8 x 2 mm).

Results and Discussion

Polysilsesuqioxane precursor

Fluorescent hybrid glass microspheres were synthesized by forming a surfactant supported emulsion of a dye-containing polyphenylsilsesquioxane precursor. The precursor was prepared by an acid-catalyzed polycondensation reaction of phenyltrimethoxysilane forming partially cross-linked structures (**Scheme 18**).[105,175]

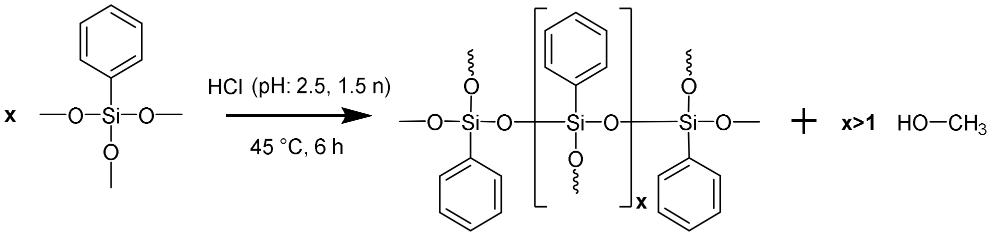

Scheme 18. Polycondensation of Phenyltrimethoxysilane under acidic conditions.

During a gelation step the organic fluorescence dyes are addable to the synthesis procedure and the material respectively (**Figure 26**). The obtained samples are solid, transparent, and rigid and soften reversible at temperatures > 80 °C.

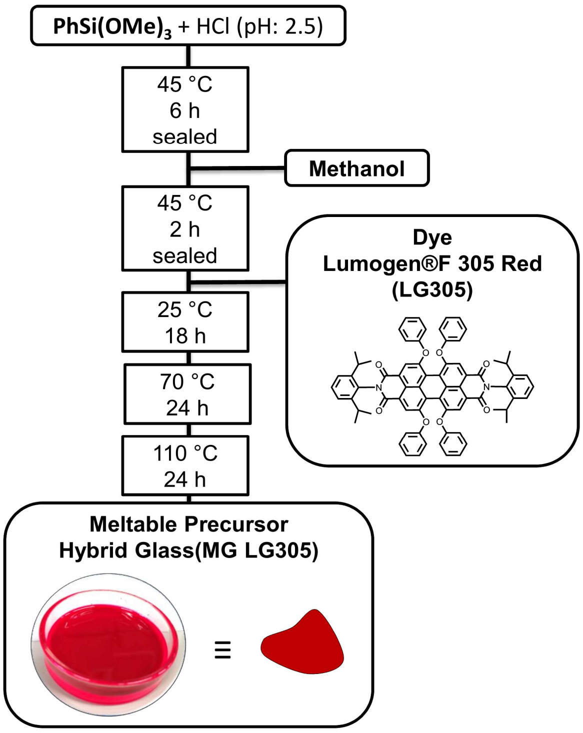

Figure 26. The synthesis procedure of a polysilsesquioxane precursor hybrid glass.

The precursor was characterized by FTIR and NMR spectroscopy. The FTIR spectra show the expected vibration bands of a **MG** polyphenylsilsesquioxane network indicated by broad ν(Si–O) vibration bands at 1052, 1016, 806 cm^{-1} and phenyl side groups at 3050, 3072, 2953, 2910 [ν(C–H)AR]; 1130 δ(Si– C)AR; 726 cm^{-1} [ρ(C–H)], and 694 cm^{-1} [ν(Si–C)] (Figure ESI20). Additionally, vibration bands at 3380 ν(O–H), 2840 [ν(C–H[O–CH$_3$])], and 846 [δ(Si–O–CH$_3$)] are caused by the polymers pendant and terminal methoxy groups as well as unreacted monomers, methanol, or water. The ^{1}H and ^{13}C NMR spectra show the chemical shifts of the phenyl protons [8.07 – 6.84 (m, phenyl)] and the alkoxy protons [3.96 – 2.97 (m, MeOR [R= H, CH$_3$])] as well as the corresponding carbon chemical shifts at -134.26…-127.93 ppm [Phenyl] and -50.78 ppm [MeOR [R= H, CH$_3$] (Figure ESI3). Signals of the integrated dye are not detectable due to the low dye concentration. Two-dimensional ^{1}H-^{29}Si HMBC NMR spectroscopy was used to characterize the cross-linking of the silicon atoms in the precursor (Figure ESI4). To the chemical shifts of the trifunctional T^2 units of phenyltrimethoxysilane monomers, there are also T^3 units detectable (**Table 1**). The additional chemical shift at -22 ppm can be assigned to small traces of silicon grease.

Table 1. *^{29}Si and ^{1}H chemical shift of the polyphenylsilsesquioxane precursor detected by two-dimensional ^{1}H-^{29}Si HMBC NMR spectroscopy.*

^{29}Si [Ph**Si**(OR)$_{3-x}$]	^{1}H [**Ph**Si(OMe)$_{3-x}$]	^{1}H [PhSi(O**Me**)$_{3-x}$]	**Functional Group**
-75…-80	8.07…6.84	-	**T^3**
-64…-74	8.07…6.84	3.96…2.97	**T^2**

The prepared polysilsesquioxane precursor consists of a partially cross-linked structure of T^2 and T^3 units. The material softens and even melts at higher temperatures is caused by the flexibility of the polymer chains, which consist of a high amount of linearly connected T^2 phenyltrimethoxysilane units. During the reaction procedure, a completely cross-linked polysilsesquioxane with the composition PhSiO$_{1.5}$ is formed, but some alkoxy groups are still not hydrolyzed, which can be concluded from the T^2 units by the 2D NMR. This partially cross-linking of phenyltrialkoxysilanes was already reported for silsesquioxane based particles obtained by sol-gel reactions.[61,176,177] The bulky phenyl substituents should hinder the formation of dense T^3 networks for sterical reasons. The cross-peak of the ^{29}Si NMR chemical shift of the T^2 units and the methoxy protons also confirms the presence of unreacted methoxy groups at the silicon atoms. The number of methoxy groups left was calculated by the change of intensity of the ^{1}H methoxy chemical shift before and after the synthesis. 10 % of the initial amount of methoxy groups are still present in the polymer. The number of T^2 units cannot be calculated from the NMR data because hydrolyzed and non-hydrolyzed units cannot be separated in the ^{1}H spectrum and due to the ^{1}H-^{29}Si HMBC experiment a quantitative evaluation of the ^{29}Si NMR peak areas is not reasonable.

Precursor Consolidation

The precursor material is soluble in organic solvents and can be thermally consolidated by an additional heat treatment at temperatures >200°C. The consolidation is caused by the condensation of still existing methoxy and hydroxy groups left in the partially cross-linked precursor.[181] After consolidation, the material is not meltable anymore but still soluble in organic solvents. Thermal analysis of the precursor shows the differences in the behavior of the material before and after thermal consolidation. Heat treatment of the precursor leads to an irreversible consolidation of the material caused by a further condensation of T^2 units. [81,100] The TG measurement of **MG** shows a mass loss of 3% starting at 216 °caused by this condensation reaction (**Figure 27**). The FTIR spectra of the gases being released at this temperatures show exclusively vibrations of the condensation product methanol and water at 3082 [ν(O-H)], 2980, 1467 [ν(C-H [O-CH_3])], 1033 cm^{-1}[ν(C-O)].[182] After this event, the methanol vibrations signal intensity decreases, and the material is consolidated irreversible.

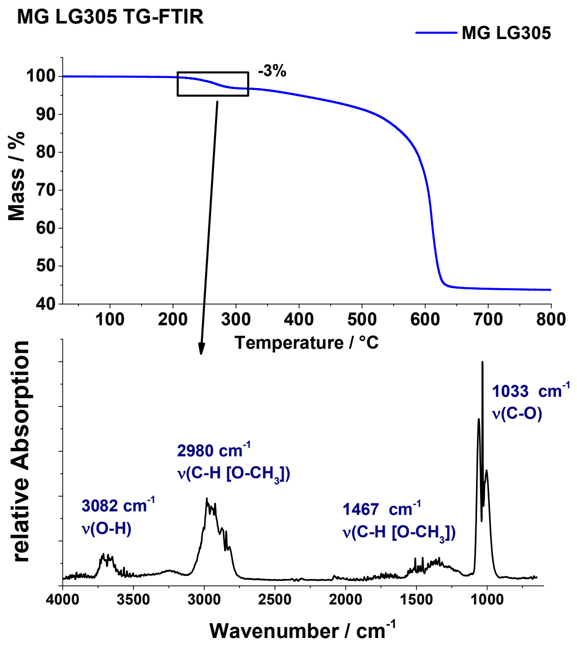

Figure 27. TG and FTIR spectrum of MG during heat treatment from 25 – 800 °C under air.

No additional mass loss caused by further condensation reactions or by formed side products like cyclosiloxanes was observed, which was described in the literature for comparable condensation reactions of materials containing tri- and dialkoxysilanes monomers. [54,55,81,100] After this consolidation step the **MG Cons.** degradation begins at 488 °C defined by the T_{95} value at which 95 % of the initial mass is left (Figure ESI30). The ATR-FTIR spectra of the consolidated material do not show any relevant changes compared to the unconsolidated material, only the water vibrations at 3380 cm^{-1} [ν(O–H)] are disappeared (Figure ESI18, 19). In the ^{29}Si NMR spectrum of the consolidated sample T^3 and T^2 units are still detectable -80 and -72 ppm as well as carbon from remaining methoxy groups in the and ^{13}C CP-MAS-NMR at -50.38 ppm (Figure ESI6-8). This concludes that the material is irreversibly consolidated by the heat treatment, but it is not fully cross-linked afterward. A semi-quantitative analysis of the peak areas of the chemical shifts in the ^{29}Si CP-MAS-NMR by fitting a Lorentz function leads to a total percentage of T^3 units of 55 % and a degree of condensation (DC) of 85 %. This forming of partially-crosslinked structures consisting of T^2 and T^3 units by a thermal consolidation has already been discussed in the literature for polysiloxanes based hybrid glasses containing dialkoxysilanes as well.[81,100]

Hybrid Glass Microspheres

For the subsequent formation of microspheres, the unconsolidated polysilsesquioxane precursor was added to a boiling solution of a nonionic surfactant in water (Triton™ X-405). The material softens, and a hot emulsion is formed (**Figure 28**).

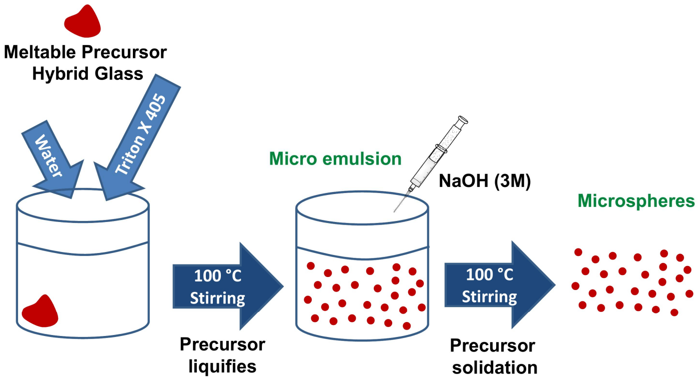

Figure 28. Preparation of the polyphenylsilsesquioxane microspheres in water.

The hydrophobic properties of the integrated perylene based dye, let it remain solved in the precursor phase without being leached to the solution. By adding sodium hydroxide to the solution the materials droplets surface molecules start to cross-link due to base-catalyzed hydrolysis and condensation reactions of hydroxy groups with the silicon atoms (**Scheme 19**).

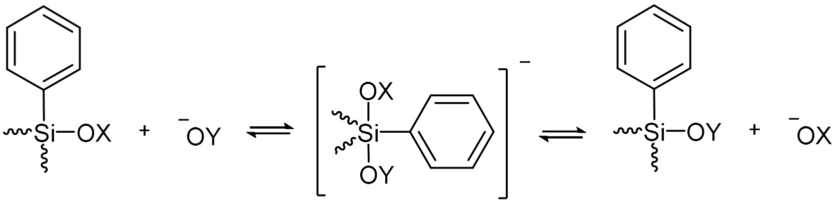

Hydrolysis reaction: X = Me, Y = H
Condensation reation: X = Me or H, Y = PhSi(OR)$_3$

***Scheme 19.** Reaction mechanism of the condensation of a phenyltrialkoxysilane or a polyphenylsilsesquioxane under basic conditions.*

As a result, the droplets start to consolidate chemically preserving their spherical morphology. After cooling the solution to room temperature the microspheres can be isolated by centrifugation. After the particles were isolated and dried at 80°C under reduced pressure the color of the material changed from red to pinkish due to light scattering effects (**Figure 29**). The obtained microspheres are insoluble in water or ethanol and are still coated by the surfactant used in the synthesis. The surfactant causes the sphere to be hydrophilic. A further heat treatment at 200 °C leads to the removal of the surfactant and a more hydrophobic sphere surface respectively. At the same time, the microsphere structure is further cross-linked, which makes the material insoluble in organic solvents as well.

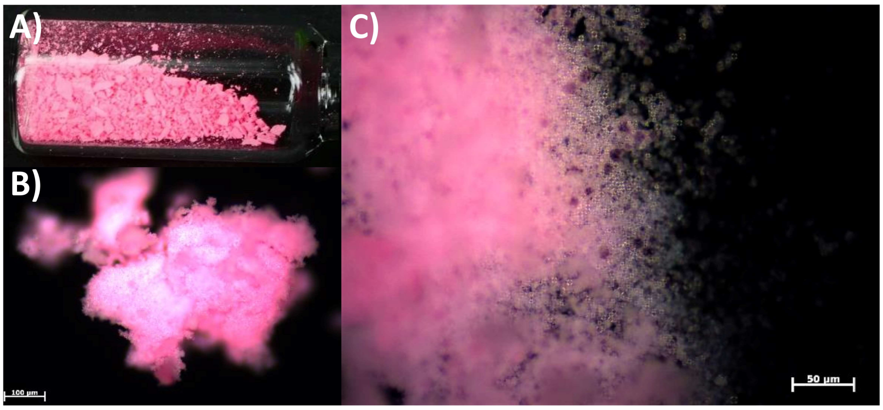

Figure 29. *Images of the isolated microspheres* ***MGP-3*** *A) without magnification. B)-C) light microscopy images.*

A variation of the mean sphere size was realized by altering the stirring method and stirring speed was used to synthesize different sized spheres. The hybrid glass precursor (MG) and the hybrid glass microspheres (MGP) properties have been investigated by 1D and 2D nuclear magnetic resonance spectroscopy (^{1}H, ^{29}Si, and ^{1}H-^{29}Si HMBC 2D NMR, MAS-NMR), infrared spectroscopy (ATR-FTIR) as well as thermogravimetric methods (TG, TG-FTIR).

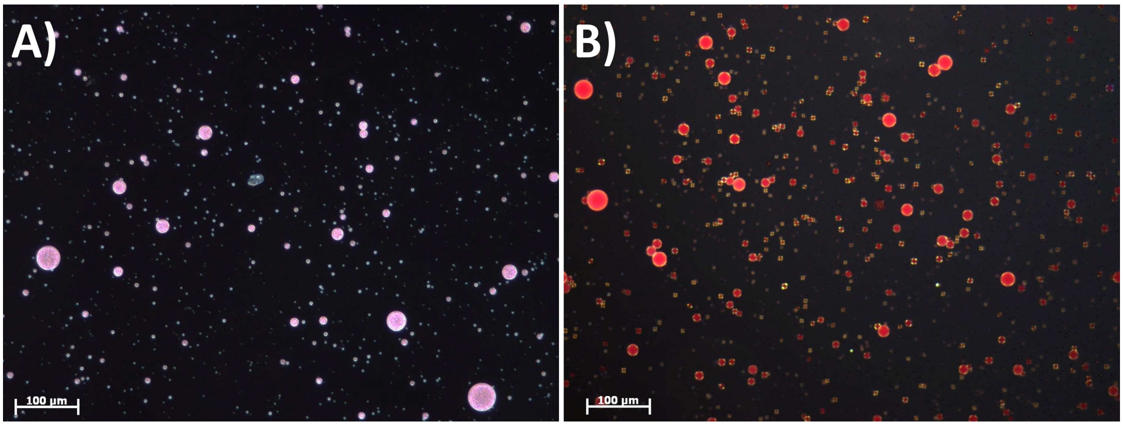

Figure 30. *(A) Dark-field microscopy image of the hybrid glass microspheres* ***MGP-1*** *with Lumogen®F Red 305 integrated dispersed in water before the removal of the surfactant. (B) Fluorescence microscopy image of the same material showing the red fluorescence of the dye molecules (Mercury UV ARC Lamp λ = 254 – 579 nm).*

The microspheres size and morphology were investigated by light microscopy, and the optical properties of the integrated dye were studied by fluorescence spectroscopy and quantum yield determination (**Figure 30**).

A subsequent heat treatment at 200 °C for 4 h was also performed to compare the properties like structure, solubility, and surface coating with untampered microspheres. The untampered microspheres are denoted with **MGP** and the additional heat treated with **MGP-T**. For further characterization of the structure of the material, ^{29}Si and ^{13}C CP-MAS-NMR, as well as FTIR spectroscopy and thermal analysis methods were performed. The ATR-FTIR spectra of **MG** and **MGP-T** do not show significant differences compared to the precursor or the consolidated precursor of the microspheres (Figure ESI20, 21). Furthermore, no vibration bands caused by a surface coating of **MG** with Triton™ X-405 could be detected. The morphology of the **MGP-T** particles is also not influenced by the heat treatment.

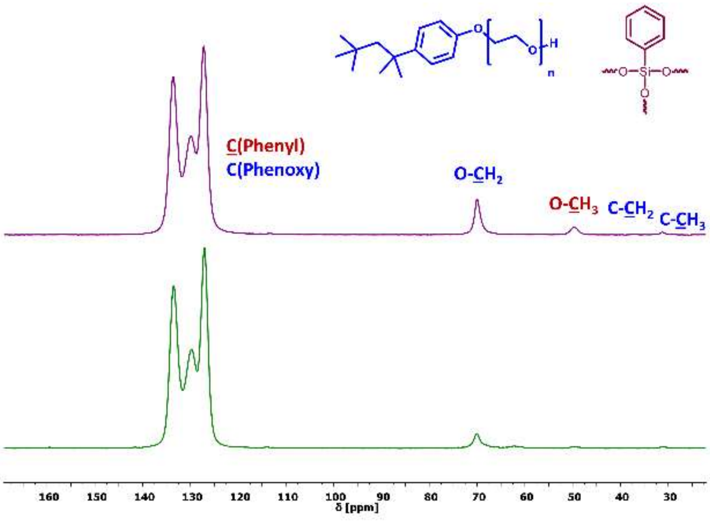

***Figure 31**. ^{13}C MAS-NMR spectra of **MGP and MGP-T** showing the removal of the surfactant and the further condensation of the microspheres structure.*

In the ^{13}C MAS-NMR spectra of **MGP,** the surfactant could be detected by the chemical shifts generated by the Triton™ X-405 structure (**Figure 31**). The chemical shifts at and 133, 129, 127 ppm (C-H [phenoxy/phenyl]) are generated by the aromatic protons of the phenyl and phenoxy groups of the polyphenylsilsesquioxane structure and the surfactant. Other shifts of the surfactant are detected at 70 (O-CH_2), 37 (C-CH_2) and 31 ppm (C-CH_3). The additional chemical shift at 49 ppm is caused by the unreacted methoxy groups of T^2 units of the polysilsesquioxane. The presence of this shift also indicates that chemical consolidation also leads to partially cross-linked structures. After the heat treatment, the signal intensity of the surfactant and the methoxy groups' chemical shifts decreased or even disappeared.

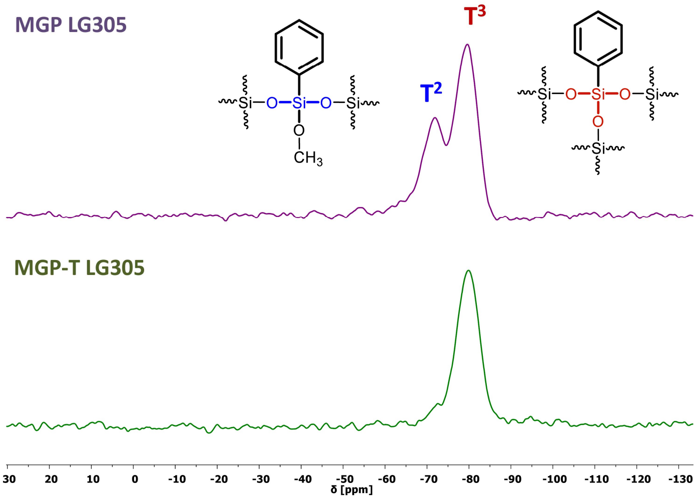

Figure 32. *^{29}Si CP-MAS-NMR spectra of **MGP and MGP-T** showing the change from T^2 and T^3 units in **MGP** to T^3 units only for MGP-T.*

This finding is verified by the ^{29}Si CP-MAS-NMR data. In the chemically consolidated **MGP** microspheres' NMR spectrum, T^2 and T^3 units can be detected at -71 and -79 ppm (**Figure 32**). The calculated percentage of T^3 units is 53 %, and DC is 84 %, which is slightly less than calculated for the thermally consolidated precursor. For other thermally untampered polyphenylsilsesquioxane based particles the DC varies between 40 – 90 %.[61,176] The reason for the partially-crosslinked structure was discussed above [61,176,177]

In the spectrum of the thermally consolidated **MGP-T** particles, only the T^3 chemical shift at -79 ppm can be assigned certainly, indicating a fully cross-linked $PhSiO_{1.5}$ structure (**Figure 32**). It reveals that the thermal consolidation process of the microspheres is different from the thermal consolidation process of the precursor, in which T2 units are still present afterward. It also indicates a direct influence of the spheres pretreatment with sodium hydroxide to the further structure formation. The subsequent thermal treatment leads to a cross-linking degree of 100 %. As a result, two different processes can be studied.

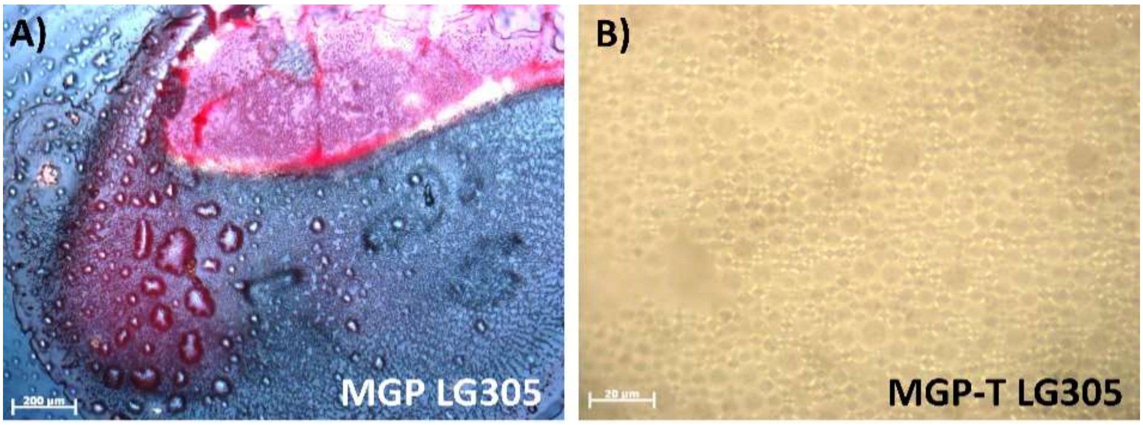

Figure 33. *Microscopy images of A) **MGP-1** and B) **MGP-1-T** after treatment with acetone for 15 minutes.*

After the base initialized chemical consolidation of the liquid precursor droplets, their structure is partially cross-linked, and their surface is coated with a layer of the Triton™ X-45 surfactant. This leads to a hydrophilic surface very well dispersible in water. After the heat treatment the surfactant is removed from the surface, and the T^2 methoxy and hydroxy groups condensate to a fully cross-linked polyphenylsilsesquioxane structure with T^3 units only. The particles cannot be suspended homogeneously in water anymore, indicating that the surface is now hydrophilic.

The solubility of the untampered **MGP** materials is equal to that of the precursor material. The untampered **MGP** microspheres with a partially cross-linked structure are soluble in organic solvents, the additional heat-treated and fully crosslinked **MGP-T** particles are insoluble, and their spherical morphology is retained. This variety in solubility is also caused by the different cross-linking degrees of the microspheres as discussed above. The **MGP-T** microspheres consist of fully-crosslinked $PhSiO_{1.5}$ structure, whereas the **MGP** microspheres are partially-crosslinked. The integrated dye is leached out of both materials structures, as shown in acetone for **MGP** and **MGP-T** (**Figure 33**). For applications in which the particles are used in solvent-free media or in polar solvents like water or ethanol, the dye is not leaching out of the particle structure. Due to the leaching behavior, SEM images from the fresh made and from temperature treated particles were recorded to see the morphology of surface structure in detail (**Figure 34**). The particles structure is smooth, and there is no change in morphology due to the heat treatment. There are some holes in few of the particles, but there is no porous structure detectable from this images. One reason for the leaching of the dye can be domains in which the structure is less closed-meshed. The T^3 network still have some space, in which the dye can diffuse trough the particles structure. A higher resolution TEM image is needed to characterize the surface even more.

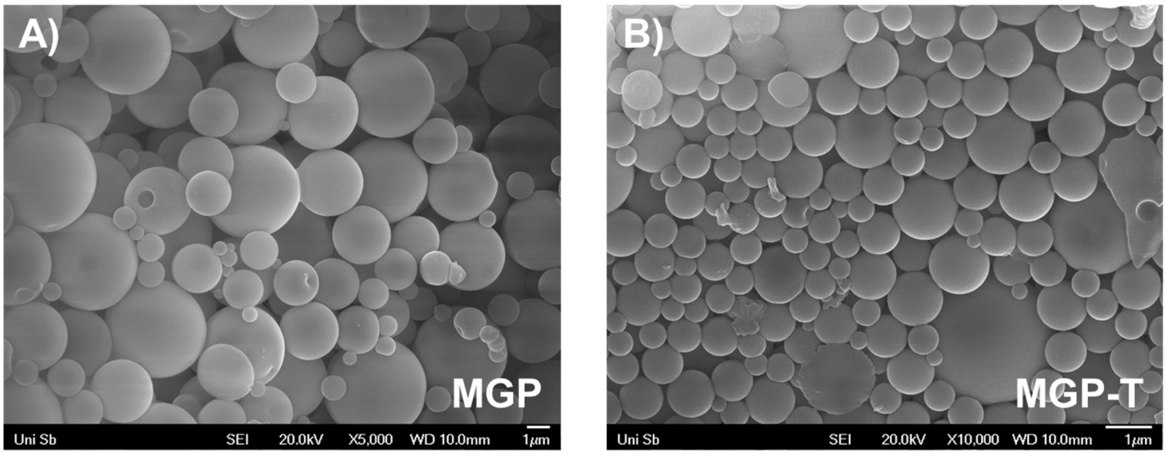

*Figure 34. Electron microscopy images of A) **MGP-1** and B) **MGP-1-T** after a heat treatment at 200 °C for 4 h.*

Microspheres thermal Analysis

The ^{13}C MAS-NMR data indicated the presence of a Triton™ X-405 layer on the microsphere surface after the chemical consolidation and isolation which is removed by the thermal initiated post-consolidation process of these spheres at 200 °C for 4 h. By performing a thermal analysis of the untampered microspheres **MGP,** this process was verified. A mass loss of 5% was detected, starting at 213 °C (**Figure 35**). This mass loss could be assigned to the removal of Triton™ X-405 by FTIR spectroscopy. The vibration bands detected at 2863 [ν(O-H)], 2358 [ν(C-H)] and 1745, 1164, 669 cm^{-1}[ν(C-O)] could be assigned to Triton™ X-405 (Figure 9). This was verified by an isothermal TG-FTIR measurement of the MGP microspheres and the used Triton™ X-405 solution at 220 °C (Figure ESI 31). The IR spectra of the gas released from the particles and the Triton™ X-405 solution are identical (Figure ESI 32).

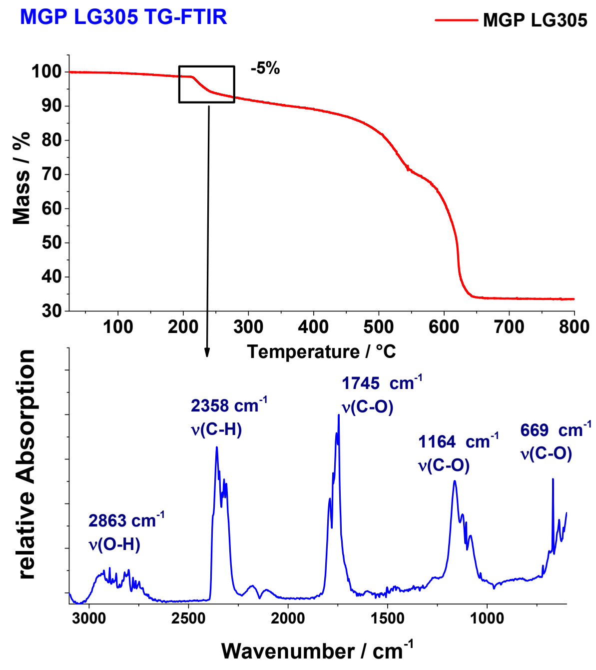

Figure 35. *TG and FTIR spectrum of MGP during a heat treatment from 25 – 800 °C under air.*

The thermally consolidated **MGP-T** microspheres show no more mass loss caused by further condensation reactions. After this consolidation step, the degradation of the materials begins at 438 °C defined by the T_{95} value (Figure ESI30). It is slightly decreased compared to **MG Cons.** due to the powder state. As a result, the Triton™ X-405 layer on the microsphere surface can be easily removed by a heat treatment at 200 °C verified by the 5% mass loss shown in the TG-FTIR spectra. At the same time, the particle structure is getting fully-crosslinked as described before.

Stirring Influence on the Particle Size Distribution

During the synthesis of the microspheres, an emulsion is formed. By just stirring the emulsion at different stirring rates applying a standard laboratory stirrer a narrow size distribution can be obtained. For the optimization of the particle size and distribution, five additional experiments were performed by changing the stirring rate, speed, or method (Table 2). The stirring rate with a standard bar was changed from 500 (**MGP-1**) to 800 rpm (**MGP-3**) and the stirring time was changed from 1 h (**MGP-1**) to 2 h (**MGP-2**) at 500 rpm.

Table 2. Sample name and differences in stirring rate and time used for the synthesis of the hybrid glass microspheres.

Sample	Stirring Rate / rpm	Stirring time / min	Mean particle size / µm
MGP-1	500	1 h	7.22 ± 3.11
MGP-2	500	2 h	7.50 ± 3.16
MGP-3	800	1 h	5.73 ± 2.28
MGP-US	1. 500 2. only ultra-sonic (150 W)	10 min 2 min	7.28 ± 6.04
MGP-UT	1. 500 2. 10000 (disperser)	10 min 2 min	3.09 ± 0.71

By using an Ultra-Sonic finger (150 W [**MGP-US**]) or an Ultra-Turrax™ dispenser (10000 rpm [**MGP-UT**]) after stirring at 500 rpm for 10 min, the influence of high energy processes to the particle morphology was studied (Figure 36). All experiments were performed with the hot emulsion of the precursor material before adding the sodium hydroxide to start the chemical consolidation and forming a suspension, respectively.

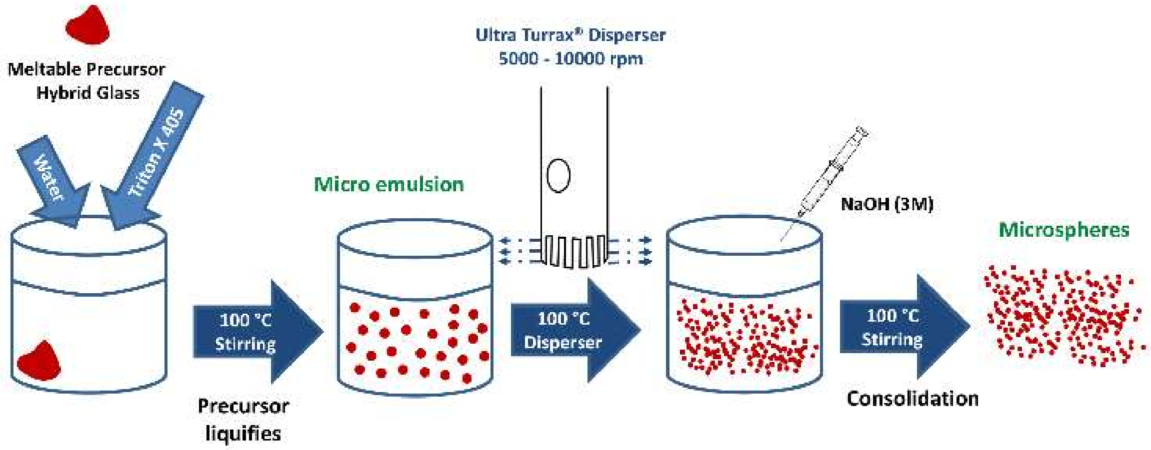

Figure 36. Schematic preparation of polyphenylsilsesquioxane microspheres using a Ultra-Turrax™ dispenser.

The particle size and distribution was determined by measuring and counting particles from microscopy images (Figure ESI25-28). All particles measured are smaller than 20 µm independent of the procedure. By just stirring the emulsion at 500 rpm for 1 or 2 h (**MGP-1/2**), the particle size distribution does not change significantly (Figure 37). By increasing the stirring speed to 800 rpm, the distribution gets more narrow, and the particle size decreases (**MGP-3**). The additional ultrasonic treatment leads to broader distribution and larger particle sizes (**MGP-US**). The narrowest distribution and the smallest particles were obtained by using the Ultra-Turrax™ dispenser (**MGP-UT**). As a result, using a standard stirring bar, an increase of stirring velocity leads to a decrease of particle size and distribution. Increasing the stirring time at the same velocity does not lead to any significant change in particle size. In other sol-gel based particle preparation procedures an ultra-sonic mediated synthesis leads to decreased particle sizes as well.[183,184] The use of an ultra-sonic finger during our synthesis, results in an increased particle size distribution. One reason for this is the absence of mechanical stirring during the sonification and the high viscosity of the liquid hybrid glass emulsion droplets. The final droplet size distribution, in general, is equal to the distribution directly after a droplet disruption by mechanical energy, and it depends on the droplets phase viscosity.[185,186] The high viscosity hinders the disruption of the droplets by ultra-sonic energy introduction. By using the disperser, small particles with a narrow distribution are formed. The reason for this is the high rotation speed of the rotor, which generates extremely strong shear and thrust forces disrupting the droplets. As a result, mechanical energy is required to form smaller particles by disruption. The energy introduced to the system by ultra-sonic waves does not promote the size reduction of the droplets.

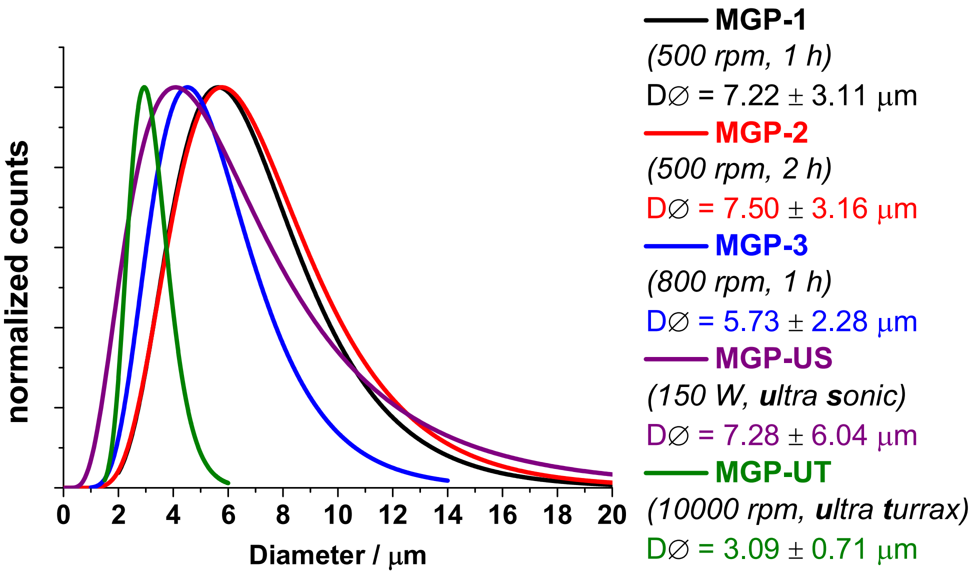

Figure 37. Particle size distribution of the different experiments MGP-1, MGP-2, MGP-3 MGP-US and MGP-UT.

Fluorescence and Quantum Efficiency

The perylene dye Lumogen®F Red 305 was integrated into the polyphenylsilsesquioxane hybrid glass in the gelation step of its synthesis (see experimental section). The dye solved immediately in the polymer due to its very good solubility in phenyl containing materials.[187] During the preparation of the emulsion the dye stays solved in the polymer phase. The isolated and heat-treated microspheres (**MGP-T**) show red fluorescence (Figure 12). At 500 nm (20000 cm^{-1}) excitation wavelength two emission bands at 622 (16077 cm^{-1}) and 647 nm (15456 cm^{-1}) are detectable. At 650 nm (15384 cm^{-1}) emission wavelength three excitation bands at 578 nm (17301 cm^{-1}), 530 nm (18867 cm^{-1}) and 440 nm (22727 cm^{-1}) can be detected. Compared to the fluorescence spectra of Lumogen®F Red 305 in toluene, a small bathochromic shift of the emission occurs.[187] The Stokes shift in toluene was determined with 29 nm (840 cm^{-1}) in the microspheres it is 44 nm (1224 cm^{-1}). The absolute quantum yield of the microspheres was 0.87 (λ_{ex}=570 nm) and 0.82 (λ_{ex}=450 nm). In the precursor material (MG LG305) and in other curable polyphenylmethylsiloxanes the quantum yield of Lumogen®F Red 305 is slightly higher with 1.00 (λ_{ex}=450 nm).[187] A particle morphology and size effected decrease of the quantum in silica, and polymeric particles have already been reported.[156,178] The reason for the shifted emission and the decreased quantum yields are reabsorption processes in the sample caused by the relatively high dye concentration (1 µmol g^{-1}) and spectral distortions caused by scattering and reabsorption processes evoked by the change in solid-phase morphology from transparent hybrid glass to a microparticle powder.[108,179] Incomparable polyphenylmethylsiloxanes with Lumogen®F Red 305 integrated there is no change of quantum yield detectable even for a high concentration of 3000 ppm.[187]

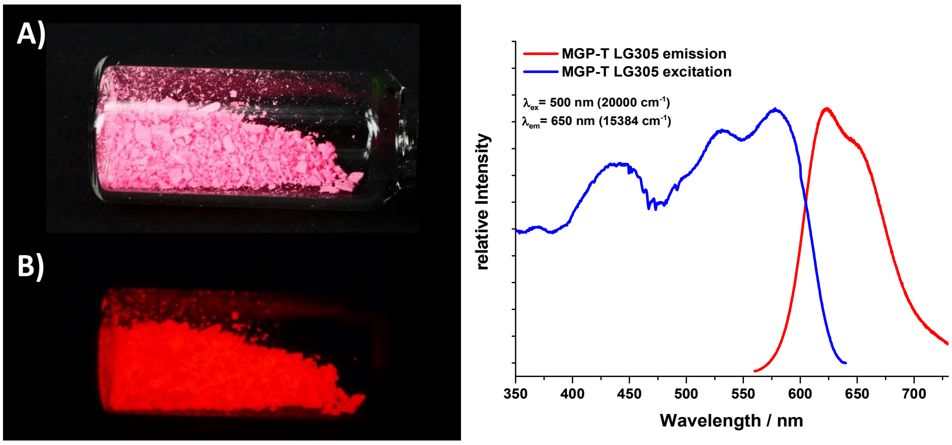

Figure 38. (A) Image of the hybrid glass microspheres MGP-T with Lumogen®F Red 305 integrated (B) Image of the same material showing the red fluorescence of the dye molecules (LED λ = 450 nm). Emission and excitation spectrum of MGP-T LG305 at 500 nm(20000 cm^{-1}) excitation and 650 nm(15384 cm^{-1}) emission wavelength.

Particle Integration into a Polyphenylmethylsiloxan Resin

For the use in an organic hybrid LED application, the hybrid glass microspheres have to be homogeneously encapsulated by a silicon resin. Afterward, the particles and the integrated dye must withstand the working conditions of the LED device, especially the high radiation at 450 nm wavelength. A first estimation of the long-time photostability has been determined by a long-time irradiation experiment. Therefore, the temperature treated **MGP-3T** were integrated into polyphenylmethylsiloxane resin [Dow Corning OE6630; Dow(1)], which was cast into an aluminum frame and thermally cured at 150°C for 4 h. The finished sample [Dow(1)MGP-3T] show a homogenous distribution of the particles inside the sample and strong fluorescence under light exposure with a wavelength of 450 nm (**Figure 40**). Furthermore, the dye did not leach out of the particles due to the procedure.

The sample and one sample of the consolidated precursor hybrid glass were irradiated with a 450 nm light source for >35 h at ~0.85 W/cm^2. To investigate the photophysical stability of the incorporated dye, the absorbance of the sample was measured periodically during the irradiation process. The relative absorbance to the initial value at 450 nm was determined (**Figure 39**). The decrease in absorbance of the consolidated hybrid glass and the hybrid glass microspheres inside the cured polysiloxane resin is nearly equal within the experiment. It decreases by 10 % after ~990 h (~39 d). The hybrid glass and the hybrid glass particles show a significant increase of the incorporated dyes photostability compared to the commercially available polysiloxanes samples, in which LG305 was directly incorporated into the material. There, the dyes absorbance decreased 10% after 25 hours in Dow Corning OE6630 (see chapter 4.1).

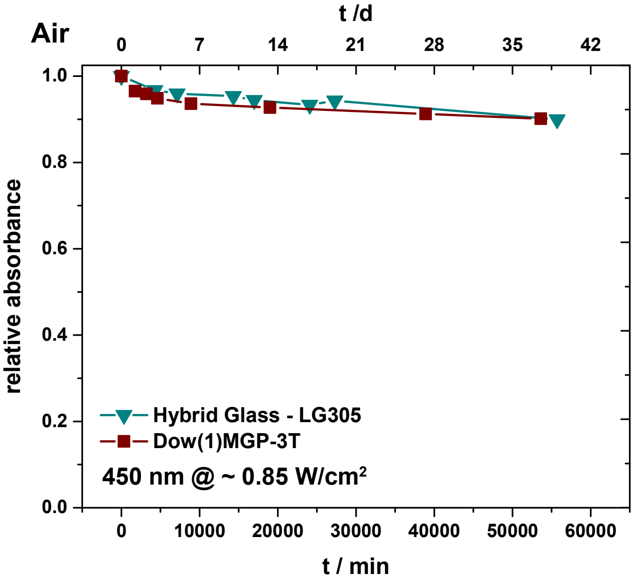

Figure 39. *Relative absorbance of the consolidated precursor hybrid glass with LG305 and Dow(1)MGP-3T at different times measured during a light exposure with 450 nm light source with 850 mW/cm^2.*

The main difference of the materials is the cross-linking degree, which also can influence the oxygen permeability and thus the dyes photostability. The polysiloxane resins are cross-linked by hydrosilylation and still elastic. The hybrid glass is a highly cross-linked by polycondensation of trialkoxysilanes, making it hard and rigid, and probably less permeable for oxygen. This has also been indicated by gas barrier experiments with other hybrid glass compositions.[175] It has also been shown, that the change in morphology from a hybrid glass to microparticles does not influence the dyes photostability properties. Therefore, the dye-containing microparticles are suitable for the use in organic hybrid LED applications and have to be tested under working conditions.

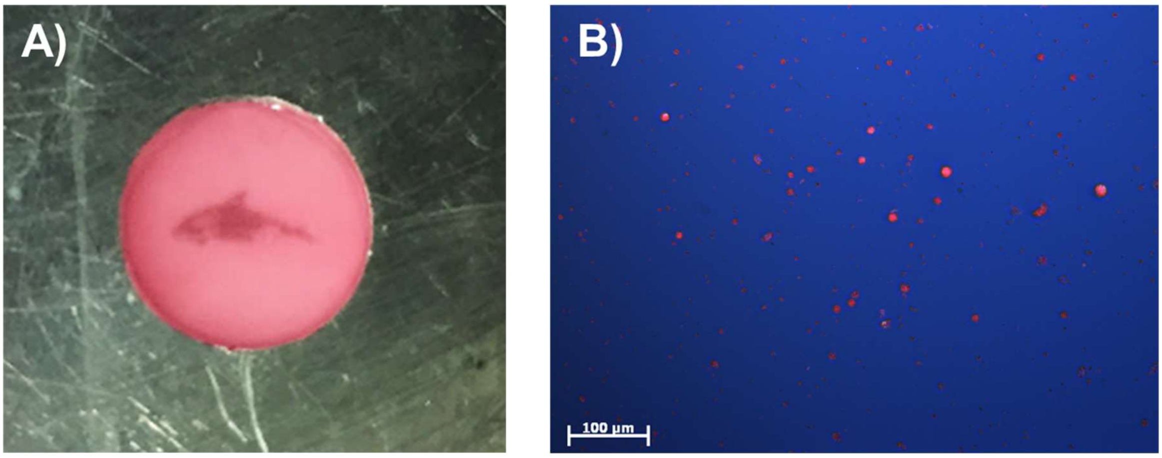

Figure 40. *(A) Cured, MGP-3T containing Dow Corning OE660 resin, (B) microscope image of the sumple under 450 nm light.*

As a result, the integration of a hydrophobic perylene dye into polyphenylsilsesquioxane microspheres could be realized leading to a high fluorescent microsphere powder. Under common conditions like in optoelectronic applications or in medical sensing or imaging, where usually water is used as a solvent or polymers are used as host material the dye stays in the particle structure. As described before the dye is leachable out of the microspheres by treating it with organic solvents, whereas the microspheres integrity is retained. The particles can also be encapsulated into curable polysiloxanes and thus into organic hybrid LED applications.

Conclusion

A fluorescent solid polyphenylsilsesquioxane hybrid glass was synthesized, able to be melted at >80 °C and consolidated at >150 °C without any platinum catalyst by performing an acid-catalyzed condensation reaction of phenyltrimethoxysilane and subsequent addition of Lumogen®F Red305 before gelation. The obtained material was transferred into a boiling solution of Triton™ X-405, forming a hot emulsion of the liquid precursor in water. Adding sodium hydroxide to this emulsion starts a condensation and solidification of the microspheres. A further cross-linking to a fully condensed $PhSiO_{1.5}$ structure and the removal of Triton™ X-405 molecules from the microspheres' surface was performed by subsequent heat treatment of the particles. The polyphenylsilsesquioxane hybrid glass (**MG**) ^{29}Si and ^{13}C chemical shifts, caused by the consistency of T^2 and T^3 units, indicate partially cross-linked structures. It was subsequently consolidated at 200 °C leading to a still incomplete condensation of the structure (**D**egree of **C**ondensation: 85 %).

The FTIR spectra of the gases being released by the consolidation during the TG measurement show exclusively vibrations of the condensation products methanol and water. The consolidated hybrid glass (**MG Cons.**) shows no further mass loss caused by consolidation. Its T^{95} value was determined with 488 °C. The material is still partially cross-linked shown by ^{29}Si and ^{13}C spectroscopy.

The fresh made and untampered microspheres (**MGP**) also show partially cross-linked polyphenylsilsesquioxane structures indicated by ^{29}Si and ^{13}C chemical shifts of T^2 and T^3 units (**DC**: 84 %). The particles are not meltable anymore, which verifies a structural change and a further cross-linking by the microsphere synthesis procedure. The NMR data of the subsequently heat treated microspheres (**MGP-T**, 200 °C, 4h) verify a full condensation to a $PhSiO_{1.5}$ network by the exclusive presence of T^3 units. This structural change explains primarily the solubility behavior of these materials in organic solvents like acetone. The less cross-linked materials consisting of T^2 and T^3 units are soluble, the fully cross-linked and heat-treated **MGP-T** microspheres are not and their morphology is retained.

The microspheres (**MGP-T**) show red fluorescence with an emission maximum at 647nm (15456 cm^{-1}). The quantum yield of 0.82 is slightly decreased compared to the one of **MG,** which is caused by scattering and reabsorption processes evoked by the change in solid phase morphology from transparent hybrid glass to the microparticle powder. The dye is leachable from the microspheres by treating it with organic solvents like acetone despite the fully cross-linked structure of the matrix. The particles can be incorporated in curable polysiloxane resins, homogeneously, showing a slight decrease of 10% of absorbance at 450 nm after 25 hours by irradiation with 450 nm wavelength at ~0.85 mW/m^2, and therefore, a high photostability.

The mean particle size distribution was optimized by performing five experiments with different stirring velocities or energy input. The narrowest distribution and the smallest particles with 3.09±0.71 µm were obtained by using the Ultra-Turrax™ dispenser.

Acknowledgments: This research has been funded by the Federal Ministry of Education and Research (BMBF, Germany) in the project ORCA - Organic and rare-earth reduced conversion materials for LED-based lightning (project number **03XP0050**). We would like to thank Dr. Michael Zimmer for CP-MAS-NMR support and Silvia Beetz for technical support.

5. Conclusion and Perspective

In the context of this thesis, the synthesis and interaction of several siloxane-based materials and organic fluorescence dyes and their combination were investigated regarding their physical and chemical properties. The obtained results are of current interest in the research and development of optoelectronic devices, especially for rare-earth reduced organic hybrid light-emitting diodes. In the following, the initially stated research objectives are addressed more specifically, and the prime conclusions are drawn for a better overview.

In the first part of the thesis, two different perylene dyes have been incorporated in different concentrations into commercially available polydimethylsiloxane, and a polyphenylmethylsiloxane two-component resins that are thermally curable by platinum catalyzed hydrosilylation reaction. It could be shown, that the presence of phenyl groups in a polysiloxane encapsulation is required to generate an outstanding environment for the incorporation of perylene dyes in organic hybrid LEDs. It leads to an enhanced solubility, an increased quantum yield, and an increased thermal and photophysical stability with regard to the dyes incorporated and to the host material itself compared to the pure polydimethylsiloxane matrix. The covalent integration of the dye molecules to the structure of the polymer prevents dye precipitation, and leaching phenomena in any polysiloxane and the impact of oxygen could be evaluated in the degradation photo-initiated dye degradation mechanism.

In a second approach, the covalently incorporable perylene dye was integrated into polysiloxane chains, leading to liquid linear and cross-linked perylene polysiloxanes. These fluorescent liquids were subsequently integrated covalently into the already known polyphenylmethylsiloxane resin that is thermally curable by a platinum-catalyzed hydrosilylation reaction. Due to the preceding synthesis of the liquid perylene polysiloxanes, the separation of the molecule and the dye concentration could be enhanced furthermore. The subsequent integration of the liquid polysiloxanes to the thermally curable polyphenylmethylsiloxane resin leads to samples with high quantum yields, high thermal and photophysical stabilities, and considerable new properties compared to the pure resin. By increasing the perylene polysiloxane concentration incorporated to the cured resin the materials, mechanical properties like cross-linking degree and hardness are decreased simultaneously, making this flexible, functional material accessible and especially interesting for many more optoelectronic applications like photovoltaics or luminescent solar collectors. The longtime photostability of these materials was still not sufficient for the implementation of an organic hybrid LED.

Based on the experiences and the results obtained due to the studies of perylenes and perylene polysiloxanes in the commercially available systems, the requirements for the development of new platinum-free curable siloxane-based materials, able to incorporate and protect a high concentration of perylene based dyes without changing their optical properties were evaluated.

As a consequence, the synthesis of a novel one-component and platinum-free thermally curable polysiloxane encapsulation with tunable mechanical properties were realized. The pre-curing, gel-like material was prepared by a stepwise, acid-catalyzed polycondensation reaction of trialkoxysilanes, dialkoxysilanes, and oligosiloxanes. By changing the ratio of monomers the mechanical properties like viscosity, cross-linking degree and hardness get tunable under preservation of high transparencies, and high thermal and photophysical stabilities. It could also be shown that, if necessary, the curing procedure can be catalyzed with eco-friendly and sustainable inorganic or organic bases.

Due to the waiver of metal catalysts for the curing procedure, these materials are sustainable and at the same time suitable to be used in many different applications where flexibility and transparency are required. Especially for the use in organic hybrid LEDs, these materials are eminently suitable. The material combination of these materials with Lumogen®F Red 305 incorporated show long-time stability up to 80 days with a fluorescence loss of 10 %.

As a result, these materials are the first step for the successful preparation of an organic hybrid LED.

In the last part, dye-doped polysilsesquioxane hybrid glasses were synthesized, showing the best photostability properties measured during this thesis with a fluorescence intensity loss of less than 5 % under nitrogen atmosphere and less than 15 % under ambient conditions. Unfortunately, after casting and consolidation, the material got very hard and rigid, and crack formation started early. But by developing a new preparation method, the material was transformed into microparticles, able to be used in organic hybrid LEDs as a powder type conversion material. A dye-doped polyphenylsilsesquioxane was, therefore synthesized. The material was melted in aqueous solution forming a surfactant mediated emulsion. A base-catalyzed condensation reaction followed by a post-synthetic thermal consolidation led to highly fluorescent fully condensed polyphenylsilsesquioxane microspheres. Optimization of the preparation procedure resulted in nearly monodispersed 3 µm sized microspheres, making them also suitable for many different other purposes like bioimaging or drug delivery.

Up to now, the ORCA project is still running. The generated knowledge and the developed materials are still tested and optimized for the goal of creating a sustainable and efficient organic hybrid LED prototype. It can be concluded that the best combination of polymer encapsulation and organic dye was found. Phenyl containing polysiloxanes are definitely needed for the preservation of the properties of the dye and adequate protection. At the same time, the change from a less cross-linked polysiloxane system cured by hydrosilylation to a highly cross-linked polysilsesquioxane system cured by polycondensation led to an additional increase of photostability.

Nevertheless, all tested materials did not meet the reliability requirements for white light LED yet. The main reason is still the degradation of the red light-emitting perylenes like Lumogen®F Red 305 that are excited by high power radiation with a wavelength of 450 nm. The ORCA project goal is not limited to a white light LED. The basic understanding of the interaction of perylene dyes and siloxanes can also be transferred to several perylene based dyes with other absorption and emission maxima. This is the reason why the ORCA project associates started to investigate a whole range of dyes emitting green, yellow, orange, and especially infra-red light. After the evaluation of possible use in the different application, the IR emitters started to get the most interesting ones concerning the implementation in organic hybrid LEDs for IR spectroscopy, for example. The reason for this is the low accessibility of IR efficient inorganic IR-phosphor alternatives for such applications.

As a result, the basic concepts of the perylene dye and siloxane interactions and properties, and the resulting new platinum-free curable materials like the one-component encapsulations or the polyphenylsilsesquioxane microspheres investigated and characterized within this thesis are significant contributions for the prospective process of creating organic hybrid LED. The main goal of increasing the thermal and photophysical stabilities of perylene dyes in siloxane-based materials by developing new platinum-free curablesiloxane-based materials and meeting all requirements for LED encapsulations was successfully reached.

6. References

(1) Cho, J.; Park, J. H.; Kim, J. K.; Schubert, E. F. White Light-Emitting Diodes: History, Progress, and Future. *Laser Photonics Rev.* **2017**, *11* (2), 1–17. https://doi.org/10.1002/lpor.201600147.

(2) Feldmann, C.; Jüstel, T.; Ronda, C. R.; Schmidt, P. J. Inorganic Luminescent Materials: 100 Years of Research and Application. *Adv. Funct. Mater.* **2003**, *13* (7), 511–516. https://doi.org/10.1002/adfm.200301005.

(3) Born, M.; Jüstel, T. Elektrische Lichtquellen: Chemie in Lampen. *Chem. Unser Zeit* **2006**, *40* (5), 294–305. https://doi.org/10.1002/ciuz.200600377.

(4) Ye, S.; Xiao, F.; Pan, Y. X.; Ma, Y. Y.; Zhang, Q. Y. Phosphors in Phosphor-Converted White Light-Emitting Diodes: Recent Advances in Materials, Techniques and Properties. *Mater. Sci. Eng. R Reports* **2010**, *71* (1), 1–34. https://doi.org/10.1016/j.mser.2010.07.001.

(5) Xia, Z.; Liu, Q. Progress in Discovery and Structural Design of Color Conversion Phosphors for LEDs. *Prog. Mater. Sci.* **2016**, *84*, 59–117. https://doi.org/10.1016/j.pmatsci.2016.09.007.

(6) Lin, Y. H.; You, J. P.; Lin, Y. C.; Tran, N. T.; Shi, F. G. Development of High-Performance Optical Silicone for the Packaging of High-Power LEDs. *IEEE Trans. Components Packag. Technol.* **2010**, *33* (4), 761–766. https://doi.org/10.1109/TCAPT.2010.2046488.

(7) Zhou, B.; Li, Z.; Chen, C. Global Potential of Rare Earth Resources and Rare Earth Demand from Clean Technologies. *Minerals* **2017**, *7* (203), 1–14. https://doi.org/10.3390/min7110203.

(8) Mancheri, N. A. Chinese Monopoly in Rare Earth Elements: Supply-Demand and Industrial Applications. *China Rep.* **2012**, *48* (4), 449–468. https://doi.org/10.1177/0009445512466621.

(9) Mancheri, N. A.; Sprecher, B.; Bailey, G.; Ge, J.; Tukker, A. Effect of Chinese Policies on Rare Earth Supply Chain Resilience. *Resour. Conserv. Recycl.* **2019**, *142* (July 2018), 101–112. https://doi.org/10.1016/j.resconrec.2018.11.017.

(10) World Economic Forum. Rare earths are the new battlefront in the US-China trade war. But what are they? https://www.weforum.org/agenda/2019/06/rare-earths-are-the-new-battlefront-in-the-us-china-trade-war-but-what-precisely-are-they/ (accessed Jun 5, 2019).

(11) Rademaker, J. H.; Kleijn, R.; Yang, Y. Recycling as a Strategy against Rare Earth Element Criticality: A Systemic Evaluation of the Potential Yield of NdFeB Magnet Recycling. *Environ. Sci. Technol.* **2013**, *47* (18), 10129–10136. https://doi.org/10.1021/es305007w.

(12) Schlotter, P.; Schmidt, R.; Schneider, J. Luminescence Conversion of Blue Light Emitting Diodes. *Appl. Phys. A Mater. Sci. Process.* **1997**, *A 64*, 417–418. https://doi.org/10.3389/fnins.2011.00005.

(13) Chang, M. H.; Das, D.; Varde, P. V.; Pecht, M. Light Emitting Diodes Reliability Review. *Microelectron. Reliab.* **2012**, *52* (5), 762–782. https://doi.org/10.1016/j.microrel.2011.07.063.

(14) Jüstel, T.; Nikol, H.; Ronda, C. New Developments in the Field of Luminescent Materials for Lighting and Displays. *Angew. Chemie - Int. Ed.* **1998**, *37* (22), 3084–3103. https://doi.org/10.1002/(SICI)1521-3773(19981204)37:22<3084::AID-ANIE3084>3.0.CO;2-W.

(15) Ronda, C. R. Phosphors for Lamps and Displays: An Applicational View. *J. Alloys Compd.* **1995**, *225* (1–2), 534–538. https://doi.org/10.1016/0925-8388(94)07065-2.

(16) Arukawa, Y. N.; Iki, I. N.; Zuno, K. I.; Amada, M. Y.; Urazaki, Y. M.; Ukai, T. M. Phosphor-Conversion White Light Emitting Diode Using InGaN Near-Ultraviolet Chip. *Jpn. J. Appl. Phys.* **2002**, *41*, 371–373. https://doi.org/10.1143/JJAP.41.L371.

(17) Xie, R.-J.; Hirosaki, N.; Li, H.-L.; Li, Y. Q.; Mitomo, M. Synthesis and Photoluminescence Properties of β-Sialon:Eu2+. *J. Electrochem. Soc.* **2007**, *154* (10), J314–J319. https://doi.org/10.1149/1.2768289.

(18) Tanabe, S.; Fujita, S.; Yoshihara, S.; Sakamoto, A.; Yamamoto, S. YAG Glass-Ceramic Phosphor for White LED (II): Luminescence Characteristics. *Fifth Int. Conf. Solid State Light.* **2005**, *5941* (Ii), 594112. https://doi.org/10.1117/12.614681.

(19) Yeh, N.; Ding, T. J.; Yeh, P. Light-Emitting Diodes' Light Qualities and Their Corresponding Scientific Applications. *Renew. Sustain. Energy Rev.* **2015**, *51*, 55–61. https://doi.org/10.1016/j.rser.2015.04.177.

(20) Bui, D. A.; Hauser, P. C. Analytical Devices Based on Light-Emitting Diodes - A Review of the State-of-the-Art. *Anal. Chim. Acta* **2015**, *853* (1), 46–58. https://doi.org/10.1016/j.aca.2014.09.044.

(21) Macka, M.; Piasecki, T.; Dasgupta, P. K. Light-Emitting Diodes for Analytical Chemistry. *Annu. Rev. Anal. Chem.* **2014**, *7* (1), 183–207. https://doi.org/10.1146/annurev-anchem-071213-020059.

(22) OSRAM Opto Semiconductors GmbH. Golden Dragon White Light LED.

(23) Dai, X.; Deng, Y.; Peng, X.; Jin, Y. Quantum-Dot Light-Emitting Diodes for Large-Area Displays: Towards the Dawn of Commercialization. *Adv. Mater.* **2017**, *29* (14), 1607022. https://doi.org/10.1002/adma.201607022.

(24) Tsutsui, T.; Takada, N. Progress in Emission Efficiency of Organic Light-Emitting Diodes: Basic Understanding and Its Technical Application. *Jpn. J. Appl. Phys.* **2013**, *52* (11 PART 1), 1–10. https://doi.org/10.7567/JJAP.52.110001.

(25) Jang, H. J.; Lee, J. Y.; Kwak, J.; Lee, D.; Park, J. H.; Lee, B.; Noh, Y. Y. Progress of Display Performances: AR, VR, QLED, OLED, and TFT. *J. Inf. Disp.* **2019**, *20* (1), 1–8. https://doi.org/10.1080/15980316.2019.1572662.

(26) Galeotti, F.; Mróz, W.; Catellani, M.; Kutrzeba-Kotowska, B.; Kozma, E. Tailorable Perylene-Loaded Fluorescent Nanostructures: A Multifaceted Approach Enabling Their Application in White Hybrid LEDs. *J. Mater. Chem. C* **2016**, *4* (23), 5407–5415. https://doi.org/10.1039/c6tc00486e.

(27) Wagenblast, G.; Könemann, M.; Ivanovici, S.; Keyzer, de G.; Send, R.; Pepers, M. Novel Illumination Devices. US20160084477 A1, 2016.

(28) Könemann, M.; Wagenblast, G.; Ivanovici, S.; Keyzer, de G.; Send, R. Novel Color Converters. US20140076397 A1, 2014.

(29) Könemann, M.; Wagenblast, G.; Send, R.; Ivanovici, S.; Dekeyzer, G. Novel Color Converter. US20160284947 A1, 2016.

(30) Bierhuizen, S.; Krames, M.; Harbers, G.; Bierhuizen, S.; Krames, M.; Harbers, G.; Weijers, G. Performance and Trends of High Power Light Emitting Diodes. In *SPIE 6669, Seventh International Conference on Solid State Lighting*; 2007; Vol. 66690B. https://doi.org/10.1117/12.735102.

(31) Chang, L. B.; Pan, K. W.; Yen, C. Y.; Jeng, M. J.; Wu, C. Te; Hu, S. C.; Kuo, Y. K. Comparison of Silicone and Spin-on Glass Packaging Materials for Light-Emitting Diode Encapsulation. *Thin Solid Films* **2014**, *570* (PB), 496–499. https://doi.org/10.1016/j.tsf.2014.03.033.

(32) Hoelen, C.; Borel, H.; Graaf, J. De; Lankhorst, M.; Hoelen, C.; Borel, H.; Graaf, J. De; Keuper, M.; Mutter, C.; Waumans, L.; et al. Remote Phosphor LED Modules for General Illumination: Toward 200 Lm/W General Lighting LED Light Sources. In *SPIE 7058, Eighth International Conference on Solid State Lighting*; 2019; Vol. 70580M. https://doi.org/10.1117/12.799502.

(33) He, J.; Yang, S.; Zheng, K.; Zhang, Y.; Song, J.; Qu, J. One-Pot Synthesis of Dispersible Thermally Stable Organic Downconversion Materials under DBU Catalyzation for High Performance Hybrid-LED Lamps. *Green Chem.* **2018**, *20* (15), 3557–3565. https://doi.org/10.1039/c8gc01390j.

(34) Tsai, M. Y.; Tang, C. Y.; Wang, C. H.; Tsai, Y. Y.; Chen, C. H. Investigation on Some Parameters Affecting Optical Degradation of LED Packages during High-Temperature Aging. *IEEE Trans. Device Mater. Reliab.* **2015**, *15* (3), 335–341. https://doi.org/10.1109/TDMR.2015.2441751.

(35) Zibold, A.; Dammann, M.; Schmidt, R.; Konstanzer, H.; Kunzer, M. Influence of Air Pollutants on the Lifetime of LEDs and Analysis of Degradation Effects. *Microelectron. Reliab.* **2017**, *76–77*, 566–570. https://doi.org/10.1016/j.microrel.2017.07.019.

(36) Singh, P.; Tan, C. M.; Chang, L. B. Early Degradation of High Power Packaged LEDs under Humid Conditions and Its Recovery - Myth of Reliability Rejuvenation. *Microelectron. Reliab.* **2016**, *61*, 145–153. https://doi.org/10.1016/j.microrel.2015.12.036.

(37) Chen, X.; Wang, S.; Chen, M.; Liu, S. Phosphor Settling Induced Mechanical Degradation of Silicone/Phosphor Composite in Light Emitting Diode Packages. *J. Appl. Polym. Sci.* **2015**, *132* (22), 2–9. https://doi.org/10.1002/app.42006.

(38) Zweben, C. Advances in LED Packaging and Thermal Management Materials. In *SPIE 6910, Light-Emitting Diodes: Research, Manufacturing, and Applications XII*; 2008; Vol. 691018. https://doi.org/10.1117/12.761839.

(39) Permal, A.; Devarajan, M.; Hung, H. L.; Zahner, T.; Lacey, D.; Ibrahim, K. Controlled High Filler Loading of Functionalized Al2O3-Filled Epoxy Composites for LED Thermal Management. *J. Mater. Eng. Perform.* **2018**, *27* (3), 1296–1307. https://doi.org/10.1007/s11665-018-3151-y.

(40) Chen, H.; Wei, H.; Chen, M.; Meng, F.; Li, H.; Li, Q. Enhancing the Effectiveness of Silicone Thermal Grease by the Addition of Functionalized Carbon Nanotubes. *Appl. Surf. Sci.* **2013**, *283*, 525–531. https://doi.org/10.1016/j.apsusc.2013.06.139.

(41) Liou, B. H.; Chen, C. M.; Horng, R. H.; Chiang, Y. C.; Wuu, D. S. Improvement of Thermal Management of High-Power GaN-Based Light-Emitting Diodes. *Microelectron. Reliab.* **2012**, *52* (5), 861–865. https://doi.org/10.1016/j.microrel.2011.04.002.

(42) Huang, J. H.; Li, C. P.; Chang-Jian, C. W.; Lee, K. C.; Huang, J. H. Preparation and Characterization of High Refractive Index Silicone/TiO2 Nanocomposites for LED Encapsulants. *J. Taiwan Inst. Chem. Eng.* **2015**, *46*, 168–175. https://doi.org/10.1016/j.jtice.2014.09.008.

(43) He, Y.; Wang, J. A.; Pei, C. L.; Song, J. Z.; Zhu, D.; Chen, J. Novel Epoxy-Silicone Thermolytic Transparent Packaging Adhesives Chemical Modified by ZnO Nanowires for HB LEDs. *J. Nanoparticle Res.* **2010**, *12* (8), 3019–3024. https://doi.org/10.1007/s11051-010-9895-4.

(44) Dow Corning Corporation. *Silicone Chemistry Overview*; 1997.

(45) Ren, Z.; Yan, S. Polysiloxanes for Optoelectronic Applications. *Prog. Mater. Sci.* **2016**, *83*, 383–416. https://doi.org/10.1016/j.pmatsci.2016.07.004.

(46) Kamino, B. A.; Bender, T. P. The Use of Siloxanes, Silsesquioxanes, and Silicones in Organic Semiconducting Materials. *Chem. Soc. Rev.* **2013**, *42* (12), 5119–5130. https://doi.org/10.1039/c3cs35519e.

(47) Shea, K. J.; Loy, D. A. Bridged Polysilsesquioxanes. Molecular-Engineered Hybrid Organic-Inorganic Materials. *Chem. Mater.* **2001**, *13* (10), 3306–3319. https://doi.org/10.1021/cm011074s.

(48) Lee, K. R.; Sotzing, G. A. Green and Blue Electrochromic Polymers from Processable Siloxane Precursors. *Chem. Mater.* **2013**, *25* (14), 2898–2904. https://doi.org/10.1021/cm401498f.

(49) Elkins, C. L.; Long, T. E. Living Anionic Polymerization of Hexamethylcyclotrisiloxane (D 3) Using Functionalized Initiation . *Macromolecules* **2004**, *37* (17), 6657–6659. https://doi.org/10.1021/ma049188n.

(50) Jiesheng, L.; Ke, L.; Lian, X.; Xiang, H. Synthesis of Polysiloxanes in Microemulsion Via Ring Opening of D 4. *Nanochem Res* **2016**, *1* (12), 229–236. https://doi.org/10.7508/ncr.2016.02.010.

(51) Sigwalt, P. New Developments in Cationic Polymerization of Cyclosiloxanes. *Polymer Journal*. 2005, pp 567–580. https://doi.org/10.1295/polymj.19.567.

(52) Perju, E.; Cuervo-Reyes, E.; Shova, S.; Opris, D. M. Synthesis of Novel Cyclosiloxane Monomers Containing Push-Pull Moieties and Their Anionic Ring Opening Polymerization. *RSC Adv.* **2018**, *8* (14), 7569–7578. https://doi.org/10.1039/c8ra00707a.

(53) Zheng, P.; McCarthy, T. J. D4H/D4Vi Silicone: A Replica Material with Several Advantages for Nanoimprint Lithography and Capillary Force Lithography. *Langmuir* **2011**, *27* (13), 7976–7979. https://doi.org/10.1021/la201141k.

(54) Schubert, U. *The Sol-Gel Handbook: Synthesis, Characterization, and Applikations, Volume 1*; Levy, D., Zayat, M., Eds.; Wiley-VCH, 2015.

(55) Arkles, B.; Steinmetz, J. R.; Zazyczny, J.; Mehta, P. *Silanes and Other Coupling Agents: Factors Contributing to the Stability of Alkoxysilanes in Aqueous Solutions*; 1992.

(56) Ahmed, A.; Abdelmagid, W.; Ritchie, H.; Myers, P.; Zhang, H. Investigation on Synthesis of Spheres-on-Sphere Silica Particles and Their Assessment for High Performance Liquid Chromatography Applications. *J. Chromatogr. A* **2012**, *1270*, 194–203. https://doi.org/10.1016/j.chroma.2012.11.008.

(57) Masalov, V.; Sukhinina, N.; Kudrenko, E.; Emelchenko, G. Mechanism of Formation and Nanostructure of Stöber Silica Particles. *Nanotechnology* **2011**, *22* (27), 275718. https://doi.org/10.1088/0957-4484/22/27/275718.

(58) Bae, J. Y.; Kim, Y. H.; Kim, H. Y.; Kim, Y. B.; Jin, J.; Bae, B. S. Ultraviolet Light Stable and Transparent Sol-Gel Methyl Siloxane Hybrid Material for UV Light-Emitting Diode (UV LED) Encapsulant. *ACS Appl. Mater. Interfaces* **2015**, *7* (2), 1035–1039. https://doi.org/10.1021/am507132a.

(59) Kim, Y. H.; Lim, Y.-W.; Lee, D.; Kim, Y. H.; Bae, B. A Highly Adhesive Siloxane LED Encapsulant Optimized for High Thermal Stability and Optical Efficiency. *J. Mater. Chem. C* **2016**, *4* (46), 10791–10796. https://doi.org/10.1039/C6TC04305D.

(60) Kim, J. S.; Yang, S.; Bae, B. S. Thermally Stable Transparent Sol-Gel Based Siloxane Hybrid Material with High Refractive Index for Light Emitting Diode (LED) Encapsulation. *Chem. Mater.* **2010**, *22* (11), 3549–3555. https://doi.org/10.1021/cm100903b.

(61) Odenwald, C.; Kickelbick, G. Additive-Free Continuous Synthesis of Silica and ORMOSIL Micro- and Nanoparticles Applying a Microjet Reactor. *J. Sol-Gel Sci. Technol.* **2019**, *89* (1), 343–353. https://doi.org/10.1007/s10971-018-4626-x.

(62) Engelhardt, G.; Jancke, H.; Mägi, M.; Pehk, T.; Lippmaa, E. Über Die 1H-, 13C- Und 29Si-NMR Chemischen Verschiebungen Einiger Linearer, Verzweigter Und Cyclischer Methylsiloxan-Verbindungen. *J. Organomet. Chem.* **1971**, *28* (3), 293–300. https://doi.org/10.1016/S0022-328X(00)88009-2.

(63) Engelhardt, G. 29Si-NMR-Spektroskopische Untersuchungen an Methyl- Und Methyl-Phenyl-Siloxanen Und Ihre Anwendung in Der Silikonanalytik. *J. Organomet. Chem.* **1973**, *54*, 115–122. https://doi.org/10.1016/S0022-328X(00)84998-0.

(64) Li, J.; Zhang, L.; Wang, A.; Zhao, C.; Li, J.; Zhang, L.; Wang, A.; Zhao, C.; Lin, L. Effect of Junction Temperature on the Performance of High-Power White LEDs. *SPIE 7852, LED Disp. Technol.* **2010**, *78521H* (November 2010). https://doi.org/10.1117/12.871700.

(65) Kim, D. S.; Han, B. Effect of Junction Temperature on Heat Dissipation of High Power Light Emitting Diodes. *J. Appl. Phys.* **2016**, *119* (12). https://doi.org/10.1063/1.4944800.

(66) Han, N.; Jung, E.; Han, M.; Ryu, B. D.; Ko, K. B.; Park, Y. J.; Cuong, T.; Cho, J.; Kim, H.; Hong, C. H. Reduced Junction Temperature and Enhanced Performance of High Power Light-Emitting Diodes Using Reduced Graphene Oxide Pattern. *J. Phys. D. Appl. Phys.* **2015**, *48* (26). https://doi.org/10.1088/0022-3727/48/26/265102.

(67) Yazdan Mehr, M.; van Driel, W. D.; Zhang, G. Q. (Kouchi). Progress in Understanding Color Maintenance in Solid-State Lighting Systems. *Engineering* **2015**, *1* (2), 170–178. https://doi.org/10.15302/J-ENG-2015035.

(68) Huang, J. C.; Chu, Y. P.; Wei, M.; Deanin, R. D. Comparison of Epoxy Resins for Applications in Light-Emitting Diodes. *Adv. Polym. Technol.* **2004**, *23* (4), 298–306. https://doi.org/10.1002/adv.20018.

(69) Krauklis, A. E.; Echtermeyer, A. T. Mechanism of Yellowing: Carbonyl Formation during Hygrothermal Aging in a Common Amine Epoxy. *Polymers (Basel).* **2018**, *10* (9). https://doi.org/10.3390/polym10091017.

(70) Yin, M.; Yang, L.; Li, X. Y.; Ma, H. B. Synthesis and Properties of Methyl Hexahydrophthalic Anhydride-Cured Fluorinated Epoxy Resin 2,2-Bisphenol Hexafluoropropane Diglycidyl Ether. *J. Appl. Polym. Sci.* **2013**, *130* (4), 2801–2808. https://doi.org/10.1002/app.39517.

(71) Andraschek, N.; Wanner, A. J.; Ebner, C.; Riess, G. Mica/Epoxy-Composites in the Electrical Industry: Applications, Composites for Insulation, and Investigations on Failure Mechanisms for Prospective Optimizations. *Polymers (Basel).* **2016**, *8* (5). https://doi.org/10.3390/polym8050201.

(72) Matějka, L.; Lövy, J.; Pokorný, S.; Bouchal, K.; Dušek, K. Curing Epoxy Resins with Anhydrides. Model Reactions and Reaction Mechanism. *J. Polym. Sci. Polym. Chem. Ed.* **2003**, *21* (10), 2873–2885. https://doi.org/10.1002/pol.1983.170211003.

(73) Yang, S.; Kwak, S.-Y.; Jin, J.; Kim, J.-S.; Choi, Y.; Paik, K.-W.; Bae, B.-S. Thermally Resistant UV-Curable Epoxy–Siloxane Hybrid Materials for Light Emitting Diode (LED) Encapsulation. *J. Mater. Chem.* **2012**, *22* (18), 8874. https://doi.org/10.1039/c2jm16355a.

(74) Yazdan Mehr, M.; Van Driel, W. D.; Jansen, K. M. B.; Deeben, P.; Zhang, G. Q. Lifetime Assessment of Bisphenol-A Polycarbonate (BPA-PC) Plastic Lens, Used in LED-Based Products. *Microelectron. Reliab.* **2014**, *54* (1), 138–142. https://doi.org/10.1016/j.microrel.2013.09.009.

(75) Mark, J. E. Some Interesting Things about Polysiloxanes. *Acc. Chem. Res.* **2004**, *37* (12), 946–953. https://doi.org/10.1021/ar030279z.

(76) Wen, R.; Huo, J.; Lv, J.; Liu, Z.; Yu, Y. Effect of Silicone Resin Modification on the Performance of Epoxy Materials for LED Encapsulation. *J. Mater. Sci. Mater. Electron.* **2017**, *28* (19), 1–14. https://doi.org/10.1007/s10854-017-7316-5.

(77) Lewis, L. N.; Stein, J.; Gao, Y.; Colborn, R. E.; Hutchins, G. Platinum Catalysts Used in the Silicone Industry. *Platin. Matals Rev.* **1997**, *41* (2), 66–75.

(78) Dow Corning Corporation. LED Packaging - Advanced silicone technology for LED applications www.ellsworth.com/globalassets/literature-library/manufacturer/dow-corning/dow-corning-brochure-silicone-technology-for-led-packaging.pdf.

(79) Shin-Etsu Chemical Co. Ltd. Encapsulation materials for optical devices http://www.shinetsu-encap-mat.jp/e/product/k_l/lds/.

(80) Velderrain, M. Designing Low Permeability, Optical- Grade Silicone Systems: Guidelines for Choosing a Silicone Based on Transmission Rates for Barrier Applications. In *SPIE 8280, Advances in Display Technologies II*; 2012; Vol. 82800O. https://doi.org/10.1117/12.910642.

(81) Steinbrück, N.; Pohl, S.; Kickelbick, G. Platinum Free Thermally Curable Siloxanes for Optoelectronic Application – Synthesis and Properties. *RSC Adv.* **2019**, *9* (4), 2205–2216. https://doi.org/10.1039/C8RA09801H.

(82) Zhang, B.; Soleimaninejad, H.; Jones, D. J.; White, J. M.; Ghiggino, K. P.; Smith, T. A.; Wong, W. W. H. Highly Fluorescent Molecularly Insulated Perylene Diimides: Effect of Concentration on Photophysical Properties. *Chem. Mater.* **2017**, *29* (19), 8395–8403. https://doi.org/10.1021/acs.chemmater.7b02968.

(83) Buffa, M.; Carturan, S.; Debije, M. G.; Quaranta, A.; Maggioni, G. Dye-Doped Polysiloxane Rubbers for Luminescent Solar Concentrator Systems. *Springer Ser. Mater. Sci.* **2014**, *190*, 247–266. https://doi.org/10.1007/978-3-319-01988-8_9.

(84) Krumer, Z.; van Sark, W. G. J. H. M.; Schropp, R. E. I.; de Mello Donega, C. Compensation of Self-Absorption Losses in Luminescent Solar Concentrators by Increasing Luminophore Concentration. *Sol. Energy Mater. Sol. Cells* **2017**, *167* (July 2016), 133–139. https://doi.org/10.1016/j.solmat.2017.04.010.

(85) Higashihara, T.; Ueda, M. Recent Progress in High Refractive Index Polymers. *Macromolecules* **2015**, *48* (7), 1915–1929. https://doi.org/10.1021/ma502569r.

(86) Wang, J.; Du, M.-L.; Xu, C.-S.; Zhu, H.; Fu, Y.-Q. Synthesis of Transparent Densely Crosslinked Polysiloxane with High Refractive Index. *J. Macromol. Sci. Part B* **2012**, *51* (12), 2462–2472. https://doi.org/10.1080/00222348.2012.679140.

(87) Chen, M.; Zhang, G.; Liang, X.; Zhang, W.; Zhou, L.; He, B.; Song, P.; Yuan, X.; Zhang, C.; Zhang, L.; et al. Thermally Stable Transparent Sol-Gel Based Active Siloxane-Oligomer Materials with Tunable High Refractive Index and Dual Reactive Groups. *RSC Adv.* **2016**, *6* (75). https://doi.org/10.1039/c6ra13164f.

(88) Macdonald, E. K.; Shaver, M. P. Intrinsic High Refractive Index Polymers. *Polym. Int.* **2015**, *64* (1), 6–14. https://doi.org/10.1002/pi.4821.

(89) Lee, Y. S.; Kim, K. H.; Kim, W. H.; Choi, M. H.; Jung, C. H.; Choi, J. H.; Kim, J. P. Effect of Cross-Linking Density of Silicone Encapsulant on Sulfur Compound Gas Permeability of Light-Emitting Diode. *IEEE Trans. Components, Packag. Manuf. Technol.* **2015**, *5* (2), 163–167. https://doi.org/10.1109/TCPMT.2014.2387195.

(90) Mura, G.; Cassanelli, G.; Fantini, F.; Vanzi, M. Sulfur-Contamination of High Power White LED. *Microelectron. Reliab.* **2008**, *48* (8–9), 1208–1211. https://doi.org/10.1016/j.microrel.2008.07.005.

(91) Zhou, L.; An, B.; Wu, Y.; Liul, S. Analysis of Delamination and Darkening in High Power LED Packaging. *Proc. Int. Symp. Phys. Fail. Anal. Integr. Circuits, IPFA* **2009**, 656–660. https://doi.org/10.1109/IPFA.2009.5232549.

(92) Badur, T.; Dams, C.; Hampp, N. High Refractive Index Polymers by Design. *Macromolecules* **2018**, *51* (11), 4220–4228. https://doi.org/10.1021/acs.macromol.8b00615.

(93) Yang, X.; Huang, W.; Yu, Y. Synthesis, Characterization, and Properties of Silicone–Epoxy Resins. *J. Appl. Phys.* **2011**, *120*, 1216–1224. https://doi.org/10.1002/app.

(94) Gao, N.; Liu, W.; Yan, Z.; Wang, Z. Synthesis and Properties of Transparent Cycloaliphatic Epoxy-Silicone Resins for Opto-Electronic Devices Packaging. *Opt. Mater. (Amst).* **2013**, *35* (3), 567–575. https://doi.org/10.1016/j.optmat.2012.10.023.

(95) Tsai, C. W.; Wu, K. H.; Yang, C. C.; Wang, G. P. Adamantane-Based Epoxy Resin and Siloxane-Modified Adamantane-Based Epoxy Resin: Characterization of Thermal, Dielectric and Optical Properties. *React. Funct. Polym.* **2015**, *91–92*, 11–18. https://doi.org/10.1016/j.reactfunctpolym.2015.04.002.

(96) Tao, P.; Li, Y.; Rungta, A.; Viswanath, A.; Gao, J.; Benicewicz, B. C.; Siegel, R. W.; Schadler, L. S. TiO2 Nanocomposites with High Refractive Index and Transparency. *J. Mater. Chem.* **2011**, *21*, 18623. https://doi.org/10.1039/c1jm13093e.

(97) Lei, I. A.; Lai, D. F.; Don, T. M.; Chen, W. C.; Yu, Y. Y.; Chiu, W. Y. Silicone Hybrid Materials Useful for the Encapsulation of Light-Emitting Diodes. *Mater. Chem. Phys.* **2014**, *144* (1–2), 41–48. https://doi.org/10.1016/j.matchemphys.2013.12.009.

(98) Kim, Y. H.; Bae, J. Y.; Jin, J.; Bae, B. S. Sol-Gel Derived Transparent Zirconium-Phenyl Siloxane Hybrid for Robust High Refractive Index LED Encapsulant. *ACS Appl. Mater. Interfaces* **2014**, *6* (5), 3115–3121. https://doi.org/10.1021/am500315y.

(99) Lai, Y.; Jin, L.; Hang, J.; Sun, X.; Shi, L. Highly Transparent Thermal Stable Silicone/Titania Hybrids with High Refractive Index for LED Encapsulation. *J. Coatings Technol. Res.* **2015**, *12* (6), 1185–1192. https://doi.org/10.1007/s11998-015-9681-4.

(100) Jitianu, A.; Cadars, S.; Zhang, F.; Rodriguez, G.; Picard, Q.; Aparicio, M.; Mosa, J.; Klein, L. C. 29Si NMR and SAXS Investigation of the Hybrid Organic-Inorganic Glasses Obtained by Consolidation of the Melting Gels. *Dalt. Trans.* **2017**, *46* (11), 3729–3741. https://doi.org/10.1039/c6dt04394a.

(101) Nenashev, R. N.; Kotova, N. M.; Vishnevskii, A. S.; Vorotilov, K. A. Effect of Methyltrimethoxysilane Hydrolysis and Condensation Conditions on the Properties of Thin Polymethylsilsesquioxane Films. *Inorg. Mater.* **2016**, *52* (6), 625–629. https://doi.org/10.1134/S0020168516060108.

(102) Klein, L. C.; Kallontzi, S.; Fabris, L.; Jitianu, A.; Ryan, C.; Aparicio, M.; Lei, L.; Singer, J. P. Applications of Melting Gels. *J. Sol-Gel Sci. Technol.* **2018**, *89* (1), 66–77. https://doi.org/10.1007/s10971-018-4599-9.

(103) Jitianu, A.; Amatucci, G.; Klein, L. C. Phenyl-Substituted Siloxane Hybrid Gels That Soften below 140°C. *J. Am. Ceram. Soc.* **2009**, *92* (1), 36–40. https://doi.org/10.1111/j.1551-2916.2008.02841.x.

(104) Klein, L. C.; Jitianu, A. Erratum: Organic-Inorganic Hybrid Melting Gels (Journal of Sol-Gel Science and Technology). *J. Sol-Gel Sci. Technol.* **2011**, *59* (3), 424–431. https://doi.org/10.1007/s10971-011-2414-y.

(105) Jitianu, A.; Doyle, J.; Amatucci, G.; Klein, L. C. Methyl Modified Siloxane Melting Gels for Hydrophobic Films. *J. Sol-Gel Sci. Technol.* **2010**, *53* (2), 272–279. https://doi.org/10.1007/s10971-009-2087-y.

(106) Jitianu, A.; Cadars, S.; Zhang, F.; Rodriguez, G.; Picard, Q.; Aparicio, M.; Mosa, J.; Klein, L. C. 29Si NMR and SAXS Investigation of the Hybrid Organic-Inorganic Glasses Obtained by Consolidation of the Melting Gels. *Dalt. Trans.* **2017**, *46* (11), 3729–3741. https://doi.org/10.1039/c6dt04394a.

(107) Ahn, T. S.; Al-Kaysi, R. O.; Müller, A. M.; Wentz, K. M.; Bardeen, C. J. Self-Absorption Correction for Solid-State Photoluminescence Quantum Yields Obtained from Integrating Sphere Measurements. *Rev. Sci. Instrum.* **2007**, *78* (8), 2007–2009. https://doi.org/10.1063/1.2768926.

(108) Wilson, L. R.; Richards, B. S. Measurement Method for Photoluminescent Quantum Yields of Fluorescent Organic Dyes in Polymethyl Methacrylate for Luminescent Solar Concentrators. *Appl. Opt.* **2009**, *48* (2), 212. https://doi.org/10.1364/AO.48.000212.

(109) Huang, C.; Barlow, S.; Marder, S. R. Perylene-3,4,9,10-Tetracarboxylic Acid Diimides: Synthesis, Physical Properties, and Use in Organic Electronics. *J. Org. Chem.* **2011**, *76* (8), 2386–2407. https://doi.org/10.1021/jo2001963.

(110) Fan, L.; Xu, Y.; Tian, H. 1,6-Disubstituted Perylene Bisimides: Concise Synthesis and Characterization as near-Infrared Fluorescent Dyes. *Tetrahedron Lett.* **2005**, *46* (26), 4443–4447. https://doi.org/10.1016/j.tetlet.2005.04.137.

(111) Li, C.; Wonneberger, H. Perylene Imides for Organic Photovoltaics: Yesterday, Today, and Tomorrow. *Adv. Mater.* **2012**, *24* (5), 613–636. https://doi.org/10.1002/adma.201104447.

(112) Clark, A. E.; Qin, C.; Li, A. D. Q. Beyond Exciton Theory: A Time-Dependent DFT and Franck-Condon Study of Perylene Diimide and Its Chromophoric Dimer. *J. Am. Chem. Soc.* **2007**, *129* (24), 7586–7595. https://doi.org/10.1021/ja0687724.

(113) Würthner, F. Perylene Bisimide Dyes as Versatile Building Blocks for Functional Supramolecular Architectures. *Chem. Commun.* **2004**, *4* (14), 1564–1579. https://doi.org/10.1039/b401630k.

(114) Song, P.; Guan, B.; Zhou, Q.; Zhao, M.; Huang, J.; Ma, F. Effect of the Phenoxy Groups on PDIB and Its Derivatives. *Sci. Rep.* **2016**, *6* (September), 1–8. https://doi.org/10.1038/srep35555.

(115) Griffini, G.; Brambilla, L.; Levi, M.; Del Zoppo, M.; Turri, S. Photo-Degradation of a Perylene-Based Organic Luminescent Solar Concentrator: Molecular Aspects and Device Implications. *Sol. Energy Mater. Sol. Cells* **2013**, *111*, 41–48. https://doi.org/10.1016/j.solmat.2012.12.021.

(116) Dincalp, H.; Kizilok, S.; Icli, S. Fluorescent Macromolecular Perylene Diimides Containing Pyrene or Indole Units in Bay Positions. *Dye. Pigment.* **2010**, *86* (1), 32–41. https://doi.org/10.1016/j.dyepig.2009.11.005.

(117) Rademacher, A.; Märkle, S.; Langhals, H. Lösliche Perylen-Fluoreszenzfarbstoffe Mit Hoher Photostabilität. *Chem. Ber.* **1982**, *115* (8), 2927–2934. https://doi.org/10.1002/cber.19821150823.

(118) Zhang, B.; Soleimaninejad, H.; Jones, D. J.; White, J. M.; Ghiggino, K. P.; Smith, T. A.; Wong, W. W. H. Highly Fluorescent Molecularly Insulated Perylene Diimides: Effect of Concentration on Photophysical Properties. *Chem. Mater.* **2017**, *29* (19), 8395–8403. https://doi.org/10.1021/acs.chemmater.7b02968.

(119) BASF AG. *Lumogen(R)F - Technical Information, TI/P 3201 e (9125)*; 1997.

(120) BASF. Lumogen(R) F Rot 305 basf.com.

(121) Chen, K.; Chang, C. 1,7-Bis-(N,N-Dialkylamino)Perylene Bisimides: Facile Synthesis and Characterization as Near-Infrared Fluorescent Dyes. *Materials (Basel).* **2014**, *7* (11), 7548–7565. https://doi.org/10.3390/ma7117548.

(122) Chang, C. W.; Tsai, H. Y.; Chen, K. Y. Green Perylene Bisimide Dyes: Synthesis, Photophysical and Electrochemical Properties. *Materials (Basel).* **2014**, *7* (8), 5488–5506. https://doi.org/10.3390/ma7085488.

(123) Pucci, A.; Ruggeri, G. Mechanochromic Polymer Blends. *J. Mater. Chem.* **2011**, *21* (23), 8282–8291. https://doi.org/10.1039/c0jm03653f.

(124) Mishra, A.; Behera, R. K.; Behera, P. K.; Mishra, B. K.; Behera, G. B. Cyanines during the 1990s: A Review. *Chem. Rev.* **2000**, *100* (6), 1973–2011. https://doi.org/10.1021/cr990402t.

(125) Neuteboom, E. E.; Meskers, S. C. J.; Meijer, E. W.; Janssen, R. A. J. Photoluminescence of Self-Organized Perylene Bisimide Polymers. *Macromol. Chem. Phys.* **2004**, *205* (2), 217–222. https://doi.org/10.1002/macp.200300044.

(126) Correia, S. F. H.; De Zea Bermudez, V.; Ribeiro, S. J. L.; André, P. S.; Ferreira, R. A. S.; Carlos, L. D. Luminescent Solar Concentrators: Challenges for Lanthanide-Based Organic-Inorganic Hybrid Materials. *J. Mater. Chem. A* **2014**, *2* (16), 5580–5596. https://doi.org/10.1039/c3ta14964a.

(127) Schlotter, P.; Baur, J.; Hielscher, C.; Kunzer, M.; Obloh, H.; Schmidt, R.; Schneider, J. Fabrication and Characterization of GaN/InGaN/AlGaN Double Heterostructure LEDs and Their Application in Luminescence Conversion LEDs. *Mater. Sci. Eng. B Solid-State Mater. Adv. Technol.* **1999**, *59* (1–3), 390–394. https://doi.org/10.1016/S0921-5107(98)00352-3.

(128) Kim, H. J.; Jin, J. Y.; Lee, Y. S.; Lee, S. H.; Hong, C. H. An Efficient Luminescence Conversion LED for White Light Emission, Fabricated Using a Commercial InGaN LED and a 1,8-Naphthalimide Derivative. *Chem. Phys. Lett.* **2006**, *431* (4–6), 341–345. https://doi.org/10.1016/j.cplett.2006.09.090.

(129) Kozma, E.; Mróz, W.; Galeotti, F. A Polystyrene Bearing Perylene Diimide Pendants with Enhanced Solid State Emission for White Hybrid Light-Emitting Diodes. *Dye. Pigment.* **2015**, *114* (C), 138–143. https://doi.org/10.1016/j.dyepig.2014.11.009.

(130) Assadi, M. K.; Hanaei, H.; Mohamed, N. M.; Saidur, R.; Bakhoda, S.; Bashiri, R.; Moayedfar, M. Enhancing the Efficiency of Luminescent Solar Concentrators (LSCs). *Appl. Phys. A Mater. Sci. Process.* **2016**, *122* (9), 1–12. https://doi.org/10.1007/s00339-016-0359-2.

(131) Reisfeld, R. New Developments in Luminescence for Solar Energy Utilization. *Opt. Mater. (Amst).* **2010**, *32* (9), 850–856. https://doi.org/10.1016/j.optmat.2010.04.034.

(132) Ibrahim, A. H. A. S. I.; Khyoon, S.; Alrda, A. Effects of Luminous Solar Concentrator Parameters (Dyes Mixture , Host Type and LSC Thickness) on the Si Solar Cell Performance Efficiency. *Int. J. Curr. Eng. Technol.* **2015**, *5* (4), 2439–2443.

(133) Manikandan, M; Deepa Arun, N; Sivaranjini, P; Suresh, M; Ashok Kumar, R. Developing an Equivalent Circuit Model Based M-File for Solar Photovoltaic. *Int. J. Adv. Res. Electr. Electron. Instrum. Eng.* **2015**, *4* (9), 7628–1633. https://doi.org/10.15662/IJAREEIE.2015.0409043.

(134) Jones, B. A.; Facchetti, A.; Wasielewski, M. R.; Marks, T. J. Tuning Orbital Energetics in Arylene Diimide Semiconductors. Materials Design for Ambient Stability of n-Type Charge Transport. *J. Am. Chem. Soc.* **2007**, *129* (49), 15259–15278. https://doi.org/10.1021/ja075242e.

(135) Nowak-Król, A.; Fimmel, B.; Son, M.; Kim, D.; Würthner, F. Photoinduced Electron Transfer (PET) versus Excimer Formation in Supramolecular p/n-Heterojunctions of Perylene Bisimide Dyes and Implications for Organic Photovoltaics. *Faraday Discuss.* **2015**, 507–527. https://doi.org/10.1039/C5FD00052A.

(136) Horowitz, G. Evidence for N-Type Conduction in a Perylene Tetracarboxylic Diimide Derivative. *Adv. Mater.* **1996**, *8* (3), 242–245. https://doi.org/10.1002/adma.19960080312.

(137) Shibano, Y.; Imahori, H.; Adachi, C. Organic Thin-Film Solar Cells Using Electron-Donating Perylene Tetracarboxylic Acid Derivatives. *J. Phys. Chem. C* **2009**, *113* (34), 15454–15466. https://doi.org/10.1021/jp9045726.

(138) Noimark, S.; Salvadori, E.; Gómez-Bombarelli, R.; MacRobert, A. J.; Parkin, I. P.; Kay, C. W. M. Comparative Study of Singlet Oxygen Production by Photosensitiser Dyes Encapsulated in Silicone: Towards Rational Design of Anti-Microbial Surfaces. *Phys. Chem. Chem. Phys.* **2016**, *18* (40), 28101–28109. https://doi.org/10.1039/c6cp02529c.

(139) Ford, W. E.; Kamat, P. V. Photochemistry of 3,4,9,10-Perylenetetracarboxylic Dianhydride Dyes. 3. Singlet and Triplet Excited-State Properties of the Bis(2,5-Di-Tert-Butylphenyl)Imide Derivate. *J. Phys. Chem.* **1987**, *91* (25), 6373–6380. https://doi.org/10.1021/j100309a012.

(140) Tanaka, N.; Barashkov, N.; Heath, J.; Sisk, W. N. Photodegradation of Polymer-Dispersed Perylene Di-Imide Dyes. *Appl. Opt.* **2006**, *45* (16), 3846–3851. https://doi.org/10.1364/AO.45.003846.

(141) Kim, K. M.; Jang, B. J.; Cho, W. S.; Ju, S. H. The Property of Encapsulation Using Thin Film Multi Layer for Application to Organic Light Emitting Device. *Curr. Appl. Phys.* **2005**, *5* (1), 64–66. https://doi.org/10.1016/j.cap.2003.11.081.

(142) Le Rendu, P.; Nguyen, T. P.; Carrois, L. Cellulose Acetate and PVDC Used as Protective Layers for Organic Diodes. *Synth. Met.* **2003**, *138* (1–2), 285–288. https://doi.org/10.1016/S0379-6779(02)01294-8.

(143) Kim, G. H.; Oh, J.; Yang, Y. S.; Do, L. M.; Suh, K. S. Lamination Process Encapsulation for Longevity of Plastic-Based Organic Light-Emitting Devices. *Thin Solid Films* **2004**, *467* (1–2), 1–3. https://doi.org/10.1016/j.tsf.2004.02.036.

(144) Fu, W.; He, C.; Jiang, S.; Chen, Z.; Zhang, J.; Li, Z.; Yan, S.; Zhang, R. Synthesis of a Polymeric Electron Acceptor Based on Perylenediimide-Bridged Ladder Polysiloxane. *Macromolecules* **2011**, *44* (2), 203–207. https://doi.org/10.1021/ma1025797.

(145) Langhals, H.; Unold, P. Von; Speckbacher, M. Balanced Decarboxylation of Aromatic Polyacids – A One-Step Synthesis of Perylene-3,4-Dicarboxylic Anhydride. *Liebigs Ann./Recl.* **1997**, 467–468. https://doi.org/10.1002/jlac.199719970305.

(146) Refiker, H.; Icil, H. Amphiphilic and Chiral Unsymmetrical Perylene Dye for Solid-State Dye-Sensitized Solar Cells. *Turkish J. Chem.* **2011**, *35* (6), 847–859. https://doi.org/10.3906/kim-1107-39.

(147) Nagao, Y. Synthesis and Properties of Perylene Pigments. *Prog. Org. Coatings* **1997**, *31* (1–2), 43–49. https://doi.org/10.1016/S0300-9440(97)00017-9.

(148) Yao, D.; Bender, T. P.; Gerroir, P. J.; Sundararajan, P. R. Self-Assembled Vesicular Nanostructures of Perylene End-Capped Poly(Dimethylsiloxane). *Macromolecules* **2005**, *38* (16), 6972–6978. https://doi.org/10.1021/ma051071r.

(149) Liang, Y.; Wang, D.; Wu, Y.; Lai, Q.; Xue, L.; Feng, S. Perylene-Containing Polysiloxane: An Effective Candidate for Corrosion Protection of Iron Surface. *Appl. Surf. Sci.* **2011**, *257* (24), 10576–10580. https://doi.org/10.1016/j.apsusc.2011.07.053.

(150) Cazacu, M.; Vlad, A.; Airinei, A.; Nicolescu, A.; Stoica, I. New Imides Based on Perylene and Siloxane Derivatives. *Dye. Pigment.* **2011**, *90* (2), 106–113. https://doi.org/10.1016/j.dyepig.2010.12.012.

(151) Dahan, E.; Sundararajan, P. R. Polymer Compatibilized Self-Assembling Perylene Derivatives. *Eur. Polym. J.* **2015**, *65*, 4–14. https://doi.org/10.1016/j.eurpolymj.2014.11.022.

(152) Zhang, H. Progress in Preparation of Monodisperse Polymer Microspheres. *IOP Conf. Ser. Mater. Sci. Eng.* **2017**, *274* (1). https://doi.org/10.1088/1757-899X/274/1/012107.

(153) Hsu, C. C.; Chang, K. C.; Huang, T. C.; Yeh, L. C.; Yeh, W. T.; Ji, W. F.; Yeh, J. M.; Tsai, T. Y. Preparation and Studies on Properties of Porous Epoxy Composites Containing Microscale Hollow Epoxy Spheres. *Microporous Mesoporous Mater.* **2014**, *198*, 15–21. https://doi.org/10.1016/j.micromeso.2014.06.013.

(154) Pu, W.; Fu, D.; Xia, H.; Wang, Z. Preparation of Hollow Polyurethane Microspheres with Tunable Surface Structures via Electrospraying Technology. *RSC Adv.* **2017**, *7* (79), 49828–49837. https://doi.org/10.1039/c7ra09831f.

(155) Weng, H.; Wu, Z.; Zhao, C.; Wang, M.; Ge, X.; Yamashita, S.; Tang, J.; Lin, M. Construction of Polyporous Polymer Microspheres with a Tailored Mesoporous Wall. *Polym. Chem.* **2019**. https://doi.org/10.1039/C8PY01714J.

(156) Trofymchuk, K.; Reisch, A.; Shulov, I.; Mély, Y.; Klymchenko, A. S. Tuning the Color and Photostability of Perylene Diimides inside Polymer Nanoparticles: Towards Biodegradable Substitutes of Quantum Dots. *Nanoscale* **2014**, *6* (21), 12934–12942. https://doi.org/10.1039/c4nr03718a.

(157) Slomkowski, S. Functionalized Biodegradable Nano- and Microspheres for Medical Applications. *Macromol. Symp.* **2010**, *288* (1), 121–129. https://doi.org/10.1002/masy.201050216.

(158) Gardner, K.; Aghajamali, M.; Vagin, S.; Pille, J.; Morrish, W.; Veinot, J. G. C.; Rieger, B.; Meldrum, A. Ultrabright Fluorescent and Lasing Microspheres from a Conjugated Polymer. *Adv. Funct. Mater.* **2018**, *28* (33), 1–6. https://doi.org/10.1002/adfm.201802759.

(159) Trau, M.; Surawski, P. P. T.; Miller, C. R.; Corrie, S. R.; Vogel, R.; Jack, K. S. Functionalized Organosilica Microspheres via a Novel Emulsion-Based Route. *Langmuir* **2005**, *21* (21), 9733–9740. https://doi.org/10.1021/la0514112.

(160) Lu, X.; Hou, Y.; Zha, J.; Xin, Z. Facile Synthesis of Rhodamine B-Doped Poly(3-Mercaptopropylsilsesquioxane) Fluorescent Microspheres with Controllable Size. *Ind. Eng. Chem. Res.* **2013**, *52* (17), 5880–5886. https://doi.org/10.1021/ie302556t.

(161) Chojnowski, J.; Pospiech, P.; Fortuniak, W.; Kurjata, J.; Slomkowski, S. Route to Hydrophilic, Hydrophobic and Functionalized Cross-Linked Polysiloxane Microspheres. *Polymer (Guildf).* **2013**, *54* (13), 3156–3165. https://doi.org/10.1016/j.polymer.2013.04.017.

(162) Pospiech, P.; Chojnowski, J.; Mizerska, U.; Fortuniak, W.; Slomkowski, S.; Stolarski, J. Macroporous Microspheres and Microspheroidal Particles from Polyhydromethylsiloxane. *Colloid Polym. Sci.* **2017**, *295* (5), 939–944. https://doi.org/10.1007/s00396-017-4075-z.

(163) Romeo, H. E.; Cameo, M.; Choren, M. V.; Fanovich, M. A. Functionalized Bridged Silsesquioxane-Based Nanostructured Microspheres: Ultrasound-Assisted Synthesis and in Vitro Cytotoxicity Characterization. *J. Mater. Sci. Mater. Med.* **2011**, *22* (4), 935–943. https://doi.org/10.1007/s10856-011-4261-3.

(164) Krüner, B.; Odenwald, C.; Tolosa, A.; Schreiber, A.; Aslan, M.; Kickelbick, G.; Presser, V. Carbide-Derived Carbon Beads with Tunable Nanopores from Continuously Produced Polysilsesquioxanes for Supercapacitor Electrodes. *Sustain. Energy Fuels* **2017**, *1* (7), 1588–1600. https://doi.org/10.1039/c7se00265c.

(165) Fortuniak, W.; Chojnowski, J.; Slomkowski, S.; Nyczyk-Malinowska, A.; Pospiech, P.; Mizerska, U. Solid Ceramic SiCO Microspheres and Porous Rigid Siloxane Microspheres from Swellable Polysiloxane Particles. *Mater. Chem. Phys.* **2015**, *155*, 83–91. https://doi.org/10.1016/j.matchemphys.2015.02.002.

(166) Vakifahmetoglu, C.; Balliana, M.; Colombo, P. Ceramic Foams and Micro-Beads from Emulsions of a Preceramic Polymer. *J. Eur. Ceram. Soc.* **2011**, *31* (8), 1481–1490. https://doi.org/10.1016/j.jeurceramsoc.2011.02.012.

(167) Roy, P. K.; Iqbal, N.; Kumar, D.; Rajagopal, C. Polysiloxane-Based Core-Shell Microspheres for Toughening of Epoxy Resins. *J. Polym. Res.* **2014**, *21* (1). https://doi.org/10.1007/s10965-013-0348-5.

(168) Romeo, H. E.; Fanovich, M. A. Functionalized Bridged Silsesquioxane-Based Nanostructured Microspheres: Performance as Novel Drug-Delivery Devices in Bone Tissue-Related Applications. *J. Biomater. Appl.* **2012**, *26* (8), 987–1012. https://doi.org/10.1177/0885328210389503.

(169) Arkhireeva, A.; Hay, J. N.; Manzano, M. Preparation of Silsesquioxane Particles via a Nonhydrolytic Sol-Gel Route. *Chem. Mater.* **2005**, *17* (4), 875–880. https://doi.org/10.1021/cm0496341.

(170) Cao, J.; Zhu, Q.; Dou, J.; Li, C.; Chen, W.; Li, Z. Controlling Sol-Gel Polymerization to Create Bowl-Shaped Polysilsesquioxane Particles with a Kippah Structure. *Polymer (Guildf).* **2013**, *54* (10), 2493–2497. https://doi.org/10.1016/j.polymer.2013.03.033.

(171) Ren, X.; Sun, B.; Tsai, C. C.; Tu, Y.; Leng, S.; Li, K.; Kang, Z.; Horn, R. M. V.; Li, X.; Zhu, M.; et al. Synthesis, Self-Assembly, and Crystal Structure of a Shape-Persistent Polyhedral-Oligosilsesquioxane-Nanoparticle-Tethered Perylene Diimide. *J. Phys. Chem. B* **2010**, *114* (14), 4802–4810. https://doi.org/10.1021/jp100126u.

(172) Ben, H. J.; Fan, Y.; Shi, Y. J.; Liu, R.; Chen, Y.; Ren, X. K.; Jiang, S. Polyhedral-Oligosilsesquioxane Containing Poly(Methyl Methacrylate) Perylenebisimide Microspheres with High Solid State Emission. *Dye. Pigment.* **2017**, *137*, 584–592. https://doi.org/10.1016/j.dyepig.2016.09.065.

(173) Chen, J.; Jia, S.; Ji, X.; Nourrein, M.; Xiang, H.; Zhou, Z.; Wang, C. L.; Sun, B.; Zhu, M. The Morphologies and Fluorescence Quantum Yields of Perylene Diimide Dye-Doped PS and PHVB Microspheres. *RSC Adv.* **2018**, *8* (62), 35534–35538. https://doi.org/10.1039/C8RA04158J.

(174) Liu, B.; Bai, R.; Tian, J.; Wang, H.; Jin, B.; Du, F. Synthesis and Luminescence of POSS-Containing Perylene Bisimide-Bridged Amphiphilic Polymers. *Macromolecules* **2012**, *45* (7), 3086–3093. https://doi.org/10.1021/ma300100s.

(175) Jitianu, A.; Doyle, J.; Amatucci, G.; Klein, L. C. Methyl-Modified Melting Gels for Hermetic Barrier Coatings. In *Materials Science and Technology*; 2008; pp 2171–2182.

(176) Li, Z.; Tolbert, S.; Loy, D. A. Hybrid Organic-Inorganic Membranes on Porous Supports by Size Exclusion and Thermal Sintering of Fluorescent Polyphenylsilsesquioxane Nanoparticles. *Macromol. Mater. Eng.* **2013**, *298* (7), 715–721. https://doi.org/10.1002/mame.201200091.

(177) MacAn, J.; Tadanaga, K.; Tatsumisago, M. Influence of Copolymerization with Alkyltrialkoxysilanes on Condensation and Thermal Behaviour of Poly(Phenylsilsesquioxane) Particles. *J. Sol-Gel Sci. Technol.* **2010**, *53* (1), 31–37. https://doi.org/10.1007/s10971-009-2051-x.

(178) Liang, S.; Shephard, K.; Pierce, D. T.; Zhao, J. X. Effects of a Nanoscale Silica Matrix on the Fluorescence Quantum Yield of Encapsulated Dye Molecules. *Nanoscale* **2013**, *5* (19), 9365–9373. https://doi.org/10.1039/c3nr02500d.

(179) Lagorio, M. G.; San Román, E. How Does Light Scattering Affect Luminescence? Fluorescence Spectra and Quantum Yields in the Solid Phase. *J. Chem. Educ.* **2009**, *79* (11), 1362. https://doi.org/10.1021/ed079p1362.

(180) Shinde, P.; Gupta, S. Sen; Singh, B.; Polshettiwar, V.; Prasad, B. L. V. Amphi-Functional Mesoporous Silica Nanoparticles for Dye Separation. *J. Mater. Chem. A* **2017**, *5* (28), 14914–14921. https://doi.org/10.1039/c7ta03904b.

(181) Hurwitz, F. .; Hyatt, L.; Gorecki, J.; D'Amore, L. Silsesquioxanes as Precursors to Ceramic Composites. *Ceram. Eng. Sci. Proc.* **1987**, *8*, 732.

(182) Plyler, E. K. Infrared Spectra of Methanol, Ethanol, and n-Propanol. *J. Res. Natl. Bur. Stand. (1934).* **1952**, *48* (4), 281–286.

(183) Mechrez, G.; Zelikman, E.; Yaakov, N.; Itzhaik Alkotzer, Y.; Mani, K. A Robust Fabrication Method for Amphiphilic Janus Particles via Immobilization on Polycarbonate Microspheres. *Polymers (Basel).* **2018**, *10* (8), 900. https://doi.org/10.3390/polym10080900.

(184) Romeo, H. E.; Brus, J.; Pleštil, J.; Fanovich, M. A.; Matějka, L.; Williams, R. J. J. Fast Synthesis of Nanostructured Microspheres of a Bridged Silsesquioxane via Ultrasound-Assisted Sol-Gel Processing. *Macromol. Chem. Phys.* **2008**, NA-NA. https://doi.org/10.1002/macp.200800492.

(185) Behrend, O.; Ax, K.; Schubert, H. Influence of Continuous Phase Viscosity on Emulsification by Ultrasound. *Ultrason. Sonochem.* **2000**, *7* (2), 77–85. https://doi.org/10.1016/S1350-4177(99)00029-2.

(186) Gommes, C. J.; Blacher, S.; Dunsmuir, J. H.; Tsou, A. H. Viscosity Effects in Miniemulsification via Ultrasound. *AIChE J.* **2010**, *56* (10), 2751. https://doi.org/10.1002/aic.

(187) Steinbrück, N.; Könemann, M.; Kickelbick, G. Effect of Polysiloxane Encapsulation Material Compositions on Emission Behaviour and Stabilities of Perylene Dyes. *RSC Adv.* **2018**, *8*, 18128–18138. https://doi.org/10.1039/C8RA01700J.

7. Supplementary Information

7.1. Effect of Polysiloxane Encapsulation Material Compositions on Emission behaviour and Stabilities of Perylene Dyes

Supplementary Information

Effect of Polysiloxane Encapsulation Material Compositions on Emission Behaviour and Stabilities of Perylene Dyes

Nils Steinbrück[a], Martin Könemann[b] and Guido Kickelbick[c]

[a]Saarland University, Inorganic Solid State Chemistry, Campus, Building C4 1, 66123 Saarbrücken, Germany.

[b]BASF SE, 67056 Ludwigshafen, Germany

E-mail: guido.kickelbick@uni-saarland.de

Reaction schemes of Dow(1) and Shin(1) curing process

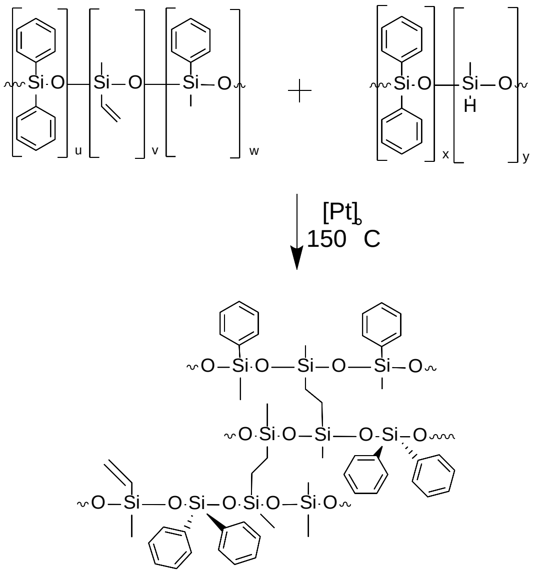

Scheme 1. Schematic chemical equation for the platinum catalysed hydrosilylation curing process of Dow(1).

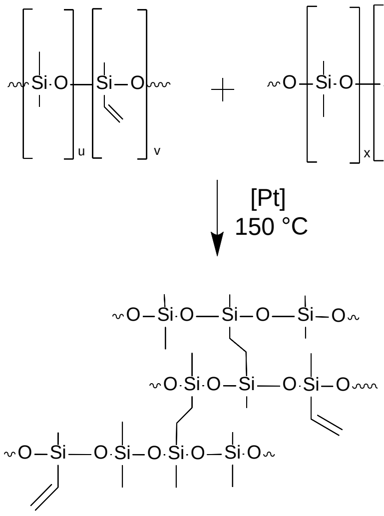

Scheme 2. Schematic chemical equation for the platinum catalysed hydrosilylation curing process of Shin(1).

Synthesis of FC546

FC546 was synthesized by BASF SE in a two-step procedure.

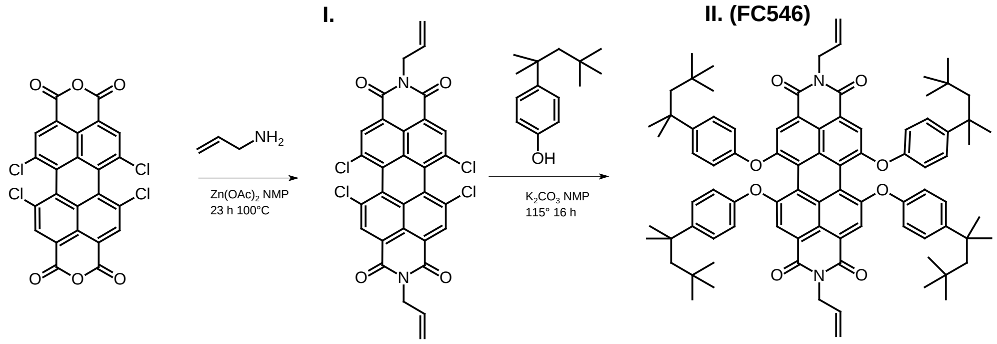

Scheme 3. Two step synthesis of FC546.

Preparation of N,N'-diallyl-1,6,7,12-tetrachloroperylene-3,4,9,10-tetracarboxylic acid diimide (I)

A mixture of 2.65 g (5 mmol) of 1,6,7,12-tetrachloroperylene-3,4;9,10-tetracarboxylic acide dianhydride, 2.75 g (15 mmol) of zinc acetate, 30 mL of N-methylpyrrolidone and 1.52 g (26 mmol) of allylamine were heated to 100°C for 23 hours. The reaction mixture was cooled to room temperature and 250 mL of brine were added. The formed solid was isolated by filtration, washed with water and dried at 70°C under reduced pressure. The product was used without further purification for the next step.

Rf (toluene:acetone 100:1) = 0.45.

Preparation of N,N'-diallyl-2,4,4-trimethylpentan-2-yl phenoxy-3,4,9,10-tetracarboxylic acid diimide (II) [FC546]

A mixture of 3.04 g (5 mmol) of the compound **I**, 70 mL of N-methylpyrrolidone, 5.16 g (25 mmol) of tert.-octylphenol, 3.46 g (25 mmol) of potassium carbonate was heated for 21 hours to 115°C. The reaction mixture was cooled to room temperature, the solid was isolated by filtration, the residue washed with water and dried at 70°C under reduced pressure. The product was subjected to column chromatography using toluene petroleum ether 1:2 and 1:1 and toluene. 1.2 g (19 %) of pure product were isolated.

Rf (toluene) = 0.36.

^{1}H NMR spectrum and chemical shifts are shown in the NMR section.

IR-Spectroscopy

Dow Corning OE6630 component A (cm^{-1}): 3049, 3072 ν(C-H)$_{AR}$; 2953, 2909 ν(C-H); 1590, 1490, 1430 [ν(C=C-C)$_{AR}$]; 1413, 1257 [δ(C-H [Si-CH$_3$])]; 1115, 1024 [ν(Si-O-Si)]; 784 [ρ(C-H [Si-(CH$_3$)$_2$])]; 726, 694 [δ(C-H)$_{AR}$].

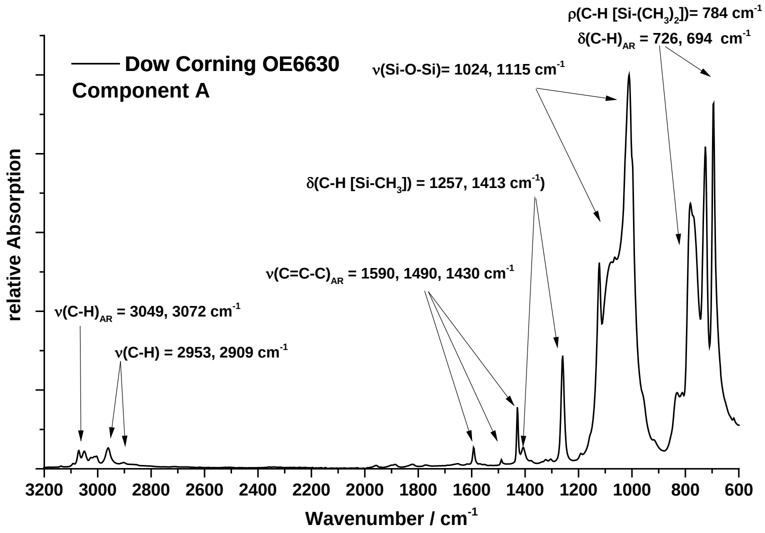

Figure 1. FTIR spectrum of Dow Corning OE6630 component A.

Dow Corning OE6630 component B (cm^{-1}): 3049, 3072 ν(C-H)$_{AR}$; 2953, 2909 ν(C-H); 2129 [ν(Si-H)]; 1590, 1490, 1430 [ν(C=C-C)$_{AR}$]; 1413, 1257 [δ(C-H [Si-CH$_3$])]; 1115, 1024 [ν(Si-O-Si)]; 896 [ρ(Si-H)]; 784 [ρ(C-H [Si-(CH$_3$)$_2$])]; 726, 694 [δ(C-H)$_{AR}$].

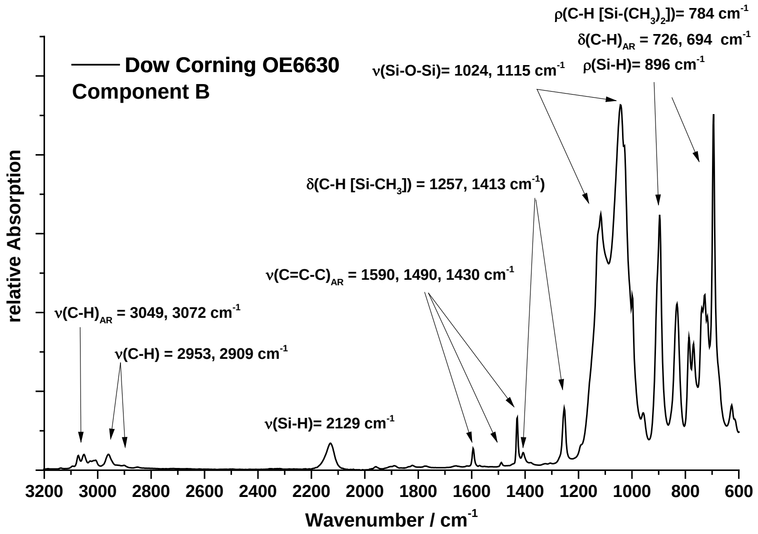

Figure 2. FTIR spectrum of Dow Corning OE6630 component B.

Shin KJR9022E component A (cm^{-1}): 2960, 2902 ν(C-H); 1412, 1257 [δ(C-H [Si-CH_3])]; 1008, 1065 [ν(Si-O-Si)]; 784 [ρ(C-H [Si-$(CH_3)_2$])].

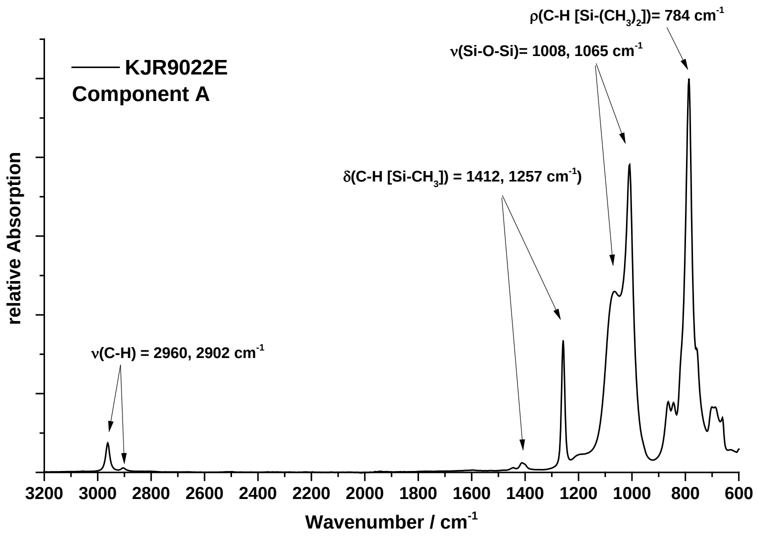

Figure 3. FTIR spectrum of Shin Etsu KJR9022E component A.

Shin KJR9022E component B (cm^{-1}): 2960, 2902 ν(C-H); 2159 [ν(Si-H)]; 1412, 1257 [δ(C-H [Si-CH_3])]; 1008, 1065 [ν(Si-O-Si)]; 906 [ρ(Si-H)]; 784 [ρ(C-H [Si-$(CH_3)_2$])].

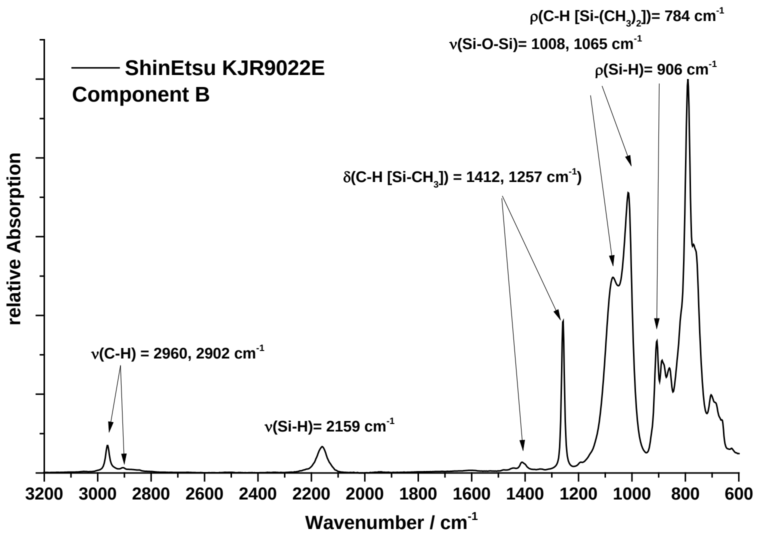

Figure 4. FTIR spectrum of Shin Etsu KJR9022E component B.

Dow Corning OE6630 cured (cm^{-1}): 3049, 3072 ν(C-H)$_{AR}$; 2953, 2909 ν(C-H); 1590, 1490, 1430 [ν(C=C-C)$_{AR}$]; 1413, 1257 [δ(C-H [Si-CH$_3$])]; 1115, 1024 [ν(Si-O-Si)]; 784 [ρ(C-H [Si-(CH$_3$)$_2$])]; 726, 694 [δ(C-H)$_{AR}$].

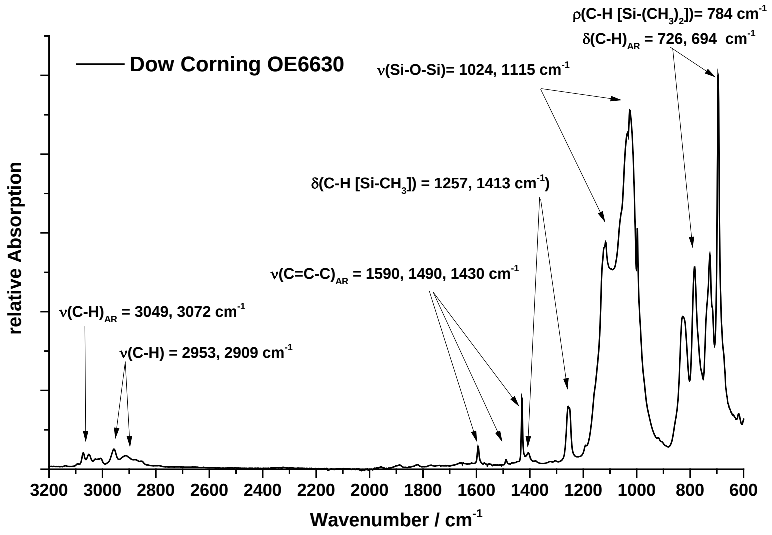

Figure 5. FTIR spectrum of cured Dow Corning OE6630.

Shin KJR9022E cured (cm^{-1}): 2960, 2902 ν(C-H); 1412, 1257 [δ(C-H [Si-CH$_3$])]; 1008, 1065 [ν(Si-O-Si)]; 784 [ρ(C-H [Si-(CH$_3$)$_2$])].

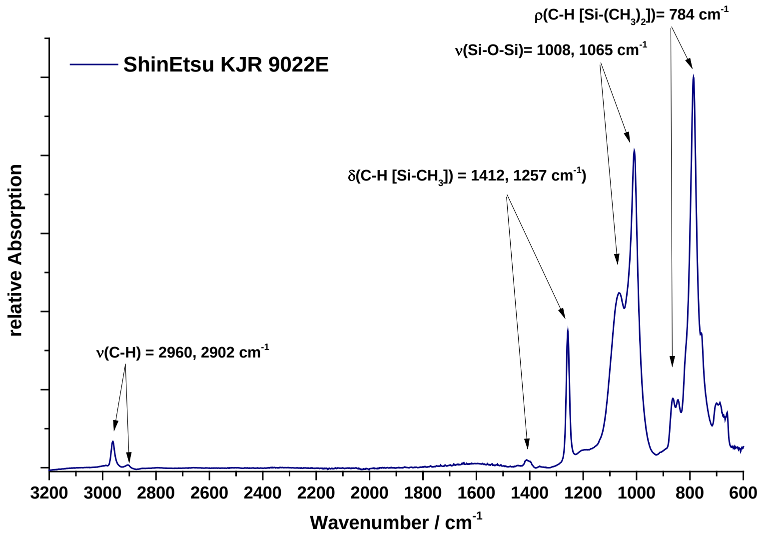

Figure 6. FTIR spectrum of cured ShinEtsu KJR9022E.

Lumogen®F Red 305 (cm^{-1}): 3030, 3064 ν(C-H)$_{AR}$; 2960, 2925 ν(C-H); 1705, 1672 ν(C=O); 1583, 1485 [ν(C=C-C)$_{AR}$]; 1407, 1338 ν(C-N); 1309, 1282, 1193 ν(C-O-C).

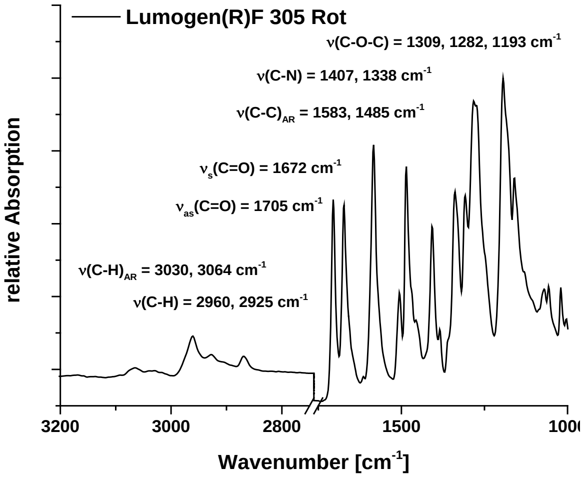

Figure 7. FTIR spectrum of Lumogen®F 305 Red.

FC546 (cm^{-1}): 3037, 3064 ν(C-H)$_{AR}$; 2920, ν(C-H); 1699, 1662 ν(C=O); 1585, 1502 [ν(C=C-C)$_{AR}$]; 1407, 1344 ν(C-N); 1303, 1282, 1172 ν(C-O-C).

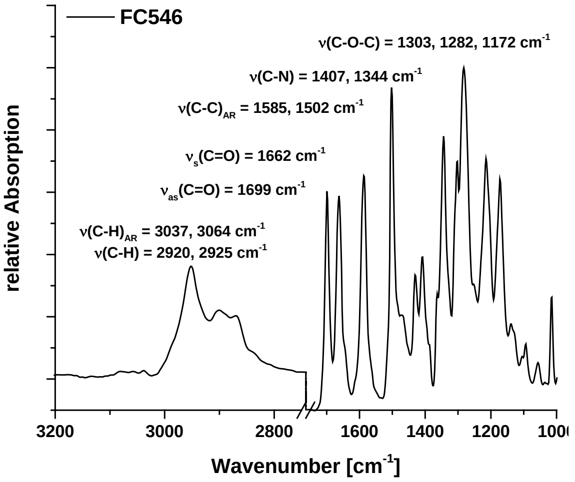

Figure 8. FTIR spectrum of FC546.

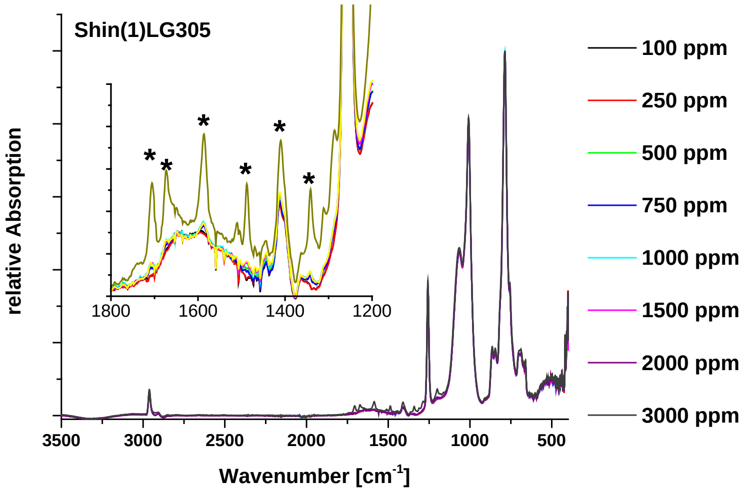

Figure 9. FTIR spectrum of Shin(1)LG305 concentration series.

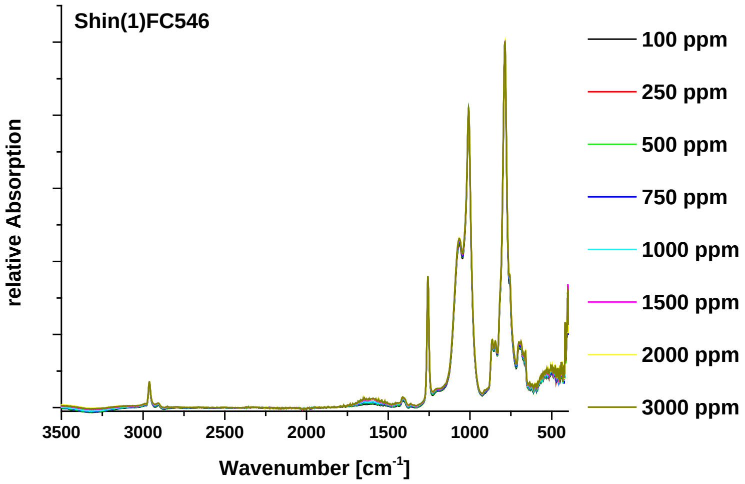

Figure 10. FTIR spectrum of Shin(1)FC546 concentration series.

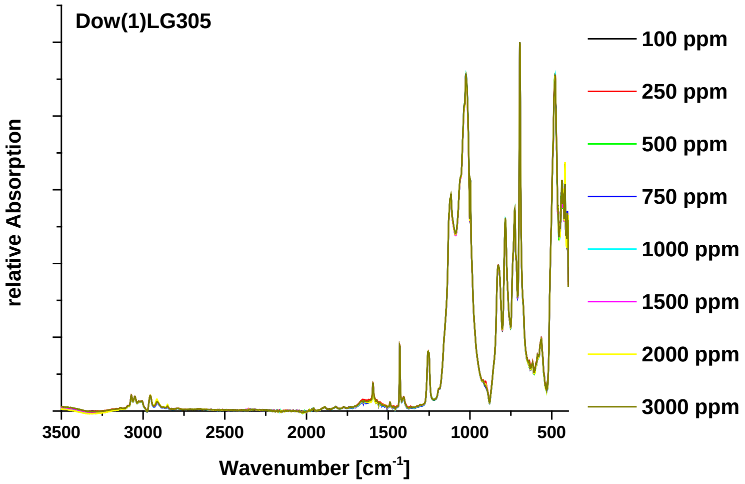

Figure 11. FTIR spectrum of Dow(1)LG305 concentration series.

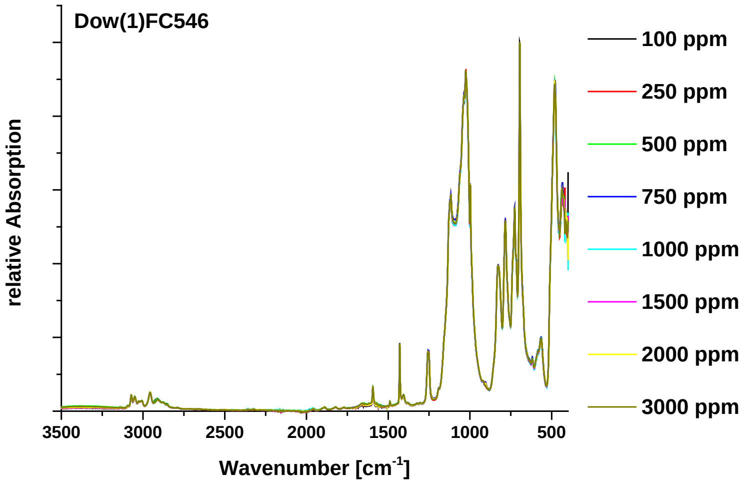

Figure 12. FTIR spectrum of Dow(1)FC546 concentration series.

NMR-Spectroscopy

Schematic structure	**Lumogen®F 305 Rot**
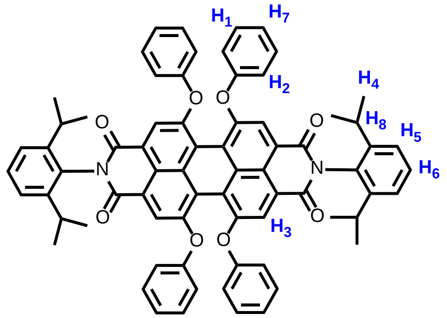	**δ_H (300 MHz, $CDCl_3$):** 8.27 (4 H, s, H_3), 7.47 – 7.39 (2 H, m, H_6), 7.31 – 7.23 (12 H, m, H_2, H_5), 7.14 – 7.07 (4 H, m, H_7), 7.02 – 6.95 (8 H, m, H_1), 2.71 (4 H, sept, J 6.7, H_8), 1.12 (24 H, d, J 6.8, H_4).

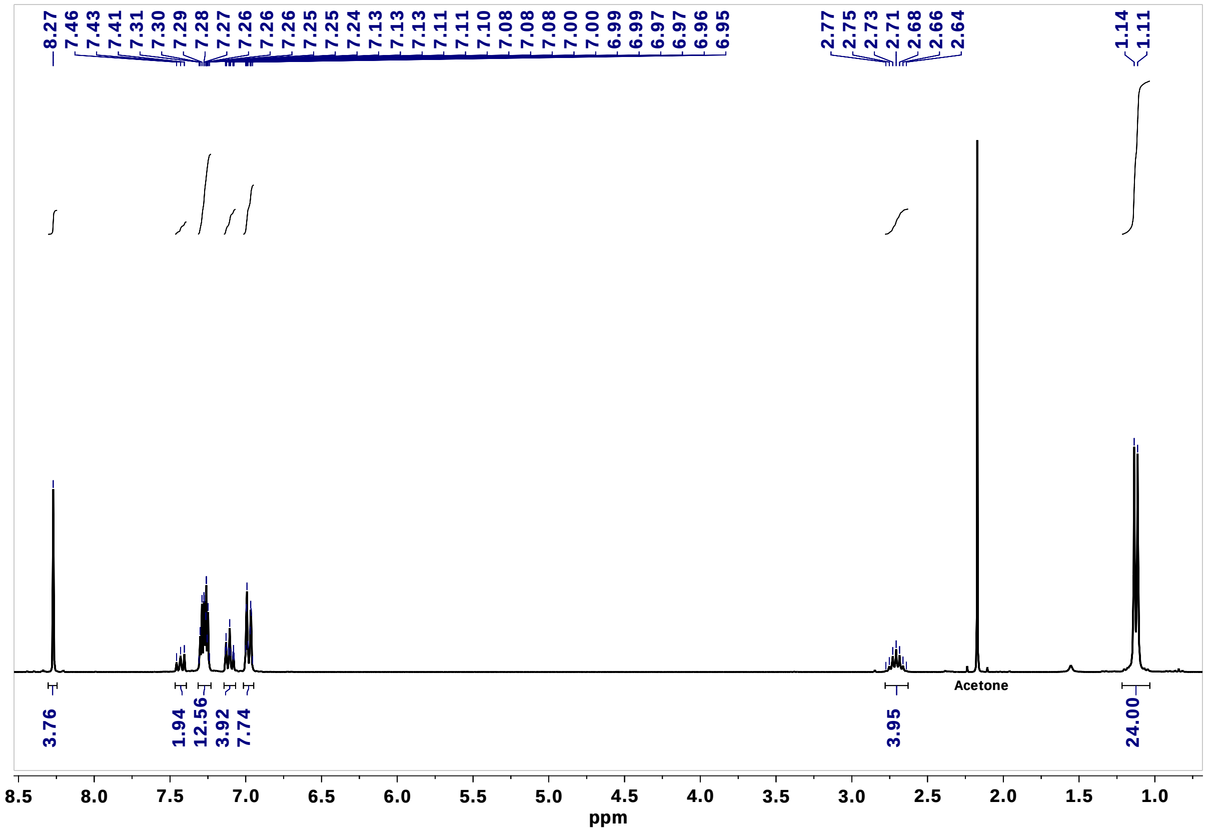

Figure 13. ^{1}H NMR spectrum of Lumogen®F 305 Red.

Schematic structure	FC546
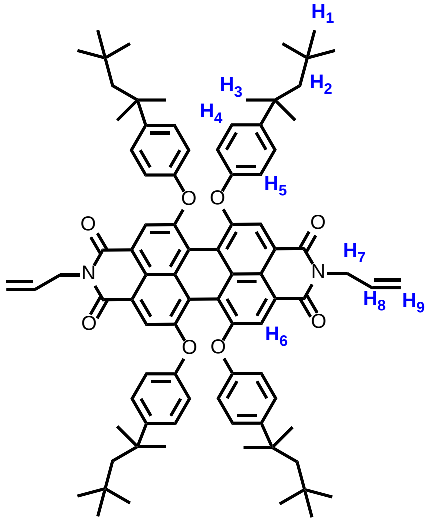	**δ_H (300 MHz, $CDCl_3$):** 8.15 (4 H, s, H_6), 7.27 (8 H, d, J 6.9, H_4), 6.86 (8 H, d, J 8.0, H_5), 6.01 – 5.83 (2 H, m, H_8), 5.33 – 5.10 (4 H, m, H_9), 4.73 (4 H, d, J 5.3, H_7), 1.73 (8 H, s, H_2), 1.54 (s, water), 1.36 (24 H, s, H_3), 0.78 (36 H, s, H_1).

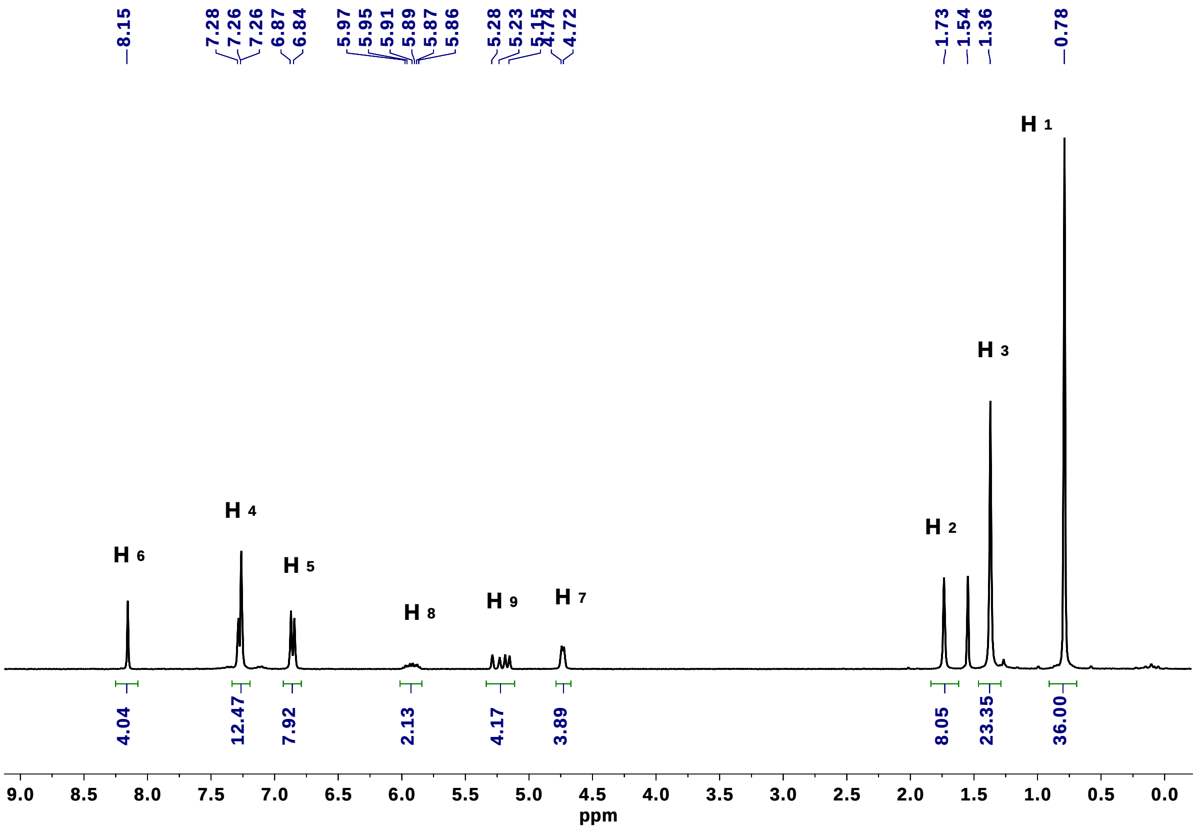

Figure 14. ^1H NMR spectrum of FC546.

Quantum yield and SA-Coefficient

Dow(1)LG305

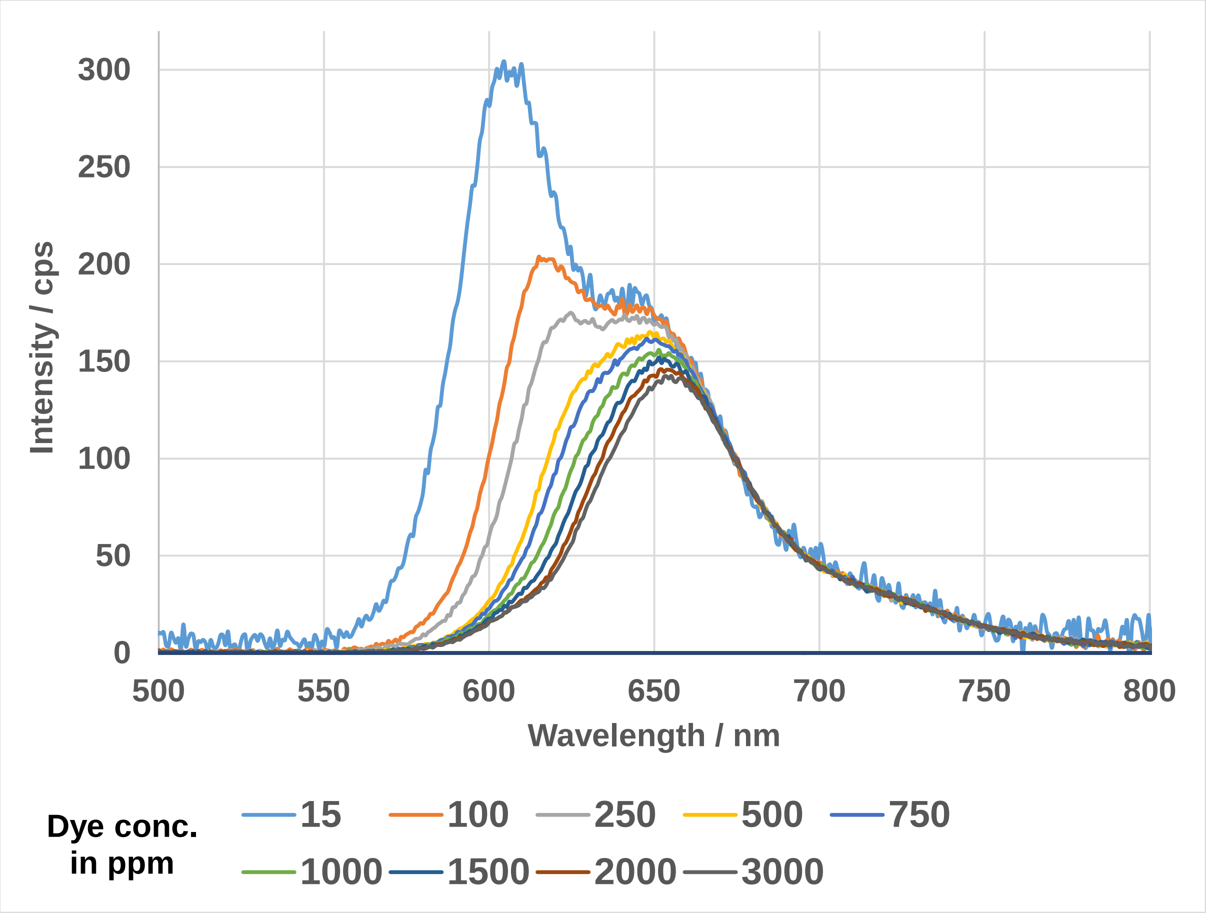

Figure 15. Fitted emission spectra of the Dow(1)LG305 concentration series quantum yield measurement and for the quantum yield correction and self-absorption coefficient calculations.

Table 1. Measured quantum yield values and calculated values of Dow(1)LG305 concentration series corrected quantum yield and the self-absorption coefficient. Goodness of the fit is calculated and given by the pearsons chi-squared test value X^2.

c / ppm	QE	QEcorr	a	$\chi2$
100	1,03	1,02	0,27	49,22
250	1,02	1,02	0,35	49,91
500	1,02	1,01	0,44	50,57
750	1,02	1,01	0,47	49,71
1000	1,00	1,00	0,50	49,91
1500	1,00	1,00	0,52	54,03
2000	1,00	1,00	0,55	53,21
3000	0,98	0,99	0,56	53,23

Dow(1)LG305 48h, 200 °C

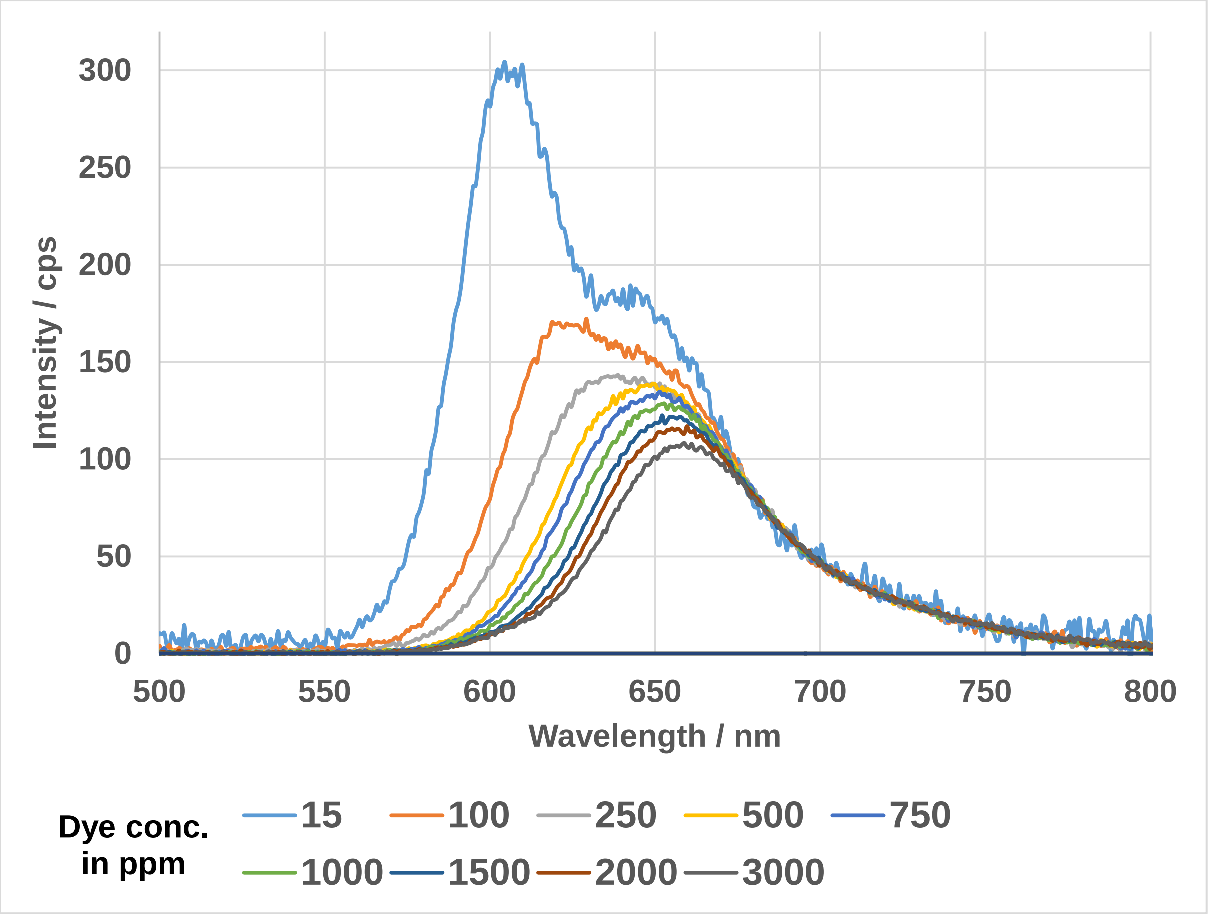

Figure 16. Fitted emission spectra of the Dow(1)LG305 48 h, 200 °C concentration series quantum yield measurement and for the quantum yield correction and self-absorption coefficient calculations.

Table 2. Measured quantum yield values and calculated values of the Dow(1)LG305 48 h, 200 °C concentration series corrected quantum yield and the self-absorption coefficient. Goodness of the fit is calculated and given by the pearsons chi-squared test value X^2.

c / ppm	QE	QEcorr	a	$\chi2$
100	0,91	0,94	0,34	65,46
250	0,93	0,96	0,45	62,54
500	0,92	0,96	0,51	56,28
750	0,91	0,96	0,54	55,58
1000	0,89	0,95	0,57	54,23
1500	0,88	0,95	0,59	54,43
2000	0,87	0,95	0,61	55,07
3000	0,85	0,94	0,64	54,94

Dow(1)LG305 120 h, 200 °C

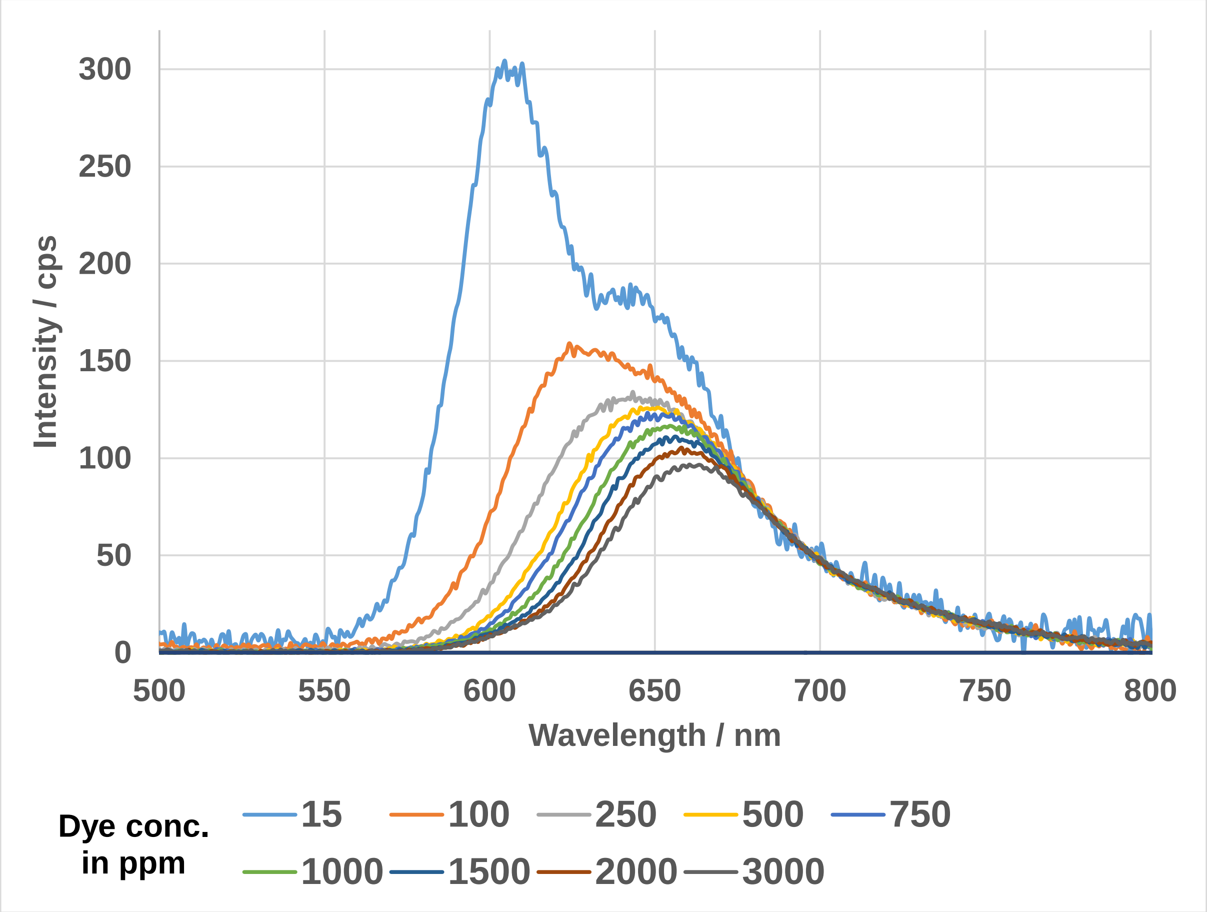

Figure 17. Fitted emission spectra of the Dow(1)LG305 120 h, 200 °C concentration series quantum yield measurement and for the quantum yield correction and self-absorption coefficient calculations.

Table 3. Measured quantum yield values and calculated values of the Dow(1)LG305 120 h, 200 °C concentration series corrected quantum yield and the self-absorption coefficient. Goodness of the fit is calculated and given by the pearsons chi-squared test value X^2.

c / ppm	QE	QEcorr	a	$\chi 2$
100	0,86	0,91	0,38	58,36
250	0,87	0,93	0,49	63,29
500	0,87	0,93	0,54	58,14
750	0,87	0,94	0,56	57,49
1000	0,84	0,93	0,59	50,45
1500	0,83	0,93	0,62	50,90
2000	0,80	0,92	0,64	49,15
3000	0,78	0,91	0,66	57,38

Dow(1)FC546

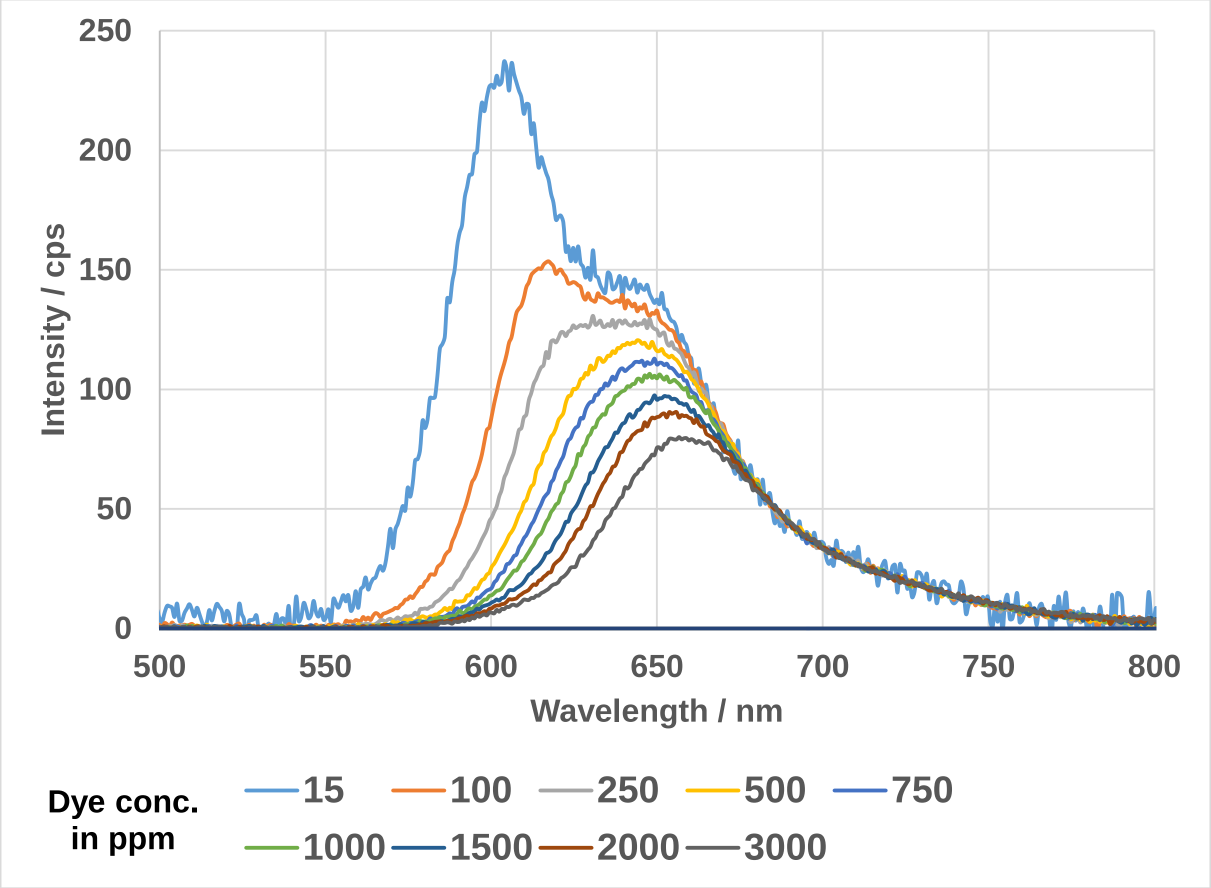

Figure 18. Fitted emission spectra of the Dow(1)FC546 concentration series quantum yield measurement and for the quantum yield correction and self-absorption coefficient calculations.

Table 4. Measured quantum yield values and calculated values of the Dow(1)FC546 concentration series quantum yield and the self-absorption coefficient. Goodness of the fit is calculated and given by the pearsons chi-squared test value X^2.

c / ppm	QE	QEcorr	a	χ2
100	0,93	0,95	0,28	47,73
250	0,97	0,98	0,38	52,63
500	0,94	0,97	0,46	48,65
750	0,93	0,96	0,51	49,80
1000	0,91	0,96	0,54	51,59
1500	0,85	0,93	0,59	52,41
2000	0,82	0,92	0,62	50,74
3000	0,77	0,91	0,66	50,89

Dow(1)FC546 48 h, 200 °C

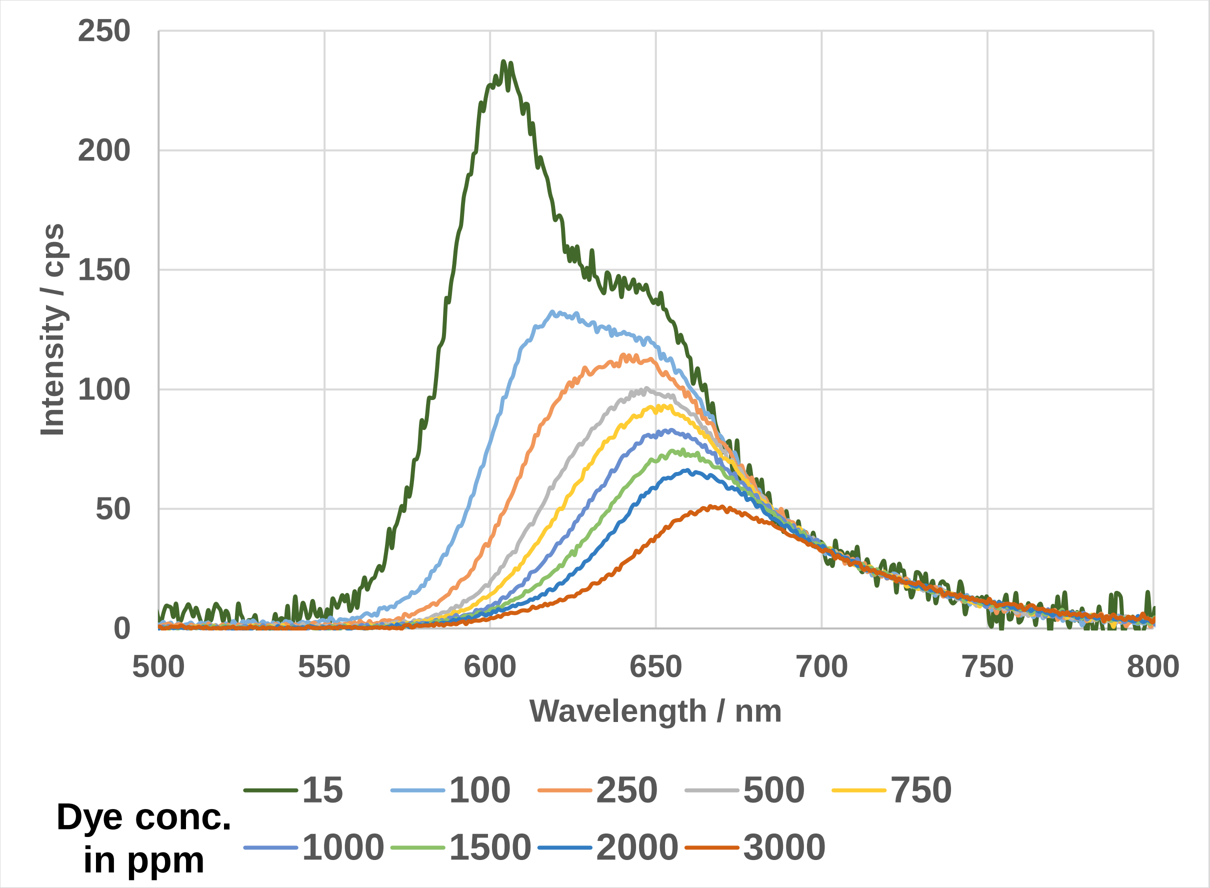

Figure 19. Fitted emission spectra of Dow(1)FC546 48 h, 200 °C concentration series quantum yield measurement and for the quantum yield correction and self-absorption coefficient calculations.

Table 5. Measured quantum yield values and calculated values of Dow(1)FC546 48 h, 200 °C concentration series corrected quantum yield and the self-absorption coefficient. Goodness of the fit is calculated and given by the pearsons chi-squared test value X^2.

c / ppm	QE	QEcorr	a	c2
100	0,87	0,91	0,33	51,79
250	0,88	0,93	0,45	54,55
500	0,84	0,92	0,54	48,00
750	0,81	0,91	0,58	51,40
1000	0,77	0,90	0,62	51,82
1500	0,72	0,88	0,66	51,56
2000	0,68	0,87	0,70	51,04
3000	0,58	0,84	0,75	49,79

Dow(1)FC546 120 h, 200 °C

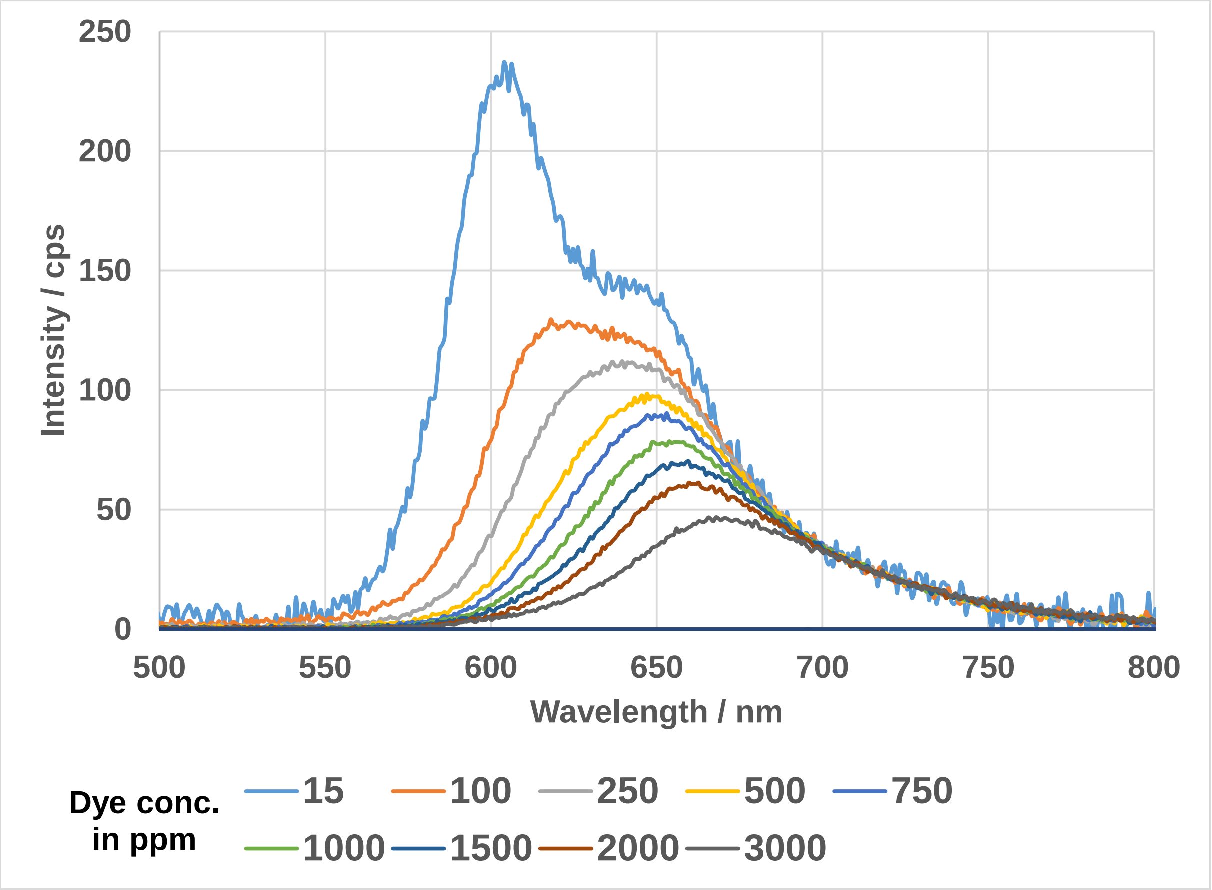

Figure 20. Fitted emission spectra of the Dow(1)FC546 120 h, 200 °C concentration series quantum yield measurement and for the quantum yield correction and self-absorption coefficient calculations.

Table 6. Measured quantum yield values and calculated values of the Dow(1)FC546 120 h, 200 °C concentration series corrected quantum yield and the self-absorption coefficient. Goodness of the fit is calculated and given by the pearsons chi-squared test value X^2.

c / ppm	QE	QEcorr	a	χ2
100	0,86	0,90	0,33	52,17
250	0,82	0,89	0,45	50,89
500	0,78	0,89	0,54	52,31
750	0,79	0,90	0,59	51,58
1000	0,73	0,88	0,63	49,74
1500	0,69	0,87	0,67	51,69
2000	0,63	0,85	0,71	55,59
3000	0,53	0,83	0,76	52,50

Shin(1)FC546

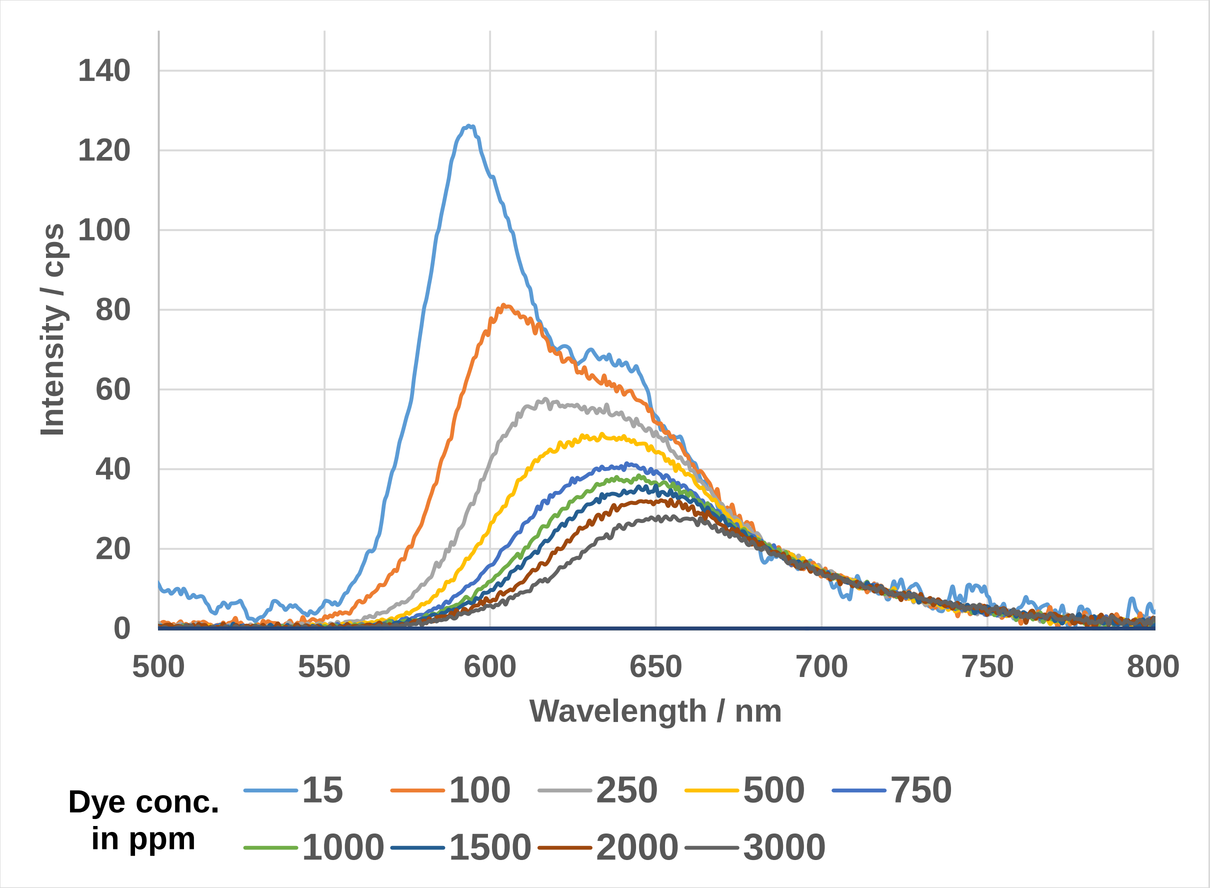

Figure 21. Fitted emission spectra of the Shin(1)FC546 concentration series quantum yield measurement and for the quantum yield correction and self-absorption coefficient calculations.

Table 7. Measured quantum yield values and calculated values of the Shin(1)FC546 concentration series corrected quantum yield and the self-absorption coefficient. Goodness of the fit is calculated and given by the pearsons chi-squared test value X^2.

c / ppm	QE	QEcorr	a	$\chi2$
100	0,93	0,95	0,24	62,22
250	0,73	0,83	0,42	64,12
500	0,65	0,79	0,51	62,39
750	0,56	0,75	0,59	59,64
1000	0,51	0,74	0,62	55,43
1500	0,48	0,72	0,64	53,50
2000	0,42	0,69	0,67	55,03
3000	0,37	0,67	0,71	50,58

Shin(1)FC546 48 h, 200 °C

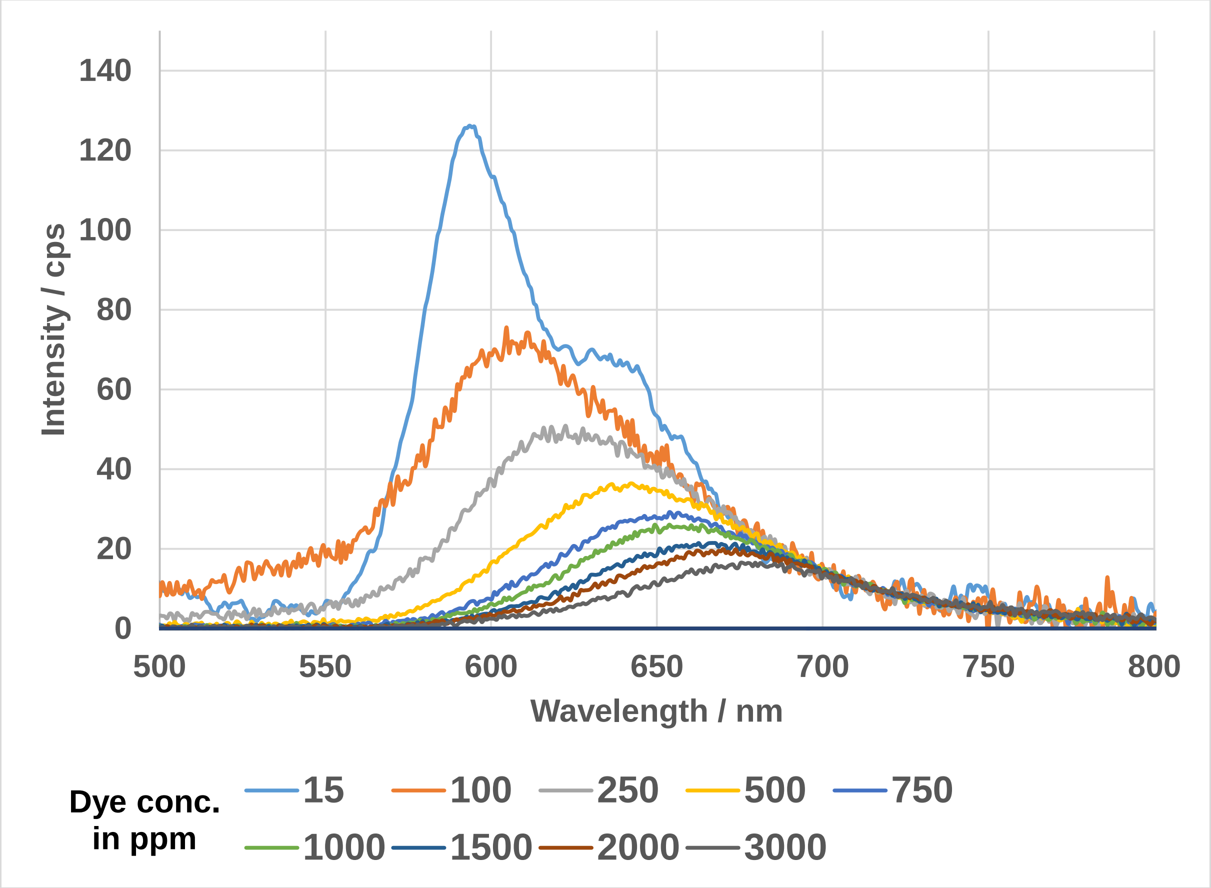

Figure 22. Fitted emission spectra of the Shin(1)FC546 48 h, 200 °C concentration series quantum yield measurement and for the quantum yield correction and self-absorption coefficient calculations.

Table 8. Measured quantum yield values and calculated values of the Shin(1)FC546 48 h, 200 °C concentration series corrected quantum yield and the self-absorption coefficient. Goodness of the fit is calculated and given by the pearsons chi-squared test value X^2.

c / ppm	QE	QEcorr	a	$\chi 2$
100	0,37	0,43	0,20	73,64
250	0,40	0,55	0,44	78,24
500	0,43	0,66	0,60	56,22
750	0,40	0,68	0,69	57,11
1000	0,37	0,68	0,72	54,02
1500	0,34	0,68	0,76	54,39
2000	0,31	0,67	0,78	52,17
3000	0,25	0,64	0,81	50,40

Shin(1)FC564 120 h, 200 °C

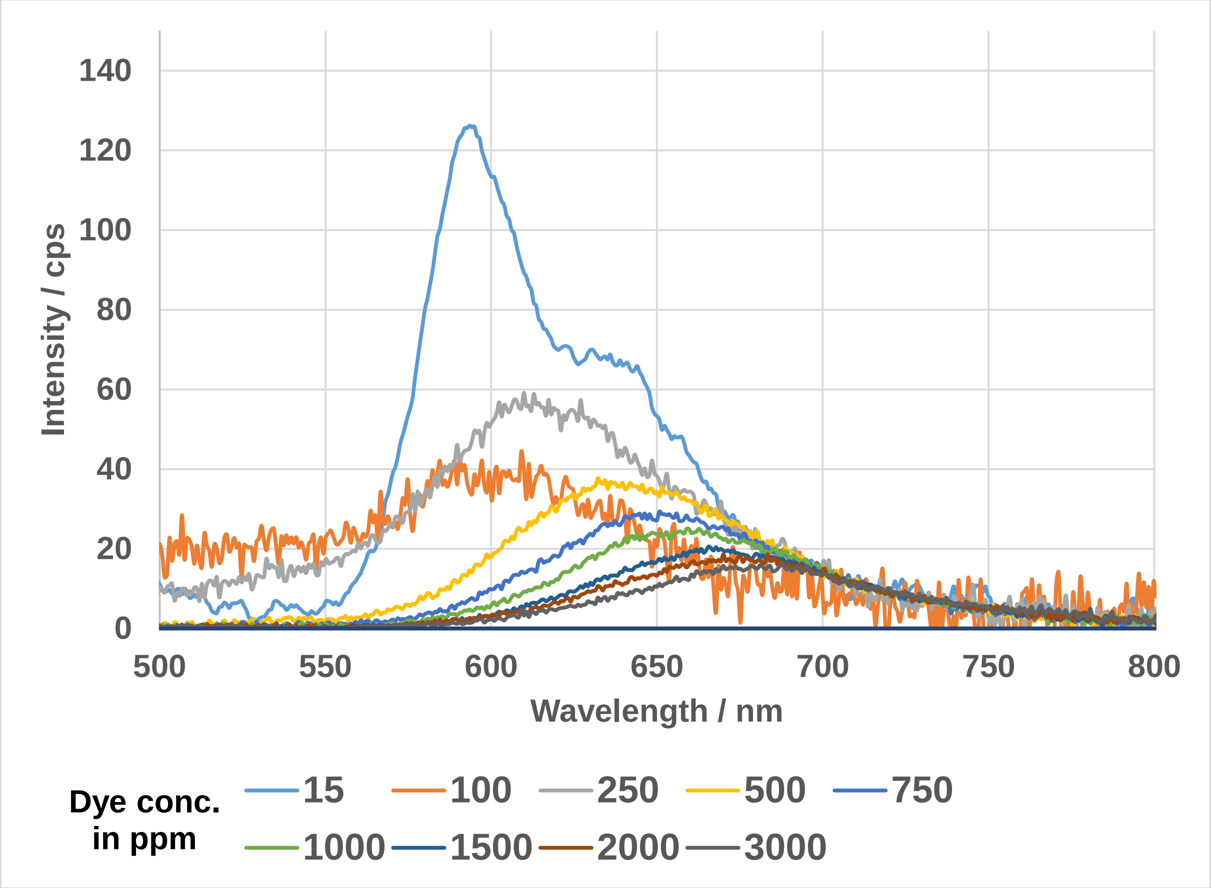

Figure 23. Fitted emission spectra of the Shin(1)FC546 120h, 200 °C concentration series quantum yield measurement and for the quantum yield correction and self-absorption coefficient calculations.

Table 9. Measured quantum yield values and calculated values of the Shin(1)FC546 120h, 200 °C concentration series corrected quantum yield and the self-absorption coefficient. Goodness of the fit is calculated and given by the pearsons chi-squared test value X^2.

c / ppm	QE	QEcorr	a	$\chi2$
100	0,00	0,00	0,49	257,62
250	0,28	0,36	0,32	74,97
500	0,38	0,59	0,58	58,84
750	0,35	0,62	0,68	63,63
1000	0,33	0,64	0,72	52,56
1500	0,30	0,65	0,78	48,48
2000	0,28	0,65	0,79	54,62
3000	0,23	0,62	0,82	45,29

Shin(1)LG305

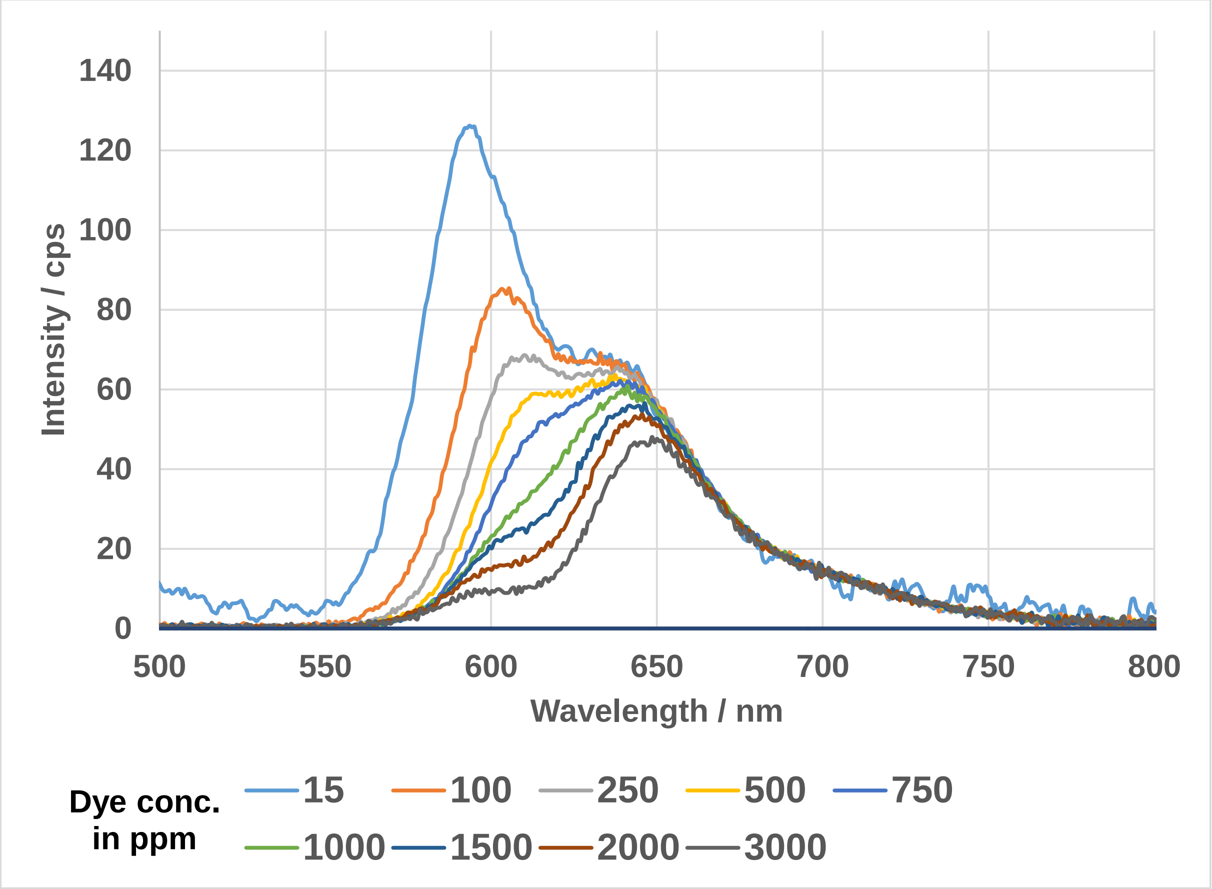

Figure 24. Fitted emission spectra of the Shin(1)LG305 concentration series quantum yield measurement and for the quantum yield correction and self-absorption coefficient calculations.

Table 10. Measured quantum yield values and calculated values of the Shin(1)LG305 concentration series corrected quantum yield and the self-absorption coefficient. Goodness of the fit is calculated and given by the pearsons chi-squared test value X^2.

c / ppm	QE	QEcorr	a	$\chi 2$
100	0,90	0,92	0,24	71,81
250	0,92	0,94	0,34	81,92
500	0,91	0,94	0,40	68,63
750	0,85	0,91	0,44	71,71
1000	0,63	0,77	0,49	69,53
1500	0,56	0,73	0,53	73,28
2000	0,38	0,59	0,57	70,53
3000	0,26	0,49	0,63	75,94

Shin(1)LG305 48 h, 200 °C

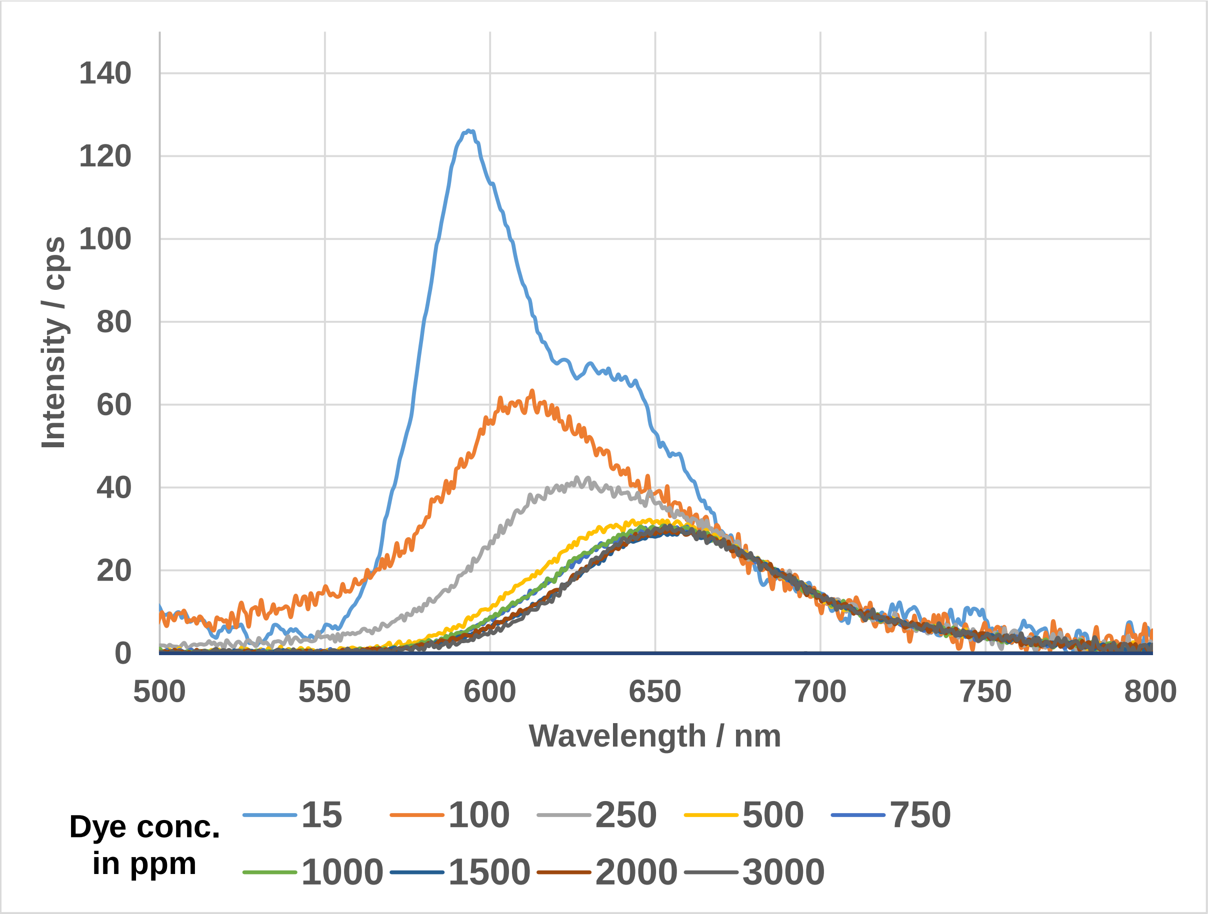

Figure 25. Fitted emission spectra of the Shin(1)LG305 48 h, 200 °C concentration series quantum yield measurement and for the quantum yield correction and self-absorption coefficient calculations.

Table 11. Measured quantum yield values and calculated values of the Shin(1)LG305 48 h, 200 °C concentration series corrected quantum yield and the self-absorption coefficient. Goodness of the fit is calculated and given by the pearsons chi-squared test value X^2.

c / ppm	QE	QEcorr	a	$\chi2$
100	0,36	0,45	0,32	105,20
250	0,41	0,60	0,53	74,73
500	0,49	0,73	0,65	67,99
750	0,50	0,76	0,68	75,67
1000	0,47	0,74	0,68	72,94
1500	0,44	0,73	0,70	70,49
2000	0,35	0,65	0,70	70,07
3000	0,28	0,57	0,70	74,68

Shin(1)LG305 120 h, 200 °C

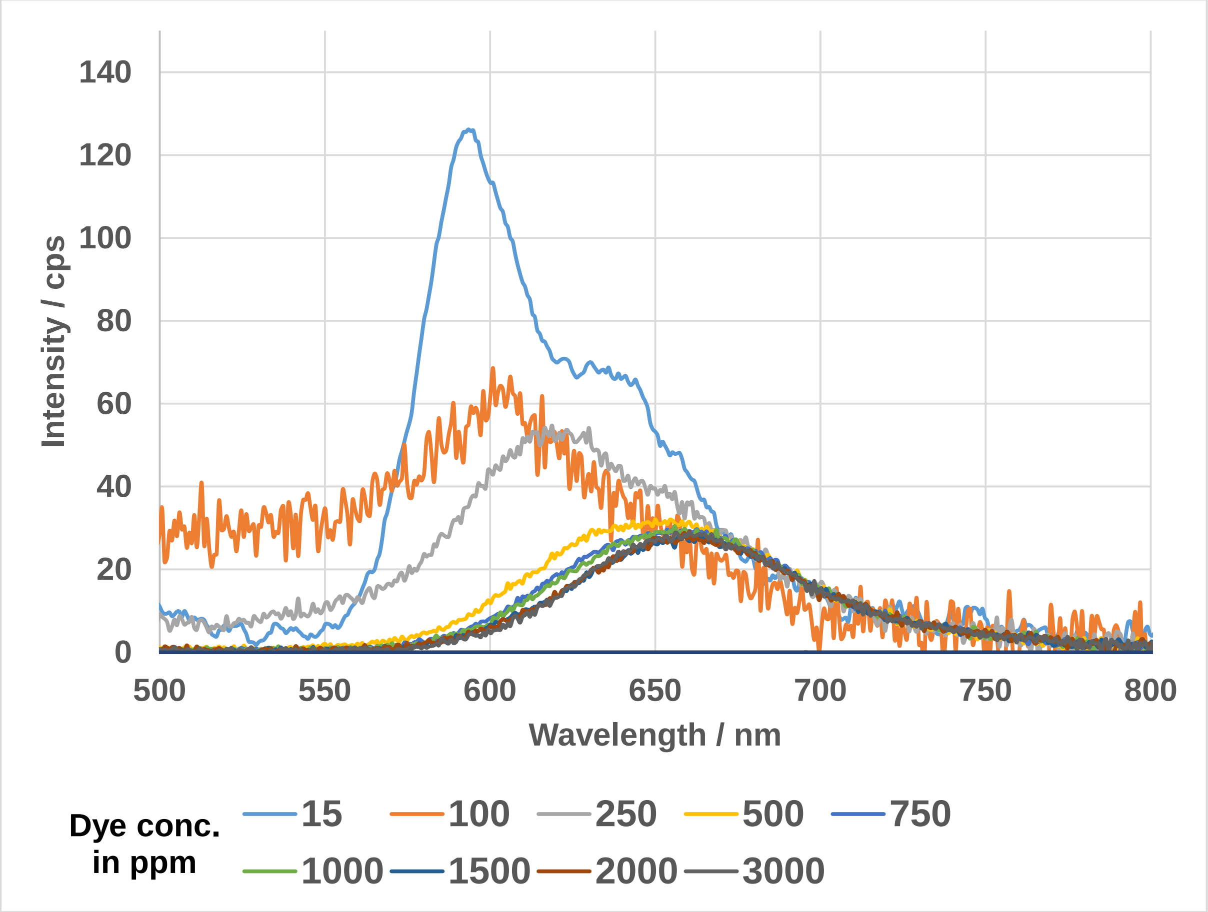

Figure 26. Fitted emission spectra of the Shin(1)LG305 120 h, 200 °C concentration series quantum yield measurement and for the quantum yield correction and self-absorption coefficient calculations.

Table 12. Measured quantum yield values and calculated values of the Shin(1)LG305 120 h, 200 °C concentration series corrected quantum yield and the self-absorption coefficient. Goodness of the fit is calculated and given by the pearsons chi-squared test value X^2.

c / ppm	QE	QEcorr	a	$\chi 2$
100	0,21	0,27	0,29	200,40
250	0,28	0,40	0,39	74,72
500	0,39	0,64	0,64	65,11
750	0,40	0,67	0,68	62,49
1000	0,39	0,66	0,68	62,44
1500	0,36	0,66	0,71	63,61
2000	0,28	0,57	0,71	64,90
3000	0,27	0,56	0,71	66,57

Bleaching UV-VIS (Air)

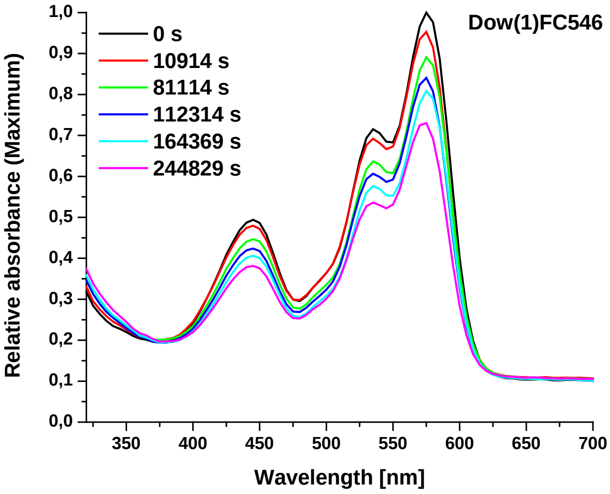

Figure 27. Relative absorbance relevant to the absorbance maximum at 0 s of light exposure and after given time of exposure to 850 mW/cm^{-1} at 450 nm wavelength under Air of the Dow(1)FC546 – 100 ppm sample.

Table 13. Absorbance and relative absorbance relevant to the absorbance at 450 nm at 0 s of light exposure and after given time of exposure to 850 mW/cm^{-1} at 450 nm wavelength under Air of the Dow(1)FC546 – 100 ppm sample.

t / sec	t/ min	Absorbance (450 nm)	Relative absorbance (450 nm)
0	0	0.22951	1
10914	181.9	0.22272	0.97044
81114	1351.9	0.20808	0.90665
112314	1871.9	0.19708	0.85871
164369	2,739	0.18886	0.82291
244829	4,080	0.17731	0.77257

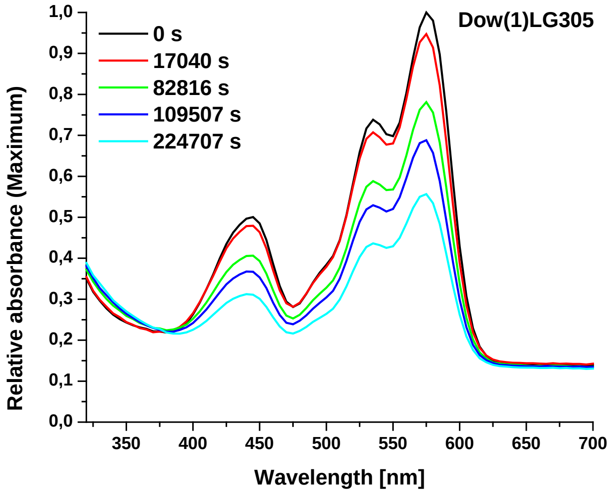

Figure 28. Relative absorbance relevant to the absorbance maximum at 0 s of light exposure and after given time of exposure to 850 mW/cm^{-1} at 450 nm wavelength under Air of the Dow(1)LG305 – 100 ppm sample.

Table 14. Absorbance and relative absorbance relevant to the absorbance at 450 nm at 0 s of light exposure and after given time of exposure to 850 mW/cm^{-1} at 450 nm wavelength under Air of the Dow(1)LG305 – 100 ppm sample.

t / sec	t/ min	Absorbance (450 nm)	Relative absorbance (450 nm)
0	0	0.26795	1
17040	284	0.25597	0.9553
82816	1380.26667	0.21707	0.81012
109507	1825.11667	0.19511	0.72815
224707	3,745	0.16628	0.62055

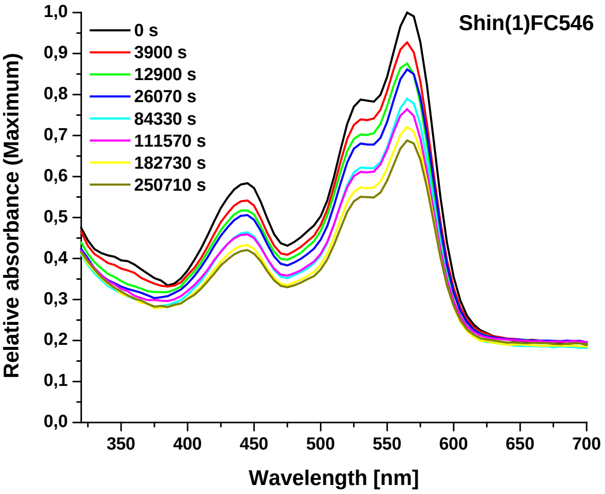

Figure 29. Relative absorbance relevant to the absorbance maximum at 0 s of light exposure and after given time of exposure to 850 mW/cm^{-1} at 450 nm wavelength under Air of the Shin(1)FC546 – 100 ppm sample.

Table 15. Absorbance and relative absorbance relevant to the absorbance at 450 nm at 0 s of light exposure and after given time of exposure to 850 mW/cm^{-1} at 450 nm wavelength under Air of the Shin(1)FC546 – 100 ppm sample.

t / sec	t/ min	Absorbance (450 nm)	Relative absorbance (450 nm)
0	0	0.1732	1
3900	65	0.16022	0.92503
12900	215	0.15374	0.88761
26070	434.5	0.14972	0.86439
84330	1,406	0.13743	0.79345
111570	1,860	0.13632	0.78703
182730	3045.5	0.12833	0.74093
250710	4178.5	0.1247	0.71997

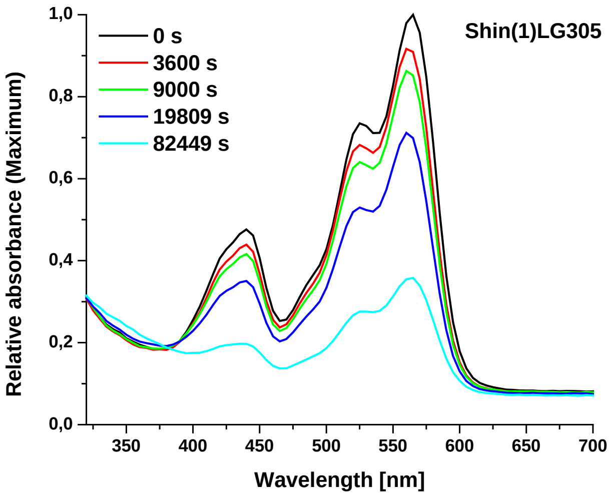

Figure 30. Relative absorbance relevant to the absorbance maximum at 0 s of light exposure and after given time of exposure to 850 mW/cm^{-1} at 450 nm wavelength under Air of the Shin(1)LG305 – 100 ppm sample.

Table 16. Absorbance and relative absorbance relevant to the absorbance at 450 nm at 0 s of light exposure and after given time of exposure to 850 mW/cm^{-1} at 450 nm wavelength under Air of the Shin(1)LG305 – 100 ppm sample.

t / sec	t/ min	Absorbance (450 nm)	Relative absorbance (450 nm)
0	0	0.19157	1
3600	60	0.17353	0.9058
9000	150	0.16436	0.85793
19809	330.15	0.13931	0.72722
82449	1,374	0.08297	0.43312

Bleaching UV-VIS (Nitrogen/Air)

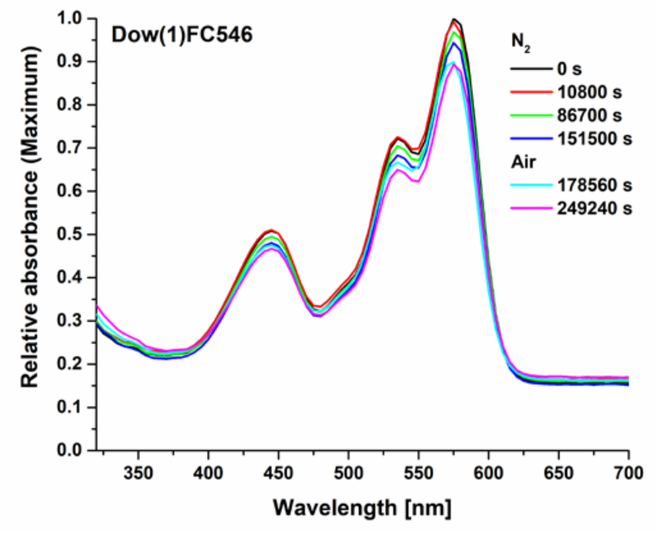

Figure 31. Relative absorbance relevant to the absorbance maximum at 0 s of light exposure and after given time of exposure to 850 mW/cm^{-1} at 450 nm wavelength under Nitrogen/Air of the Dow(1)FC546 – 100 ppm sample.

Table 17. Absorbance and relative absorbance relevant to the absorbance at 450 nm at 0 s of light exposure and after given time of exposure to 850 mW/cm^{-1} at 450 nm wavelength under Nitrogen/Air of the Dow(1)FC546 – 100 ppm sample.

t / sec	t/ min	Absorbance (450 nm)	Relative absorbance (450 nm)
0	0	0.2317	1
10800	180	0.23156	0.9994
86700	1445	0.2253	0.97235
151500	2525	0.21819	0.94167
178560	2976	0.21584	0.93155
249240	4154	0.2127	0.91796

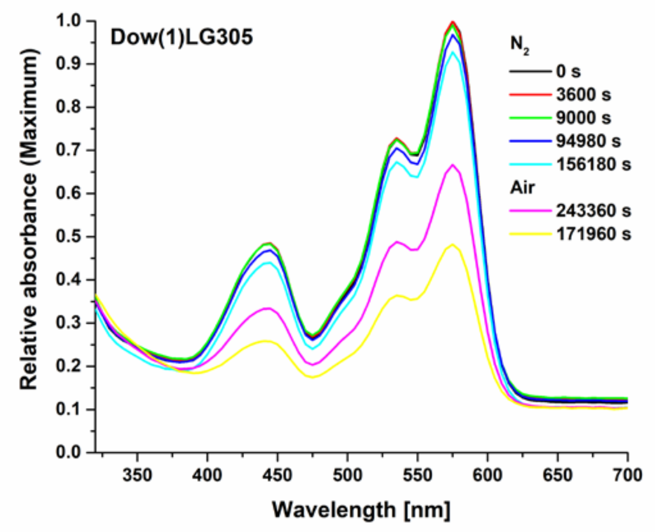

Figure 32. Relative absorbance relevant to the absorbance maximum at 0 s of light exposure and after given time of exposure to 850 mW/cm^{-1} at 450 nm wavelength under Nitrogen/Air of the Dow(1)LG305 – 100 ppm sample.

Table 18. Absorbance and relative absorbance relevant to the absorbance at 450 nm at 0 s of light exposure and after given time of exposure to 850 mW/cm^{-1} at 450 nm wavelength under Nitrogen/Air of the Dow(1)LG305 – 100 ppm sample.

t / sec	t/ min	Absorbance (450 nm)	Relative absorbance (450 nm)
0	0	0.23854	1
3600	60	0.23697	0.99344
9600	160	0.23837	0.99928
94980	1583	0.23092	0.96805
156180	2603	0.21563	0.90396
243360	4056	0.16375	0.68648

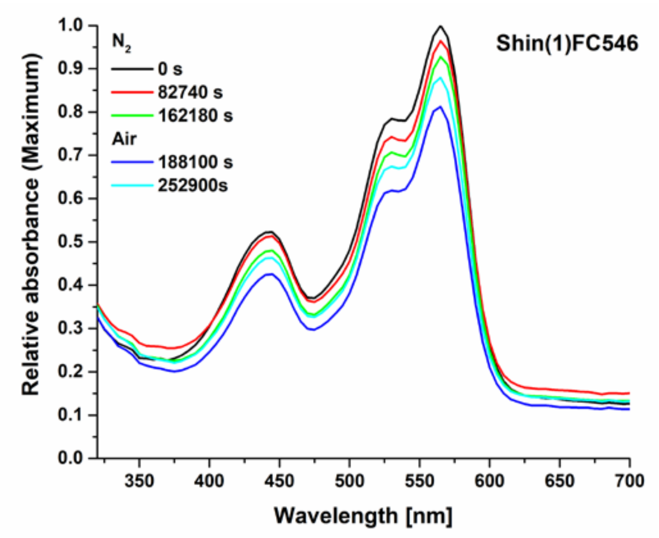

Figure 33. Relative absorbance relevant to the absorbance maximum at 0 s of light exposure and after given time of exposure to 850 mW/cm^{-1} at 450 nm wavelength under Nitrogen/Air of the Shin(1)FC546 – 100 ppm sample.

Table 19. Absorbance and relative absorbance relevant to the absorbance at 450 nm at 0 s of light exposure and after given time of exposure to 850 mW/cm^{-1} at 450 nm wavelength under Nitrogen/Air of the Shin(1)FC546 – 100 ppm sample.

t / sec	t/ min	Absorbance (450 nm)	Relative absorbance (450 nm)
0	0	0.15765	1
6900	115	0.14075	0.89279
68100	1135	0.12719	0.80678
153060	2551	0.12749	0.80868
214560	3576	0.11406	0.72348

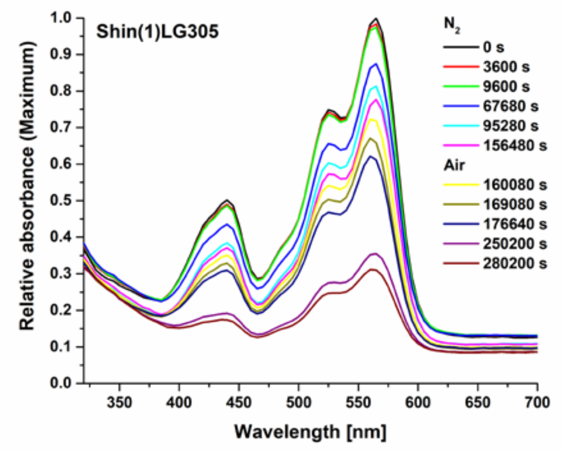

Figure 34. Relative absorbance relevant to the absorbance maximum at 0 s of light exposure and after given time of exposure to 850 mW/cm^{-1} at 450 nm wavelength under Nitrogen/Air of the Shin(1)LG305 – 100 ppm sample.

Table 20. Absorbance and relative absorbance relevant to the absorbance at 450 nm at 0 s of light exposure and after given time of exposure to 850 mW/cm^{-1} at 450 nm wavelength under Nitrogen/Air of the Shin(1)LG305 – 100 ppm sample.

t / sec	t/ min	Absorbance (450 nm)	Relative absorbance (450 nm)
0	0	0.21178	1
3600	60	0.20601	0.97279
9600	160	0.20439	0.96511
67680	1128	0.18503	0.87372
95280	1588	0.17142	0.80944
156480	2608	0.16881	0.79712
160080	2668	0.14681	0.69322
169080	2818	0.13679	0.64592
176640	2944	0.12968	0.61235
250200	4170	0.08419	0.39752

Verification of covalent bond formation between a Si-H containing polymer and FC546

In presence of a platinum based hydrosilylation catalyst a reaction between the allyl functionalyzed FC546 dye and the hydrid groups of Shin Etsu KJR9022E component B under curing conditions should lead to a cured polymer. This polymer should not show any precipitation or any Si-H vibrational Bands in the FTIR spectrum. If there is no bond-formation the dye should precipitate and Si-H vibrations should be present.

Shin Etsu KJR9022E component B (0.1 g) was mixed with a stock solution of FC546 (5.0 g [0.1 wt% in Toluol]; 5 mg FC546) and Platin- Carbonylcyclovinylmethylsiloxan (Ossko-Catalyst; 0.25 µl [2.0% Pt(0) in Xylene]; 255 µg Pt(0); 50 ppm). The solvent was removed under reduced pressure. The polymer dye mixture and the pure component B, as a reference, were transferred into a compartment drier (150 °C, 4 h). The observed solid red but transparent material and the liquid transparent component B were characterized by FTIR spectroscopy.

After the solvent was removed from the polymer dye mixture FC546 precipitated. The heat treatment leads to a cured transparent red Material. FC546 was solved completely in the matrix structure and reacted with the Si-H groups of the polymer covalent bond formation. This was verified by FTIR spectroscopy. The B component of Shin(1) shows vibration bands due to the silicon hydride bond respectively at 2159 cm^{-1} [ν(Si-H)] and 906 cm^{-1} [ρ(Si-H)]. By heating the pure B component at curing conditions this vibrational bands are still present. By adding the FC546 dye and a small amount of hydrosilylation catalyst the vibrational bands disappear. The allyl groups of the dye reacted with the Si-H groups of the polymer.

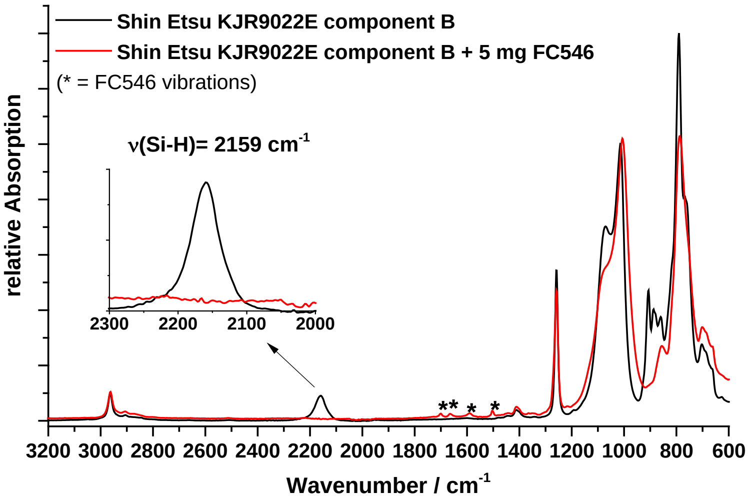

Figure 35. FTIR spectra of pure Shin component B and the dye incorporated component B after heat treatment. The Si-H vibration band disapears completely due to the formation of covalent bonds between the dye and the polymer.

7.2. Perylene Polyphenylmethylsiloxanes for Optoelectronic Applications

Supplementary Information

Perylene Polysiloxanes for Optoelectronic Applications

Supplementary Information

Nils Steinbrück, Guido Kickelbick*

Saarland University, Inorganic Solid State Chemistry, Campus, Building C4 $_1$, 66123
Saarbrücken, Germany

Correspondence to: Guido Kickelbick (E-mail: guido.kickelbick@uni-saarland.de)

Content

Fluorescence Spectrum of FC546

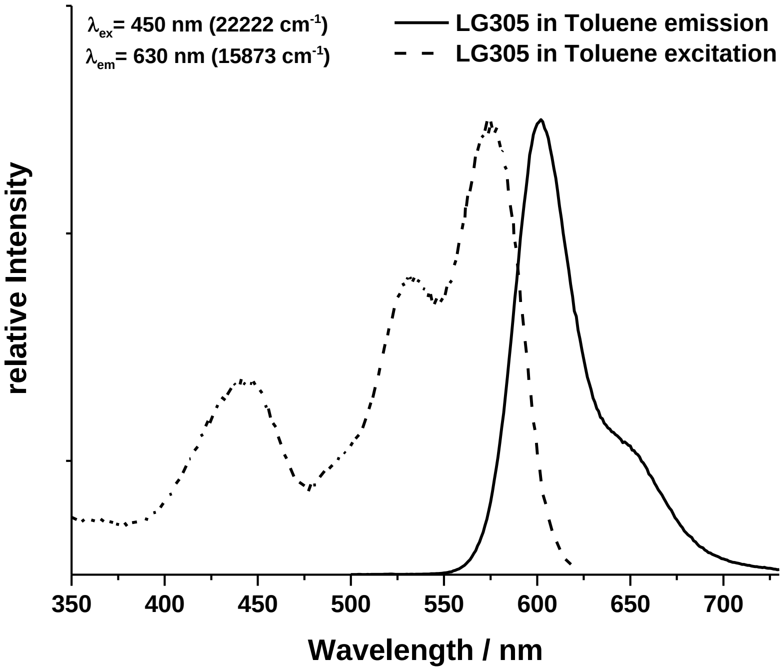

Figure S1. Emission and excitation spectra of diluted solutions (5 µmol L^{-1}) of Lumogen®F Red 305 (LG305) in toluene with an emission wavelength of 630 nm (15873 cm^{-1}) and with an excitation wavelength of 450 nm (22222 cm^{-1}).

NMR / FTIR spectra

PMS-03: Polyphenylmethylsiloxane, hydrid terminated

δ_H (300 MHz, $CDCl_3$): 7.59 – 7.40 (4 H, m, Phenyl-H), 7.33 – 7.14 (6 H, m, Phenyl-H), 4.68 (2 H, sept, *J* 2.8, *Si-H*), 1.33 (s, Impurity ~ [-OH]), 0.36 – 0.17 (7 H, m, Si-CH_3 chain), 0.14 – -0.09 (15 H, m, Si-$(CH_3)_2$, end group).

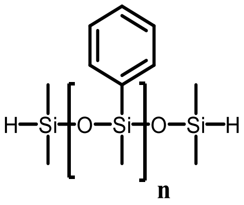

PMS-03
Polyphenylmethylsiloxane
hydride terminated
2-5 cSt.
300-500 g/Mol

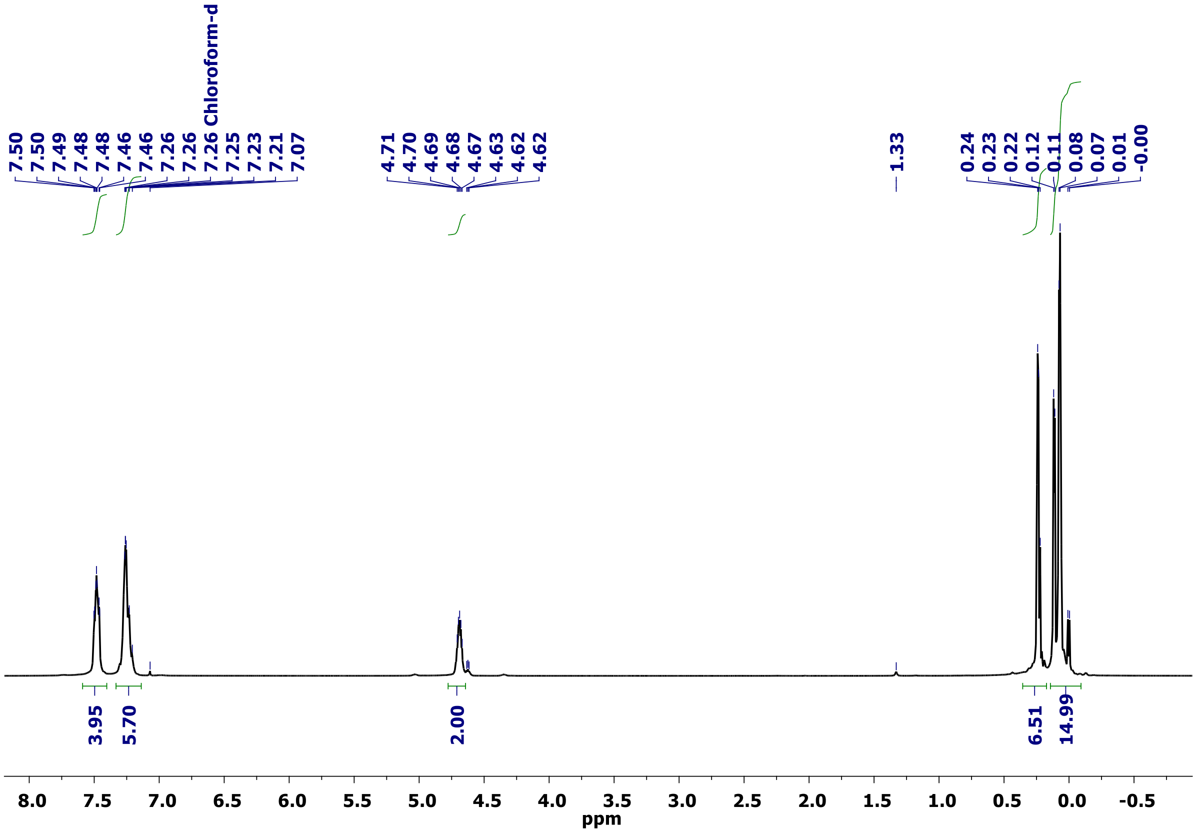

Figure S2. ^{1}H-NMR spectrum of PMS-03 in chloroform-D.

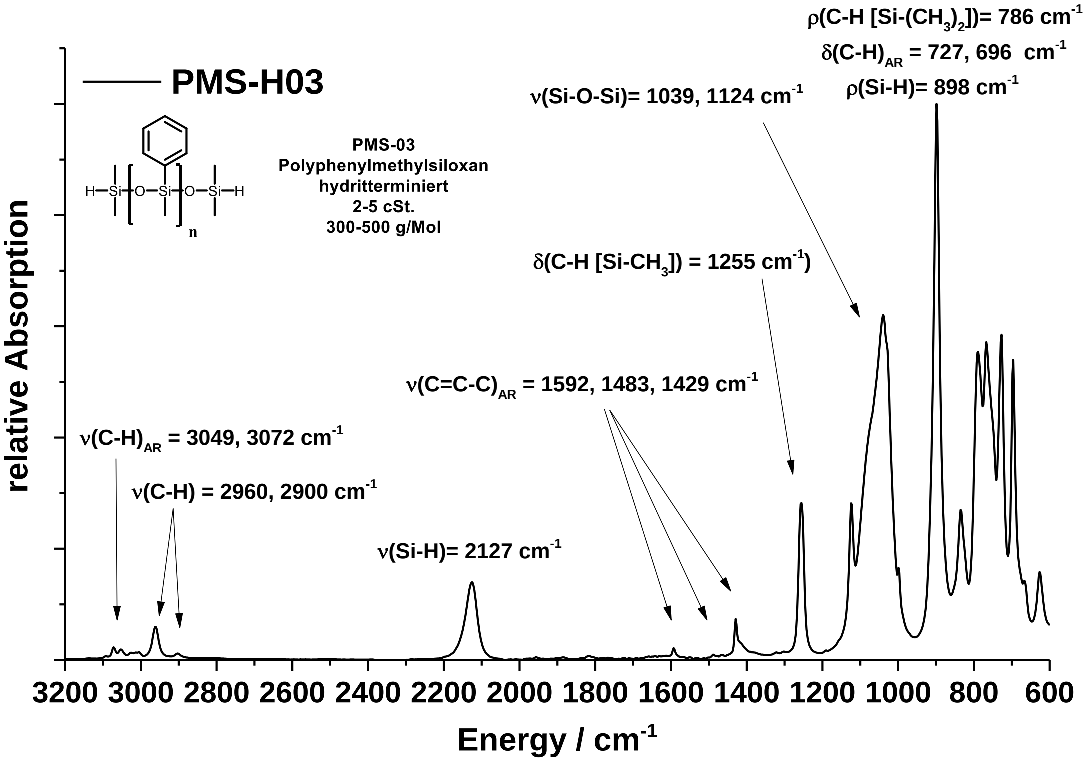

Figure S3. FTIR- spectrum of PMS-03.

PMV-9925: Polyphenylmethylsiloxane, vinyl terminated

δ_H (300 MHz, $CDCl_3$): 7.75 – 6.94 (118 H, m, Phenyl-H), 6.23 – 5.46 (6 H, m, Vinyl-H), 3.38 (s, impurity ~ [-CH_2]), 1.33 (s, impurity ~ [-OH]), 0.55 – -0.28 (89 H, m, Si-CH_3).

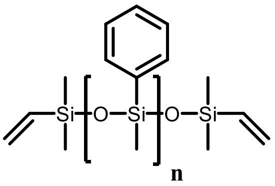

PMV-9925
Polyphenylmethylsiloxane
vinyl terminated
300-600 cSt.
2000-3000 g/Mol

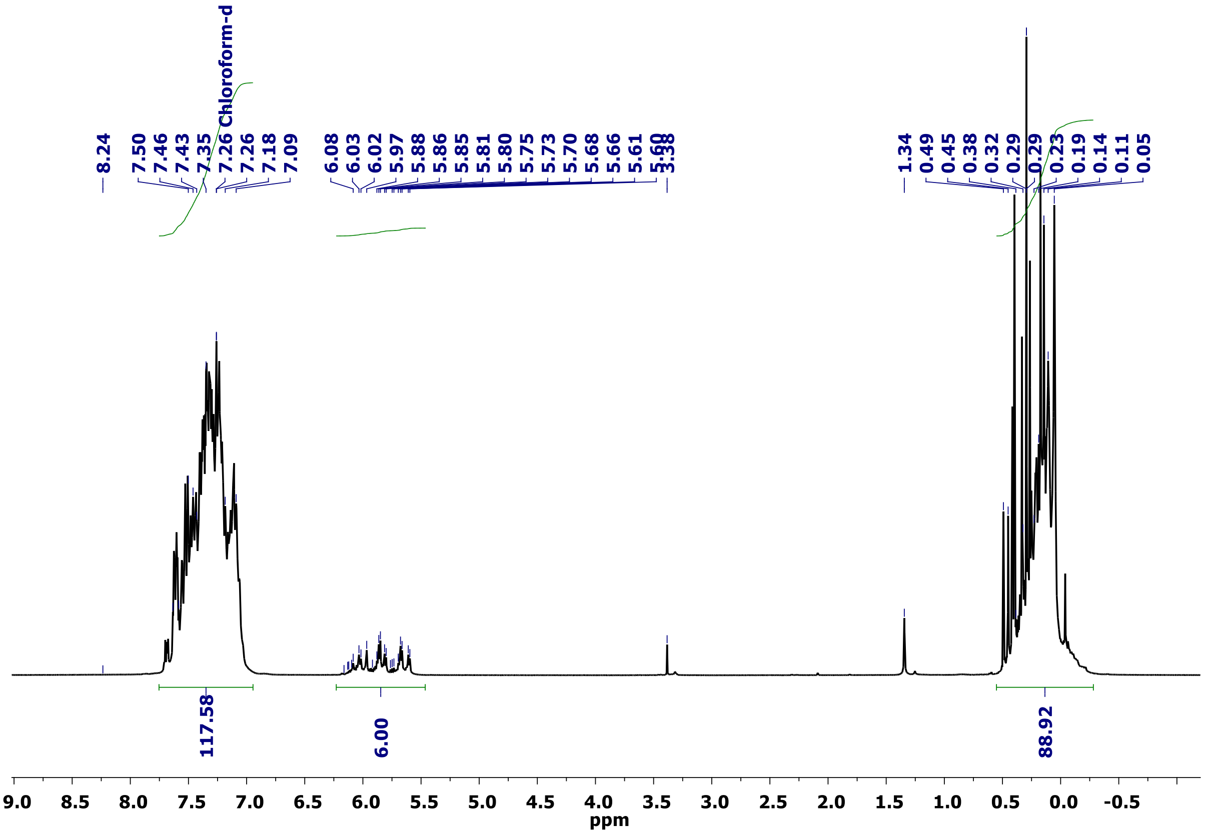

Figure S4. ^{1}H-NMR spectrum of PMV-9925 in chloroform-D.

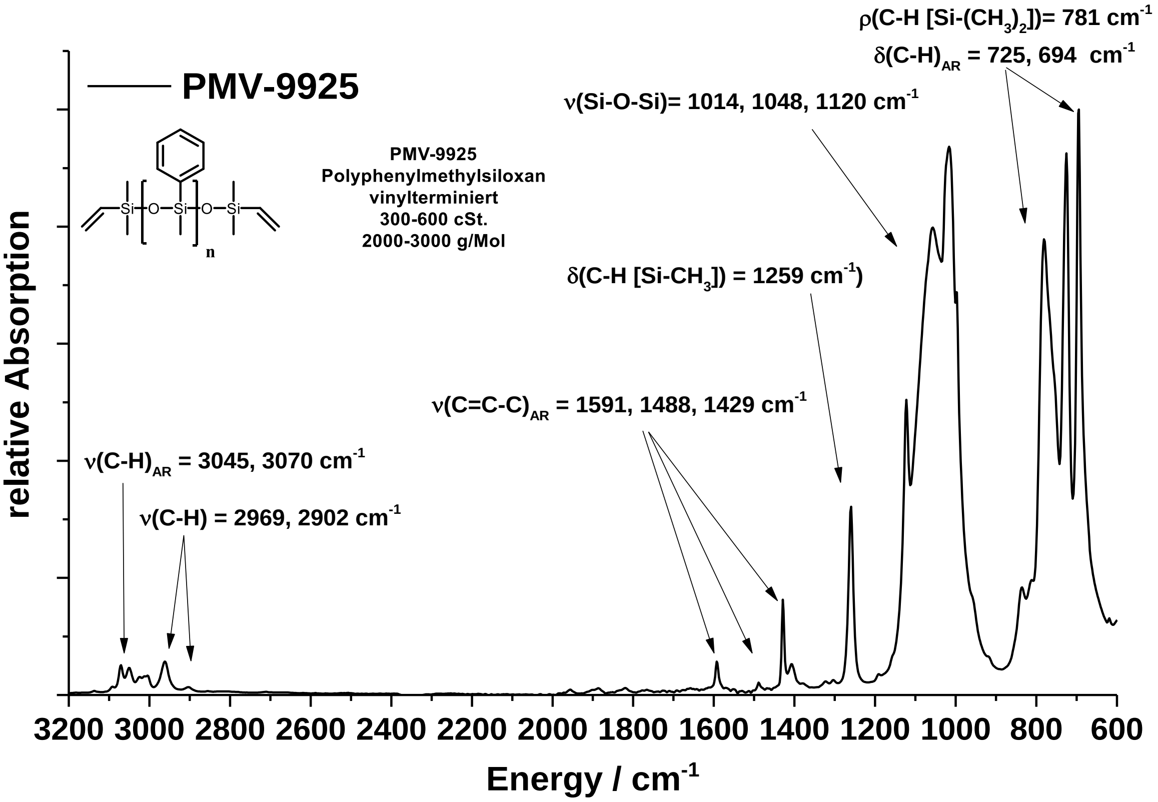

Figure S5. FTIR spectrum of PMV-9925.

OPS-B
45-50% Methylhydrosiloxane)-phenylmethylsiloxane copolymer, hydride terminated

δ_H (300 MHz, $CDCl_3$): 7.74 – 7.01 (m, Ph-H), 4.68 (m, Si-H), 2.28 (s, [impurity]), 2.06 (s, [Verunreinigung]), 1.33 (s, impurity ~ [-OH]), 1.28 (s, impurity ~ [-OH]), 0.48 – -0.20 (m, Si-CH_3).

δ_C (75 MHz, $CDCl_3$): 137.02 (Ph: C_{10}), 133.44 (C_{11}, C_{15}), 129.88 (Ph: C_{13}), 127.84 (Ph: C_{12},C_{14}), 1.5 - -1 (CH_3: C_2, C_8).

δ_{Si} (60 MHz, $CDCl_3$): -33.10 - -35.86 (Si-MePh: Si_9).

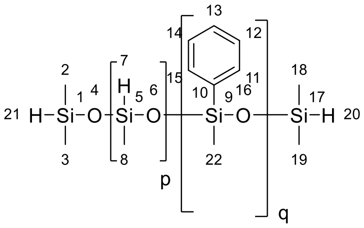

OPS- B
(45-50% Methylhydrosiloxane)-phenylmethylsiloxane copolymer, hydride terminated

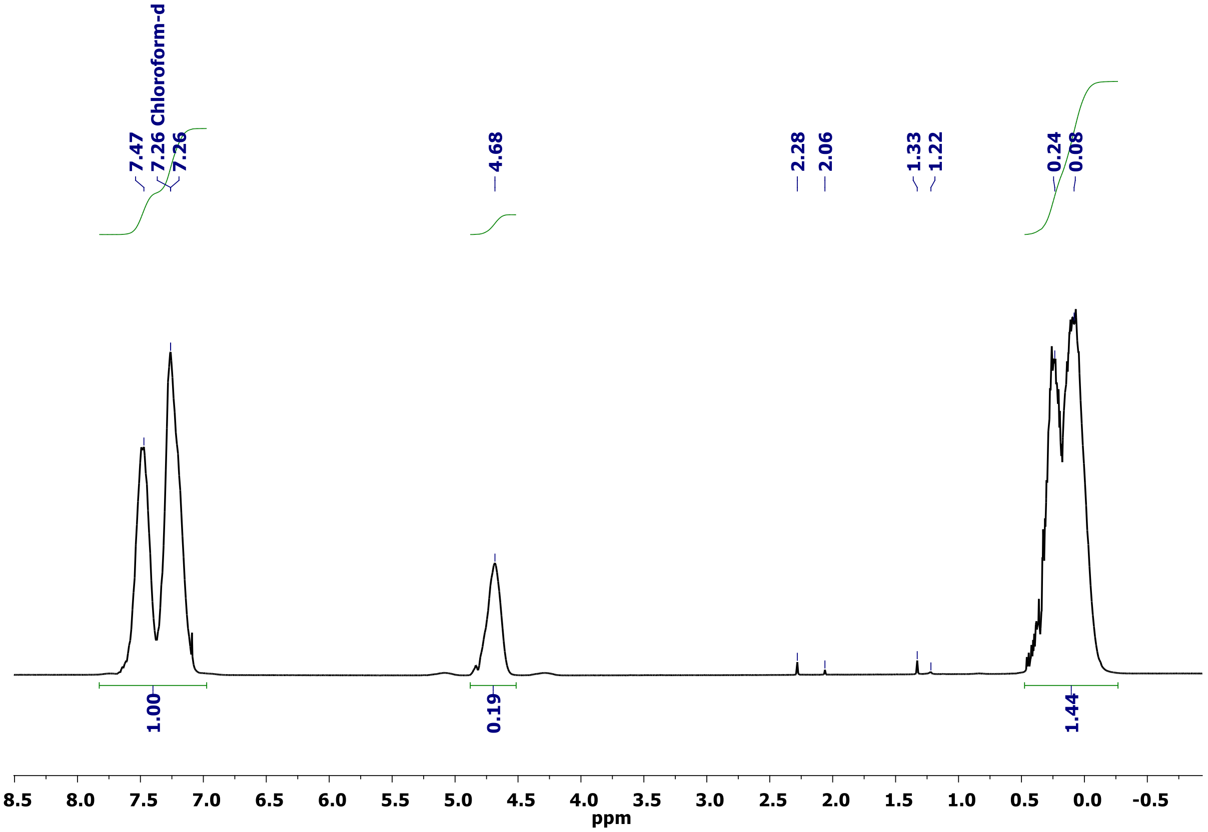

Figure S6. ^{1}H-NMR-Spektrum von OPC-B in Chloroform-D.

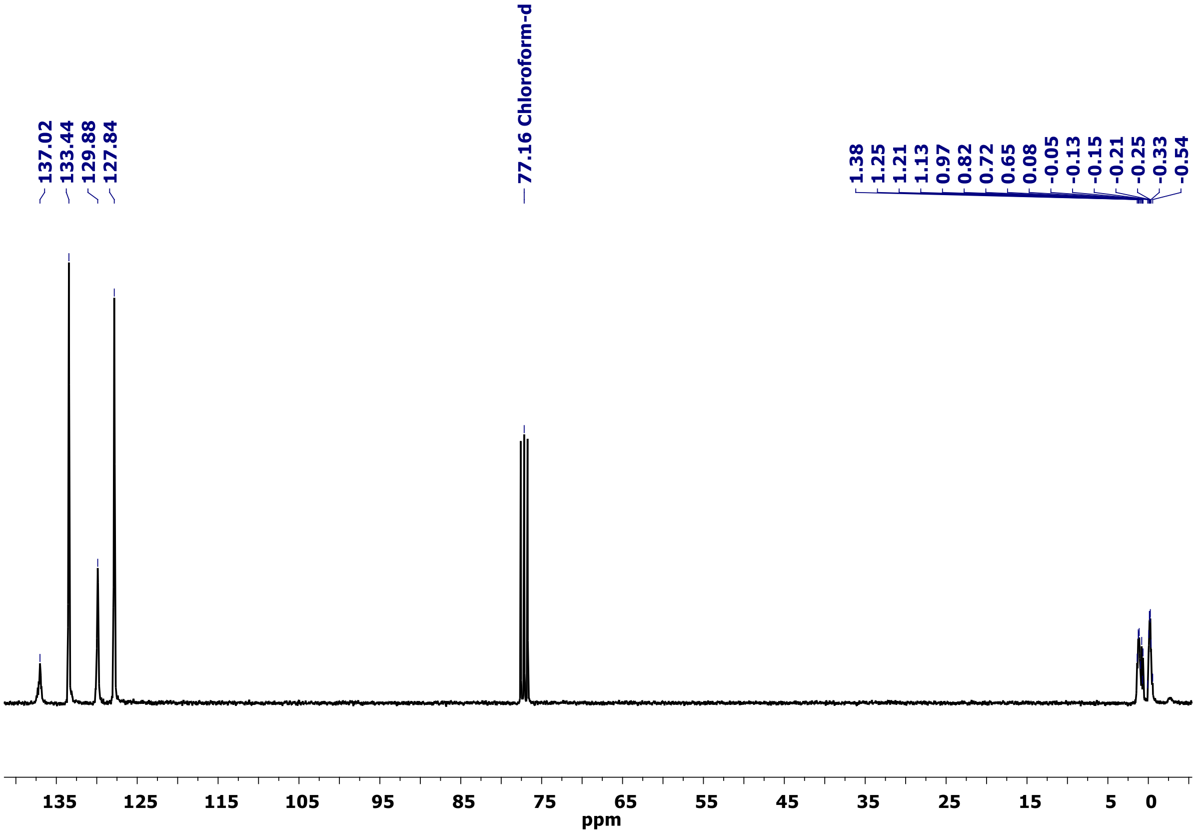

Figure S7. ^{13}C-NMR spectrum of OPS-B in chloroform-D.

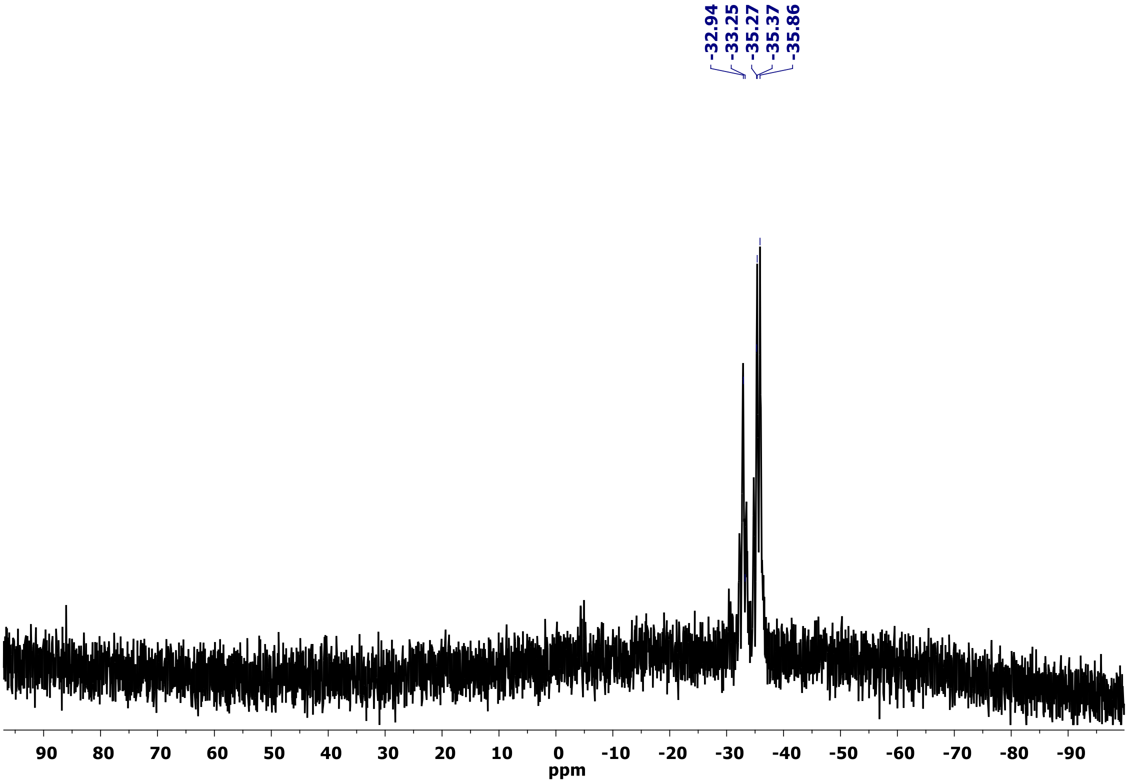

Figure S8. ^{29}Si-NMR spectrum of OPS-B in chloroform-D.

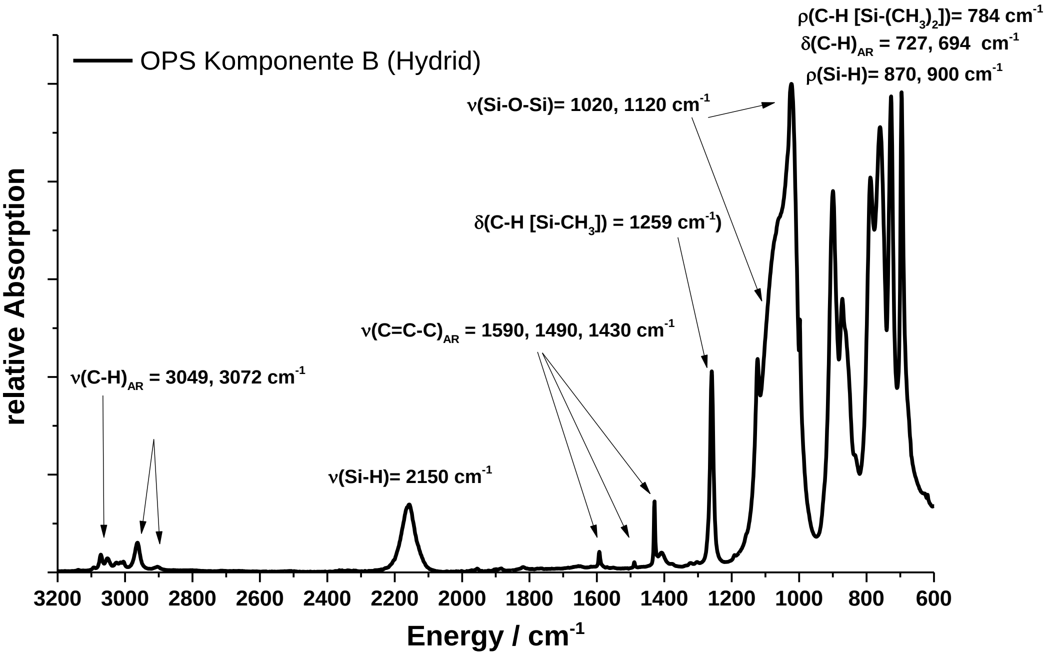

Figure S9. FTIR spectrum of OPS-B.

FC546

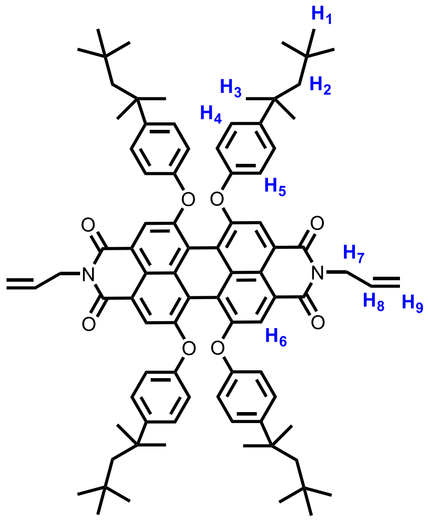

δ_H (300 MHz, CDCl$_3$): 8.15 (4 H, s, H_6), 7.27 (8 H, d, *J* 6.9, H_4), 6.86 (8 H, d, *J* 8.0, H_5), 6.01 – 5.83 (2 H, m, H_8), 5.33 – 5.10 (4 H, m, H_9), 4.73 (4 H, d, *J* 5.3, H_7), 1.73 (8 H, s, H_2), 1.54 (s, Water), 1.36 (24 H, s, H_3), 0.78 (36 H, s, H_1).

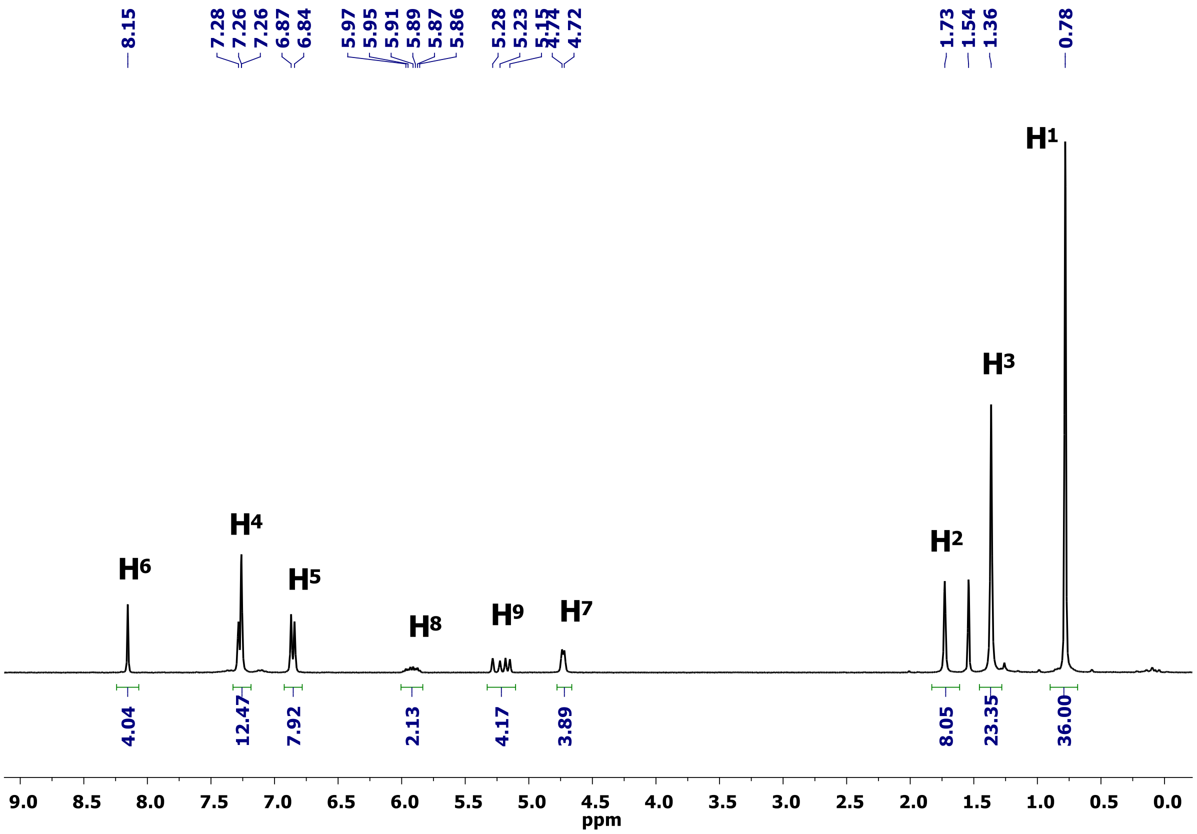

Figure S10. ^{1}H-NMR spectrum of FC546 in chloroform-D.

PX-FC546 0.1%

P2-FC546 0.1 %

δ$_H$ (300 MHz, CDCl$_3$): 7.86 – 6.88 (m, Phenyl-H), 4.76 (sept, J 2.8, Si-H), 2.00 (s, impurity), 1.55 (s, water), 1.27 (s, impurity), 1.37 (s, FC546, H$_3$), 0.79 (s, FC546, H$_1$), 0.62 – -0.26 (m, Si-CH$_3$).

P3-FC546 0.1 %

δ$_H$ (300 MHz, CDCl$_3$): 7.86 – 6.88 (m, Phenyl-H), 4.76 (sept, J 2.8, Si-H), 2.00 (s, impurity), 1.55 (s, water), 1.27 (s, impurity), 1.37 (s, FC546, H$_3$), 0.79 (s, FC546, H$_1$), 0.62 – -0.26 (m, Si-CH$_3$).

P4-FC546 0.1 %

δ$_H$ (300 MHz, CDCl$_3$): 7.86 – 6.88 (m, Phenyl-H), 4.76 (sept, J 2.8, Si-H), 2.00 (s, impurity), 1.55 (s, water), 1.27 (s, impurity), 1.37 (s, FC546, H$_3$), 0.79 (s, FC546, H$_1$), 0.62 – -0.26 (m, Si-CH$_3$).

P5-FC546 0.1 %

δ$_H$ (300 MHz, CDCl$_3$): 7.86 – 6.88 (m, Phenyl-H), 4.76 (sept, J 2.8, Si-H), 2.00 (s, impurity), 1.55 (s, water), 1.27 (s, impurity), 1.37 (s, FC546, H$_3$), 0.79 (s, FC546, H$_1$), 0.62 – -0.26 (m, Si-CH$_3$).

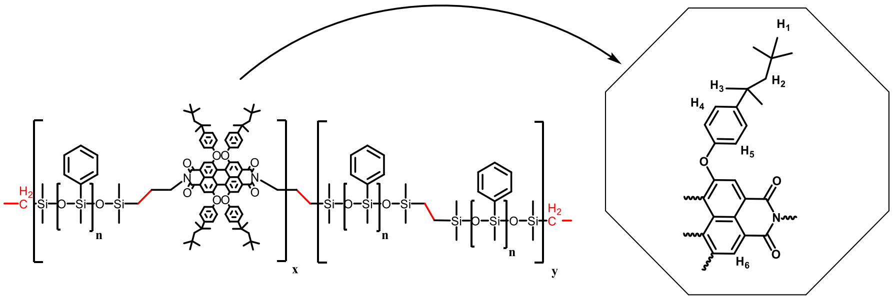

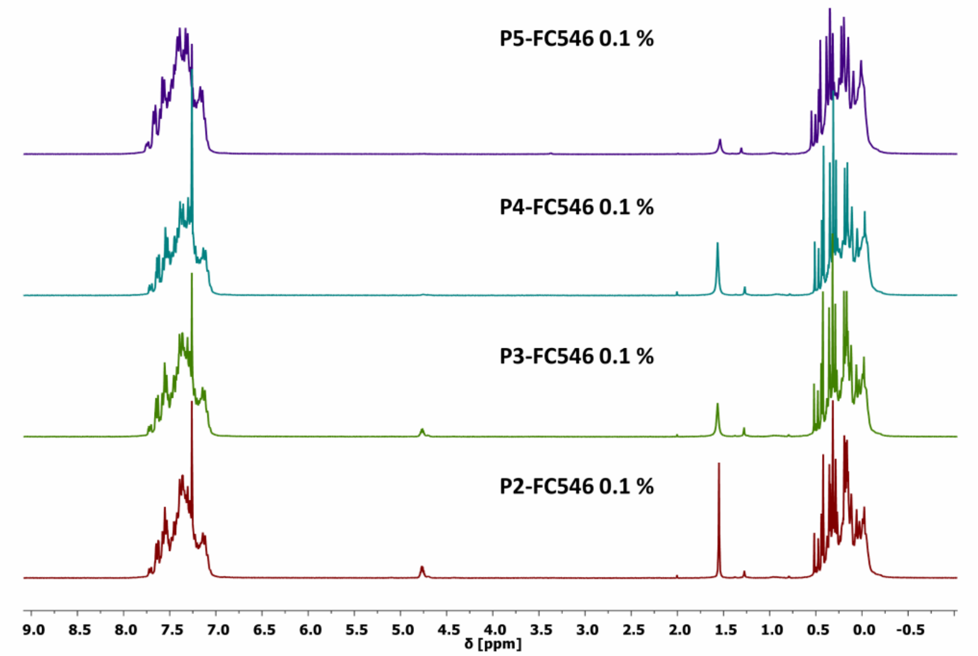

Figure S11. ^{1}H NMR spectra of PX-FC546 0.1 % (X= 2,3,4, 5)

P2-FC546 1%

δ_H (300 MHz, $CDCl_3$): 8.15 (4 H, s, FC546, H_6), 7.78 – 6.98 (m, Phenyl-H, Polymer/FC546), 6.86 (8 H, d, FC546, H_5), 3.34 (s, Polymer [impurity]), 2.00 (s, Polymer [impurity]), 1.74 (8 H, s, FC546, H_2), 1.54 (2 H, s, water), 1.37 (24 H, s, FC546, H_3), 1.28 (s, Polymer [impurity]), 0.79 (36 H, s, FC546, H_1), 0.50 – -0.25 (m, Si-CH_3, Polymer)

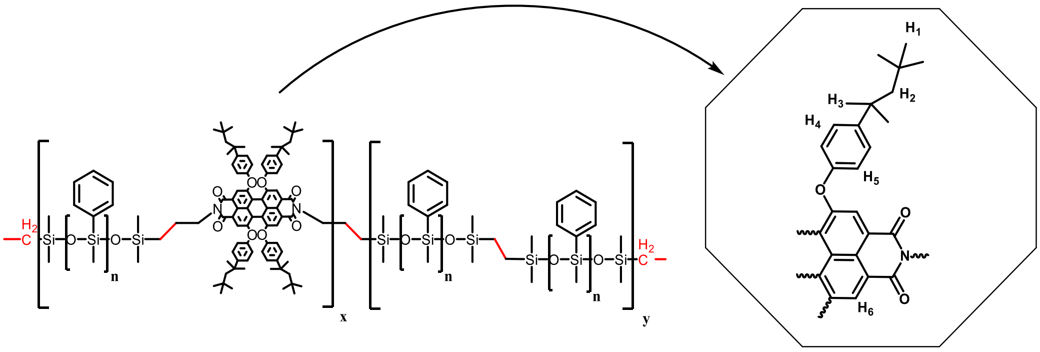

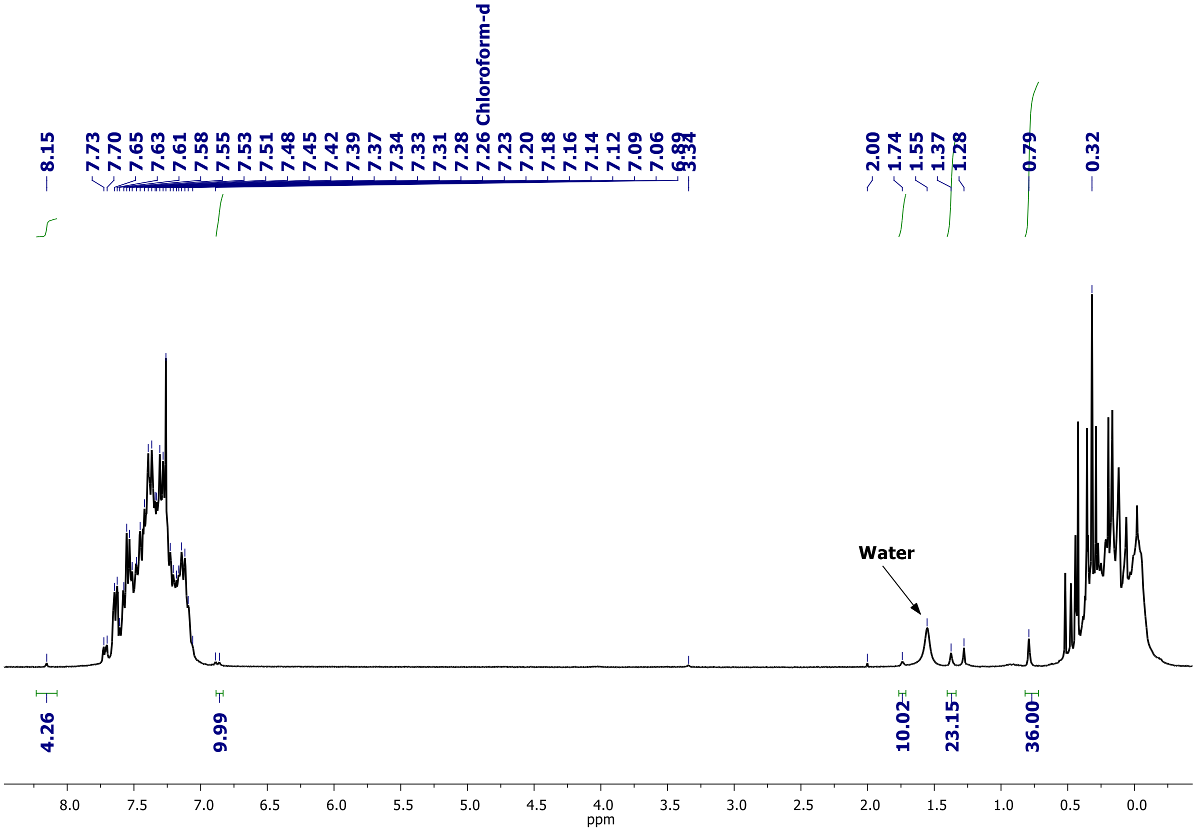

Figure S12. ^{1}H-NMR spectrum of P2-FC546 1% in chloroform-D.

OPS-B + FC546

δ_H (300 MHz, $CDCl_3$): 8.15 (4 H, s, FC546, H_6), 7.70 – 7.36 (m, Ph-H, OPS-B), 7.36 – 7.06 (m, Ph-H, OPS-B), 6.85 (8 H, d, *J* 8.1, FC546, H_5), 5.97 – 5.78 (2 H, m, FC546, H_8), 5.30 – 5.00 (4 H, m, FC546, H_9), 4.71 (m, OPS-B Si-H), 3.62 (s, OPS-B [impurity]), 1.69 (8 H, s, FC546, H_2), 1.32 (24 H, s, FC546, H_3), 0.75 (36 H, s, FC546, H_1), 0.49 – -0.22 (m, OPS-B, Si-CH_3).

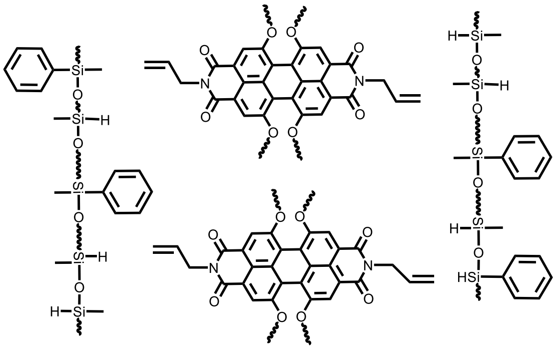

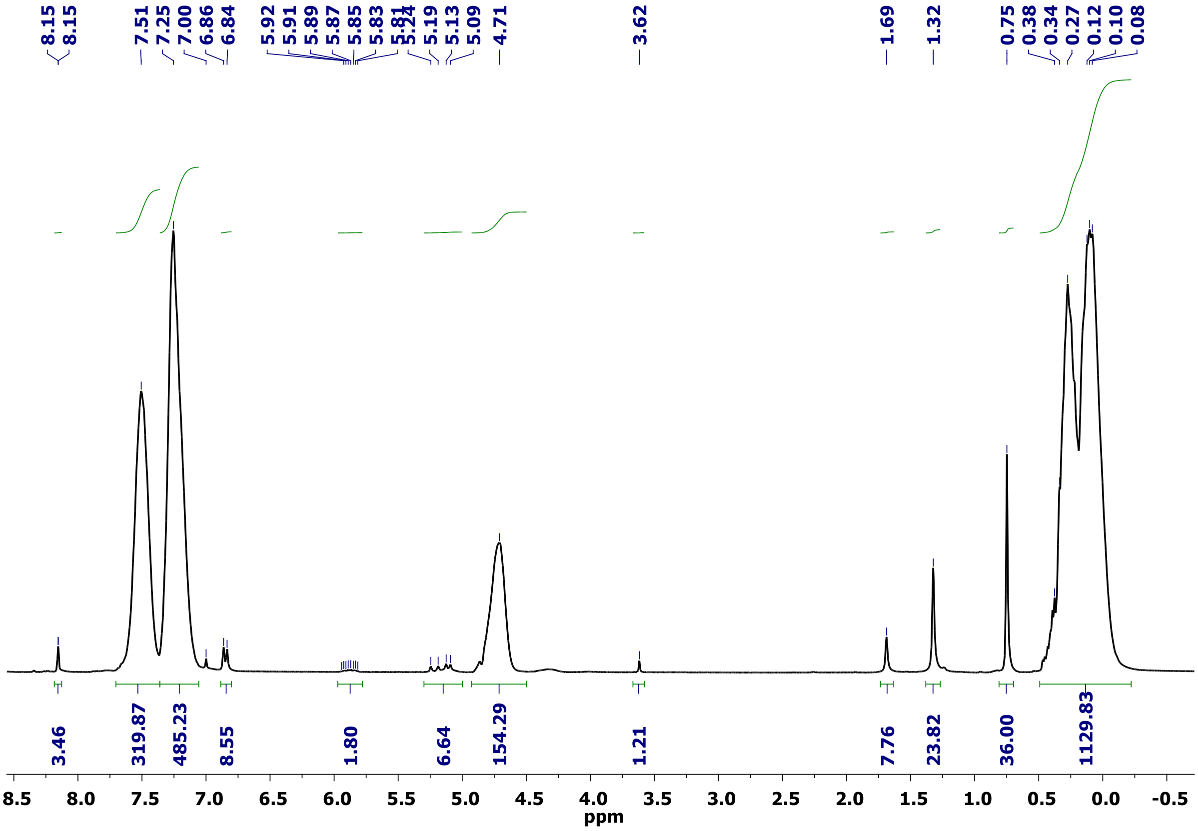

Figure S13. ^{1}H-NMR spectrum of OPS-B with FC546 8% before hydrosilylation reaction measured in chloroform-D.

OPS-B-FC546 8%

δ_H (300 MHz, $CDCl_3$): 8.15 (4 H, s, FC546, H_6), 7.75 – 7.02 (m, Ph-H, OPS-B), 6.87 (8 H, d, *J* 6.7, FC546, H_5), 4.94 – 4.52 (m, OPS-B Si-H), 2.36 (s, OPS-B [impurity]), 1.73 (8 H, s, FC546, H_2), 1.49 (s, water), 1.37 (24 H, s, FC546, H_3), 0.79 (36 H, s, FC546, H_1), 0.52 – -0.19 (m, OPS-B, Si-CH_3).

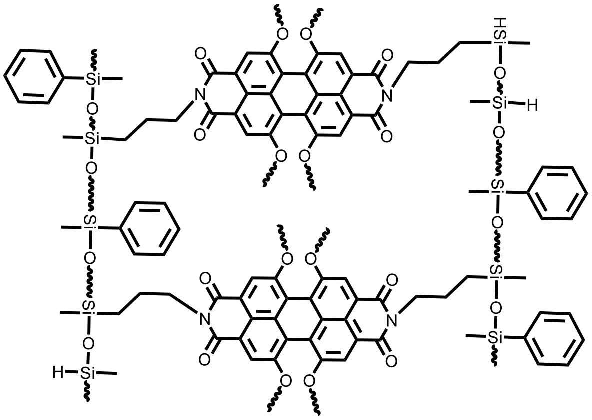

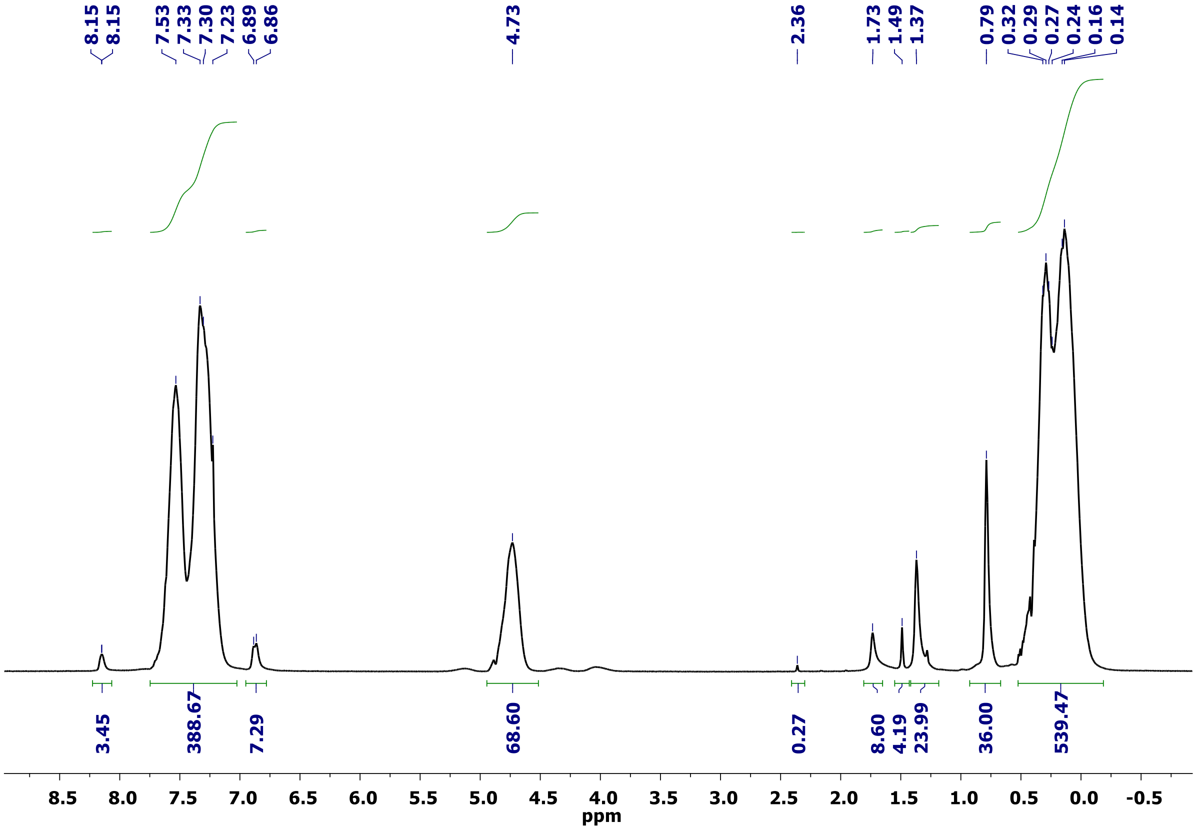

Figure S14. ^{1}H-NMR spectrum of OPS-B-FC546 8% in chloroform-D.

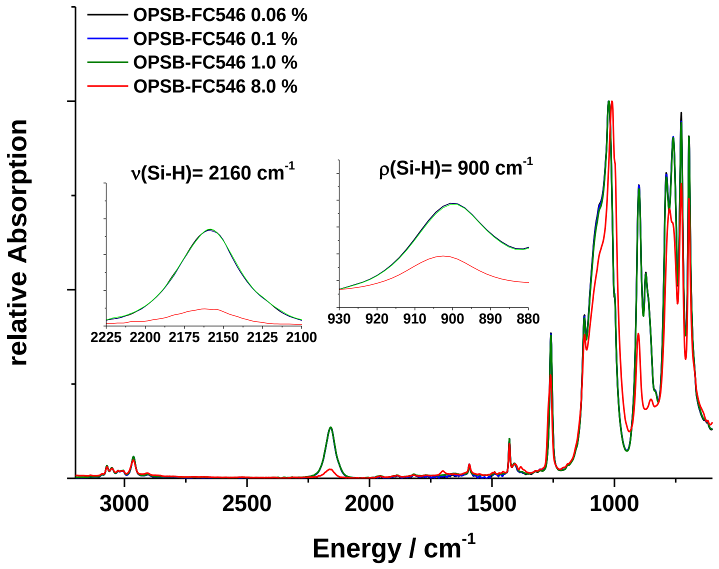

Figure S15. FTIR spectra of the OPSB-FC546 – X % series with X= 0.06, 0.1, 1.0 and 8.0. The Si-H vibration bands intensities at 2125 cm^{-1} [ν(Si-H)] and 905 cm^{-1} [ρ(Si-H)] are not decreasing significantly for samples with a low dye concentration. After the incorporation of 8 wt% of FC546 the decrease is detectable and an indication for a covalent attachment to the polymer precursor.

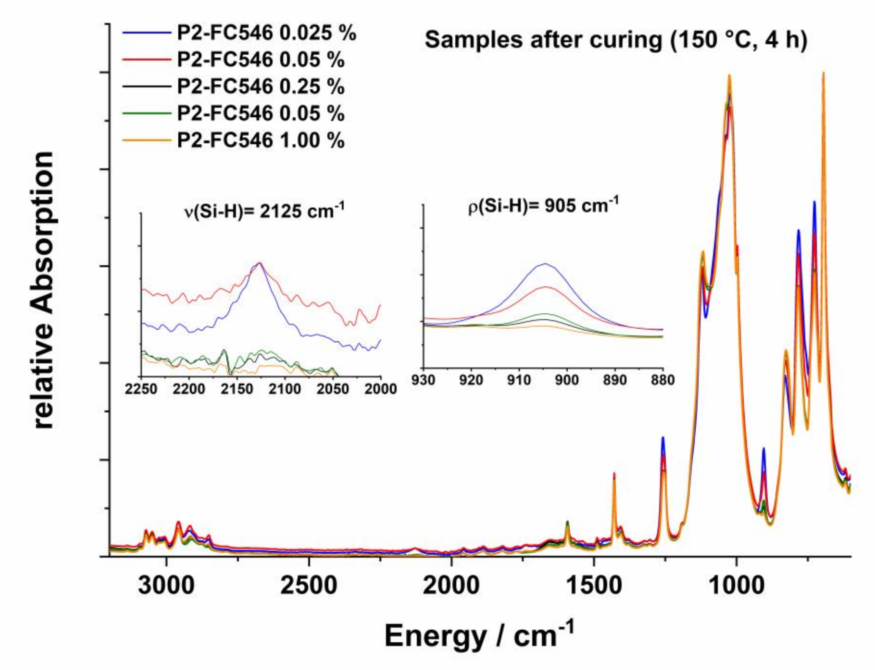

Figure S16. FTIR spectra of the Dow(1)P2-FC546 – X % series after the curing process at 150 °C for 4 h.

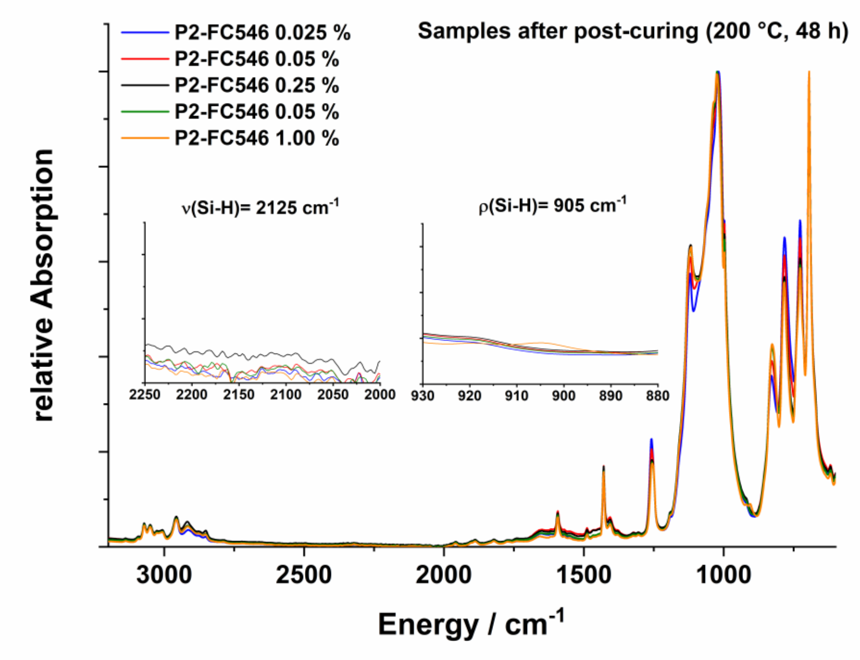

Figure S17. FTIR spectra of the Dow(1)P2-FC546 – X % series after the curing process at 200 °C for 48 h.

Thermogravimetric data

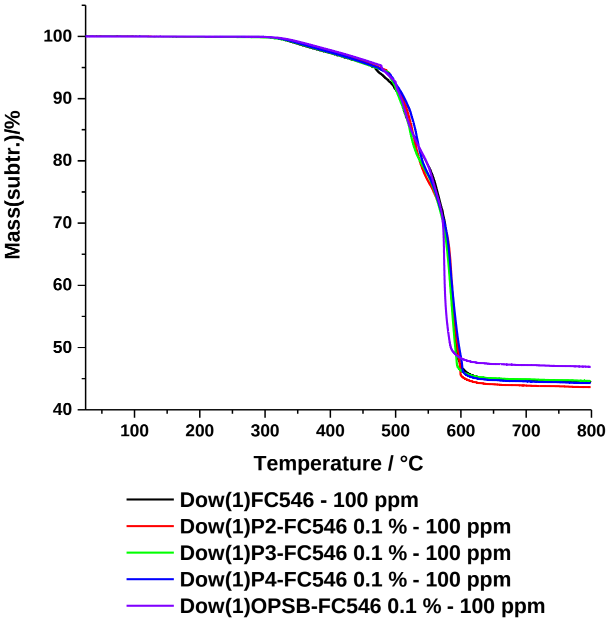

Figure S18. Thermogravimetric data of Dow(1)FC546 – 100ppm, the Dow(1)PX-FC546 0.1 % - 100 ppm series (X= 2, 3, 4) and Dow(1)OPSB-FC546 with 10 K/min to 800 °C with gas flux of N_2/O_2 of 20 ml/min respectively.

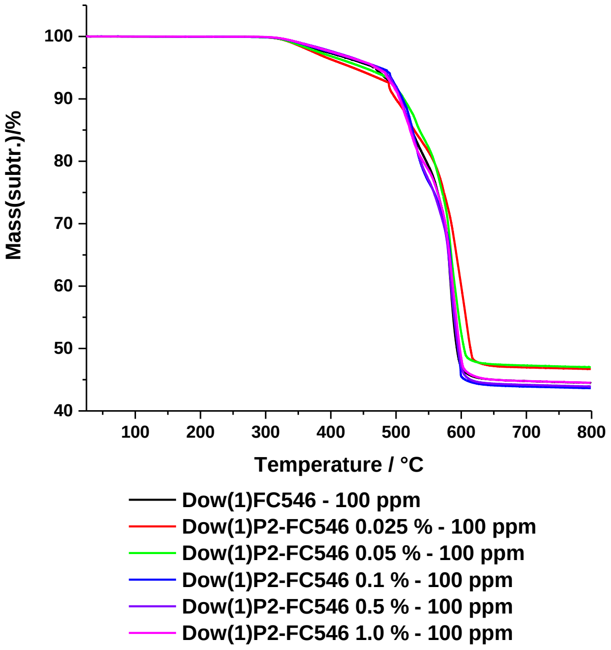

Figure S19. Thermogravimetric data of Dow(1)FC546 – 100ppm and the Dow(1)P2-FC546 X % - 100 ppm series (X=0.025, 0.05, 0.1, 0.5, 1.0) with 10 K/min to 800 °C with gas flux of N_2/O_2 of 20 ml/min respectively.

Table S1. The degradation temperature T_{95} value of the cured Dow(1) samples with the perylene polymers or the pure dye incorporated compared to the pure Dow(1) matrix. A higher concentration of perylene polysiloxane added leads to a decrease of T_{95} value.

Sample	**T_{95} / °C**
Dow(1)	465
Dow(1)FC545 - 100 ppm	468
Dow(1)P2-FC546 0.025 % - 100 ppm	433
Dow(1)P2-FC546 0.05 % - 100 ppm	450
Dow(1)P2-FC546 0.1 % - 100 ppm	474
Dow(1)P2-FC546 0.5 % - 100 ppm	472
Dow(1)P2-FC546 1.0 % - 100 ppm	470
Dow(1)P3-FC546 0.1 % - 100 ppm	469
Dow(1)P4-FC546 0.1 % - 100 ppm	472
Dow(1)OPS-B-FC546 0.1 % - 100 ppm	478

DSC

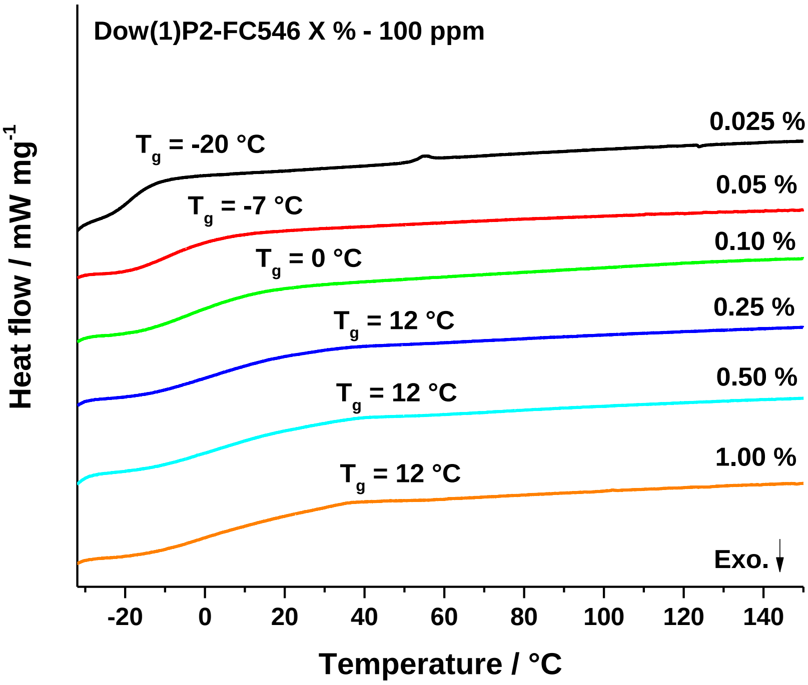

Figure S20. DSC measurements of the post cured samples measured from -40 to 400 °C with 5K/min under N_2 atmosphere (100 ml/min). The T_g value indicated by an inflection of the DSC curve increases with the hardness of the sample caused by a higher cross-linked structure.

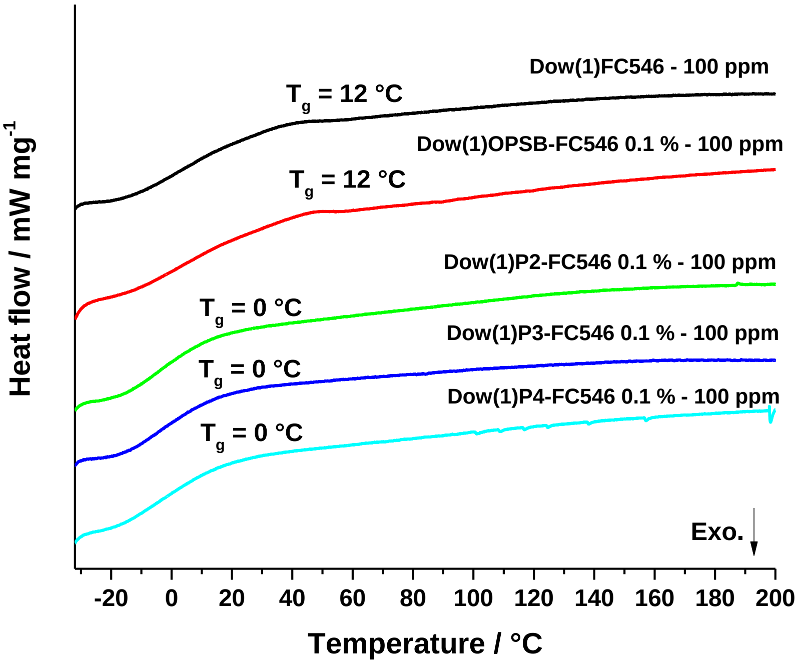

Figure S21. DSC measurements of the post cured samples measured from -40 to 400 °C with 5K/min under N_2 atmosphere (100 ml/min). The T_g value indicated by an inflection of the DSC curve increases with the hardness of the sample caused by a higher cross-linked structure.

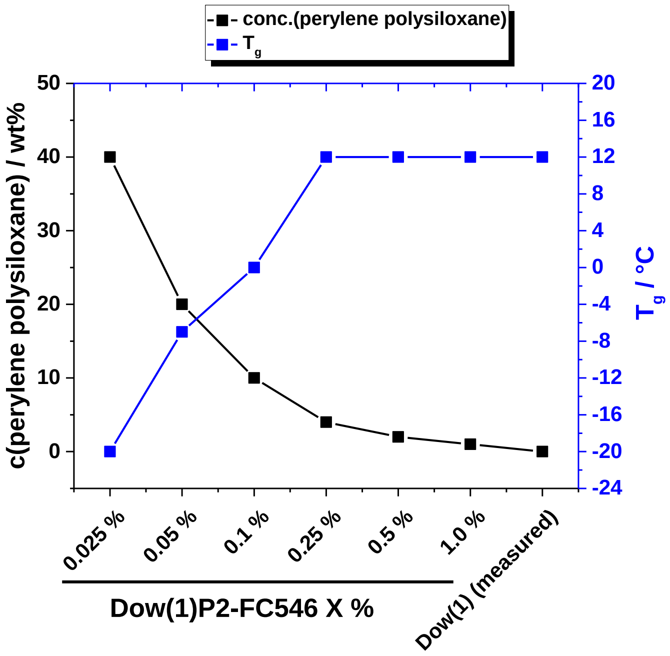

Figure S22. T_g values of the of the cured Dow(1) samples with the perylene polymers or the pure dye incorporated compared with the pure Dow(1) matrix measured after the post curing procedure (200 °C, 48 h). The decrease of the T_g and the cross-linking is directly correlated to the amount of perylene polysiloxane incorporated.

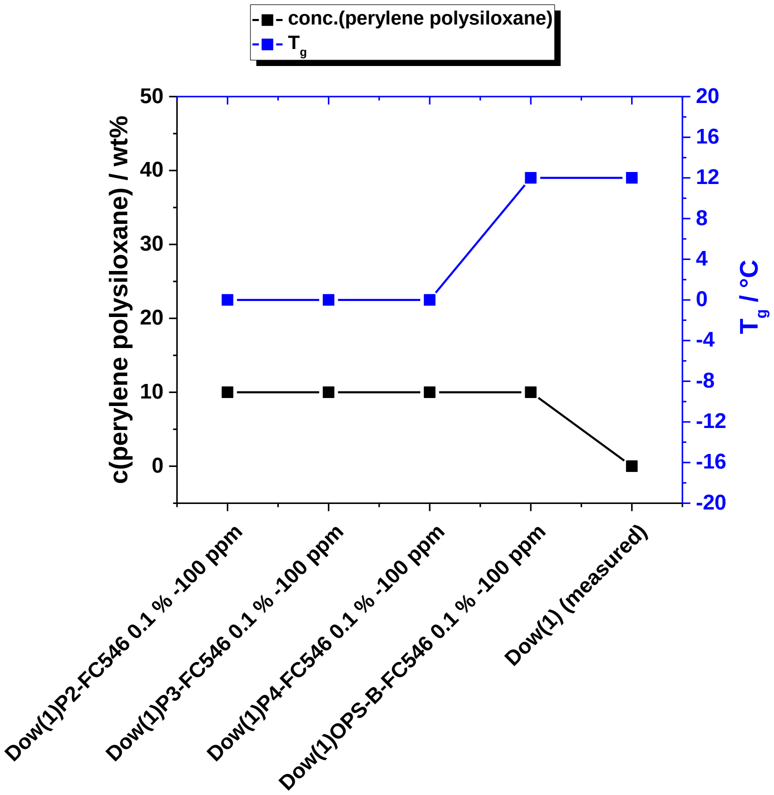

Figure S23. T_g values of the of the cured Dow(1) samples with the perylene polymers or the pure dye incorporated compared with the pure Dow(1) matrix measured after the post curing procedure (200 °C, 48 h). The decrease of the T_g and the cross-linking is directly correlated to the amount of perylene polysiloxane incorporated.

Quantum Efficiency, Self-Absorption Coefficient and Fluorescence Spectra

Table S2. Measured quantum yield values and calculated values of Dow(1)OPSB-FC546 0.1% - 100 ppm before and after additional heat treatments (200 °C, 48/120h) and the corrected quantum yield and the self-absorption coefficient. The self-absorption coefficient was calculated by using the emission spectra of a very low concentrated sample with virtually zero self-absorption (Dow(1)FC546 - 15 ppm) as described in previous studies.[1,40,41] Goodness of the fit is calculated and given by the pearsons chi-squared test value X^2.

	QE	QEcorr	a	$\chi 2$
Dow(1)FC546	1.01	1.01	0.25	65.29
Dow(1)OPS-B-FC546 0.1%	0.90	0.92	0.27	60.76
Dow(1)OPS-B-FC546 0.1%, 48h, 200 °C	0.80	0.85	0.28	66.19
Dow(1)OPS-B-FC546 0.1%, 120h, 200 °C	0.74	0.79	0.26	58.12

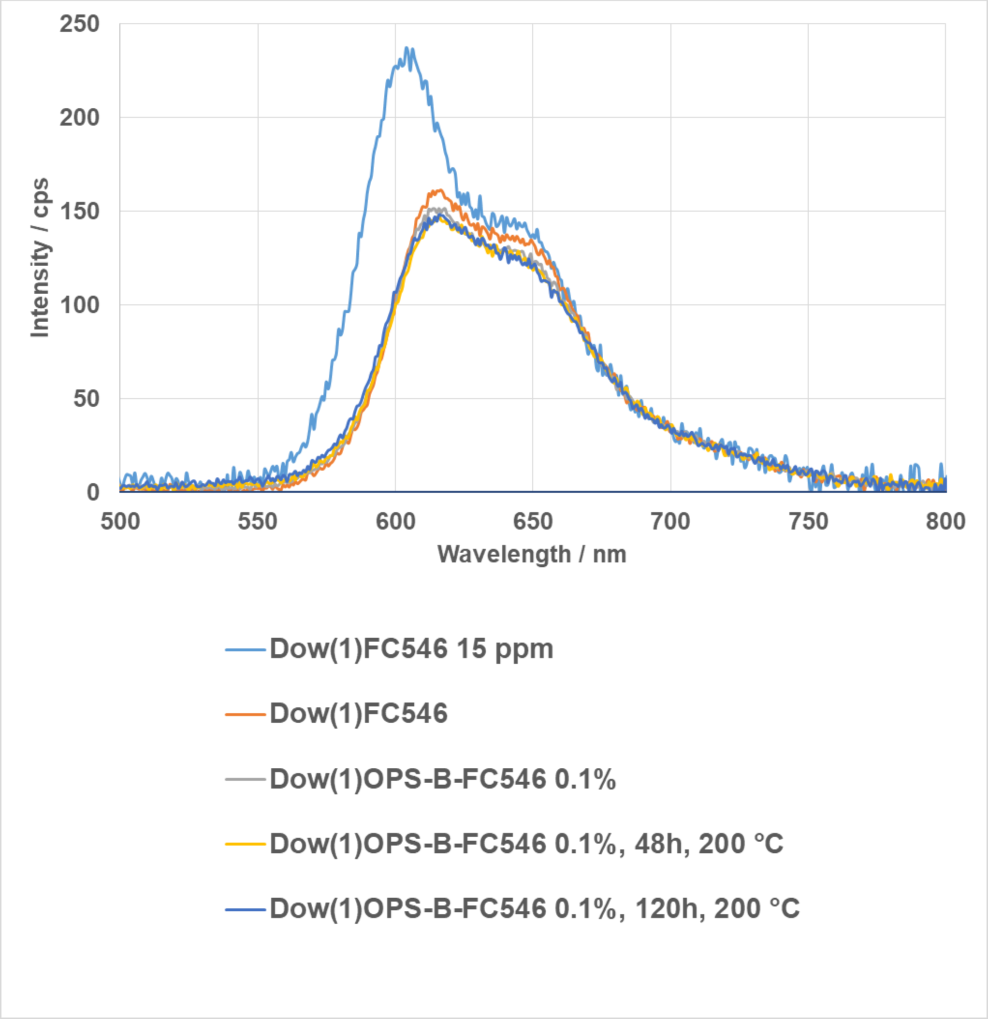

Figure S24. Fitted emission spectra of Dow(1)OPSB-FC546 0.1% - 100 ppm before and after additional heat treatments (200 °C, 48/120h) and the emission spectrum of a very low concentrated sample with virtually zero self-absorption (Dow(1)FC546 - 15 ppm) used for the quantum yield determination, the quantum yield correction and self-absorption coefficient calculations.

Table S3. Measured quantum yield values and calculated values of Dow(1)P2-FC546 0.1% - 100 ppm before and after additional heat treatments (200 °C, 48/120h) and the corrected quantum yield and the self-absorption coefficient. The self-absorption coefficient was calculated by using the emission spectra of a very low concentrated sample with virtually zero self-absorption (Dow(1)FC546 - 15 ppm) as described in previous studies.[1,40,41] Goodness of the fit is calculated and given by the pearsons chi-squared test value X^2.

	QE	QEcorr	a	$\chi2$
Dow(1)P2-FC546 0.1%	1.01	1.01	0.36	54.54
Dow(1)P2-FC546 0.1%, 200 °C, 48 h	0.82	0.88	0.39	55.45
Dow(1)P2-FC546 0.1%, 200 °C, 120 h	0.83	0.89	0.40	64.88

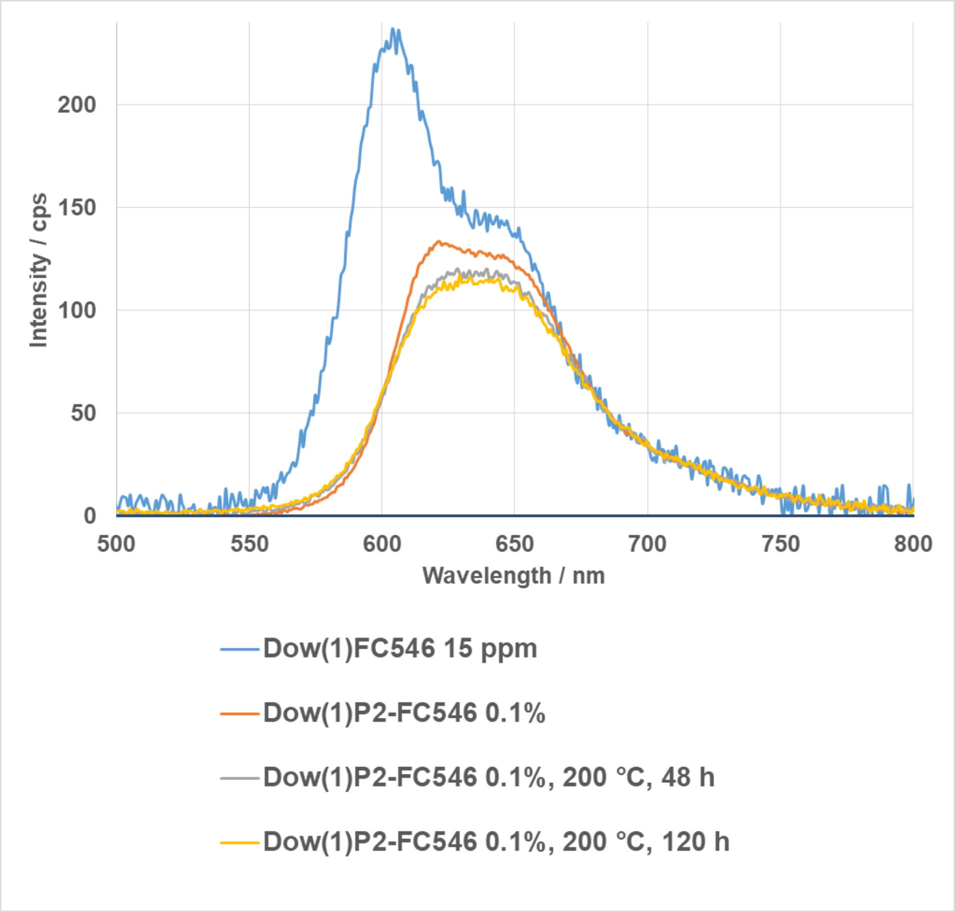

Figure S25. Fitted emission spectra of Dow(1)P2-FC546 0.1% - 100 ppm before and after additional heat treatments (200 °C, 48/120h) and the emission spectrum of a very low concentrated sample with virtually zero self-absorption (Dow(1)FC546 - 15 ppm) used for the quantum yield determination, the quantum yield correction and self-absorption coefficient calculations.

Table S4. Measured quantum yield values and calculated values of Dow(1)P3-FC546 0.1% - 100 ppm before and after additional heat treatments (200 °C, 48/120h) and the corrected quantum yield and the self-absorption coefficient. The self-absorption coefficient was calculated by using the emission spectra of a very low concentrated sample with virtually zero self-absorption (Dow(1)FC546 - 15 ppm) as described in previous studies.[1,40,41] *Goodness of the fit is calculated and given by the pearsons chi-squared test value* X^2.

	QE	QEcorr	a	$\chi 2$
Dow(1)P3-FC546 0.1%	1.01	1.00	0.31	54.42
Dow(1)P3-FC546 0.1%, 200 °C, 48 h	0.85	0.90	0.36	58.99
Dow(1)P3-FC546 0.1%, 200 °C, 120 h	0.83	0.89	0.37	82.10

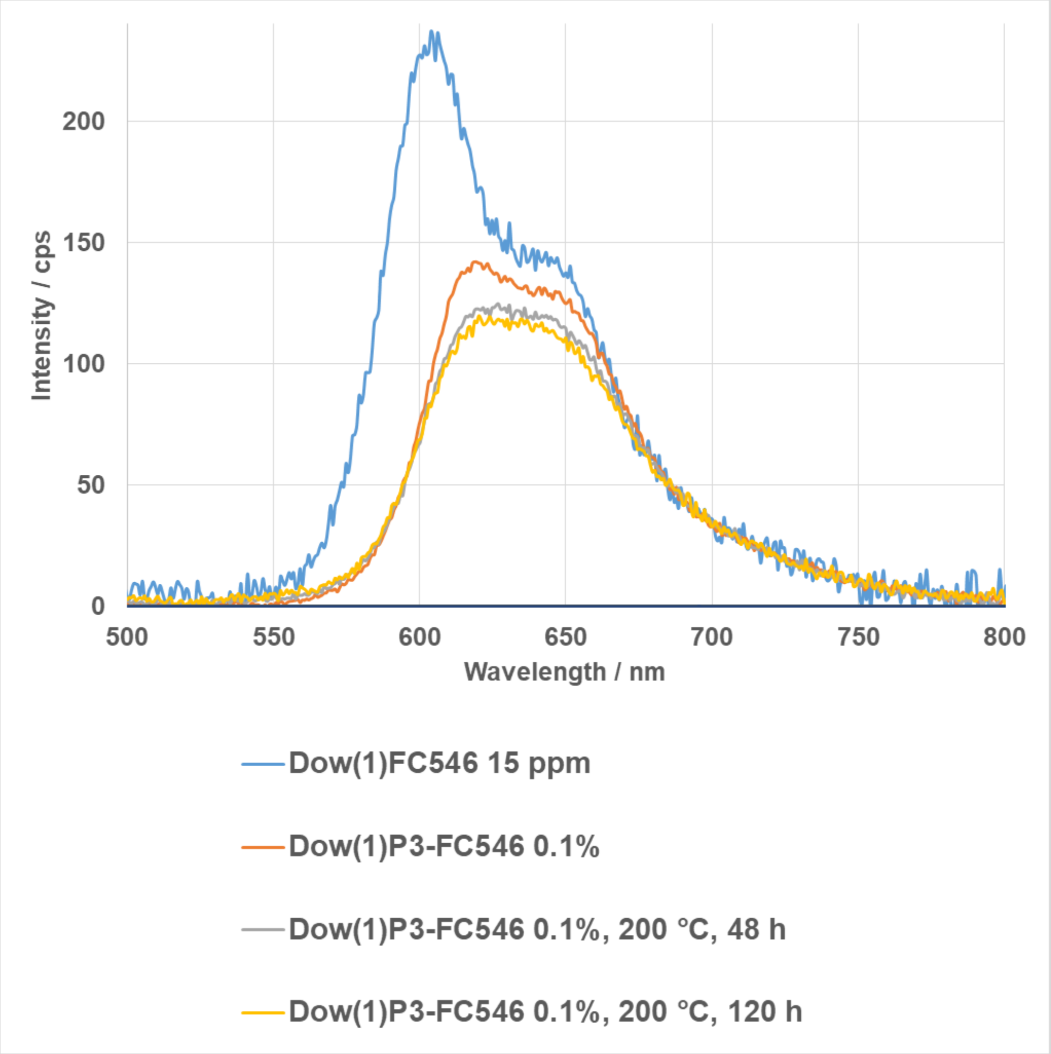

Figure S26.Fitted emission spectra of Dow(1)P3-FC546 0.1% - 100 ppm before and after additional heat treatments (200 °C, 48/120h) and the emission spectrum of a very low concentrated sample with virtually zero self-absorption (Dow(1)FC546 - 15 ppm) used for the quantum yield determination, the quantum yield correction and self-absorption coefficient calculations.

Table S5. Measured quantum yield values and calculated values of Dow(1)P4-FC546 0.1% - 100 ppm before and after additional heat treatments (200 °C, 48/120h) and the corrected quantum yield and the self-absorption coefficient. The self-absorption coefficient was calculated by using the emission spectra of a very low concentrated sample with virtually zero self-absorption (Dow(1)FC546 - 15 ppm) as described in previous studies.[1,40,41] *Goodness of the fit is calculated and given by the pearsons chi-squared test value X^2.*

	QE	QEcorr	a	$\chi 2$
Dow(1)P4-FC546 0.1%	1.00	1.00	0.36	66.89
Dow(1)P4-FC546 0.1%, 200 °C, 48 h	0.83	0.89	0.39	59.09
Dow(1)P4-FC546 0.1%, 200 °C, 120 h	0.81	0.87	0.39	67.64

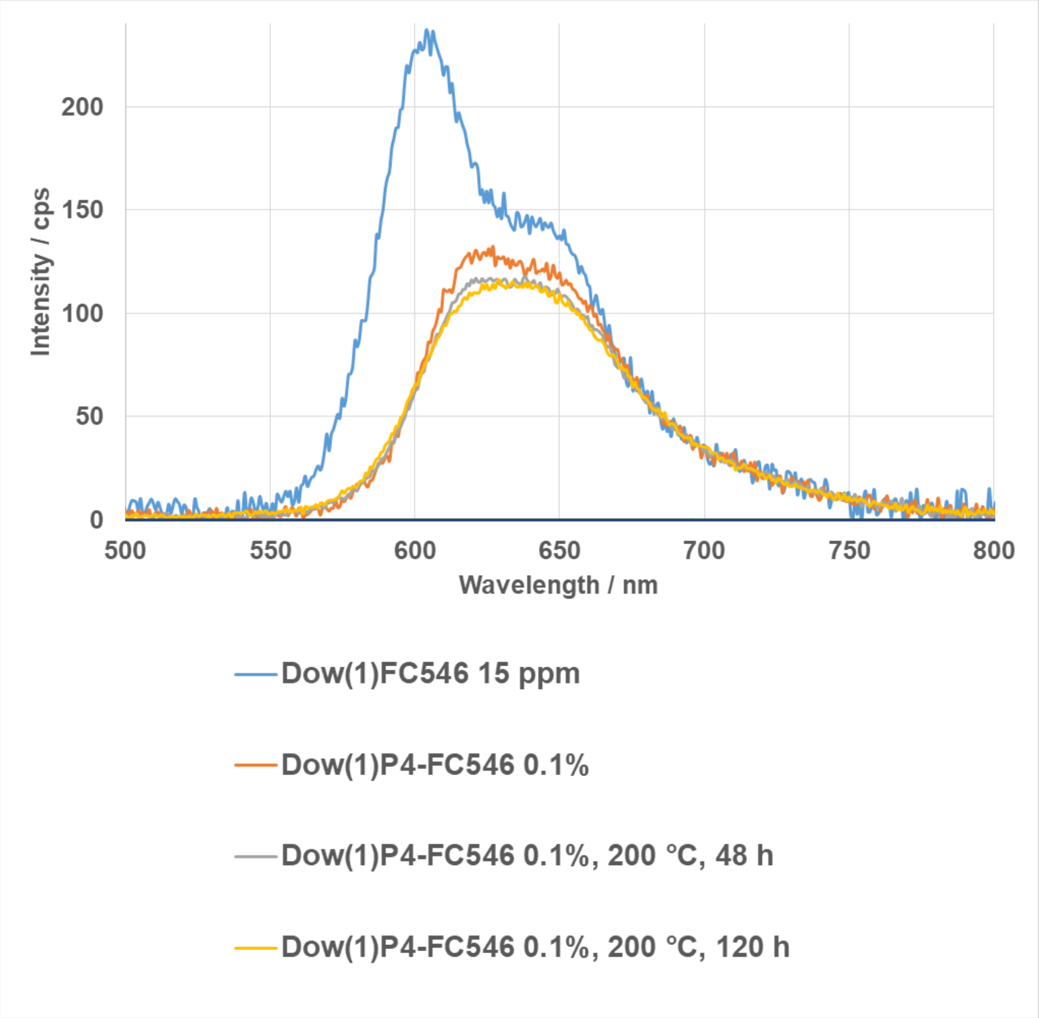

Figure S27. Fitted emission spectra of Dow(1)P4-FC546 0.1% - 100 ppm before and after additional heat treatments (200 °C, 48/120h) and the emission spectrum of a very low concentrated sample with virtually zero self-absorption (Dow(1)FC546 - 15 ppm) used for the quantum yield determination, the quantum yield correction and self-absorption coefficient calculations.

Table S6. Measured quantum yield values and calculated values of Dow(1)P2-FC546 X % - 100 ppm (X= 0.025, 0.05, 0.1, 0.25, 0.5, 1.0) before an additional heat treatments (200 °C, 48/120h) and the corrected quantum yield and the self-absorption coefficient. The self-absorption coefficient was calculated by using the emission spectra of a very low concentrated sample with virtually zero self-absorption (Dow(1)FC546 - 15 ppm) as described in previous studies.[1,40,41] Goodness of the fit is calculated and given by the pearsons chi-squared test value X^2.

Dow(1)P2-FC546 X% - 100 ppm	QE	QEcorr	a	$\chi 2$
0.025	0.98	0.99	0.32	54.98
0.05	0.98	0.99	0.34	55.79
0.1	1.01	1.01	0.35	47.66
0.25	1.00	1.00	0.28	48.33
0.5	0.97	0.98	0.35	55.28
1	0.97	0.98	0.38	52.97

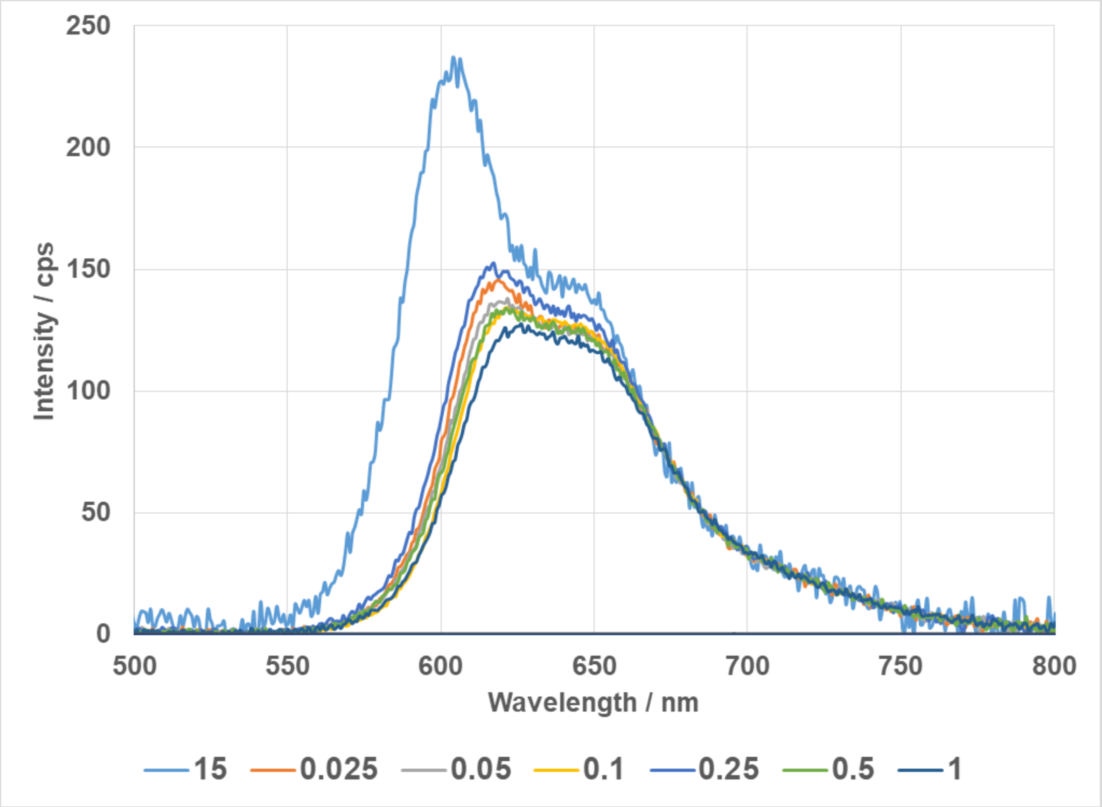

Figure S28. Fitted emission spectra of Dow(1)P2-FC546 X % - 100 ppm (X= 0.025, 0.05, 0.1, 0.25, 0.5, 1.0) before an additional heat treatments (200 °C, 48/120h) and the emission spectrum of a very low concentrated sample with virtually zero self-absorption (Dow(1)FC546 - 15 ppm) used for the quantum yield determination, the quantum yield correction and self-absorption coefficient calculations.

Table S7. Measured quantum yield values and calculated values of Dow(1)P2-FC546 X % - 100 ppm (X= 0.025, 0.05, 0.1, 0.25, 0.5, 1.0) before after additional heat treatments (200 °C, 48 h) and the corrected quantum yield and the self-absorption coefficient. The self-absorption coefficient was calculated by using the emission spectra of a very low concentrated sample with virtually zero self-absorption (Dow(1)FC546 - 15 ppm) as described in previous studies.[1,40,41] *Goodness of the fit is calculated and given by the pearsons chi-squared test value* X^2.

Dow(1)P2-FC546 X% - 100 ppm (200°C, 48h)	**QE**	**QEcorr**	**a**	**$\chi 2$**
0.025	0.84	0.89	0.36	54.25
0.05	0.87	0.91	0.35	52.79
0.1	0.82	0.88	0.39	49.16
0.25	0.87	0.90	0.30	56.99
0.5	0.86	0.90	0.35	57.86
1	0.85	0.90	0.39	47.32

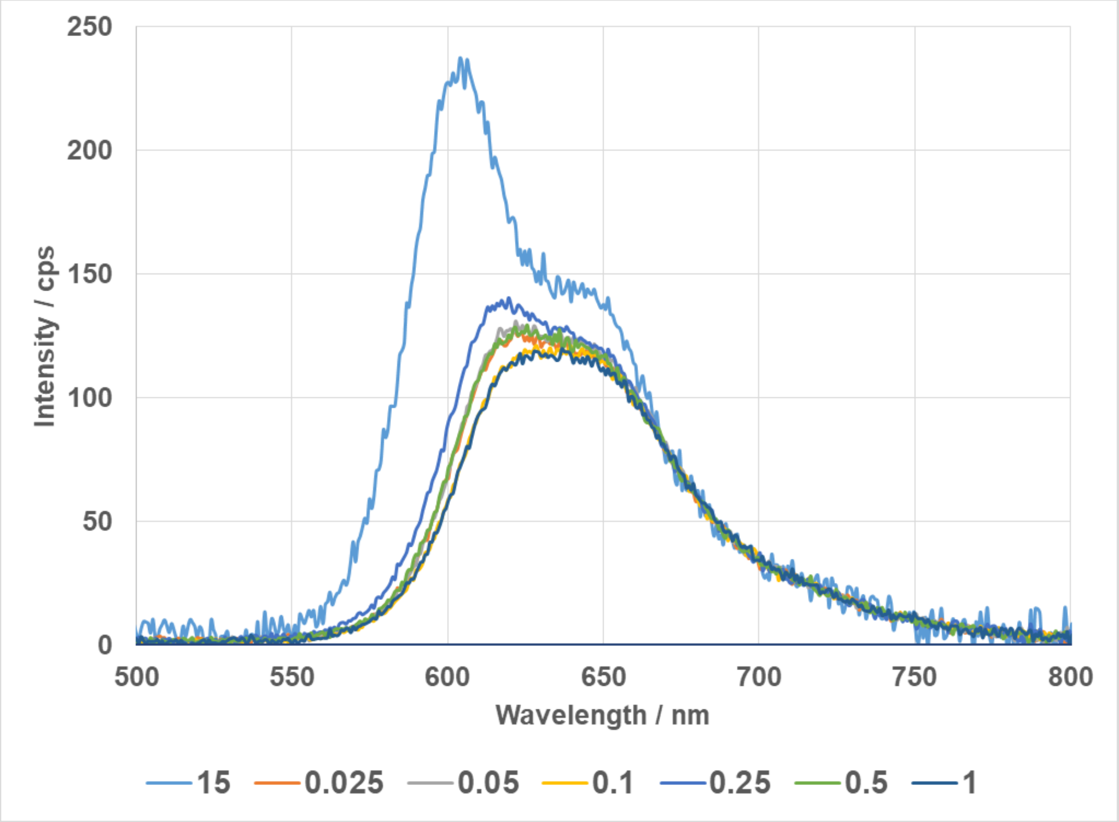

Figure S29. Fitted emission spectra of Dow(1)P2-FC546 X % - 100 ppm (X= 0.025, 0.05, 0.1, 0.25, 0.5, 1.0) after an additional heat treatments (200 °C, 48) and the emission spectrum of a very low concentrated sample with virtually zero self-absorption (Dow(1)FC546 - 15 ppm) used for the quantum yield determination, the quantum yield correction and self-absorption coefficient calculations.

Table S8. Measured quantum yield values and calculated values of Dow(1)P2-FC546 X % - 100 ppm (X= 0.025, 0.05, 0.1, 0.25, 0.5, 1.0) before after additional heat treatments (200 °C, 72 h) and the corrected quantum yield and the self-absorption coefficient. The self-absorption coefficient was calculated by using the emission spectra of a very low concentrated sample with virtually zero self-absorption (Dow(1)FC546 - 15 ppm) as described in previous studies.[1,40,41] Goodness of the fit is calculated and given by the pearsons chi-squared test value X^2.

Dow(1)P2-FC546 X% - 100 ppm (200°C, 120 h)	**QE**	**QEcorr**	**a**	**$\chi 2$**
0.025	0.78	0.85	0.38	46.64
0.05	0.82	0.88	0.36	56.22
0.1	0.83	0.89	0.40	58.40
0.25	0.82	0.87	0.31	58.99
0.5	0.83	0.88	0.34	57.14
1	0.81	0.88	0.40	49.35

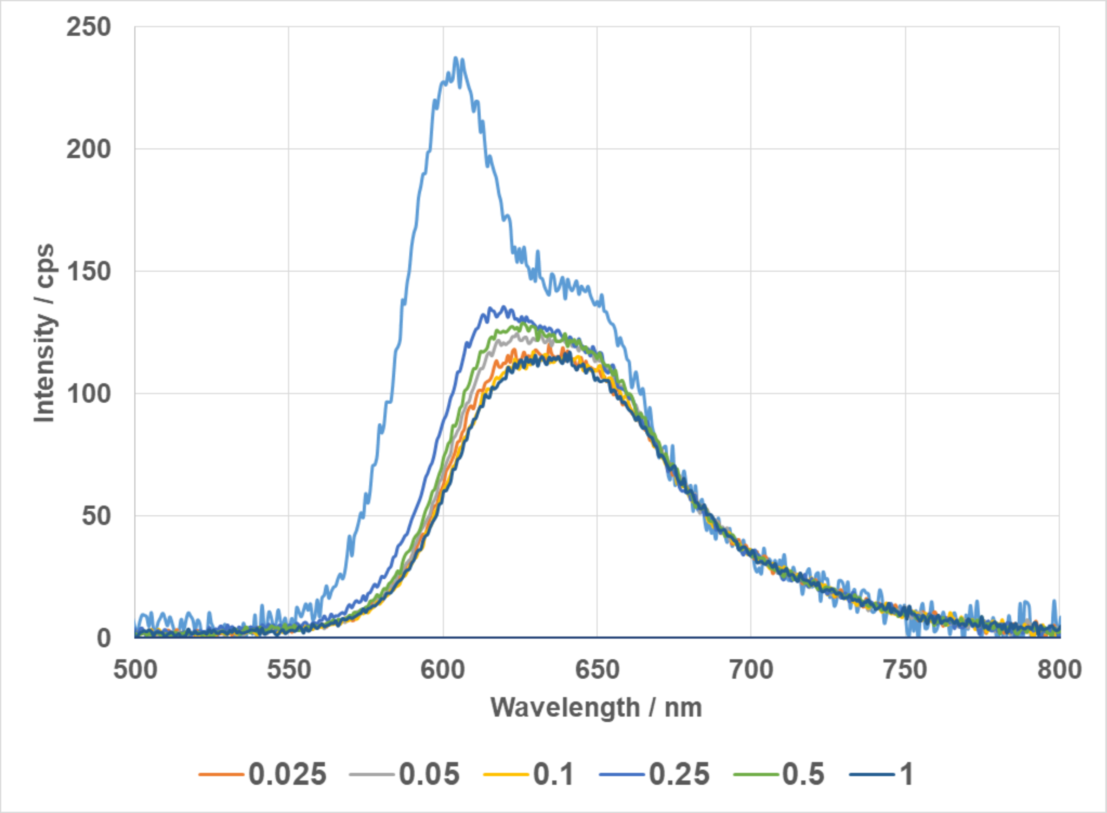

Figure S30. Fitted emission spectra of Dow(1)P2-FC546 X % - 100 ppm (X= 0.025, 0.05, 0.1, 0.25, 0.5, 1.0) after an additional heat treatments (200 °C, 72 h) and the emission spectrum of a very low concentrated sample with virtually zero self-absorption (Dow(1)FC546 - 15 ppm) used for the quantum yield determination, the quantum yield correction and self-absorption coefficient calculations.

SEC

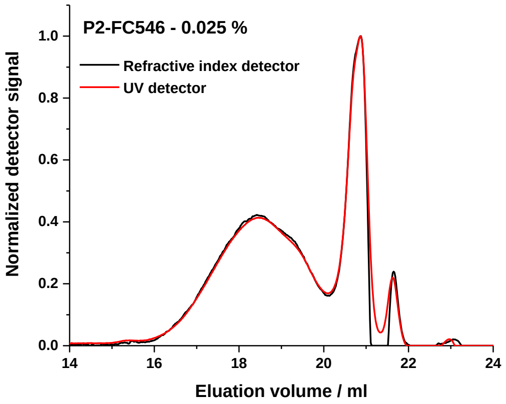

Figure S31. Elugram of P2-FC546 – 0.025 % (2g/l in THF) of the refractive index and UV detector respectively.

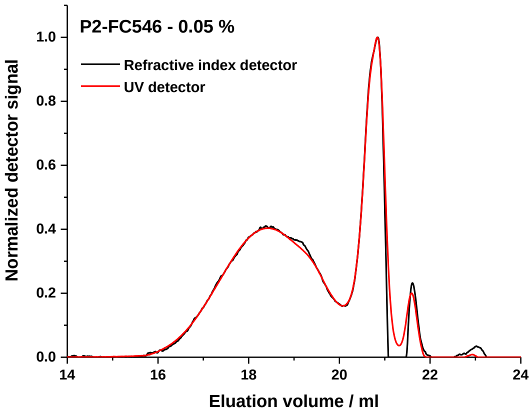

Figure S32. Elugram of P2-FC546 – 0.05 % (2g/l in THF) of the refractive index and UV detector respectively.

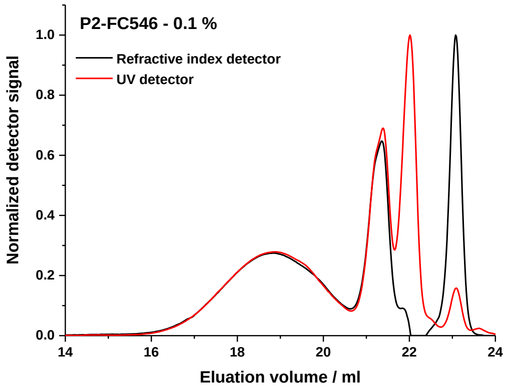

Figure S33. Elugram of P2-FC546 – 0.1 % (2g/l in THF) of the refractive index and UV detector respectively.

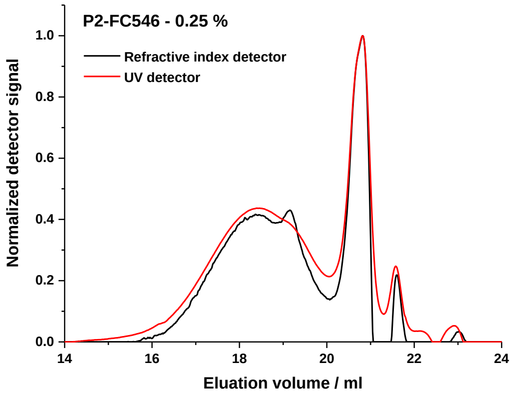

Figure S34. Elugram of P2-FC546 – 0.25 % (2g/l in THF) of the refractive index and UV detector respectively.

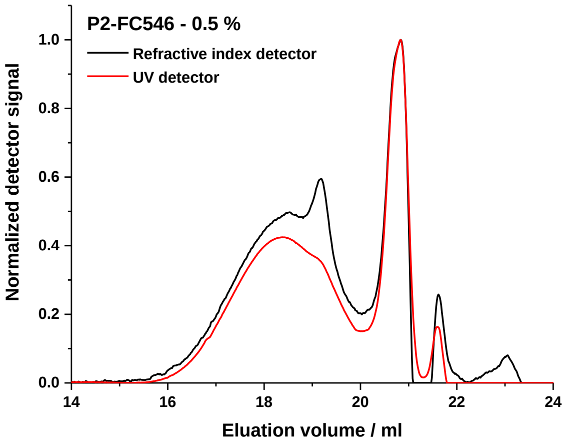

Figure S35. Elugram of P2-FC546 – 0.5 % (2g/l in THF) of the refractive index and UV detector respectively.

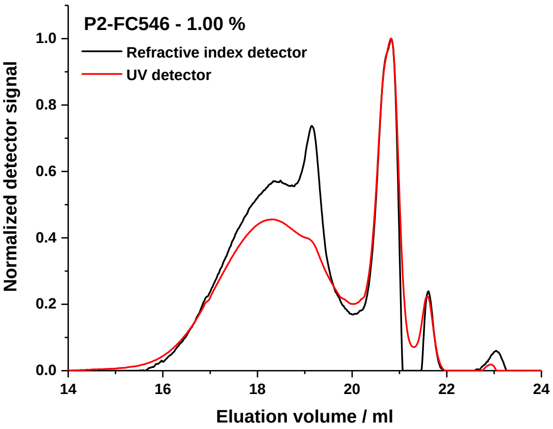

Figure S36. Elugram of P2-FC546 – 1.00 % (2g/l in THF) of the refractive index and UV detector respectively.

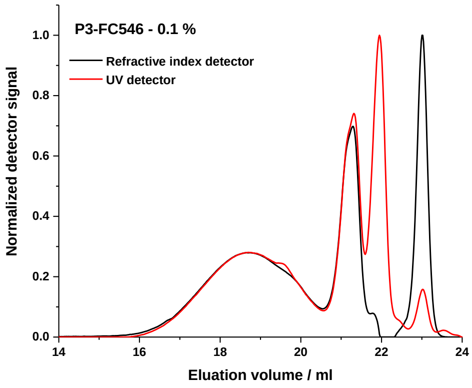

Figure S37. Elugram of P3-FC546 – 0.1 % (2g/l in THF) of the refractive index and UV detector respectively.

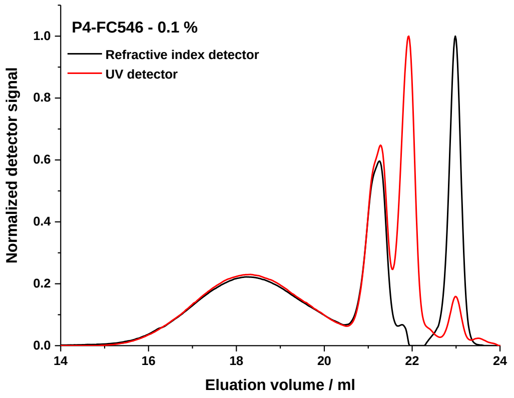

Figure 38. SElugram of P4-FC546 – 0.1 % (2g/l in THF) of the refractive index and UV detector respectively.

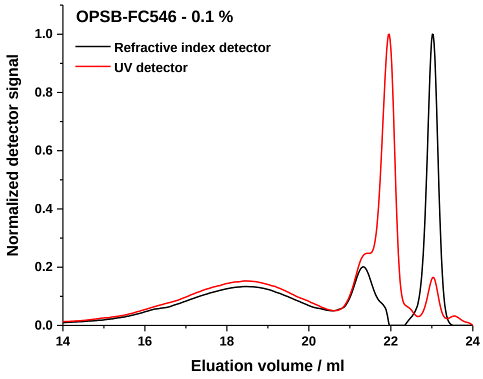

Figure S39. Elugram of OPSB-FC546 – 0.1 % (2g/l in THF) of the refractive index and UV detector respectively.

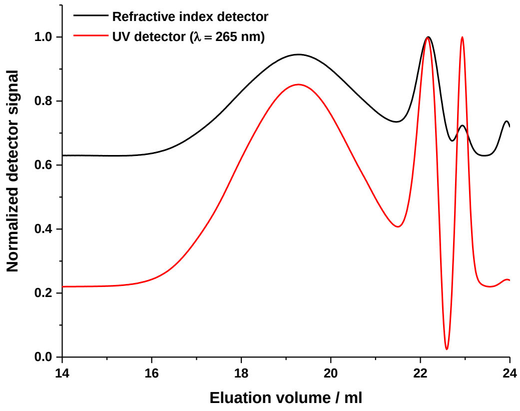

Figure S40. Elugram of OPS (4g/l in THF) of the refractive index and UV detector respectively.

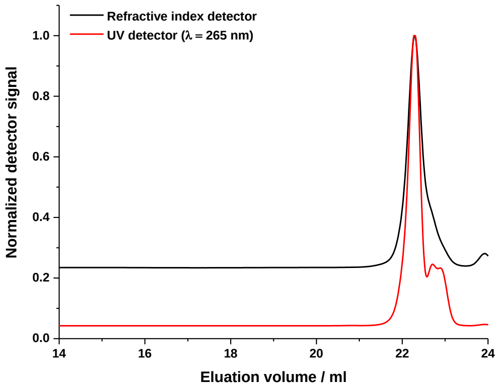

Figure S41. Elugram of PMS H03 (4g/l in THF) of the refractive index and UV detector respectively.

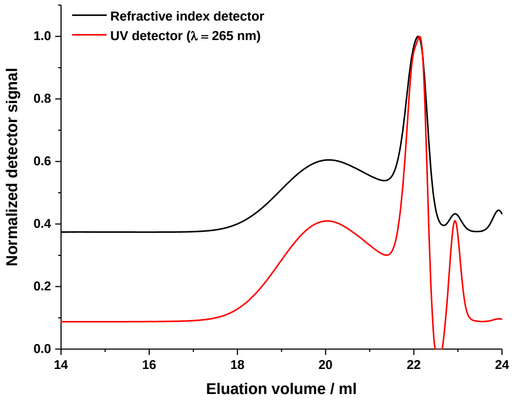

Figure S42. Elugram of PMV 9925 (4g/l in THF) of the refractive index and UV detector respectively.

Table S9. Mw, Mn and D of the measured samples.

	Refractive index detector / UV detector		
	Mw / g mol^{-1}	**Mn / g mol^{-1}**	**D**
PMS-H03	430/420	400/390	1.1
PMV-9925	2420/2500	1020/1100	2.4
OPS-B	1400/1150	5710/5750	4.1
P2-FC546 - *0.025 %*	4980/4890	3090/3090	1.6/1.6
P2-FC546 - *0.05 %*	4890/4850	3060/3060	1.6/1.6
P2-FC546 – *0.1 %*	5660/5530	3360/3360	1.7/1.6
P2-FC546 - *0.25 %*	5400/4820	3140/3140	1.7/1.5
P2-FC546 - *0.5 %*	5030/5030	3130/3130	1.7/1.6
P2-FC546 - *1.0 %*	5660/5020	3240/3240	1.7/1.6
P3-FC546 – 0.1 %	6080/5680	3600/3540	1.7/1.6
P4-FC546 – 0.1 %	8400/8080	4420/4430	1.9/1.8
OPSB-FC546 – 0.1 %	13470/14300	4440/4350	3.1/3.2

Photostability – UV/VIS Data

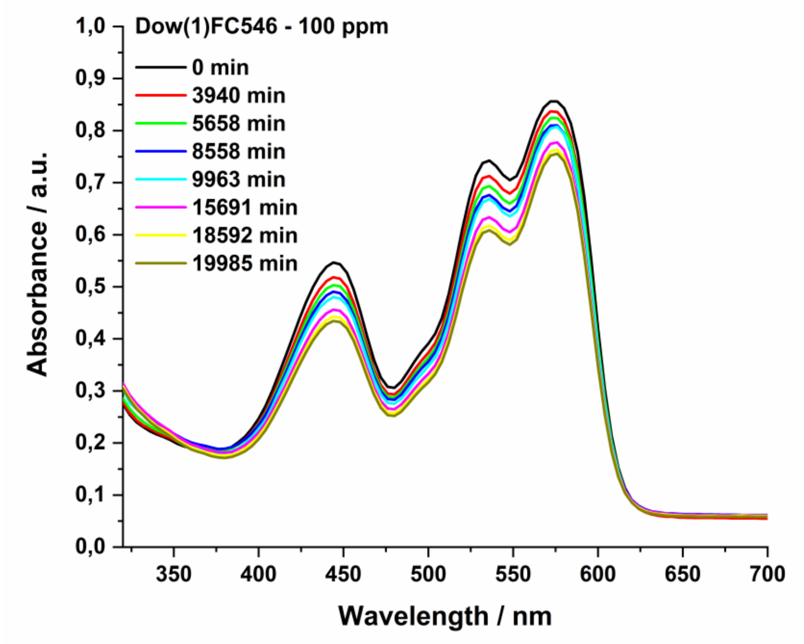

Figure S43. Absorbance spectra of Dow(1)FC546 – 100 ppm measured after given time of exposure to 710 mW LEDs (LDW5SN, 0.45 mA [max.: 0.7 mA]) at 450 nm wavelength under ambient conditions (Air).

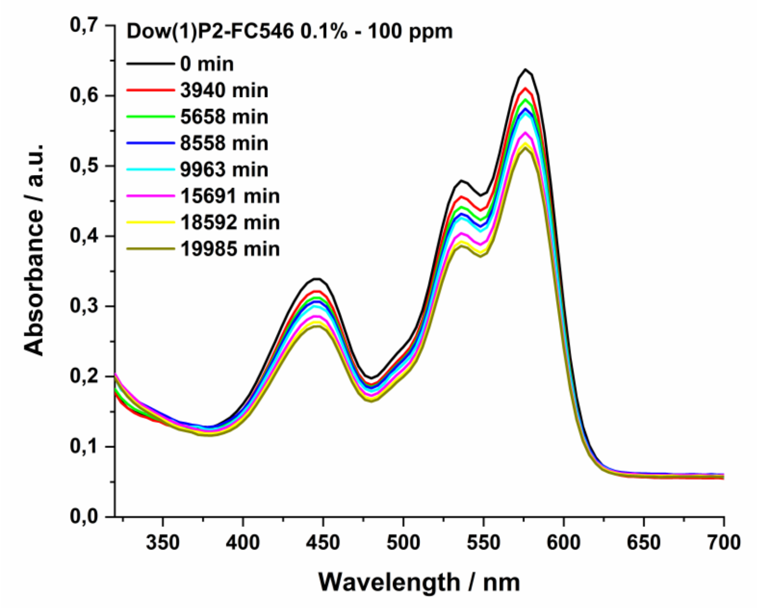

Figure S44. Absorbance spectra of Dow(1)P2-FC546 0.1 % – 100 ppm measured after given time of exposure to 710 mW LEDs (LDW5SN, 0.45 mA [max.: 0.7 mA]) at 450 nm wavelength under ambient conditions (Air).

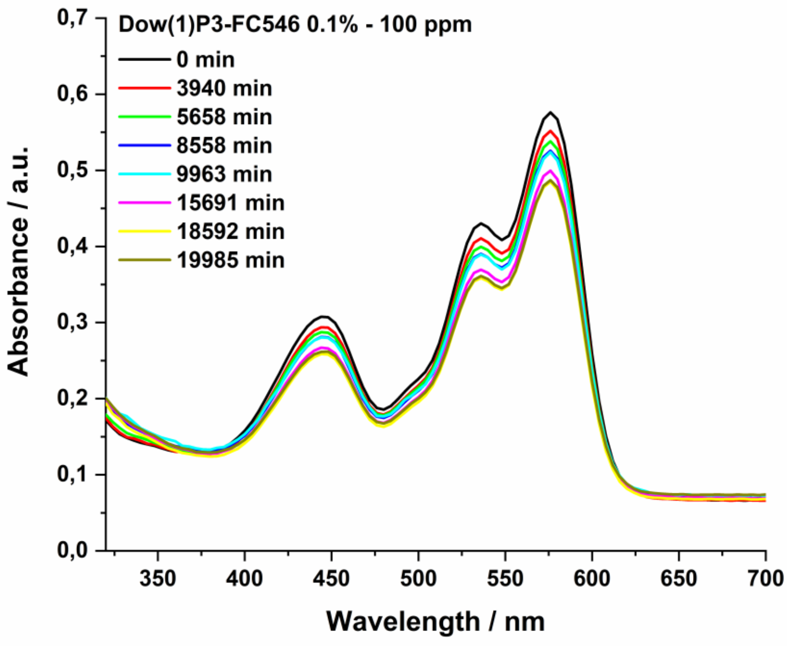

Figure S45. Absorbance spectra of Dow(1)P3-FC546 0.1 % – 100 ppm measured after given time of exposure to 710 mW LEDs (LDW5SN, 0.45 mA [max.: 0.7 mA]) at 450 nm wavelength under ambient conditions (Air).

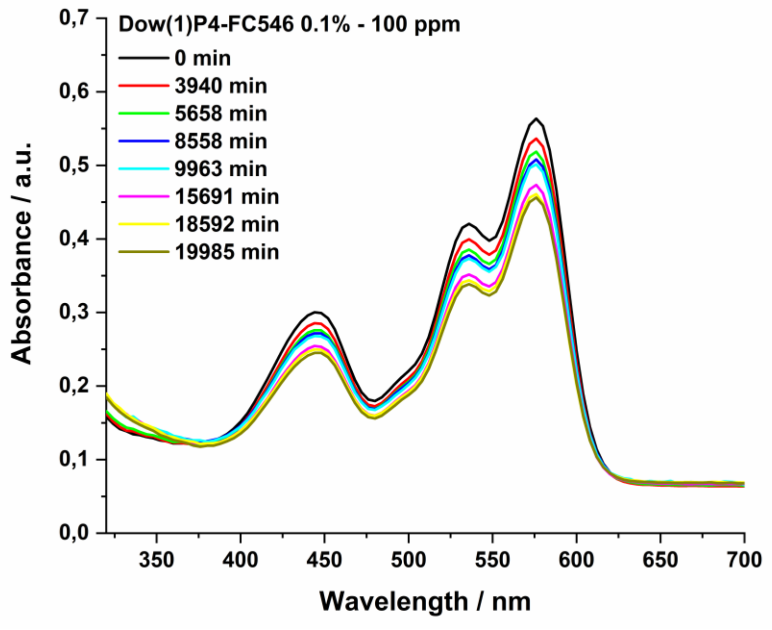

Figure S46. Absorbance spectra of Dow(1)P4-FC546 0.1 % – 100 ppm measured after given time of exposure to 710 mW LEDs (LDW5SN, 0.45 mA [max.: 0.7 mA]) at 450 nm wavelength under ambient conditions (Air).

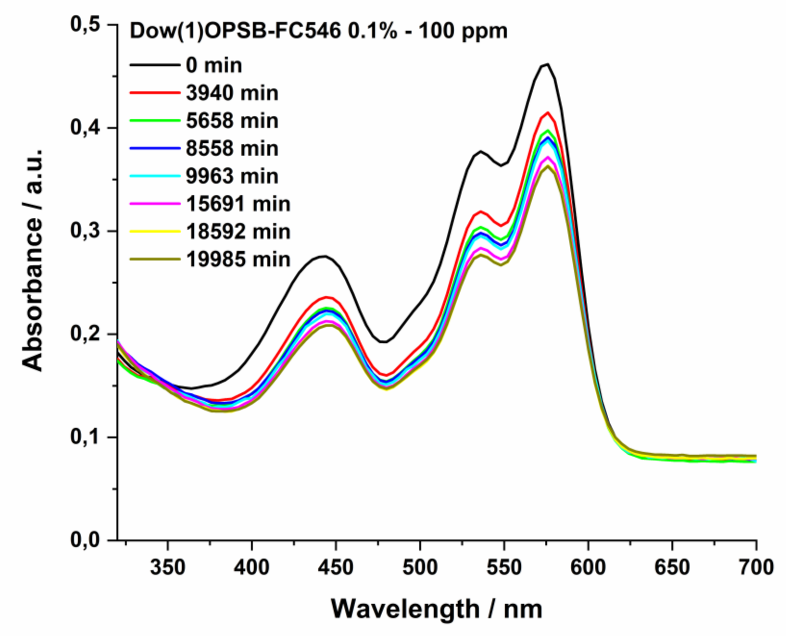

Figure S47. Absorbance spectra of Dow(1)OPSB-FC546 0.1 % – 100 ppm measured after given time of exposure to 710 mW LEDs (LDW5SN, 0.45 mA [max.: 0.7 mA]) at 450 nm wavelength under ambient conditions (Air).

7.3. Platinum free thermally curable Siloxanes for Optoelectronic Application

Supplementary Information

Electronic Supplementary Material (ESI) for RSC Advances.

Supplementary Information

Platinum Free Thermally Curable Siloxanes for Optoelectronic Application – Synthesis and Properties

Nils Steinbrück, Svenja Pohl, Guido Kickelbick*

Saarland University, Inorganic Solid State Chemistry, Campus, Building C4 $_1$, 66123 Saarbrücken, Germany.

E-mail: guido.kickelbick@uni-saarland.de

Contents

NMR spectroscopy

Phenyltrimethoxysilane

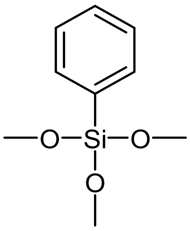

δ_H (400 MHz, $CDCl_3$): 7.71 – 7.34 (5 H, m, Si-Ph), 3.64 (9 H, s, Si-OCH_3)

δ_{Si} (80 MHz, $CDCl_3$): -54.49

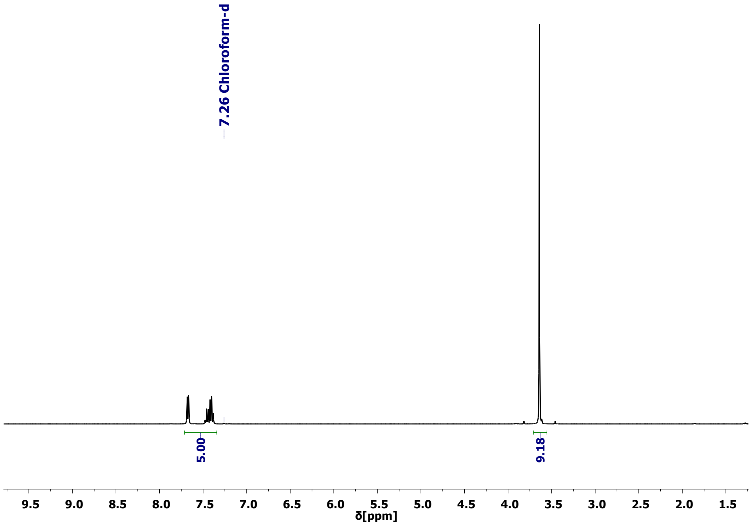

Figure ESI 1. ^1H NMR spectrum of phenyltrimethoxysilane monomer.

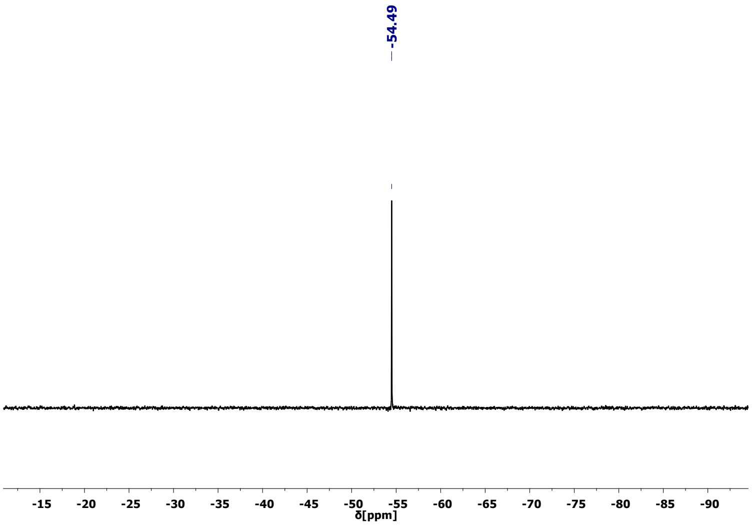

Figure ESI 2. ^{29}Si NMR spectrum of phenyltrimethoxysilane monomer.

Methyltrimethoxysilane

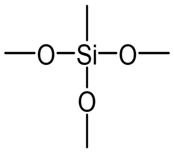

δ_H (300 MHz, $CDCl_3$): 3.50 (9 H, s, Si-OCH_3), 0.06 (3 H, s, Si-CH_3)

δ_{Si} (60 MHz, $CDCl_3$): -39.17

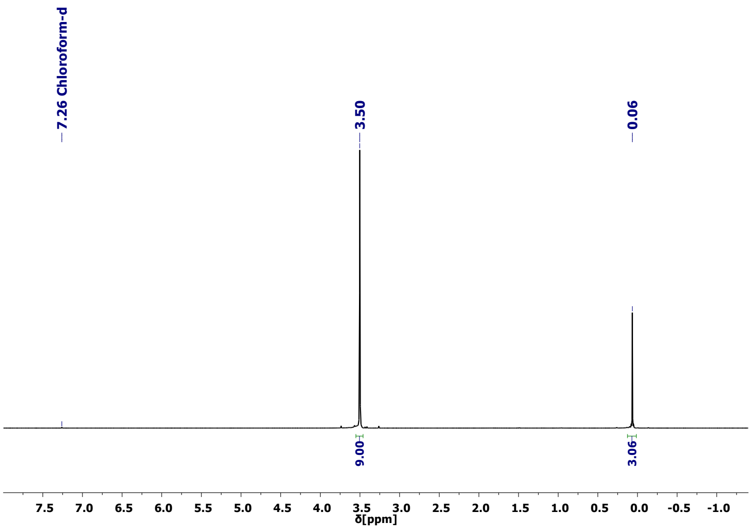

Figure ESI 3. ^{1}H NMR spectrum of methyltrimethoxysilane monomer.

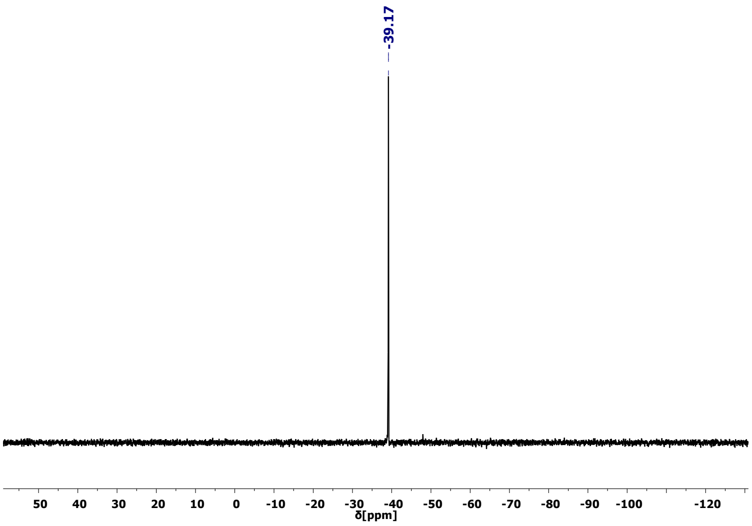

Figure ESI 4. ^{29}Si NMR spectrum of methyltrimethoxysilane monomer.

Dimethyldimethoxysilane

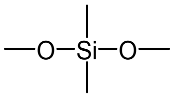

δ_H (400 MHz, $CDCl_3$): 3.39 (6 H, s, Si-OCH_3), 0.00 (6 H, s, Si-CH_3)

δ_{Si} (60 MHz, $CDCl_3$): -0.31

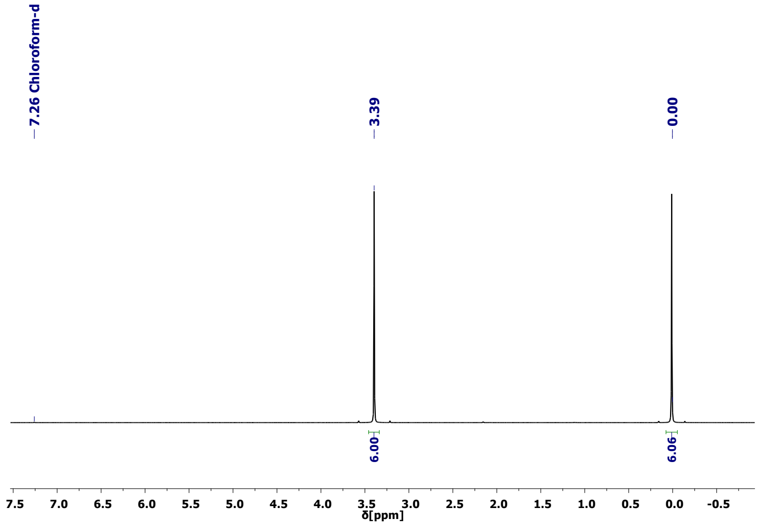

Figure ESI 5. ^1H NMR spectrum of dimethyldimethoxysilane monomer.

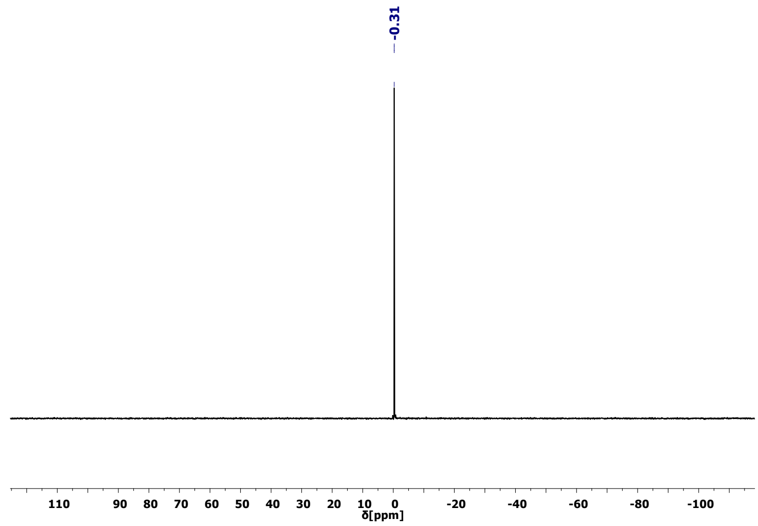

Figure ESI 6. ^{29}Si NMR spectrum of dimethyldimethoxysilane monomer.

Methoxy terminated Polydimethylsiloxane

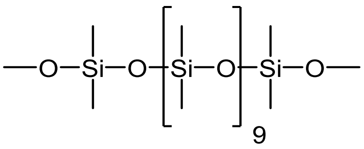

δ_H (300 MHz, $CDCl_3$): 3.45 (6 H, s, Si-OCH_3), 0.20 – -0.01 (65 H, m, Si-CH_3)

δ_{Si} (60 MHz, $CDCl_3$): -10.18 – -11.31 (m), -20.76 – -22.21 (m)

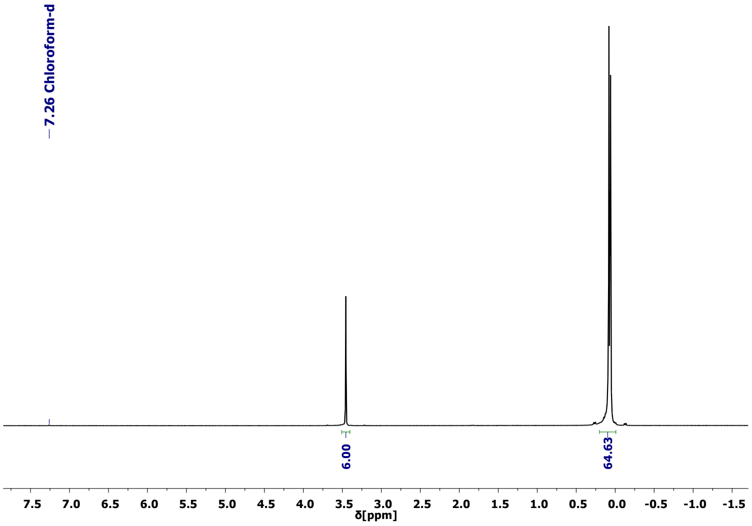

Figure ESI 7. ^{1}H NMR spectrum of methoxy-terminated polydimethylsiloxane oligomer.

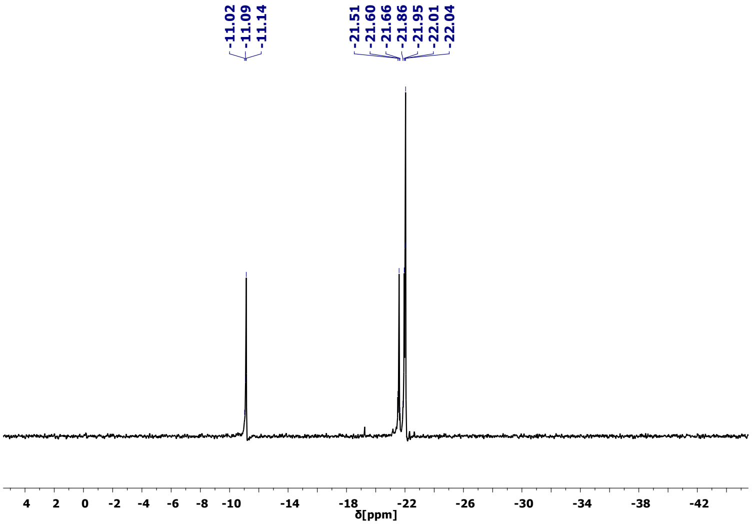

Figure ESI 8. ^{29}Si NMR spectrum of methoxy-terminated polydimethylsiloxane oligomer.

Sample 1 – after 3h of condensation

δ_H (300 MHz, $CDCl_3$): 8.08 – 6.88 (5 H, m, Si-Ph), 5.16 – 4.66 (m, $MeOD_4/H_2O$[39]), 3.80 – 2.93 (m, Si-OMe, MeOH, $MeOD_4$), 1.18 (t, *J* 7.0, EtOH[39]), 0.51 – -0.30 (m, Si-Me).

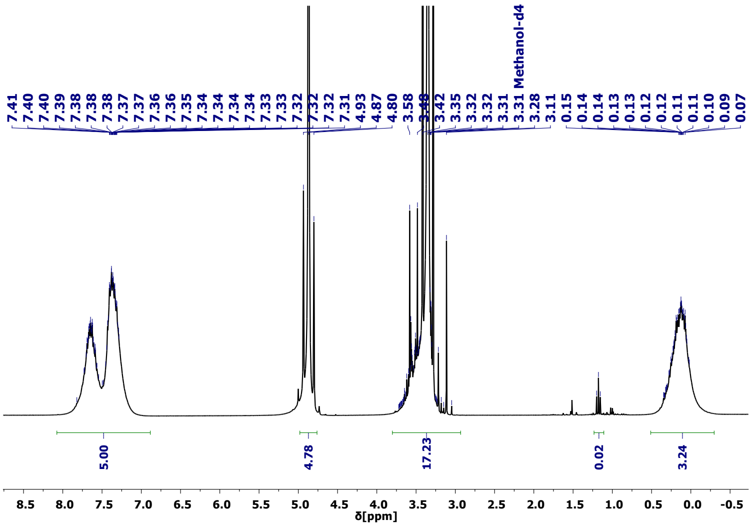

Figure ESI 9. ^1H NMR spectrum of the reaction mixture of sample 1 after 3 h of condensation reaction before methoxy-terminated polydimethylsiloxane was added.

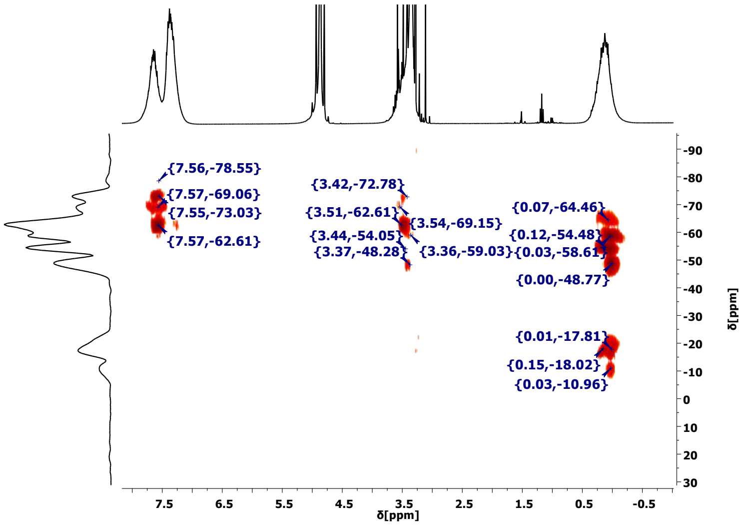

*Figure ESI 10. ^{29}Si-^1H HMBC 2D NMR spectrum of the reaction mixture of sample **1** after 3 h of condensation reaction before methoxy-terminated polydimethylsiloxane was added.*

Sample 1 – unconsolidated Gel

δ_H (300 MHz, $CDCl_3$): 8.08 – 6.88 (m, Si-Ph), 5.16 – 4.66 (m, $MeOD_4/H_2O$[39]), 3.80 – 2.93 (m, Si-OMe, MeOH, $MeOD_4$), 2.14 (s, Acetone[39]), 1.18 (t, *J* 7.0, EtOH[39]), 0.51 – -0.30 (m, Si-Me).

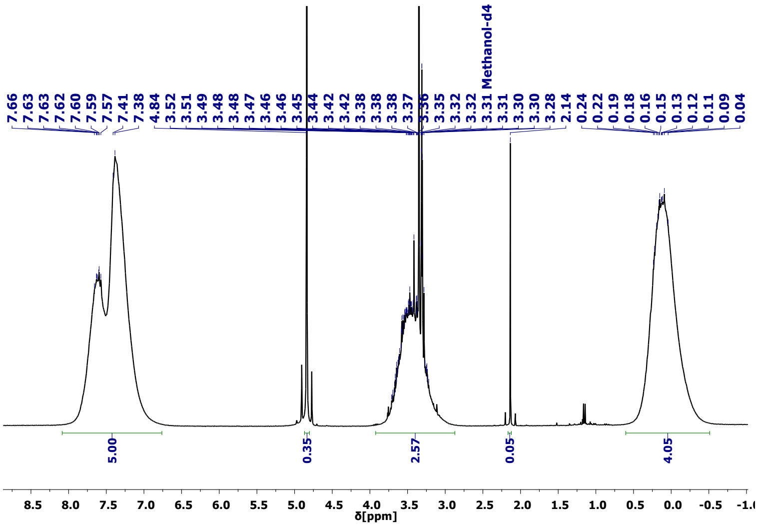

*Figure ESI 11. ^1H NMR spectrum of the unconsolidated gel like sample **1**.*

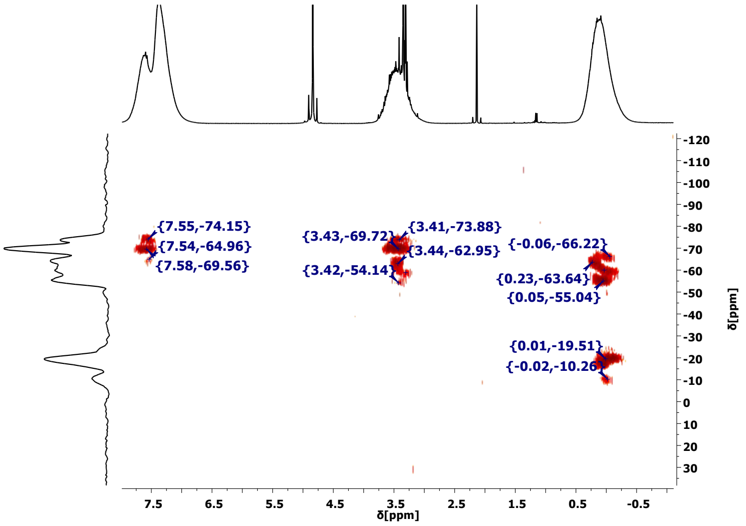

*Figure ESI 12. ^{29}Si-^1H HMBC 2D NMR spectrum of the unconsolidated gel like sample **1**.*

Sample 2 – after 3h of condensation

δ_H (300 MHz, $CDCl_3$): 8.03 – 7.02 (m, Si-Ph), 5.12 – 4.68 (m, $MeOD_4/H_2O$[39]), 3.78 – 2.95 (m, Si-OMe, MeOH, $MeOD_4$), 1.18 (t, *J* 7.0, EtOH[39]), 0.48 – -0.30 (m, Si-Me).

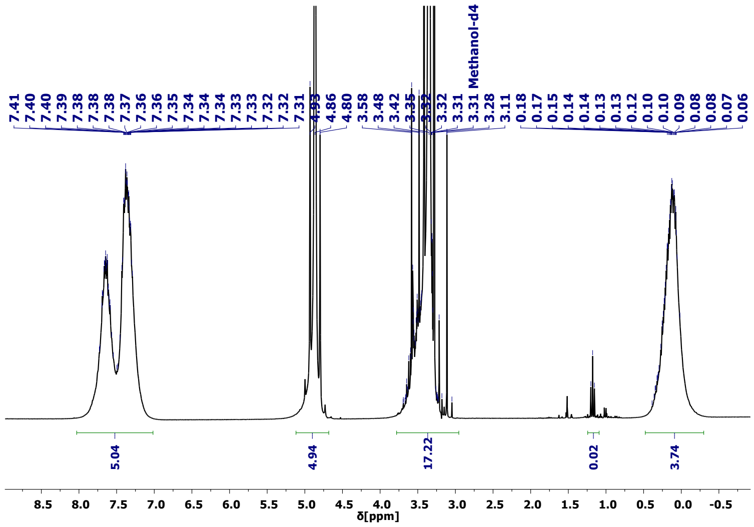

*Figure ESI 13. ^1H NMR spectrum of the reaction mixture of sample **2** after 3 h of condensation reaction before methoxy-terminated polydimethylsiloxane was added.*

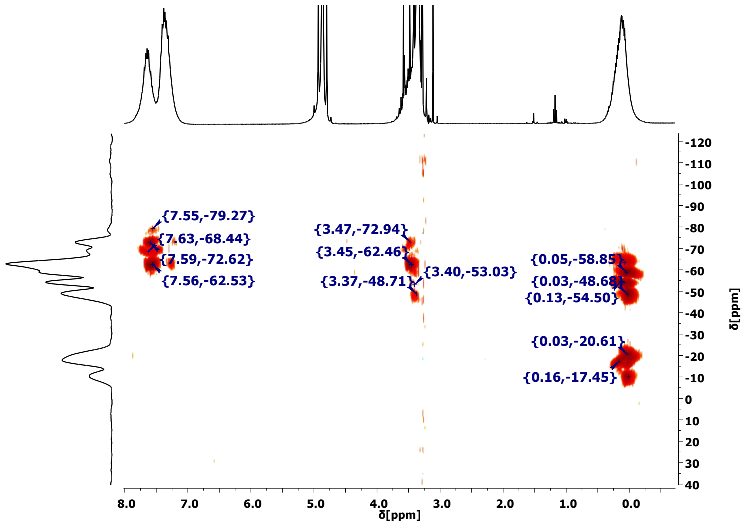

*Figure ESI 14. ^{29}Si-^1H HMBC 2D NMR spectrum of the reaction mixture of sample **2** after 3 h of condensation reaction before methoxy-terminated polydimethylsiloxane was added.*

Sample 2 – unconsolidated gel

δ_H (300 MHz, $CDCl_3$): 8.02 – 6.82 (m, Si-Ph), 5.12 – 4.68 (m, $MeOD_4/H_2O$[39]), 3.87 – 2.95 (m, Si-OMe, MeOH, $MeOD_4$), 2.13 (s, Acetone[39]), 0.52 – -0.47 (m, Si-Me).

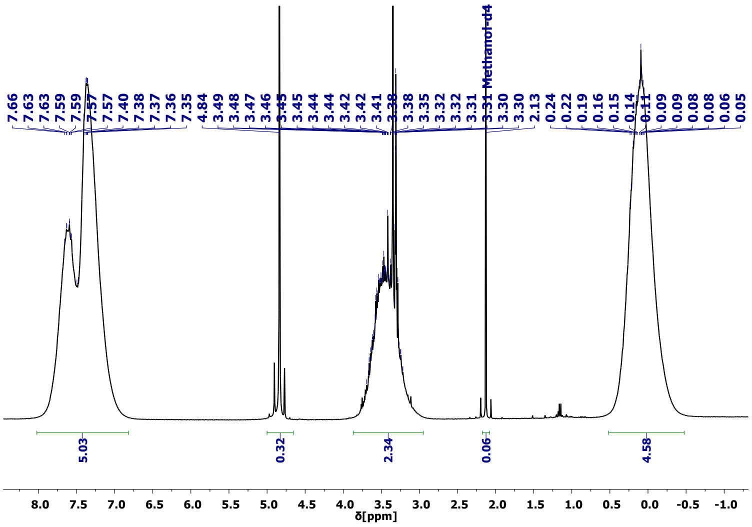

*Figure ESI 15. ¹H NMR spectrum of the unconsolidated gel like sample **2**.*

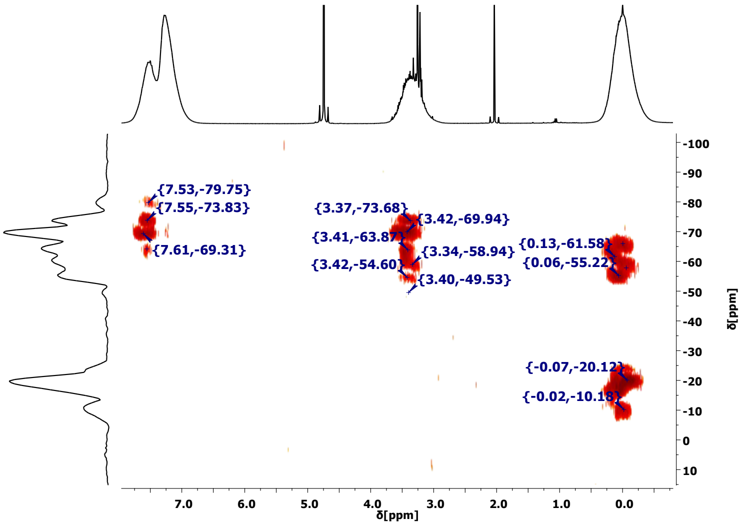

*Figure ESI 16. ^{29}Si-^{1}H HMBC 2D NMR spectrum of the unconsolidated gel like sample **2**.*

Sample 3 – after 3h of condensation

δ_H (300 MHz, $CDCl_3$): 7.95 – 7.01 (m, Si-Ph), 5.13 – 4.67 (m, $MeOD_4/H_2O$[39]), 3.75 – 2.96 (m, Si-OMe, MeOH, $MeOD_4$), 1.18 (t, *J* 7.0, EtOH[39]), 0.49 – -0.34 (m, Si-Me).

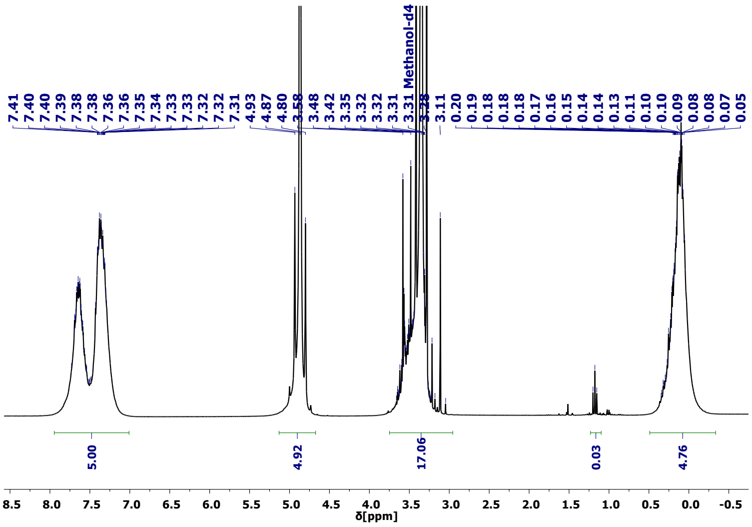

*Figure ESI 17. ^1H NMR spectrum of the reaction mixture of sample **3** after 3 h of condensation reaction before methoxy-terminated polydimethylsiloxane was added.*

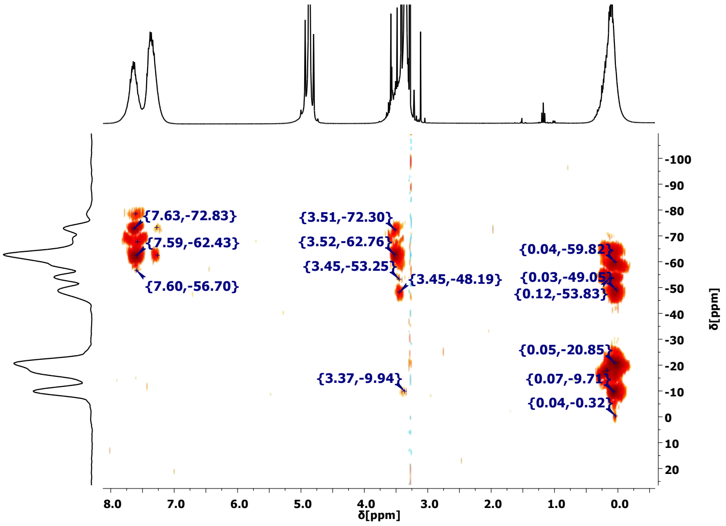

*Figure ESI 18. ^{29}Si-^1H HMBC 2D NMR spectrum of the reaction mixture of sample **3** after 3 h of condensation reaction before methoxy-terminated polydimethylsiloxane was added.*

Sample 3 – unconsolidated gel

δ_H (300 MHz, $CDCl_3$): 8.07 – 6.87 (m, Si-Ph), 5.12 – 4.68 (m, $MeOD_4/H_2O$[39]), 3.87 – 3.01 (m, Si-OMe, MeOH, $MeOD_4$), 2.13 (s, Acetone[39]), 0.47 – -0.43 (m, Si-Me).

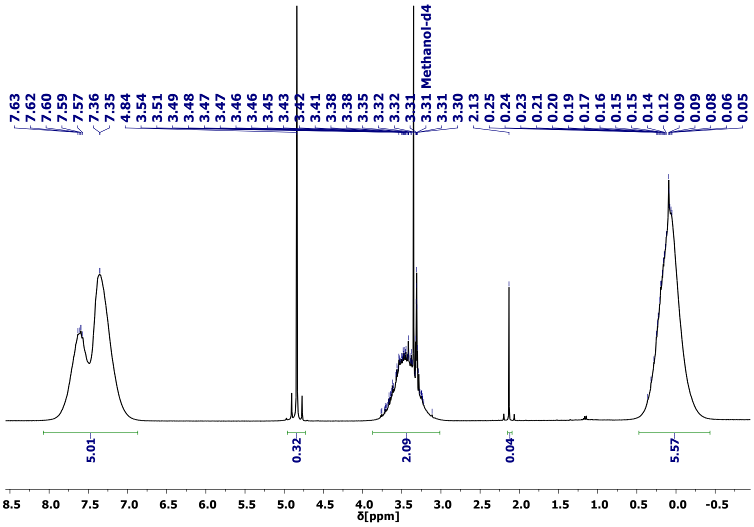

*Figure ESI 19. ^1H NMR spectrum of the unconsolidated gel like sample **3**.*

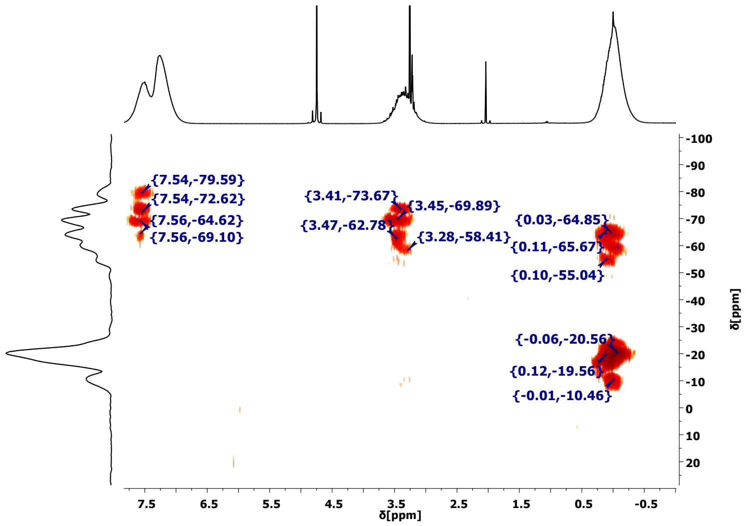

*Figure ESI 20. ^{29}Si-^1H HMBC 2D NMR spectrum of the unconsolidated gel like sample **3**.*

Sample 4 – unconsolidated gel

δ$_H$ (300 MHz, CDCl$_3$): 7.95 – 6.83 (m, Si-Ph), 5.12 – 4.68 (m, MeOD$_4$/H$_2$O[39]), 3.83 – 2.94 (m, Si-OMe, MeOH, MeOD$_4$), 1.89 – 1.82 (m, unspecific impurity), 0.55 – -0.43 (m, Si-Me).

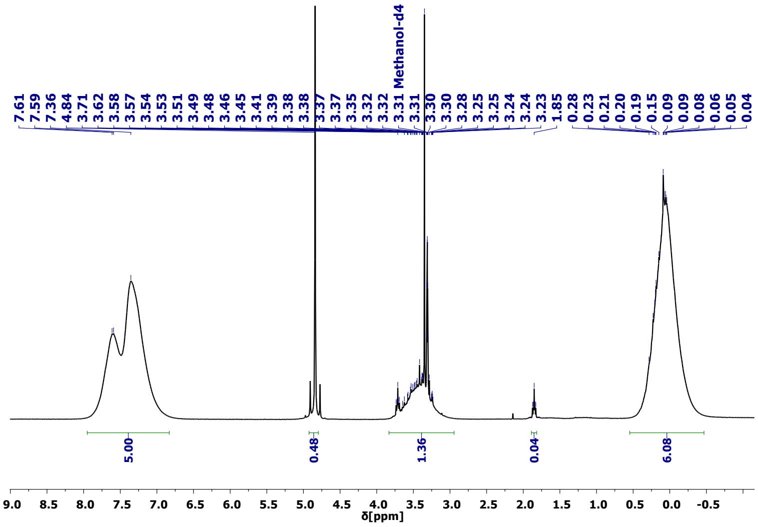

*Figure ESI 21. ^{1}H NMR spectrum of the unconsolidated gel like sample **4**.*

Sample 5 – unconsolidated gel

δ$_H$ (300 MHz, CDCl$_3$): 8.08 – 6.80 (m, Si-Ph), 5.12 – 4.68 (m, MeOD$_4$/H$_2$O[39]), 3.79 – 2.99 (m, Si-OMe, MeOH, MeOD$_4$), 0.63 – -0.52 (m, Si-Me).

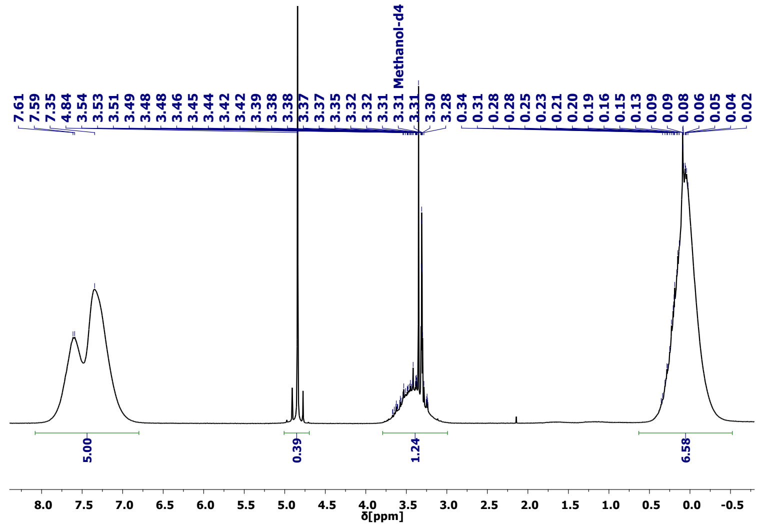

*Figure ESI 22. ^{1}H NMR spectrum of the unconsolidated gel like sample **5**.*

Sample 6 – unconsolidated gel

δ_H (300 MHz, $CDCl_3$): 7.99 – 6.78 (m, Si-Ph), 5.12 – 4.68 (m, $MeOD_4/H_2O$[39]), 3.80 – 3.06 (m, Si-OMe, MeOH, $MeOD_4$), 0.53 – -0.46 (m, Si-Me).

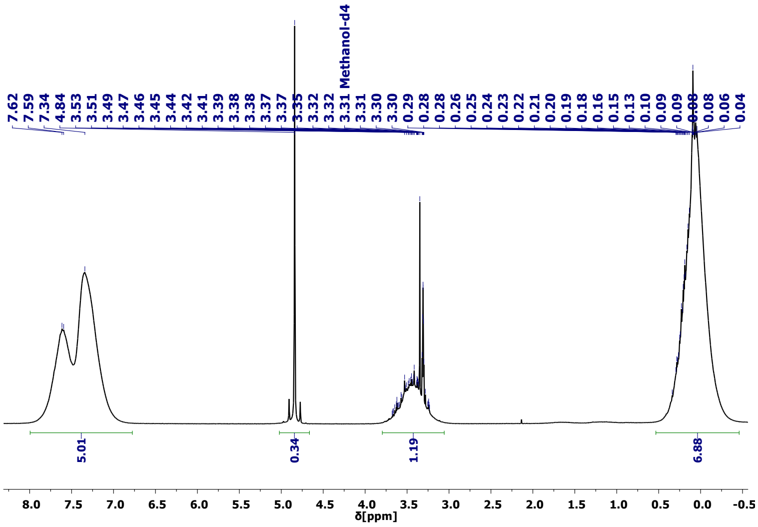

*Figure ESI 23. ^1H NMR spectrum of the unconsolidated gel like sample **6**.*

Sample 7 – unconsolidated gel

δ_H (300 MHz, $CDCl_3$): 8.02 – 6.82 (m, Si-Ph), 5.12 – 4.68 (m, $MeOD_4/H_2O$[39]), (m, Si-OMe, MeOH, $MeOD_4$), 0.57 – -0.45 (m, Si-Me).

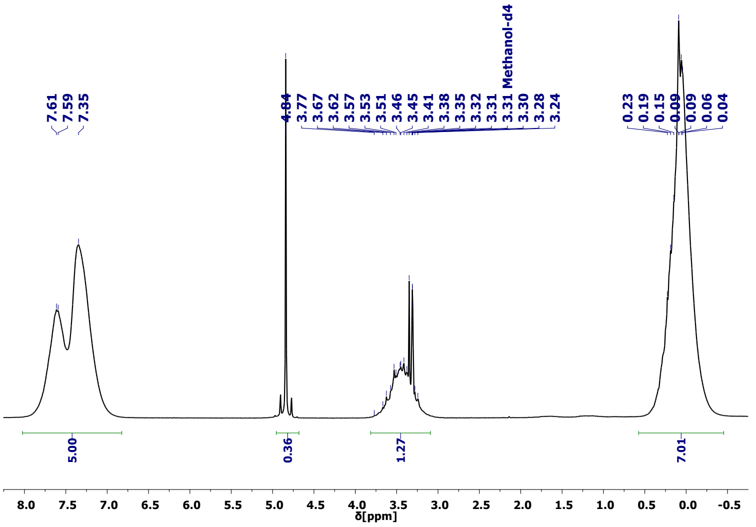

*Figure ESI 24. ^1H NMR spectrum of the unconsolidated gel like sample **7**.*

Sample 8 – after 3h of condensation

δ_H (300 MHz, CDCl$_3$): 7.85 – 7.13 (m, Si-Ph), 5.10 – 4.65 (m, MeOD$_4$/H$_2$O[39]), 3.83 – 2.89 (m, Si-OMe, MeOH, MeOD$_4$), 1.18 (t, *J* 7.0, EtOH[39]), 0.43 – -0.20 (m, Si-Me).

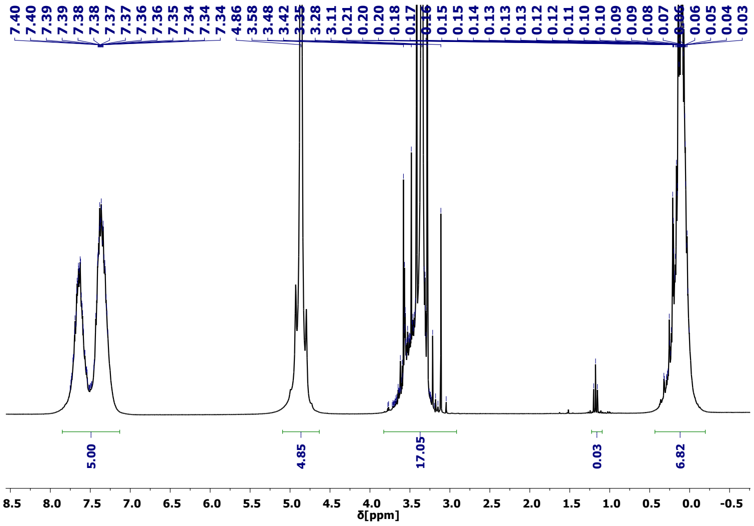

*Figure ESI 25. ^{1}H NMR spectrum of the reaction mixture of sample **8** after 3 h of condensation reaction before methoxy-terminated polydimethylsiloxane was added.*

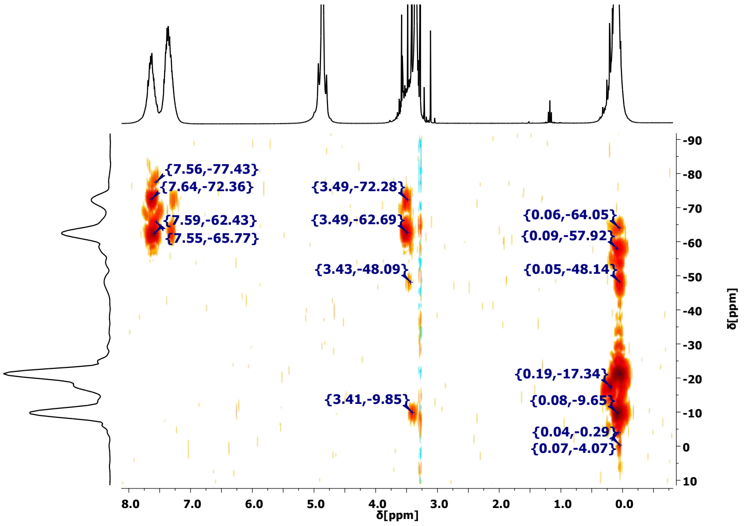

*Figure ESI 26. ^{29}Si-^{1}H HMBC 2D NMR spectrum of the reaction mixture of sample **8** after 3 h of condensation reaction before methoxy-terminated polydimethylsiloxane was added.*

Sample 8 – unconsolidated gel

δ_H (300 MHz, $CDCl_3$): 8.09 – 6.85 (m, Si-Ph), 5.12 – 4.68 (m, $MeOD_4/H_2O$[39]), 3.87 – 3.11 (m, Si-OMe, MeOH, $MeOD_4$), 2.10 (s, Acetone[39]), 0.62 – -0.38 (m, Si-Me).

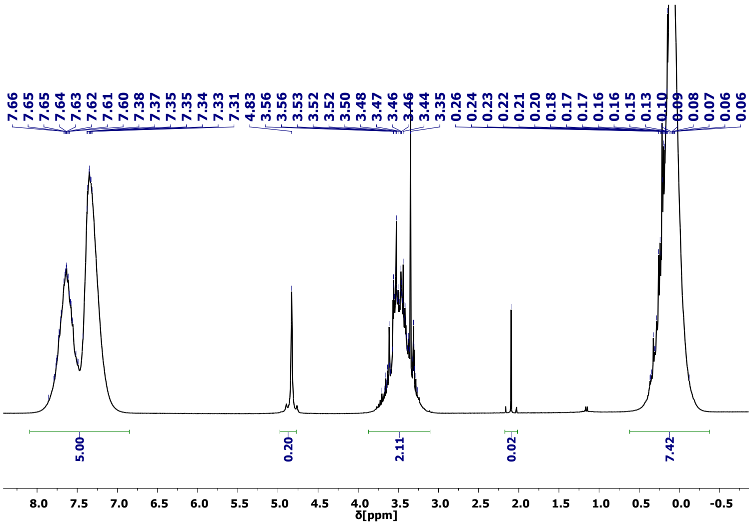

*Figure ESI 27. ^{1}H NMR spectrum of the unconsolidated gel like sample **8**.*

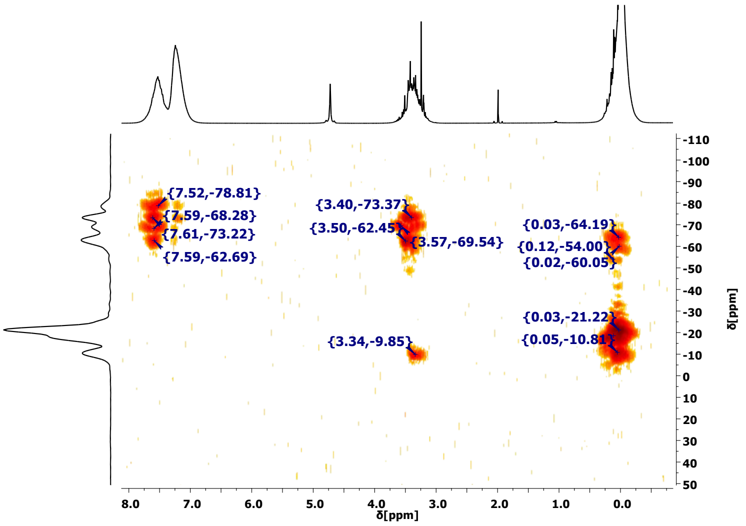

*Figure ESI 28. ^{29}Si-^{1}H HMBC 2D NMR spectrum of the unconsolidated gel like sample **8**.*

FTIR spectroscopy

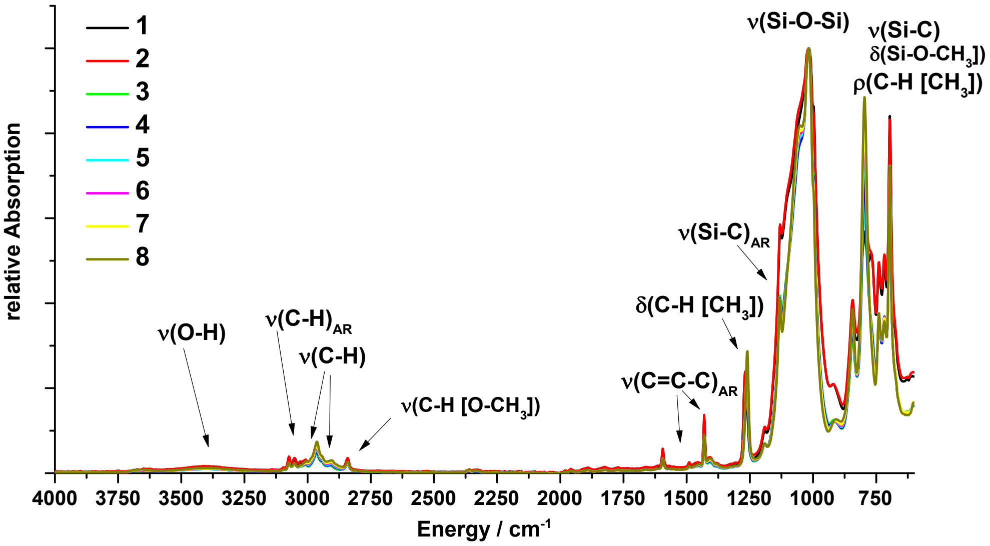

*Figure ESI 29. FTIR spectra of sample **1** – **8** with the main vibration bands noted.*

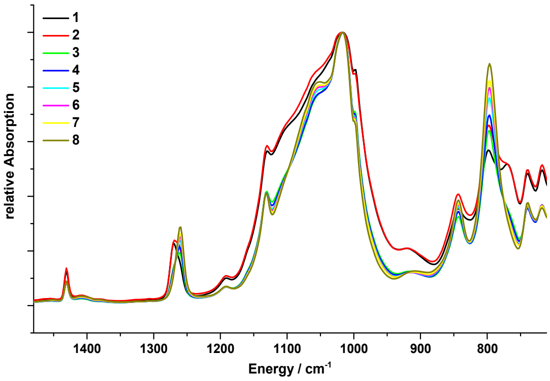

*Figure ESI 30. Enlarged segment of the FTIR spectra of sample **1** – **8**, illustrating the differences in shape of the Si-O-Si vibration bands at 1052 and 1016 cm^{-1} of the unconsolidated gels.*

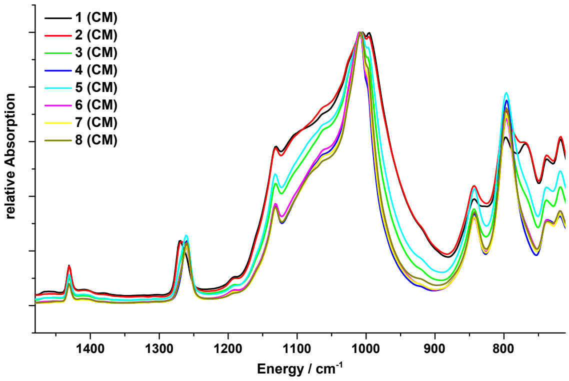

*Figure ESI 31. Enlarged segment of the FTIR spectra of sample **1** – **8**, illustrating the differences in shape of the Si-O-Si vibration bands at 1052 and 1016 cm^{-1} of the consolidated materials.*

Aging Experiments

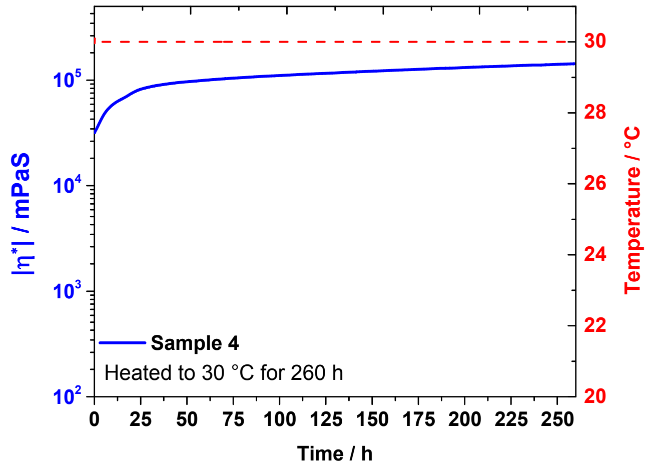

*Figure ESI 32. Absolute value of viscosity of sample **4** measured isothermally at 30 °C for 260h with an amplitude of 5%, a frequency of 1 Hz and a normal force value of 0.*

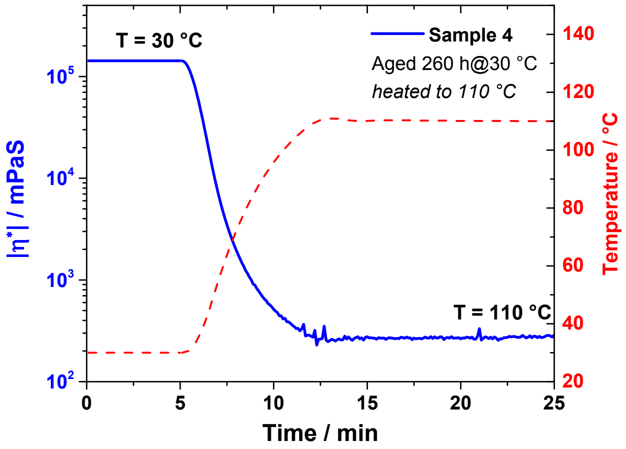

*Figure ESI 33. Absolute value of viscosity of sample **4** at 110 °C after heating it isothermally at 30 °C for 260h. Measured with an amplitude of 5%, a frequency of 1 Hz and a normal force value of 0.*

^{13}C CP-MAS-NMR

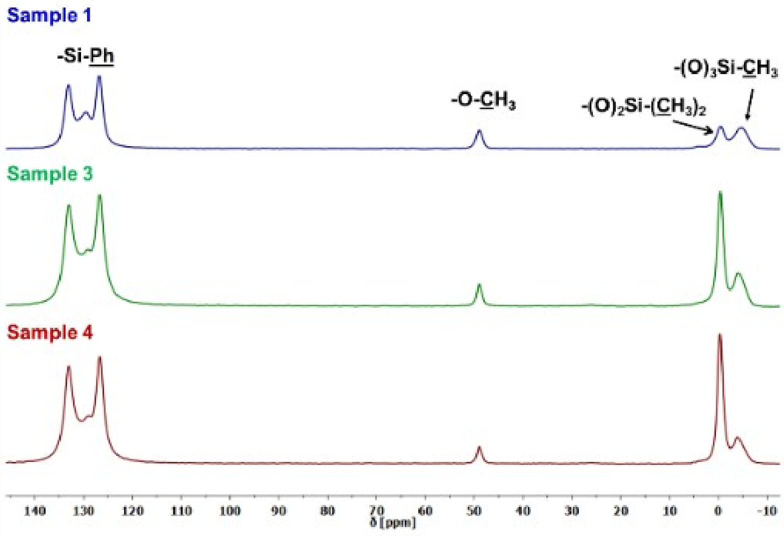

*Figure ESI 34. ^{13}C CP-MAS-NMR spectra of the cured samples **1, 3** and **5**.*

Thermogravimetric studies

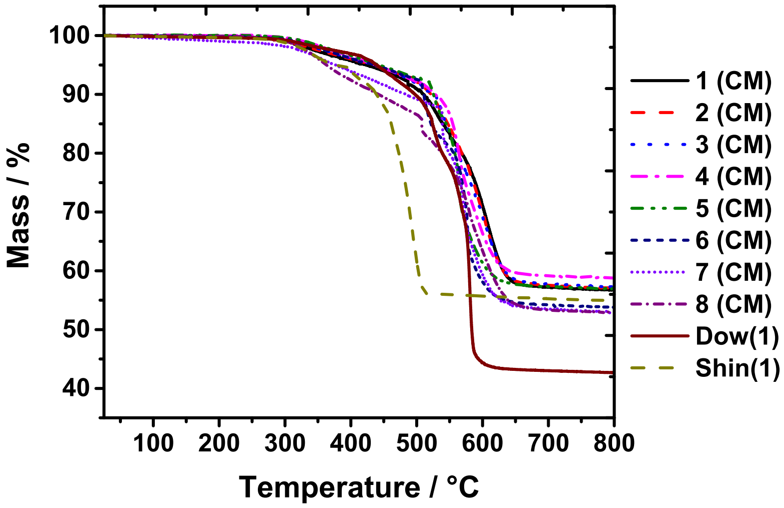

*Figure ESI 35. Thermogravimetric mass loss curve of sample **1** – **8** and the two reference encapsulation silicones Dow Corning OE6630 [Dow(1] and ShinEtsu KJR9022E [Shin(1)].*

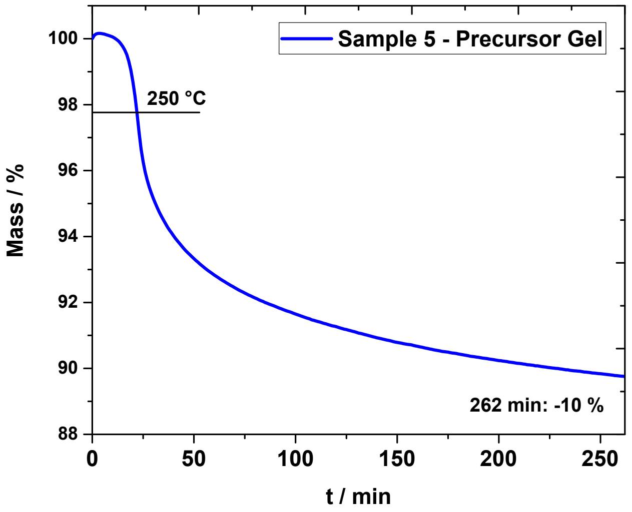

*Figure ESI 36. Thermogravimetric mass loss curve of sample **5** at isothermally 250 °C for 250 min. A mass loss of -10% was detected.*

DSC measurments

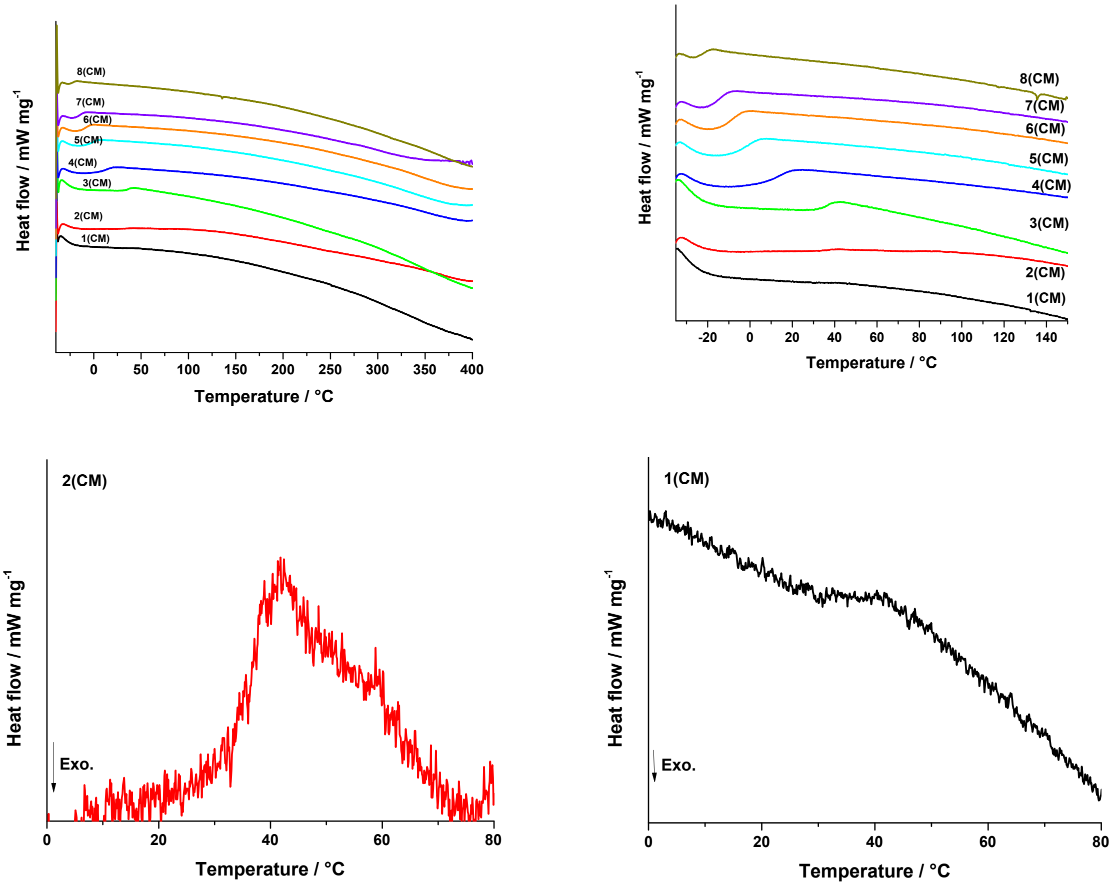

*Figure ESI 37. DSC measurements of the consolidated samples **3 – 8** measured from -40 to 400 °C with 5K/min under N_2 atmosphere (100 ml/min). The T_g value indicated by an inflection of the DSC curve increases with the hardness of the sample caused by a higher cross-linked structure. Enlarged curves of samples **1 and 2** show decrease in signal intensity.*

Transmission spectroscopy

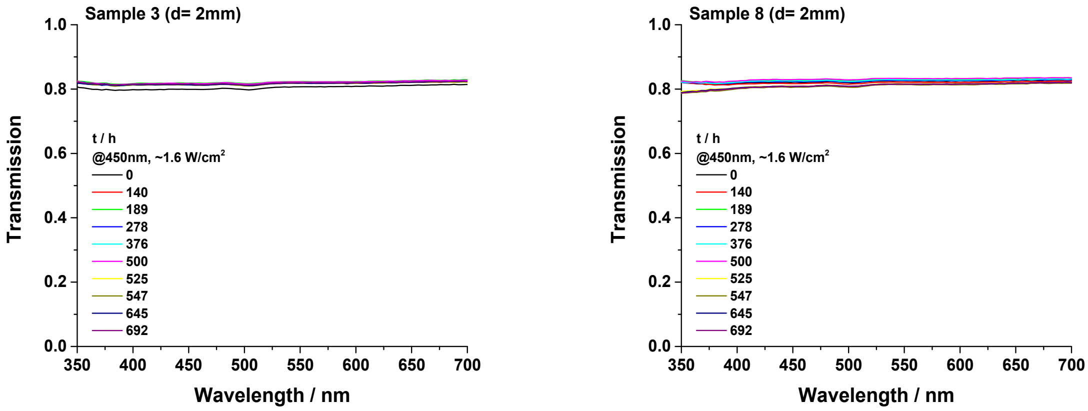

Figure ESI 38. Transmission spectra of the consolidated samples ***3*** *and* ***8*** *after the given time of irradiation at 450 nm with ~1600 mW/cm^2 and 60°C. There are no systematic changes detectable*

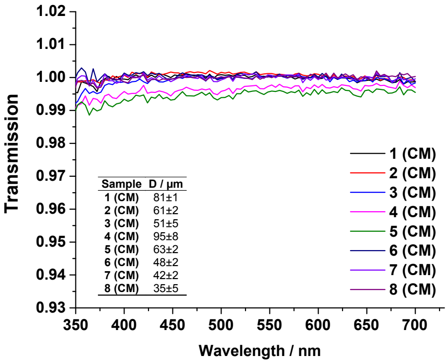

Figure ESI 39. Transmission and thickness of films of sample ***1*** *–* ***8*** *after consolidation at 200 °C for 1170 h. All samples show a minimum transmission of 0.98 in the measured wavelength range.*

.

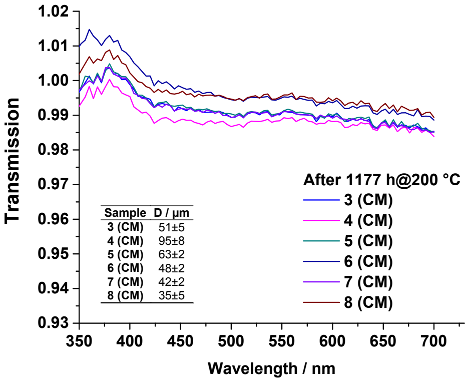

Figure ESI 40. Transmission and thickness of films of sample ***1*** *–* ***8*** *after a heat treatment at 200 °C for 1177 h.*

LED packaging demonstration

Packaging materials for optoelectronic devices needs to be castable, curable and sealed. The subsequently consolidated matrix needs to be crack and bubble free as well as elastic. To demonstrate the processability of the precursor polysiloxanes a polyphtalamide LED lead frame (1.4 x 0.7 x 0.4 mm) was casted with sample **4** and **6** by hand. The filled lead frames were heat treated to cure the polymers (160 °C, 20 h).

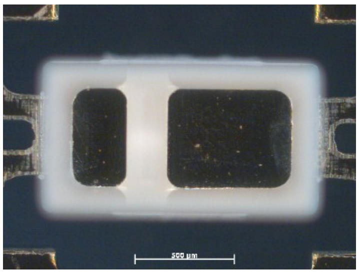

Figure ESI 41. Empty lead frame. Picture focused on the frames metal base.

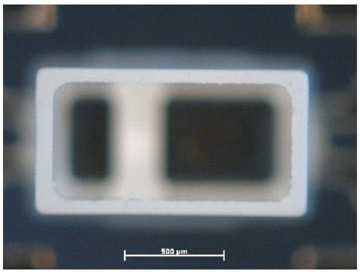

Figure ESI 42. Empty lead frame. Picture focused on the upper edge of the frame.

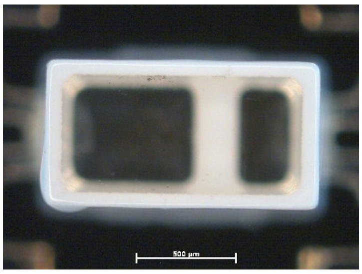

*Figure ESI 43. Lead frame filled with a smooth and transparent cast of sample **4**. Color impression is caused by the metallic base plate.*

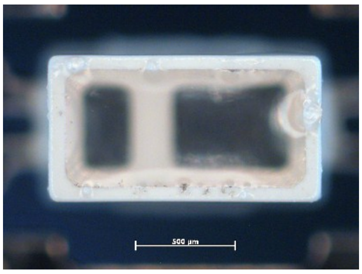

*Figure ESI 44. Lead frame with consolidated sample **4**. Color impression is caused by the metallic base plate.*

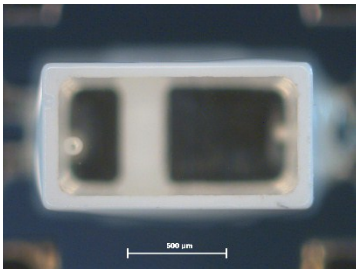

*Figure ESI 45. Lead frame filled with a smooth and transparent cast of sample **6**. Bubbles caused by the injection disappear after curing. Color impression is caused by the metallic base plate.*

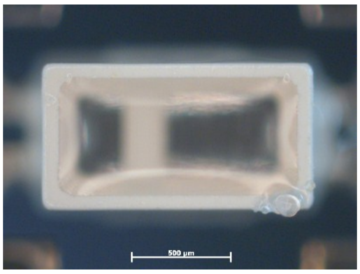

*Figure ESI 46. Lead frame with consolidated sample **6**. Color impression is caused by the metallic base plate*

Due to the difficult microscope supported injection by hand, the quality of the cast is not as good as automated industrial castings, indicated by overtopping and the small bumps of the consolidated gel on the lead frames edges. Both casted gel materials showed a very good processability. After the consolidation no bubbles or cracks inside the material can be detected. Shrinkage of the material is indicated by the convergence on the lead frames flanks. In summary, the materials are suitable as packaging material for LED applications.

7.4. Fluorescent Polysilsesquioxane Hybrid Glass Microspheres

Supplementary Information

Fluorescent Polysilsesquioxane Hybrid Glass Microspheres

Nils Steinbrück, Svenja Pohl, Guido Kickelbick*
Saarland University, Inorganic Solid State Chemistry, Campus, Building C4 $_1$,
66123 Saarbrücken, Germany.
E-mail: guido.kickelbick@uni-saarland.de

NMR Data

Phenyltrimethoxysilane

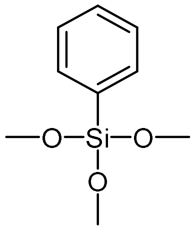

δ_H (400 MHz, $CDCl_3$): 7.71 – 7.34 (5 H, m, Si-Ph), 3.64 (9 H, s, Si-OCH_3)

δ_{Si} (80 MHz, $CDCl_3$): -54.49

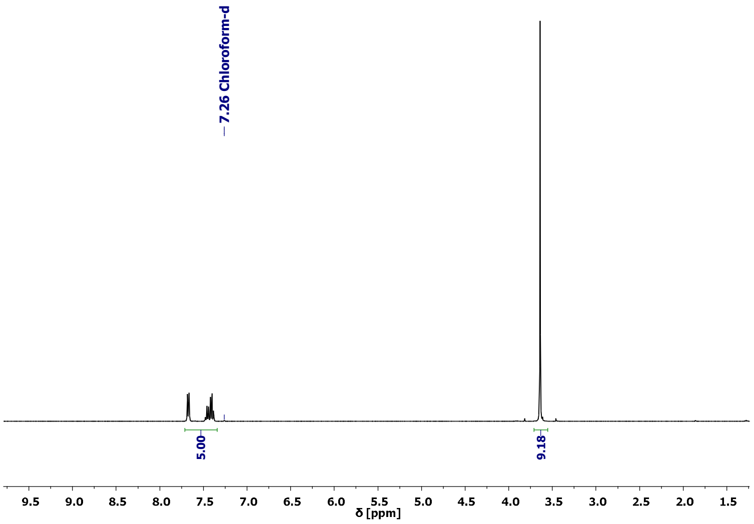

*ESI1. ^{1}H NMR spectrum of **phenyltrimethoxysilane** monomer.*

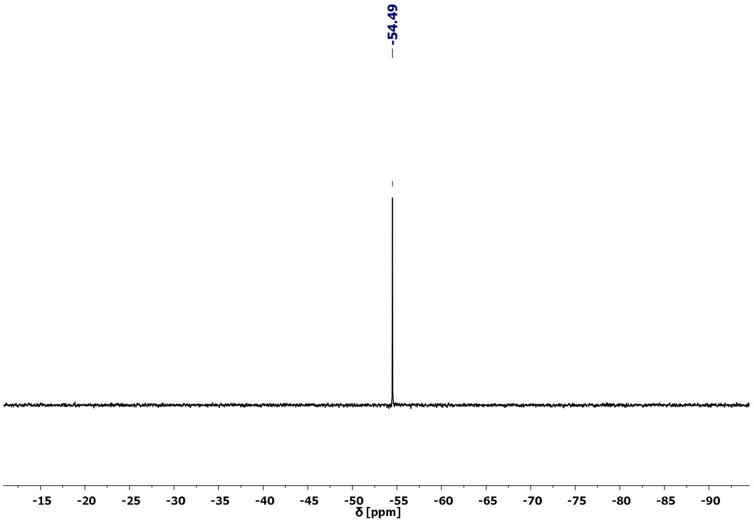

*ESI2. The ^{29}Si NMR spectrum of **phenyltrimethoxysilane** monomer.*

MG Precursor (MG LG305)

δ_H (300 MHz, $CDCl_3$): 8.07 – 6.84 (m, Phenyl), 3.96 – 2.97 (m, MeOR [R= H, CH_3]), (s, silicone grease impurity).

δ_{Si} (^{29}Si-^{1}H HMBC, 300/59 MHz, $CDCl_3$): -70 (T^2), -77.25 (T^3) , -22 (D^2, Silicone grease)

δ_C (^{13}C, 75 MHz, $CDCl_3$): -134.26, -130.67,-127.93 (Ph), -50.78 (-OMe)

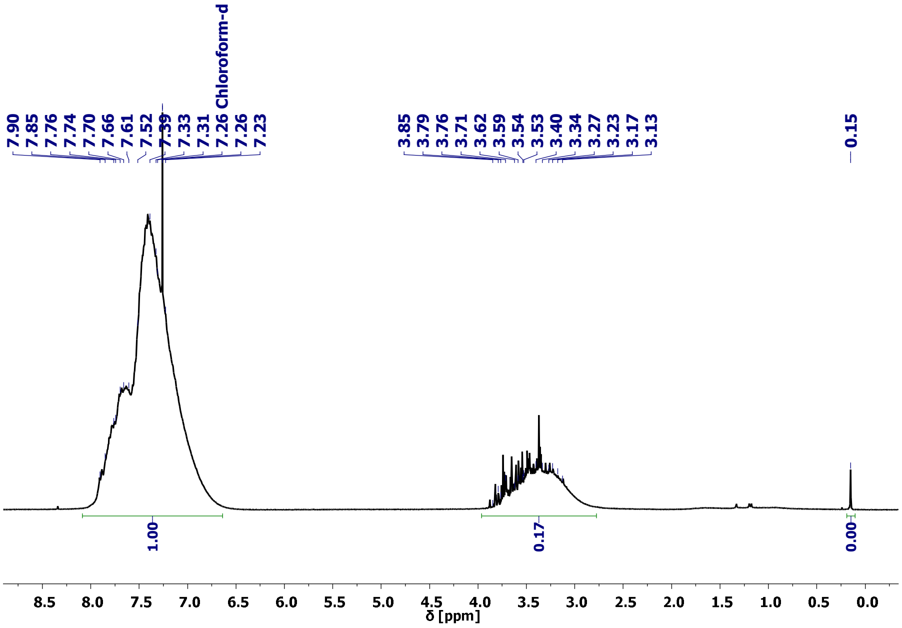

ESI3. ^{1}H NMR spectrum of MG Precursor (MG LG305)

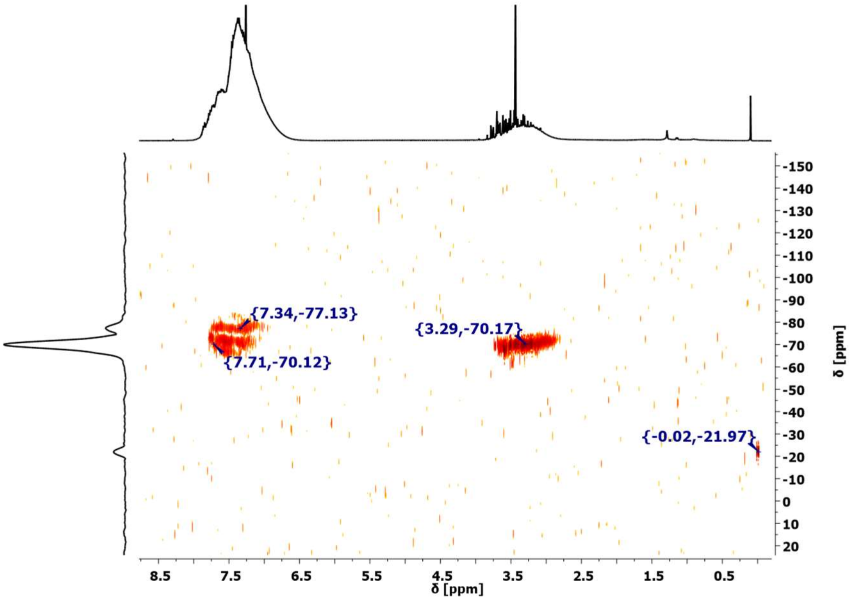

ESI4 ^{29}Si-^{1}H HMBC 2D NMR spectrum of MG Precursor (MG LG305)

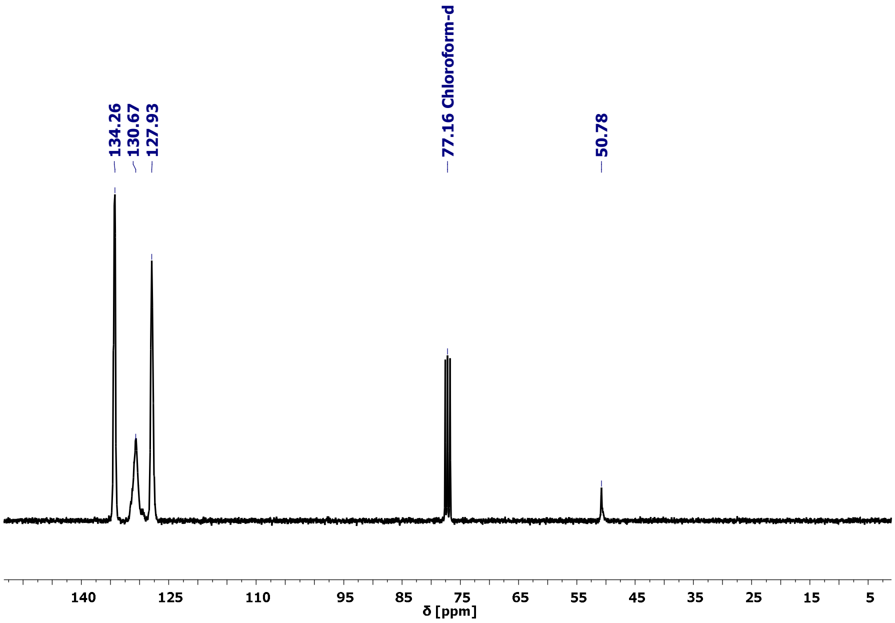

ESI5. ^{13}C NMR spectrum of MG Precursor (MG LG305)

MG Consolidated (MG cons. LG305)

δ_{Si} (^{29}Si CP-MAS-NMR, 80 MHz): -72 (T^2), -79 (T^3)

δ_{Si} (^{13}C, CP-MAS-NMR, 100 MHz,): -134.31, -130.54,-127.85 (Ph), -50.38 (-OMe)

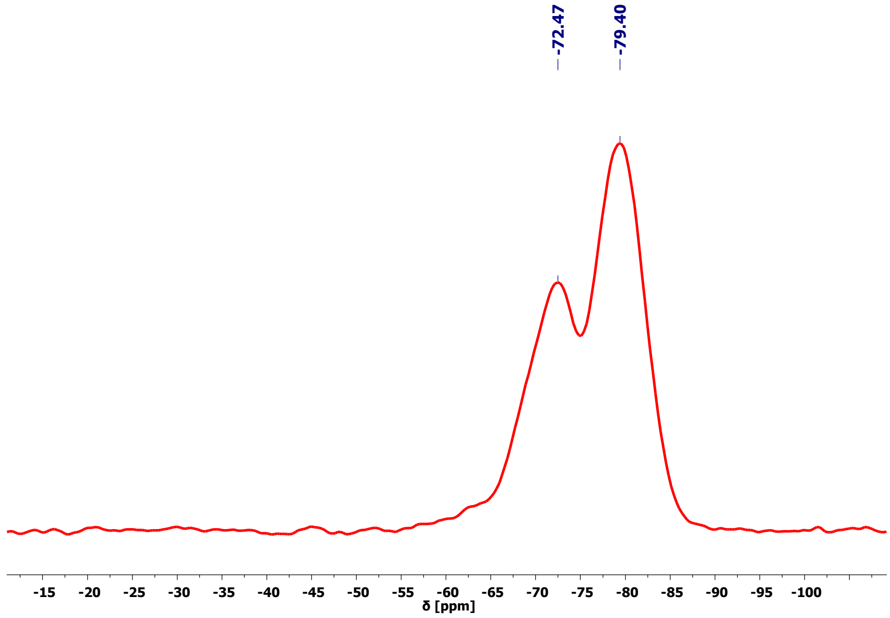

ESI6. ^{29}Si CP-MAS-NMR spectrum of MG Consolidated (MG cons. LG305)

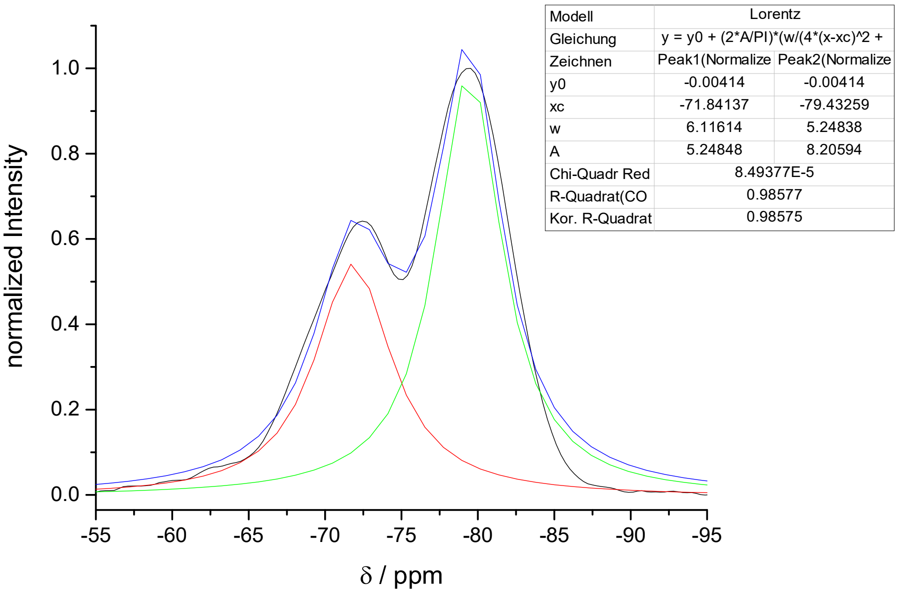

Modell	Lorentz	
Gleichung	y = y0 + (2*A/PI)*(w/(4*(x-xc)^2 +	
Zeichnen	Peak1(Normalize	Peak2(Normalize
y0	-0.00414	-0.00414
xc	-71.84137	-79.43259
w	6.11614	5.24838
A	5.24848	8.20594
Chi-Quadr Red	8.49377E-5	
R-Quadrat(CO	0.98577	
Kor. R-Quadrat	0.98575	

ESI7. Fitted ^{29}Si CP-MAS-NMR spectrum of MG Consolidated (MG cons. LG305)

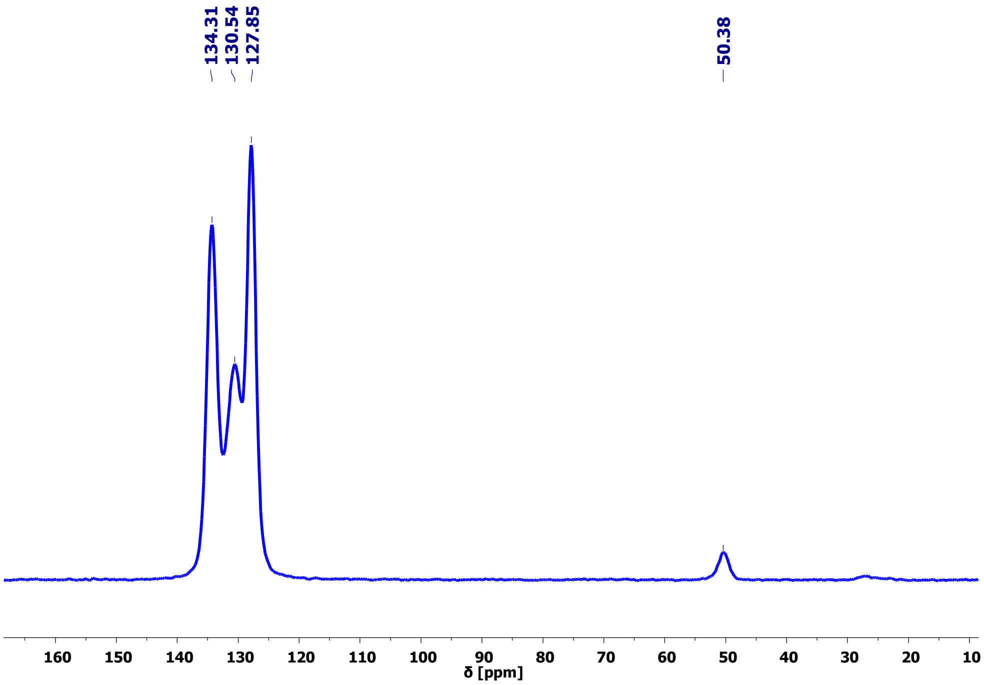

ESI8. ^{13}C CP-MAS-NMR spectrum of MG Consolidated (MG cons. LG305)

Untampered Microspheres (MGP LG305)

δ_{Si} (^{29}Si CP-MAS-NMR, 80 MHz): -72 (T^2), -80 (T^3)

δ_{Si} (^{13}C, CP-MAS-NMR, 100 MHz,): -133.59, -129.89,-127.21 (Phenyl [Polyphenylsilsesuqioxane], Phenoxy [Triton® X-405]), -70.00 (-OCH$_2$ [Triton® X-405]), -49.73 (-OMe [Polyphenylsilsesuqioxane]), -37.07 (-CCH$_2$ [Triton® X-405]), -31.24 (-CCH$_3$) [Triton® X-405])

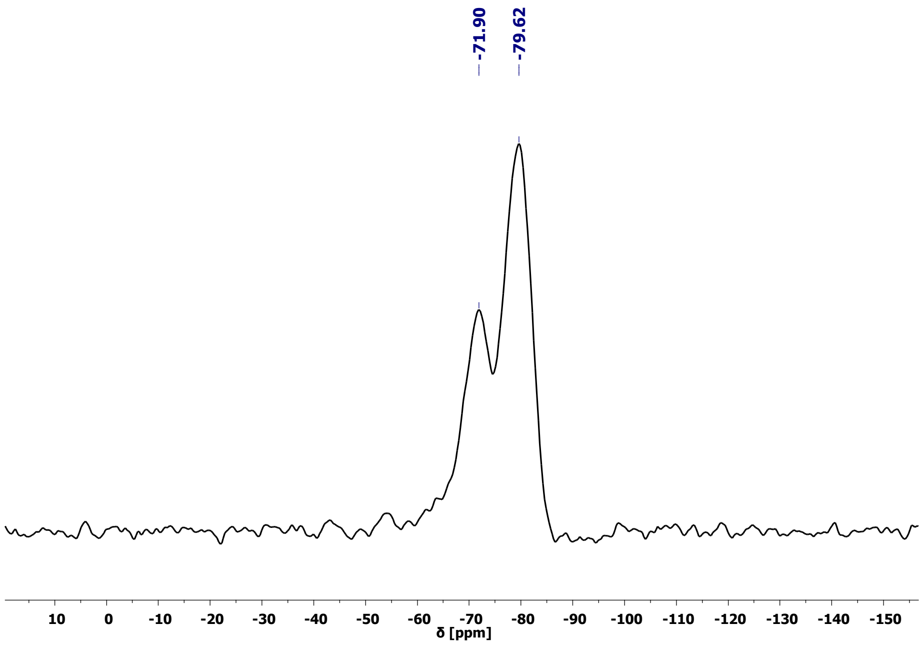

ESI9. ^{29}Si CP-MAS-NMR spectrum of Untampered Microspheres (MGP LG305)

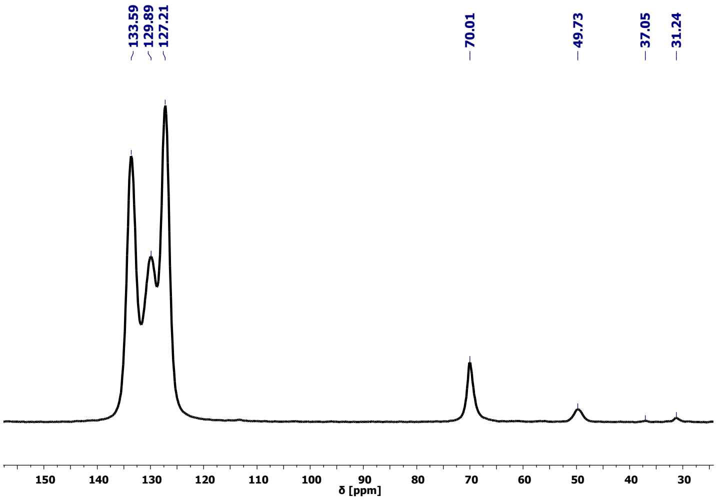

ESI10. ^{13}C CP-MAS-NMR spectrum of Untampered Microspheres (MGP LG305)

Tampered Microspheres, 200°C, 4h (MGP-T LG305)

δ_{Si} (^{29}Si CP-MAS-NMR, 80 MHz): -72 (T^2), -80 (T^3)

δ_{Si} (^{13}C, CP-MAS-NMR, 100 MHz,): -133.59, -129.89,-127.21 (Phenyl [Polyphenylsilsesuqioxane], Phenoxy [Triton® X-405]), -70.00 (-OCH$_2$ [Triton® X-405]), -49.73 (-OMe [Polyphenylsilsesuqioxane]), -37.07 (-CCH$_2$ [Triton® X-405]), -31.24 (-CCH$_3$) [Triton® X-405])

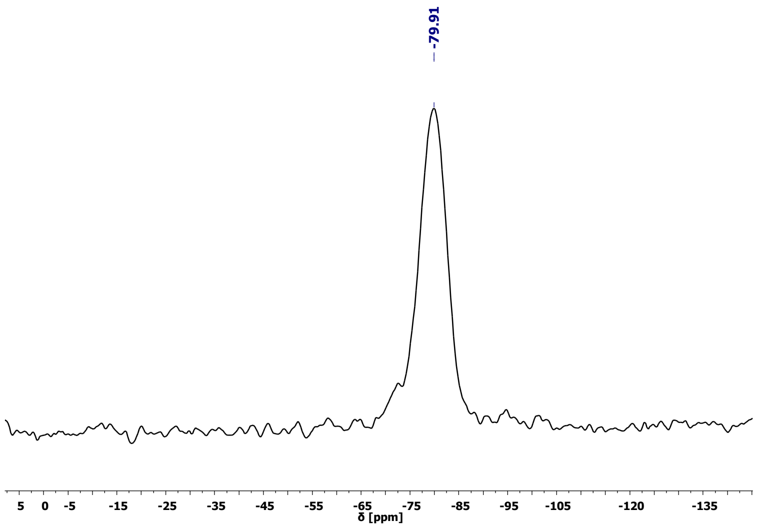

ESI11. ^{29}Si CP-MAS-NMR spectrum of tampered Microspheres, 200°C, 4h (MGP-T LG305)

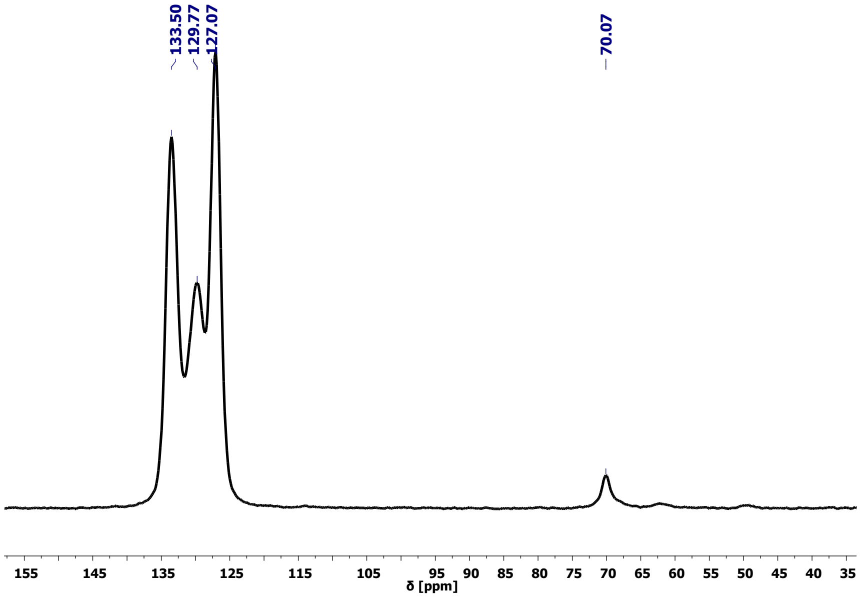

ESI12. ^{13}C CP-MAS-NMR spectrum of tampered Microspheres, 200°C, 4h (MGP-T LG305)

Lumogen®F Red 305

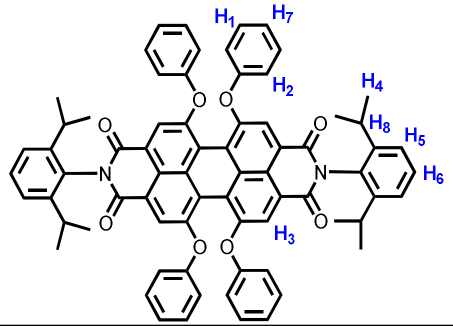

δ$_H$ (300 MHz, CDCl$_3$): 8.27 (4 H, s, H$_3$), 7.47 – 7.39 (2 H, m, H$_6$), 7.31 – 7.23 (12 H, m, H$_2$, H$_5$), 7.14 – 7.07 (4 H, m, H$_7$), 7.02 – 6.95 (8 H, m, H$_1$), 2.71 (4 H, sept, *J* 6.7, H$_8$), 1.12 (24 H, d, *J* 6.8, H$_4$).

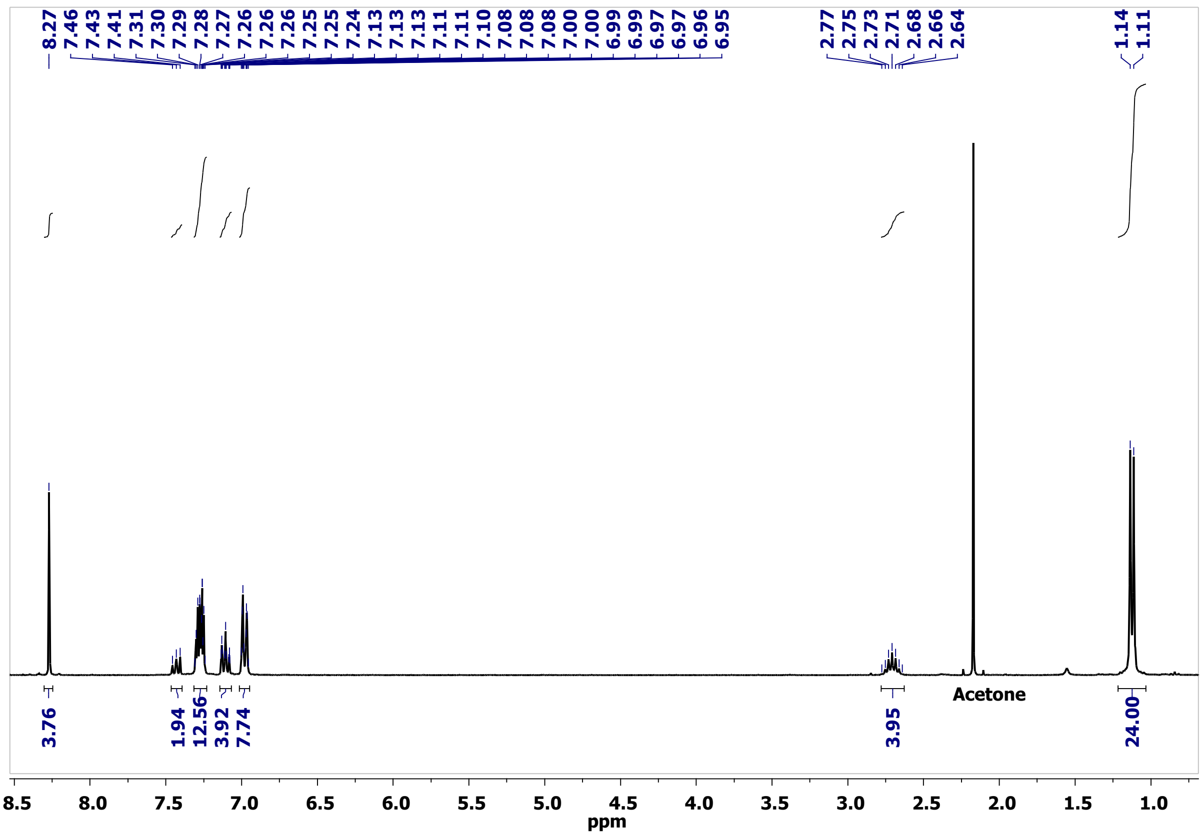

ESI13. ^{1}H NMR spectrum of Lumogen®F 305 Red.

FC546

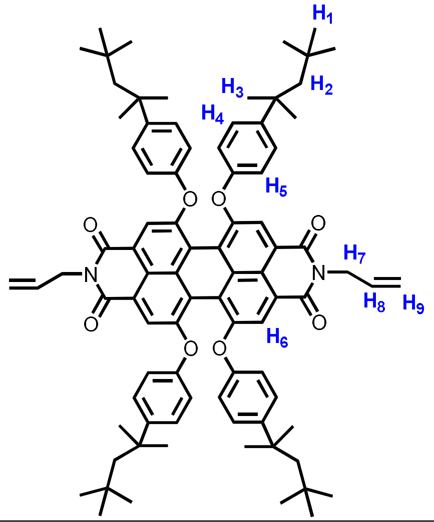

δ_H (300 MHz, $CDCl_3$): 8.15 (4 H, s, H_6), 7.27 (8 H, d, *J* 6.9, H_4), 6.86 (8 H, d, *J* 8.0, H_5), 6.01 – 5.83 (2 H, m, H_8), 5.33 – 5.10 (4 H, m, H_9), 4.73 (4 H, d, *J* 5.3, H_7), 1.73 (8 H, s, H_2), 1.54 (s, water), 1.36 (24 H, s, H_3), 0.78 (36 H, s, H_1).

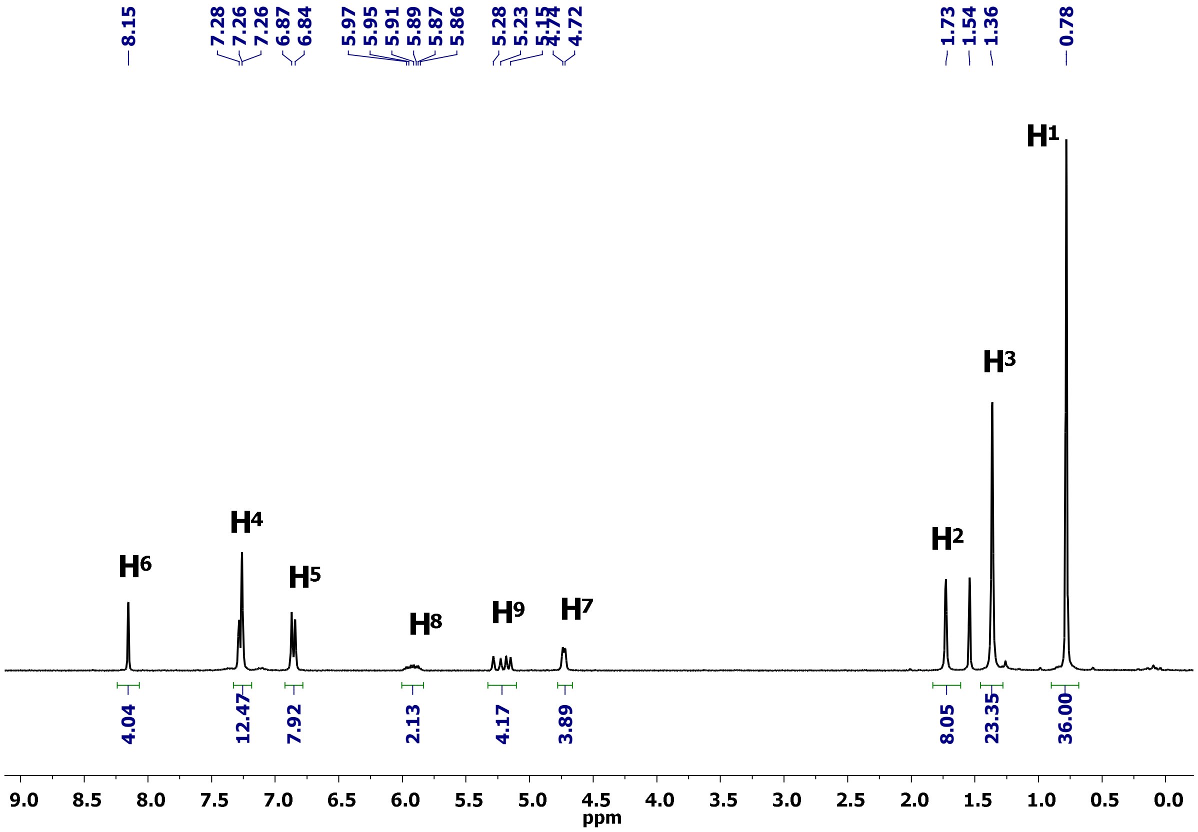

ESI14. ^1H NMR spectrum of FC546.

FC546- TES

δ_H (300 MHz, $CDCl_3$):

8.13 (4 H, s, H_6), 7.26 (8 H, d, *J* 6.9, H_4), 6.85 (8 H, d, *J* 8.7, H_5), 4.08 (4 H, t, *J* 7.0, H_7), 3.78 (12 H, q, *J* 7.0, H_{10}), 3.63 (s, educt traces), 1.85 – 1.75 (4 H, m, H^8), 1.72 (8 H, s, H_2), 1.56 (s, Wasser), 1.36 (24 H, s, H_3), 1.25 (s, Edukt), 1.18 (18 H, t, *J* 7.0, H_{11}), 0.77 (36 H, s, H_1), 0.07 (s, silicone grease).

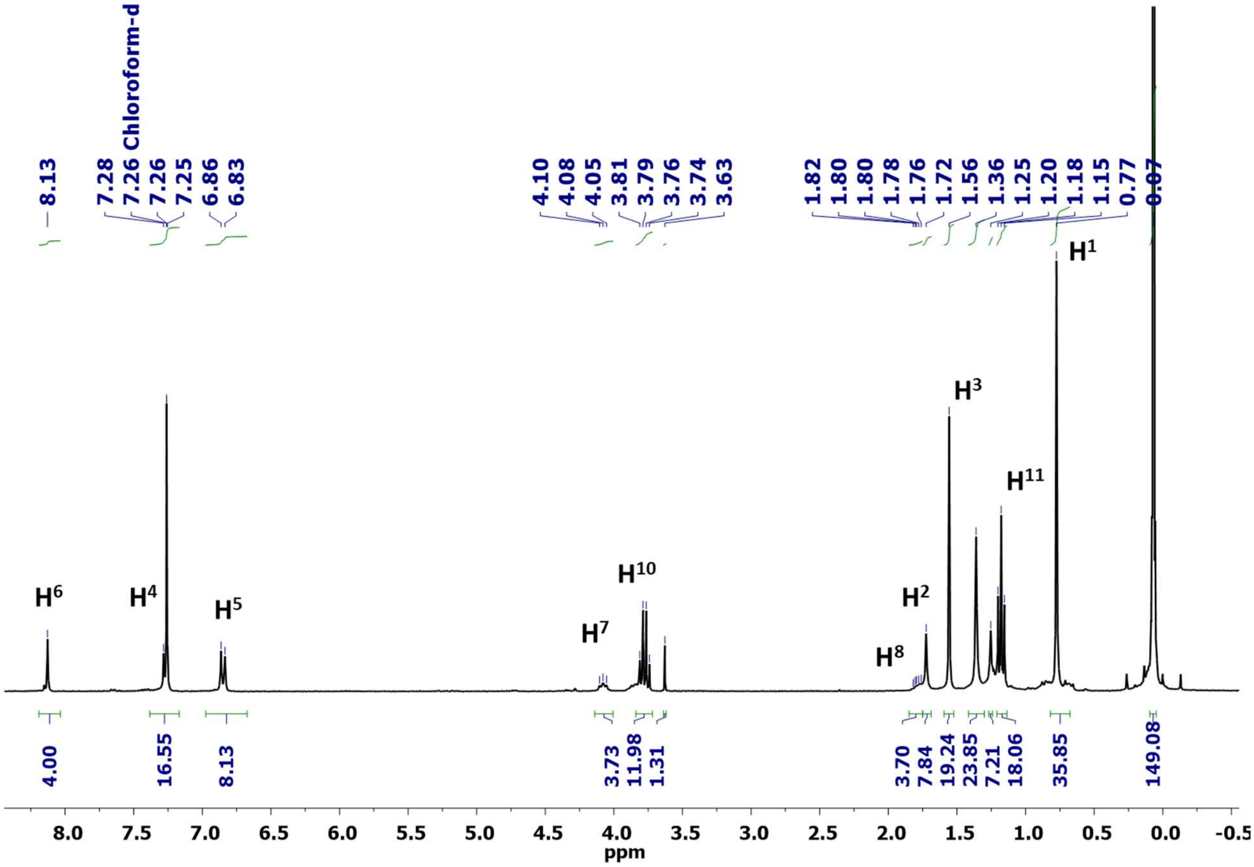

ESI15. ^1H-NMR-Spektrum von FC546 in Chloroform-D.

Triton X-405

δ_H (300 MHz, D_2O): 7.02 (4 H, dd, *J* 114.5, 8.3), 4.83 – 4.76 (D_2O, s), 4.03 (2 H, s), 3.87 – 3.51 (163 H, m), 1.66 (2 H, s), 1.28 (6 H, s), 0.70 (9 H, s).

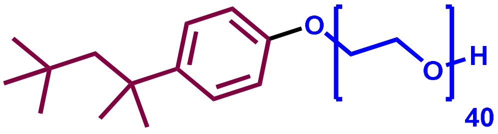

Mw = 1968,45 g mol^{-1}

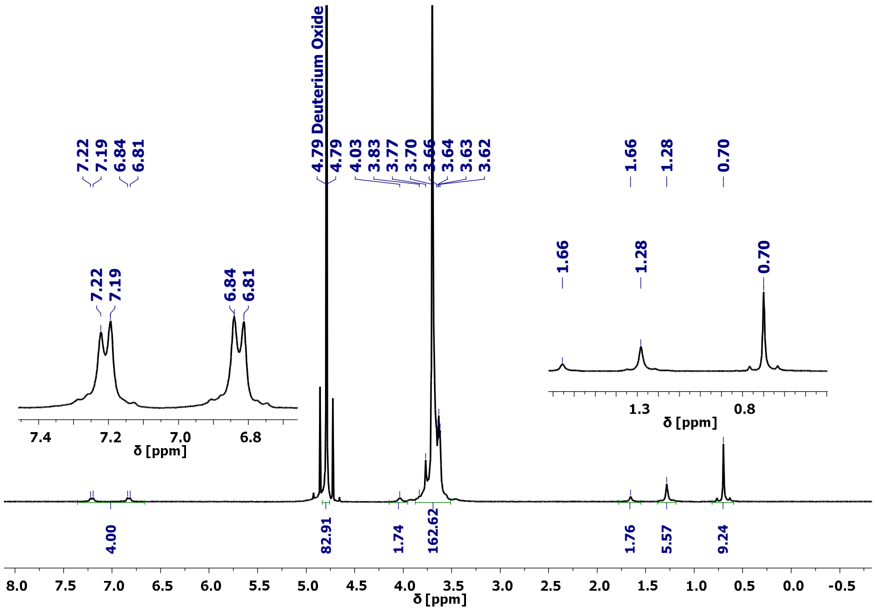

*ESI16. ^{1}H NMR spectrum of **Triton X-405.***

ATR FTIR Data

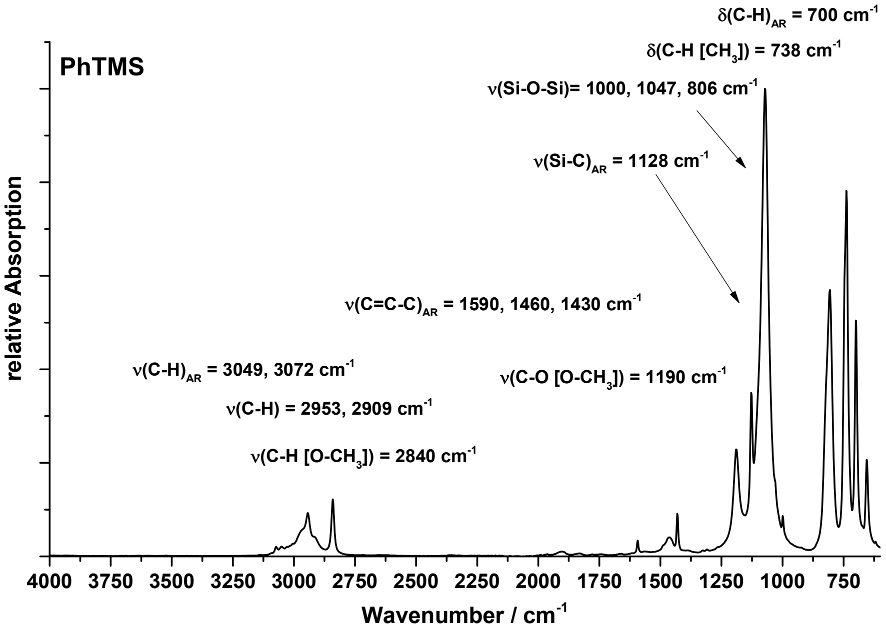

ESI17. ATR-FTIR of Phenyltrimethoxysilane.

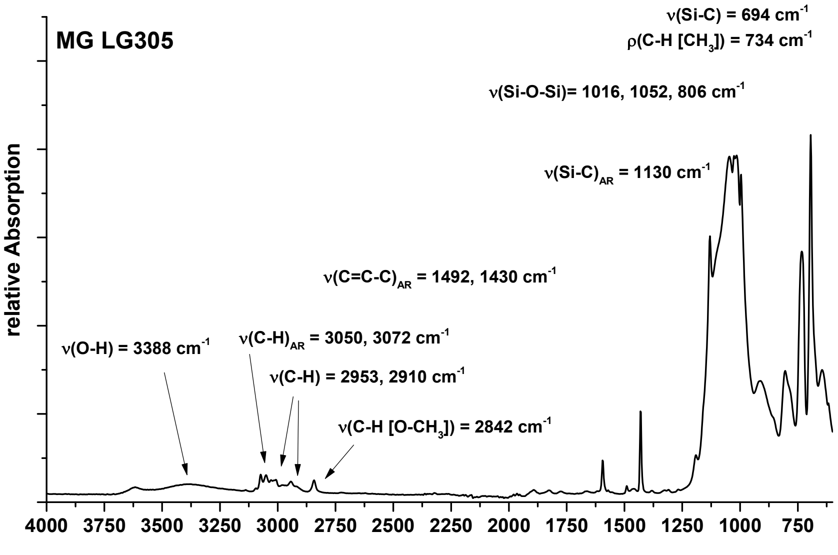

ESI18. ATR-FTIR of MG

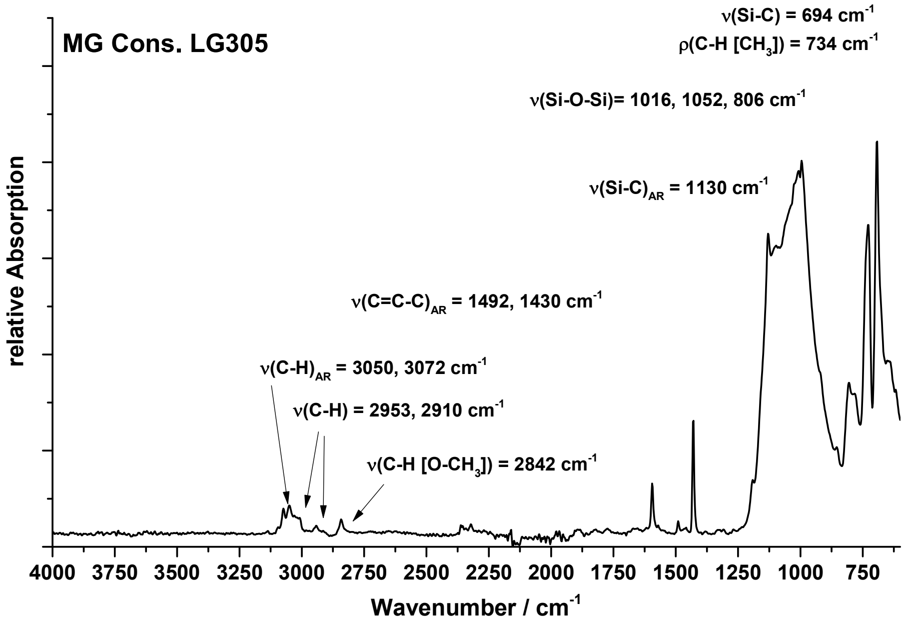

ESI19. ATR-FTIR of MG Cons.

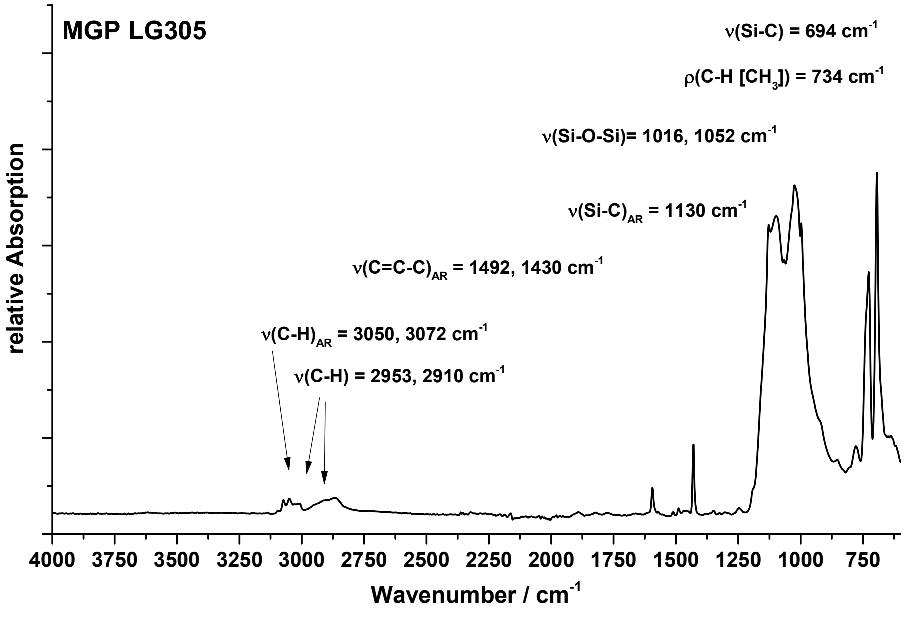

ESI20. ATR-FTIR of MGP

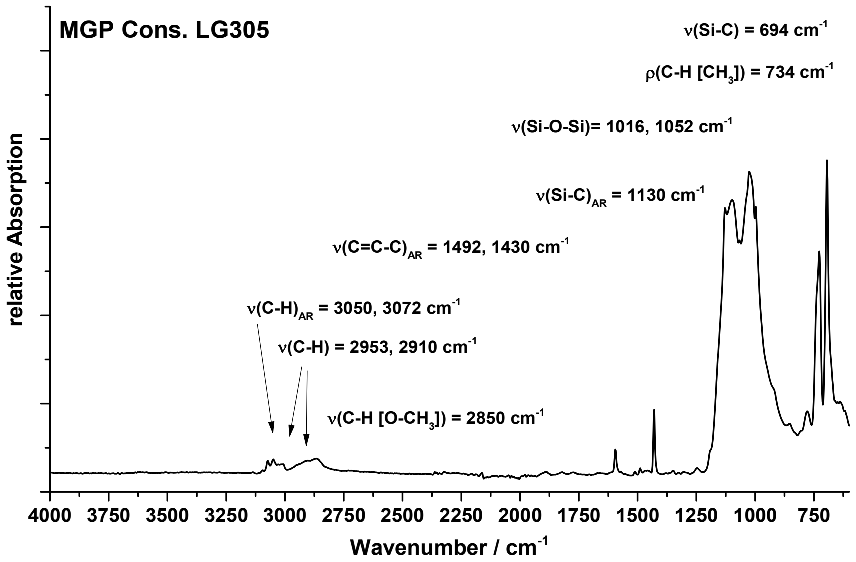

ESI21. ATR-FTIR of MGP-T

Microscopy and sphere size determination

MGP-1

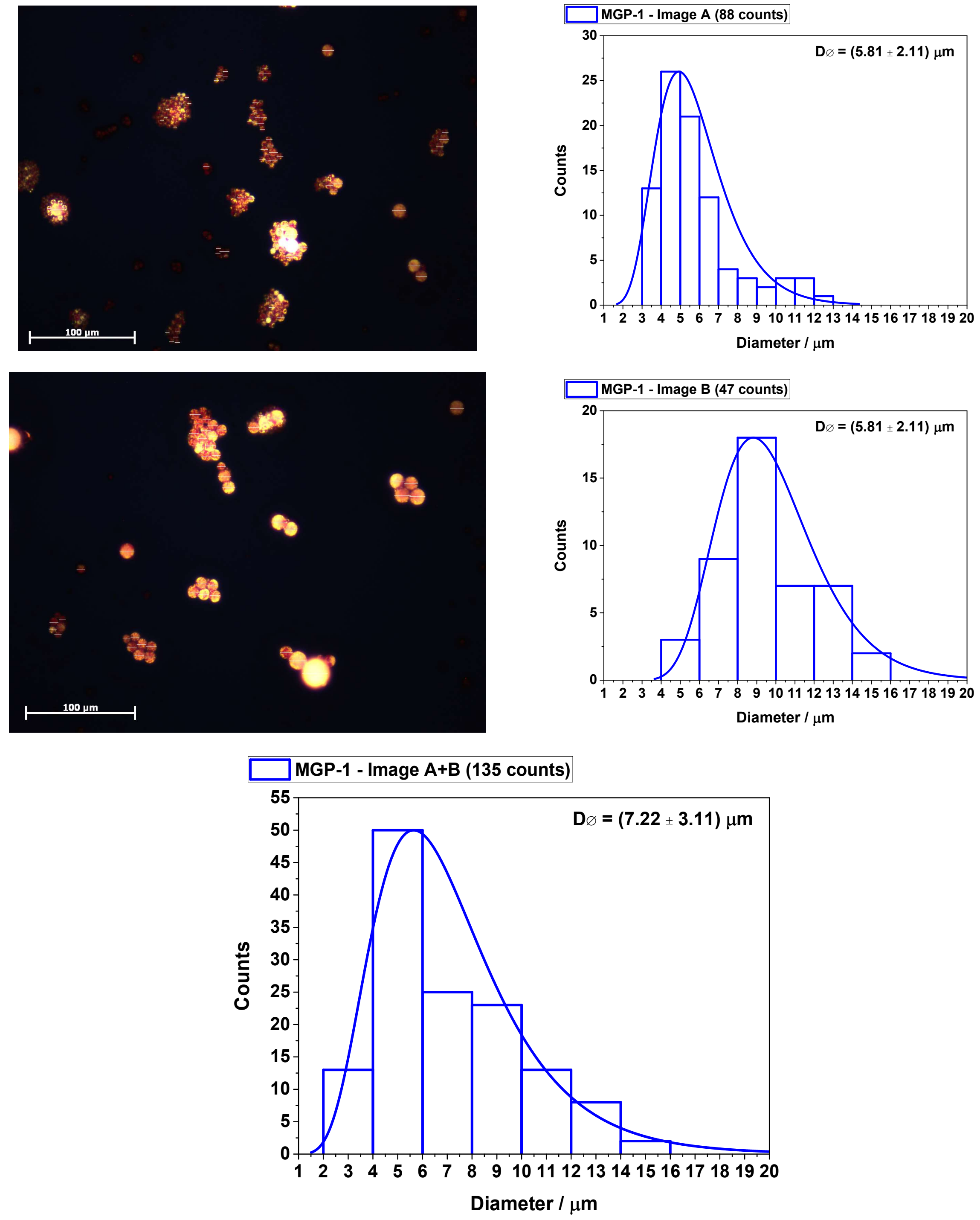

ESI22. Microscopic images and size determination of the MGP-1 particles made with 500 rpm stirring for 1h.

MGP-2

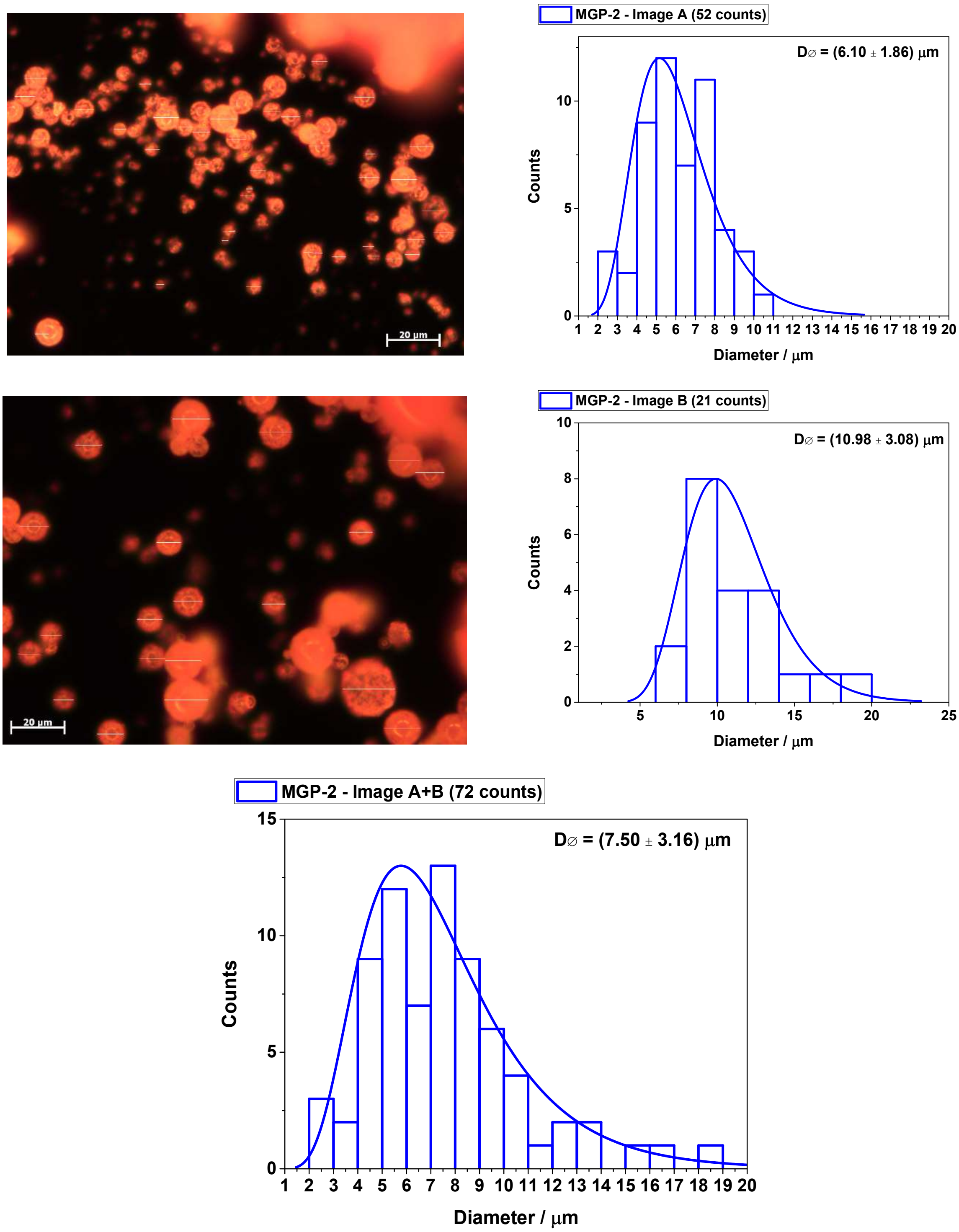

ESI23. Microscopic images and size determination of the MGP-2 particles made with 500 rpm stirring for 2h.

MGP-3

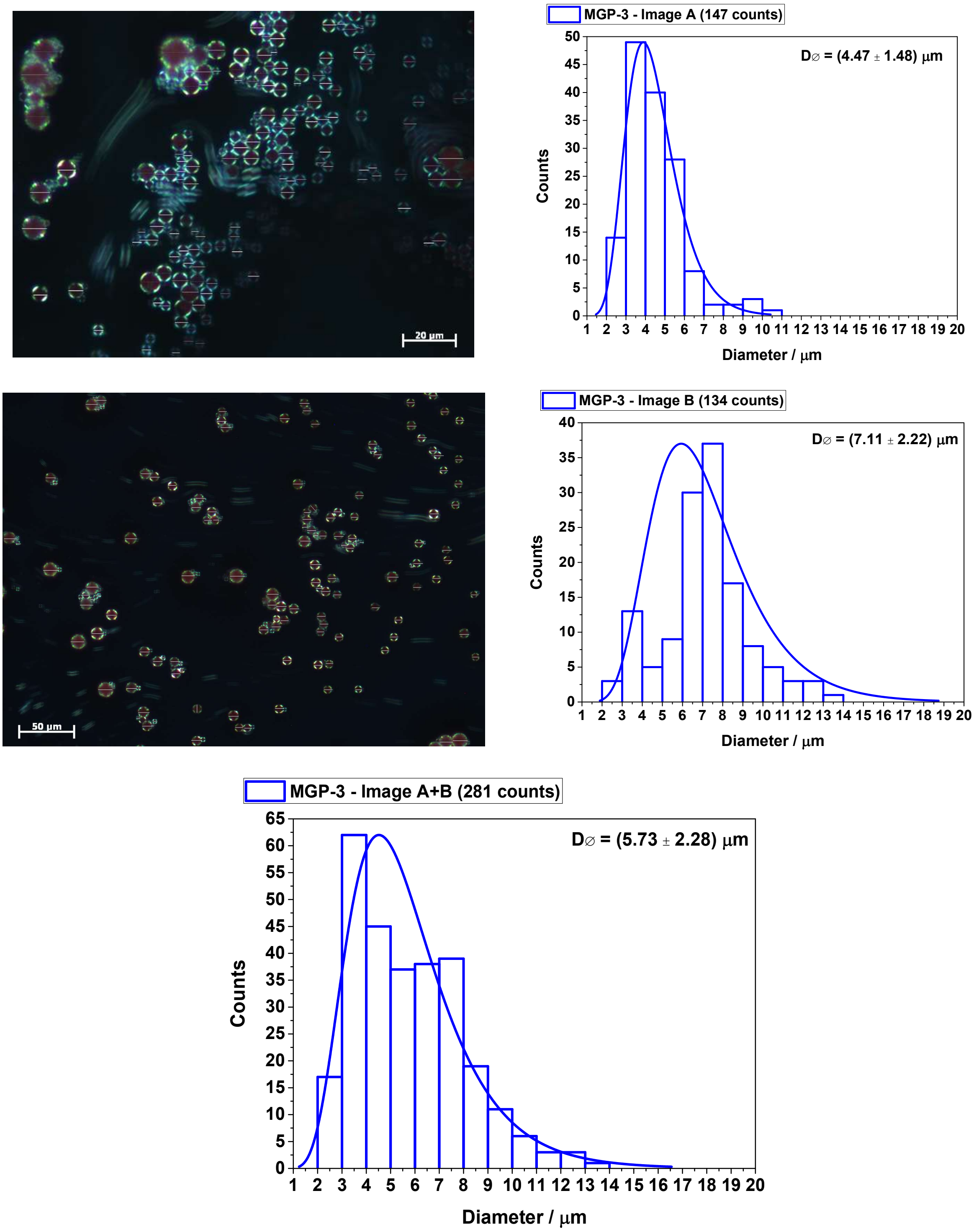

ESI24. Microscopic images and size determination of the MGP-3 particles made with 800 rpm stirring for 1h.

MGP-UT2

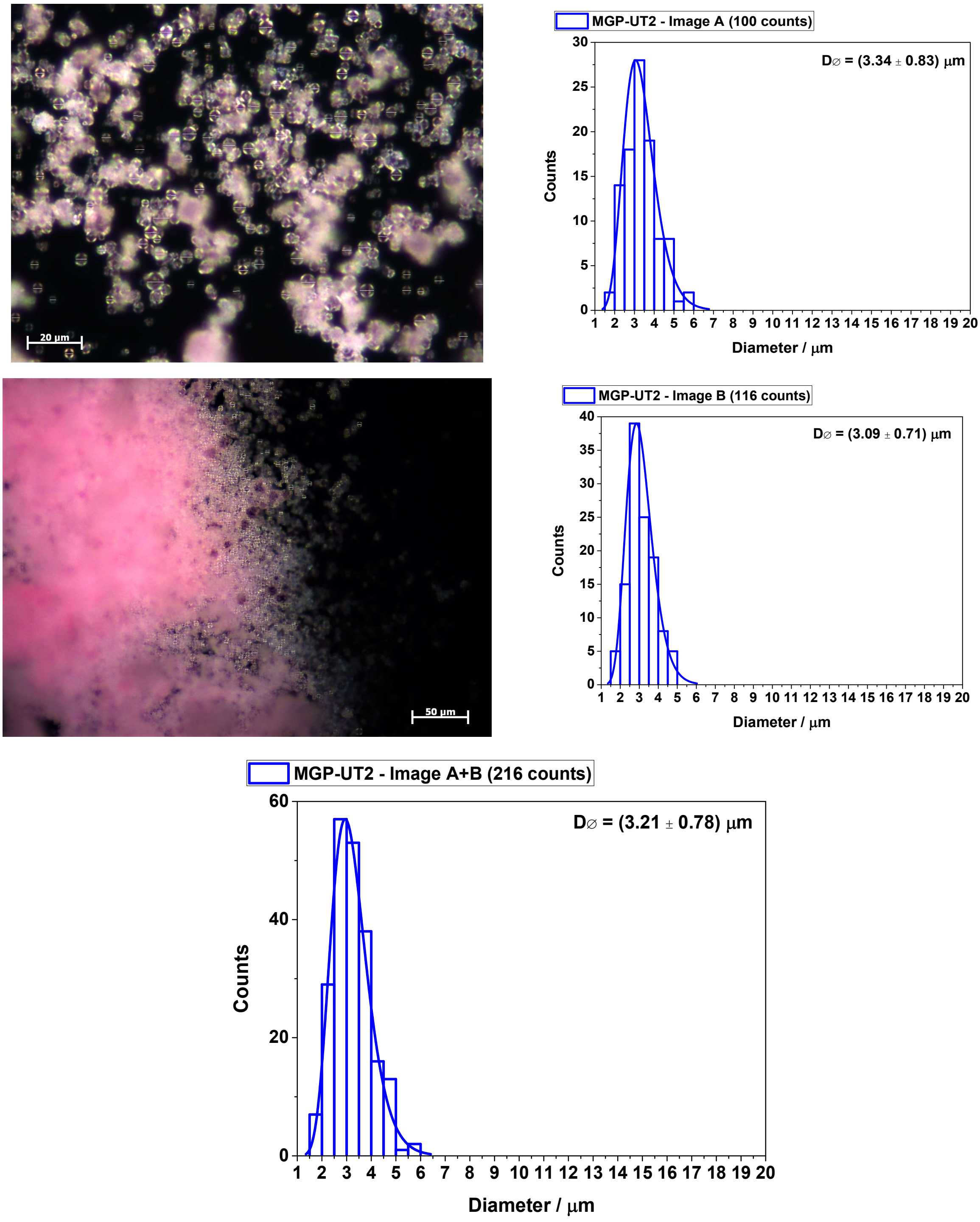

ESI25. Microscopic images and size determination of the MGP-UT particles made with 500 rpm stirring followed by 10000 rpm with an Ultra-Turrax™ dispenser.

MGP-US

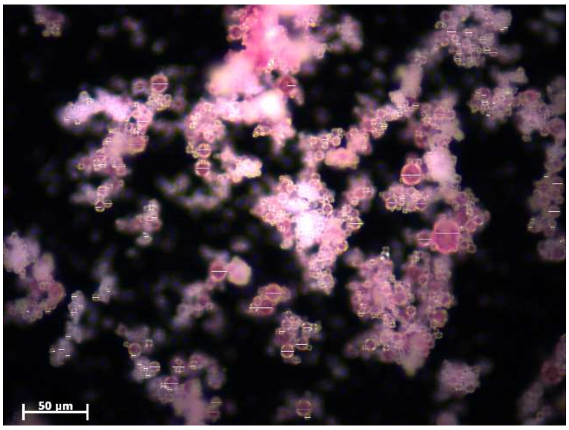

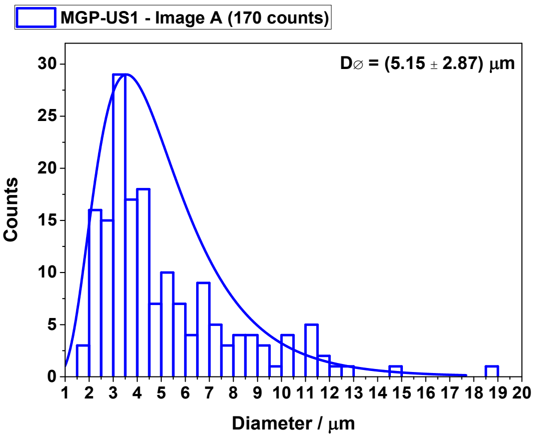

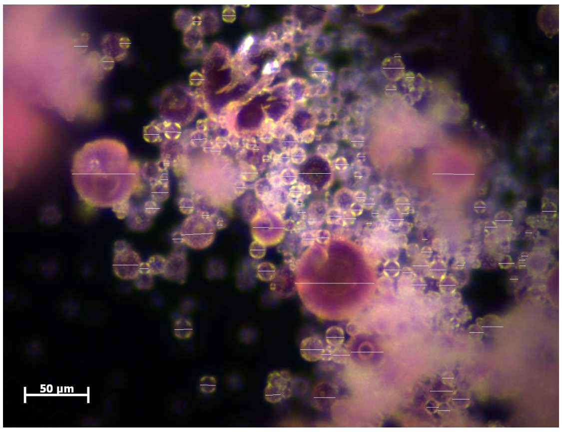

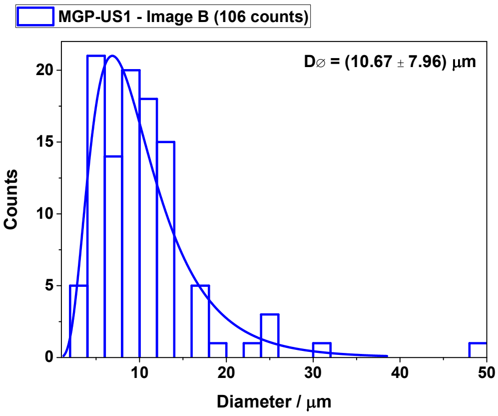

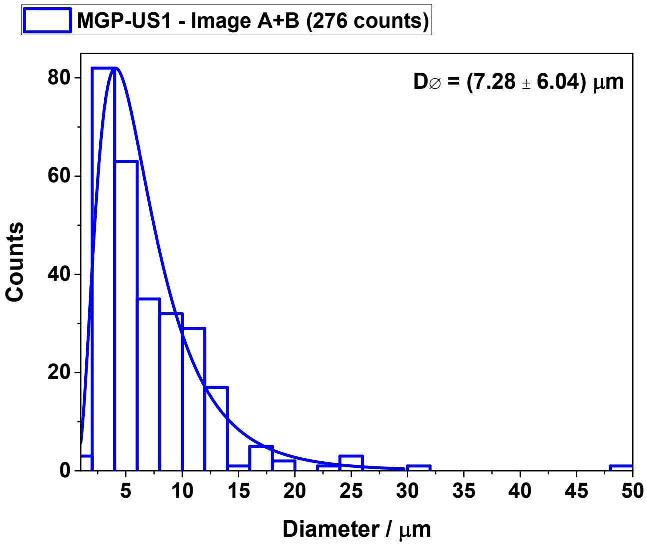

ESI26. Microscopic images and size determination of the MGP-US particles made with 500 rpm stirring followed by 150 W ultra-sonic treatment.

Thermogravimetric Data

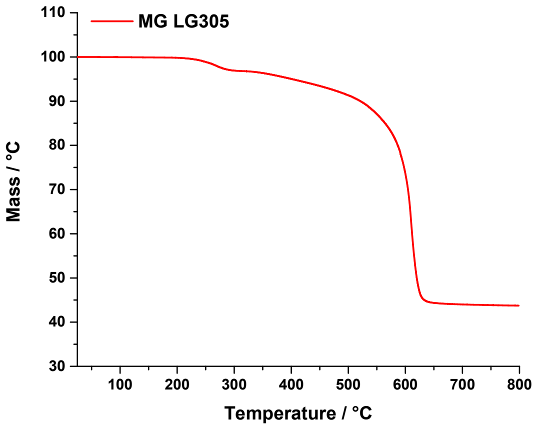

ESI27. Mass loss curve of MG

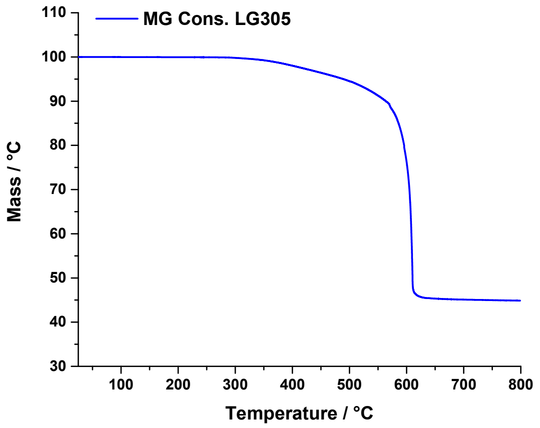

ESI28. Mass loss curve of MG Cons

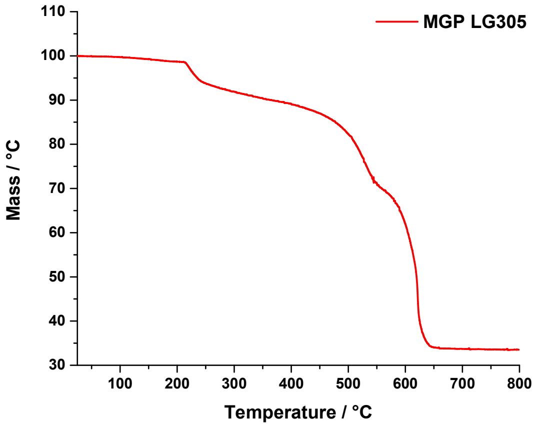

ESI29. Mass loss curve of MGP

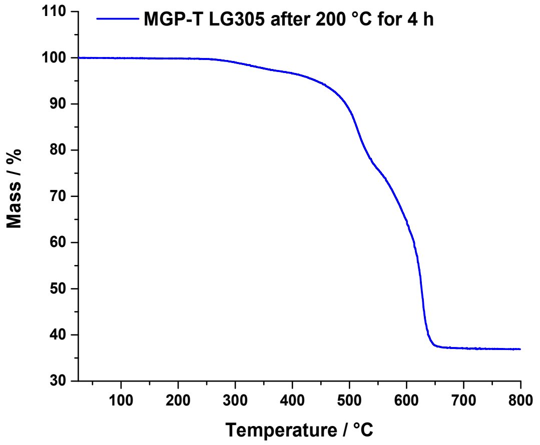

ESI30. Mass loss curve of MGP-T

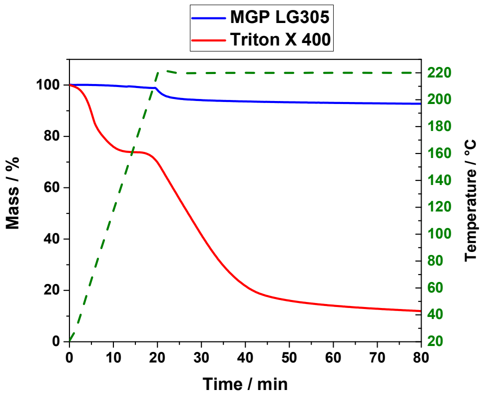

ESI31. Mass loss curve of MGP and a Triton™ X-405 solution at isothermally 220 °C for 80 min

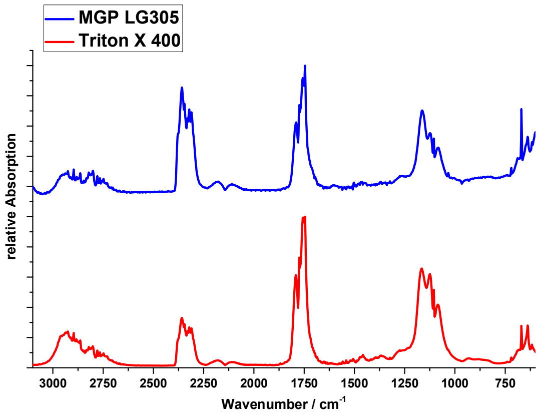

ESI32. TG-FTIR spectra of MGP and a Triton™ X-405 solution at isothermally 220 °C for 80 min.

8. Acknowledgement

Hiermit möcht ich mich bei allen Menschen bedanken, die mich während meiner Zeit als Promotionsstudent begleitet und unterstützt haben.

Mein größter Dank gilt **Prof. Dr. Guido Kickelbick**.
Er hat mir die Möglichkeit gegeben mich mit einem spannenden Forschungsthema zu verwirklichen und mich dabei jederzeit unterstützt und geleitet. Durch den großen kreativen Freiraum und die hervorragende Zusammenarbeit wurde die erfolgreiche Anfertigung dieser Dissertation und das erfolgreiche abschließen unseres gemeinsamen Projektes erst möglich. Einen weiteren Dank bedarf es für die Korrekturen und Kommentierungen der Publikationen und dieser Dissertation. Zum Schluss möchte ich mich noch für die gute gemeinsame Zeit außerhalb der Universität bedanken, die ich immer sehr genossen und geschätzt habe.

Ein besonderer Dank gilt **Svenja Pohl**, die mich tatkräftig und überaus engagiert bei meiner Arbeit und bei der Erkundung neuer experimenteller Wege unterstützt und begleitet hat.
Danke für alles Svenja!

Ich danke dem „Team Silikone“ mit **Dr. Patrick Wenderoth** und **Dennis Meier**, für die Einarbeitung in meinen ersten Wochen im Saarland, die Unterstützung bei allen Belangen und für die gemeinsame Zeit im Labor.

Ich danke **Dr. Sandra Schäfer** und **Christina Odenwald,** für die gemeinsame Zeit an der Uni, schönen kulinarische und sportliche Erlebnisse im Saarland, kreative Abende am Entenstammtisch und für unsere Freundschaft.

Ich danke den zahlreichen **Mitarbeitern des Arbeitskreises** für unsere gemeinsame Zeit und die gute Zusammenarbeit. Dennis Becker, Achim Koch, Nadja Klippel, Thomas Klein, Bastian Oberhausen, Dr. Jessica Bauer, Dr. Robert Haberkorn, Dr. Christina Hein, Kristina Brix und Dr. Ralf Kautenburger, Susanne Harling, Christel Hassler und Traudel Allgayer danke ich für die kollegiale und freundliche Arbeitsatmosphäre, den wissenschaftlichen Input, aber auch für gemeinsame Gespräche und Unternehmungen. Ebenfalls danke ich euch für alle von euch durchgeführten Messungen.

Ich denke allen, am **ORCA Projekt** beteiligten Mitarbeitern der BASF, OSRAM GmbH und OSRAM Optosemiconductors für die hervorragende Zusammenarbeit und viele schöne Stunden in Ludwigshafen, Regensburg, Schwabmünchen und natürlich in Saarbrücken.

All den **Saarländern**, auf deren Schultern ein Teil der Last dieser Arbeit ruht, und hier nicht namentlich genannt wurden, möchte ich für die Zusammenarbeit und wie wundervolle Zeit an der Universität des Saarlandes danken. Stellvertretend richtet sich mein Dank an die Mitarbeiter der Werkstatt, der Elektrotechnik und der Glasbläserei, sowie allen technischen Mitarbeitern und Laboranten.

Des Weiteren gilt mein Dank den Menschen, die mich schon länger durch mein Leben begleiten und mich auch weiterhin begleiten werden.

Besonders bedanken möchte ich mich bei **Dr. Matthias Adlung**.
Als mein Mentor und Freund hast du das Beste aus mir rausgeholt und dadurch einen enormen Anteil zu meiner persönlichen Entwicklung und zu meiner wissenschaftlichen Ausbildung beigetragen. Danke für alles Matthias!

Ich danke der gesamten ehemaligen Arbeitsgruppe der **AC-II der Universität Siegen**.
Dr. Sascha Krüger, Dr. Markus Suta, Dr. Konrad Kiefer, Dr. Kristina Großmann, Regina Stötzel und Jennifer Gellert möchte ich danken für eine unbeschwerte und erfüllte Zeit, für 100 % Liebe und 0 % Intoleranz, für schöne Wanderungen und feuchte Abende, und für unseren großartigen Zusammenhalt.

Ich danke meinen **Eltern und Geschwistern**, auf deren Liebe und Unterstützung ich immer zählen konnte und die immer an mich geglaubt haben.

Ich danke **Sina Hafner** für die Liebe, die Unterstützung und die Motivation in den letzten Jahren. Danke, dass du immer auf mich aufpasst und mir Kraft gibst. Ich liebe dich!

Ich danke **Christof Sartor** für die fortwährende Unterstützung und unsere außerordentliche Freundschaft. Egal was passiert, du bist da.

Zuletzt möchte ich **meinen Kommilitonen** Phil Marvin Pithan, Dr. Sebastian von Gradowski, Benedikt Steinhoff und Dr. Byron Staudt danken. Danke für eine wirklich gute Zeit, eure immerwährende Freundschaft und Unterstützung in all den Jahren.

9. Curriculum Vitae

Personal Data

Name: Nils Steinbrück
Birthdate: 19.08.1989

Work Experience

12/2019	Project Quality Professional, OSRAM Opto Semiconductors, Regensburg, Germany

Academic Education

03/2016 – 11/2019	PhD student and research associate, Inorganic Solid State Chemistry, Saarland University, Saarbrücken, Germany Topic: Preparation of new Polysiloxane Host Materials for Perylene based Phosphors in Optoelectronics
04/2013 – 07/2015	Consecutive, international master's program in chemistry, University of Siegen, Germany Graduation: Master of Science (final grade: 1.6)
01/2015 – 07/2015	Master thesis at the Schott Research Centre (SCHOTT AG), Mainz, Germany Topic: Investigation and Characterization of the temperature dependents of the Absorbance of an allochromatic Li_2O-Al_2O_3-SiO_2 Glass system
10/2009 – 04/2013	Bachelor's program in chemistry, University of Siegen Graduation: Bachelor of Science (Final Grade: 2.0) Topic: Synthesis, Investigation and Charactarization of the optical Properties Eu^{2+}-doped Alkaline Earth Pnictogenide Chlorides

Occupation

03/2016 – 10/2019	Research associate, Inorganic Solid State Chemistry, Saarland University, Saarbrücken, Germany
01/2011 – 09/2014	Student associate, Inorganic Chemistry, Siegen, Germany

Advanced Education

03/2019	Fire Protection Representative Qualification
04/2017	Workshop participant: Good Scientific Practice and Communication
03/2017	First Aid Training (First-Aider Qualification)
11/2016	Patent Law qualification
07/2013	First Aid training for chemistry accidents
04/2013	Workshop electroplating techniques
03/2011 – 03/2014	Annual participation at the Hemdsärmelkolloquium of the German Solid State Chemistry Community

Language

German (native speaker)
English (fluent)